

CHEMICAL BIOLOGY EDITOR'S PICK 2021

EDITED BY: John D. Wade
PUBLISHED IN: *Frontiers in Chemistry*





frontiers

Frontiers eBook Copyright Statement

The copyright in the text of individual articles in this eBook is the property of their respective authors or their respective institutions or funders. The copyright in graphics and images within each article may be subject to copyright of other parties. In both cases this is subject to a license granted to Frontiers.

The compilation of articles constituting this eBook is the property of Frontiers.

Each article within this eBook, and the eBook itself, are published under the most recent version of the Creative Commons CC-BY licence.

The version current at the date of publication of this eBook is CC-BY 4.0. If the CC-BY licence is updated, the licence granted by Frontiers is automatically updated to the new version.

When exercising any right under the CC-BY licence, Frontiers must be attributed as the original publisher of the article or eBook, as applicable.

Authors have the responsibility of ensuring that any graphics or other materials which are the property of others may be included in the CC-BY licence, but this should be checked before relying on the CC-BY licence to reproduce those materials. Any copyright notices relating to those materials must be complied with.

Copyright and source acknowledgement notices may not be removed and must be displayed in any copy, derivative work or partial copy which includes the elements in question.

All copyright, and all rights therein, are protected by national and international copyright laws. The above represents a summary only. For further information please read Frontiers' Conditions for Website Use and Copyright Statement, and the applicable CC-BY licence.

ISSN 1664-8714

ISBN 978-2-88966-796-3

DOI 10.3389/978-2-88966-796-3

About Frontiers

Frontiers is more than just an open-access publisher of scholarly articles: it is a pioneering approach to the world of academia, radically improving the way scholarly research is managed. The grand vision of Frontiers is a world where all people have an equal opportunity to seek, share and generate knowledge. Frontiers provides immediate and permanent online open access to all its publications, but this alone is not enough to realize our grand goals.

Frontiers Journal Series

The Frontiers Journal Series is a multi-tier and interdisciplinary set of open-access, online journals, promising a paradigm shift from the current review, selection and dissemination processes in academic publishing. All Frontiers journals are driven by researchers for researchers; therefore, they constitute a service to the scholarly community. At the same time, the Frontiers Journal Series operates on a revolutionary invention, the tiered publishing system, initially addressing specific communities of scholars, and gradually climbing up to broader public understanding, thus serving the interests of the lay society, too.

Dedication to Quality

Each Frontiers article is a landmark of the highest quality, thanks to genuinely collaborative interactions between authors and review editors, who include some of the world's best academicians. Research must be certified by peers before entering a stream of knowledge that may eventually reach the public - and shape society; therefore, Frontiers only applies the most rigorous and unbiased reviews.

Frontiers revolutionizes research publishing by freely delivering the most outstanding research, evaluated with no bias from both the academic and social point of view. By applying the most advanced information technologies, Frontiers is catapulting scholarly publishing into a new generation.

What are Frontiers Research Topics?

Frontiers Research Topics are very popular trademarks of the Frontiers Journals Series: they are collections of at least ten articles, all centered on a particular subject. With their unique mix of varied contributions from Original Research to Review Articles, Frontiers Research Topics unify the most influential researchers, the latest key findings and historical advances in a hot research area! Find out more on how to host your own Frontiers Research Topic or contribute to one as an author by contacting the Frontiers Editorial Office: frontiersin.org/about/contact

CHEMICAL BIOLOGY EDITOR'S PICK 2021

Topic Editor:

John D. Wade, University of Melbourne, Australia

Citation: Wade, J. D., ed. (2021). Chemical Biology Editor's Pick 2021.
Lausanne: Frontiers Media SA. doi: 10.3389/978-2-88966-796-3

Table of Contents

- 04 *Production of Glycopeptide Derivatives for Exploring Substrate Specificity of Human OGA Toward Sugar Moiety***
Shanshan Li, Jiajia Wang, Lanlan Zang, Hailiang Zhu, Jianshuang Guo, Jiabin Zhang, Liuqing Wen, Yi Chen, Yanhong Li, Xi Chen, Peng George Wang and Jing Li
- 10 *Reassessing the Host Defense Peptide Landscape***
Evan F. Haney, Suzana K. Straus and Robert E. W. Hancock
- 32 *Three Decades of Amyloid Beta Synthesis: Challenges and Advances***
Johanes K. Kasim, Iman Kavianinia, Paul W. R. Harris and Margaret A. Brimble
- 57 *Improved HaloTag Ligand Enables BRET Imaging With NanoLuc***
Ovia Margaret Thirukkumaran, Congrong Wang, Nnamdi Joseph Asouzu, Eduard Fron, Susana Rocha, Johan Hofkens, Luke D. Lavis and Hideaki Mizuno
- 64 *Cardiolipin Structure and Oxidation are Affected by Ca^{2+} at the Interface of Lipid Bilayers***
Érica G. A. Miranda, Juliana C. Araujo-Chaves, Cintia Kawai, Adrianne M. M. Brito, Igor W. R. Dias, Jeverson T. Arantes and Iseli L. Nantes-Cardoso
- 76 *Solid-Phase Synthesis of Head to Side-Chain Tyr-Cyclodepsipeptides Through a Cyclative Cleavage From Fmoc-MeDbz/MeNbz-resins***
Gerardo A. Acosta, Laura Murray, Miriam Royo, Beatriz G. de la Torre and Fernando Albericio
- 85 *Comparison Between O and OH Intermediates of Cytochrome c Oxidase Studied by FTIR Spectroscopy***
Elena Gorbikova and Ruslan Kalendar
- 91 *A New Design for the Fixed Primer Regions in an Oligonucleotide Library for SELEX Aptamer Screening***
Bin Wang
- 95 *Enhancing the Mitochondrial Uptake of Phosphonium Cations by Carboxylic Acid Incorporation***
Laura Pala, Hans M. Senn, Stuart T. Caldwell, Tracy A. Prime, Stefan Warrington, Thomas P. Bright, Hiran A. Prag, Claire Wilson, Michael P. Murphy and Richard C. Hartley



Production of Glycopeptide Derivatives for Exploring Substrate Specificity of Human OGA Toward Sugar Moiety

Shanshan Li^{2†}, Jiajia Wang^{1,2*†}, Lanlan Zang^{3†}, Hailiang Zhu², Jianshuang Guo⁴, Jiabin Zhang², Liuqing Wen², Yi Chen⁵, Yanhong Li⁵, Xi Chen⁵, Peng George Wang^{2,4*} and Jing Li^{4*}

¹ School of Basic Medical Sciences, Henan University Joint National Laboratory for Antibody Drug Engineering, Kaifeng, China, ² Department of Chemistry and Center of Diagnostics & Therapeutics, Georgia State University, Atlanta, GA, United States, ³ Central Laboratory, Linyi People's Hospital, Shandong University, Linyi, China, ⁴ State Key Laboratory of Medicinal Chemical Biology, College of Pharmacy and Tianjin Key Laboratory of Molecular Drug Research, Nankai University, Tianjin, China, ⁵ Department of Chemistry, University of California, Davis, Davis, CA, United States

OPEN ACCESS

Edited by:

Xuechen Li,
The University of Hong Kong, Hong Kong

Reviewed by:

Chang-Chun Ling,
University of Calgary, Canada
Matthew Robert Pratt,
University of Southern California,
United States

*Correspondence:

Jiajia Wang
jwang77@vip.henu.edu.cn
Peng George Wang
pwang11@gsu.edu
Jing Li
jinglink@nankai.edu.cn

[†]These authors have contributed
equally to this work

Specialty section:

This article was submitted to
Chemical Biology,
a section of the journal
Frontiers in Chemistry

Received: 08 October 2018

Accepted: 12 December 2018

Published: 14 January 2019

Citation:

Li S, Wang J, Zang L, Zhu H, Guo J, Zhang J, Wen L, Chen Y, Li Y, Chen X, Wang PG and Li J (2019) Production of Glycopeptide Derivatives for Exploring Substrate Specificity of Human OGA Toward Sugar Moiety. *Front. Chem.* 6:646. doi: 10.3389/fchem.2018.00646

O-GlcNAcase (OGA) is the only enzyme responsible for removing *N*-acetyl glucosamine (GlcNAc) attached to serine and threonine residues on proteins. This enzyme plays a key role in O-GlcNAc metabolism. However, the structural features of the sugar moiety recognized by human OGA (hOGA) remain unclear. In this study, a set of glycopeptides with modifications on the GlcNAc residue, were prepared in a recombinant full-length human OGT-catalyzed reaction, using chemoenzymatically synthesized UDP-GlcNAc derivatives. The resulting glycopeptides were used to evaluate the substrate specificity of hOGA toward the sugar moiety. This study will provide insights into the exploration of probes for O-GlcNAc modification, as well as a better understanding of the roles of O-GlcNAc in cellular physiology.

Keywords: O-GlcNAcylation, O-GlcNAcase, sugar moiety, GlcNAc derivatives, substrate specificity

INTRODUCTION

Protein glycosylation is an important protein post-translational modification in various organisms and is critical for a wide range of biological processes. Defective or aberrant glycosylation can lead to serious cellular dysfunction or diseases in humans (Wells et al., 2001). O-GlcNAcylation is a single *N*-acetylglucosamine beta-linked to the serine or threonine residues of some nucleic acids and cytoplasmic proteins, and is essential for multiple cellular signaling cascades, including gene transcription, protein translation, cell cycle, and nutrient sensing (Chen et al., 2013; Ferrer et al., 2014; Hardiville and Hart, 2014). By affecting the stability, activity, or interactions of key signaling proteins, O-GlcNAcylation is a novel and vital factor in the cause of diseases such as diabetes, cancer, and neurodegeneration (Yuzwa et al., 2012; Yuzwa and Vocadlo, 2014; Zhu et al., 2014). Because of the importance of O-GlcNAc and its crucial role in disease pathology, the enzymes controlling O-GlcNAcylation levels are considered to be therapeutic targets.

O-GlcNAcylation is a dynamic reversible process, the addition and removal of GlcNAc residues from a protein is regulated by only two enzymes. Uridine diphosphate-*N*-acetyl-D-glucosamine: polypeptidyl transferase (OGT) is responsible for transferring a single GlcNAc from uridine diphosphate- α -*N*-acetyl-D-glucosamine (UDP-GlcNAc) to proteins. O-GlcNAcase (OGA) removes GlcNAc from glycoproteins. Substrate promiscuity of OGT and OGA has been shown to be valuable for enzymatic catalysis and O-GlcNAcylation level control. The substrate specificity

of human OGT (hOGT) has been widely investigated and the hOGT crystal structure has been solved (Lazarus et al., 2011). Among the 26 UDP-sugar derivatives, 4 (UDP-GlcNPr, UDP-6-deoxy-GlcNAc, UDP-4-deoxy-GlcNAc and UDP-6-deoxy-GalNAc) were reported to highly glycosylate peptides via sOGT-catalyzed glycosylation (Ma et al., 2013). For peptide acceptor recognition, 3 positions (−2, −1, and +2) in the peptide sequence are vital for O-GlcNAcylation, and uncharged amino acids are preferred and show high reactivity (Liu et al., 2014). Recently, several research groups solved the structure of hOGA and revealed that hOGA existed as an unusual arm-in-arm homodimer. The residues of hOGA on the cleft surface enabled broad interactions with peptide substrates, indicating the important role of the peptide structure in the recognition mode (Elsen et al., 2017; Li et al., 2017; Roth et al., 2017). However, partly because of the difficulties in obtaining glycopeptides with modified GlcNAc residues, structure determination during GlcNAc-recognition by hOGA remains unclear.

We previously evaluated chemoenzymatic synthesis and purified oligosaccharides and glycopeptides (Wen et al., 2016a,b; Wu et al., 2016; Wang et al., 2018). As an extension of these studies, glycopeptides containing different GlcNAc derivatives were successfully synthesized and purified. Further, we investigated the substrate specificity of hOGA and found that hOGA was less promiscuous in tolerating substrates with modified GlcNAc.

RESULTS

Synthesis of GlcNAc Derivatives

GlcNAc and GalNAc were purchased from *Carbosynth* (San Diego, CA, USA). GlcNPh, GlcNGc, GlcNTFA, and 6-N₃-GlcNAc were gifted from Dr. Xi Chen's lab (UC Davis, USA). 4-Deoxy-GlcNAc and GlcNAz were synthesized according to our previous report (Li et al., 2016). The other three new compounds, GlcNPr, 4-OMe-GlcNAc, and 6-deoxy-GlcNAc, were synthesized for the first time in this study (Figure 1). GlcNPr was generated in the presence of propionyl chloride

and pyridine after global deprotection. A convergent route was designed to synthesize 6-deo-GlcNAc and 4-OMe-GlcNAc; GlcNAc as the starting material was first protected with benzylidene and then subjected to 1,3-diacetylation to afford intermediate 5. Selective deprotection of benzylidene was carried out in the presence of NBS and calcium sulfate to afford 6. The desired target compound 8 was obtained after reduction of the bromide and full deacetylation. For 4-OMe-GlcNAc, benzylidene in 5 was removed and selective acetylation of the 6-OH freed the 4-OH, which was O-methylated in the presence of iodomethane and silver oxide. 11 was obtained after global deprotection.

Protein Expression and Purification

According to previous studies, we overexpressed *Bifidobacterium infantis* N-acetylhexosamine 1-kinase ATCC#15697 (BiNahK), human UDP-N-acetylglactosamine pyrophosphorylase (hAGX1), human OGT (ncOGT), and human OGA (hOGA) in *Escherichia coli* (Gross et al., 2005; Guan et al., 2010; Li et al., 2011, 2012). Enzymes were expressed by induction with 1 mM of isopropyl 1-thio-β-D-galactopyranoside followed by incubation at 16°C for 24 h with vigorous shaking (200 rpm). After purification, 15 mg ncOGT, 20 mg hOGA, 40 mg BiNahK, and 20 mg hAGX1 were obtained from 1 L of an *E. coli* culture. As shown in Figure S1, enzymes with an N-terminal His₆ tag showed 80% purity with a high yield. The apparent molecular weights of the enzymes according to SDS-PAGE were well-correlated with the calculated molecular weights of each protein.

Production of Glycopeptides and Determination of Substrate Specificity of OGT

UDP-GlcNPh, UDP-GlcNGc, UDP-GlcNTFA, and UDP-6-N₃-GlcNAc were synthesized as reported previously (Chen et al., 2011). Other sugar nucleotides were obtained through a chemoenzymatic strategy by chemical synthesis of GlcNAc derivatives, which were used as the substrates in a one-pot two-enzyme system containing BiNahK and hAGX1 (Figure 2A).

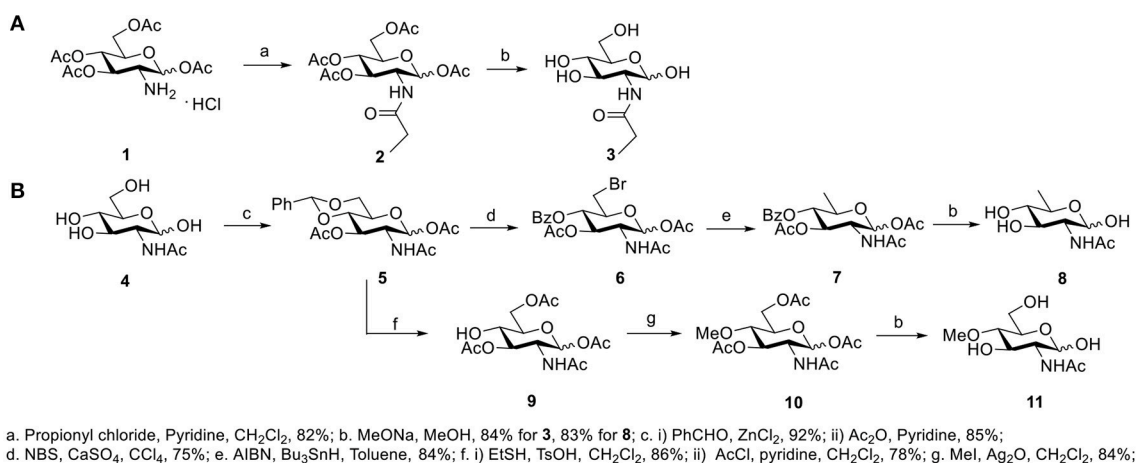


FIGURE 1 | Synthetic methods of compounds: (A) GlcNPr, (B) 4-OMe-GlcNAc, and 6-deoxy-GlcNAc.

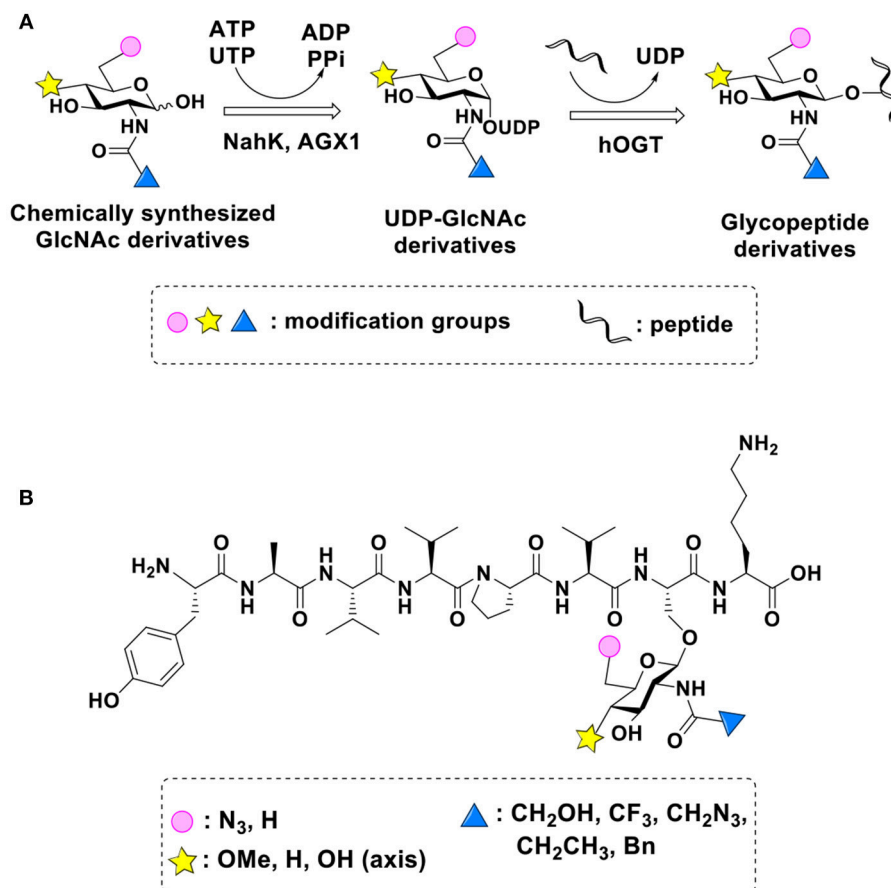


FIGURE 2 | (A) Production of glycopeptides by hOGT-catalyzed reaction using chemoenzymatically synthesized UDP-GlcNAc derivatives. **(B)** The structures of glycopeptide derivatives used in the study.

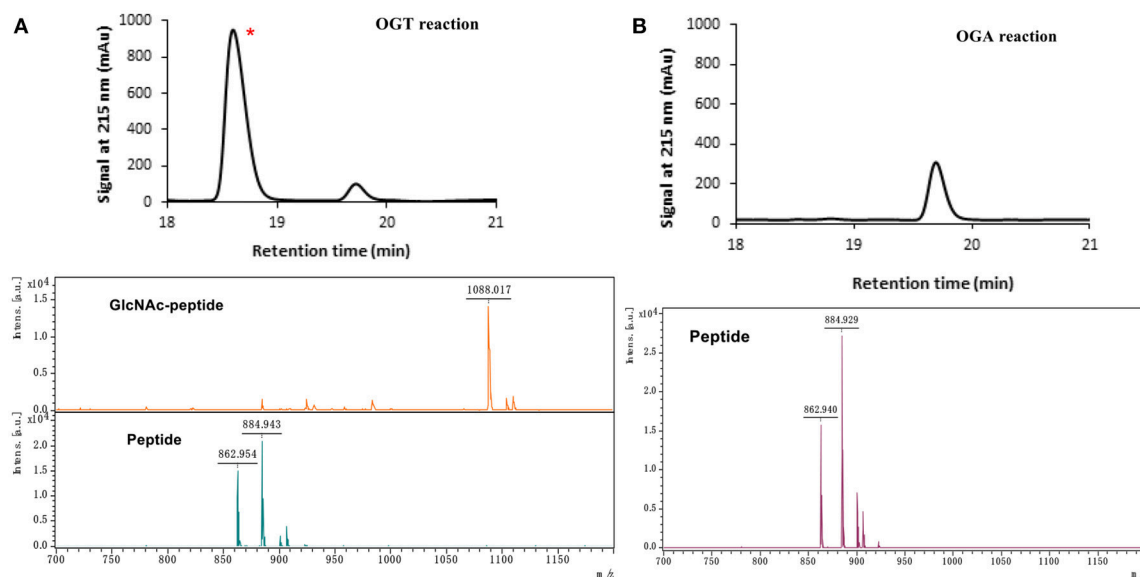
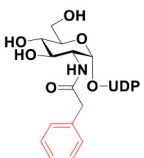
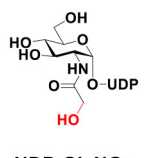
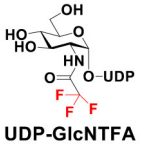
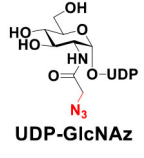
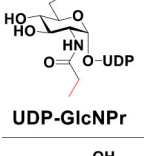
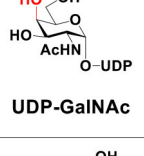
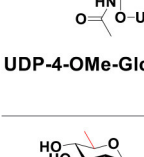
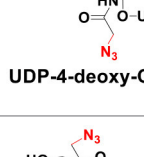
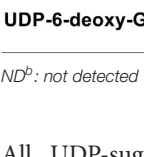
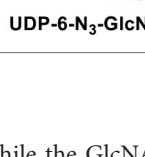


FIGURE 3 | The HPLC and MALDI-TOF profile for OGT **(A)** and OGA **(B)** reactions toward UDP-GlcNAc substrates. * represents the glycopeptide peak.

TABLE 1 | The yields of OGT and OGA reactions.

| UDP-GlcNAc derivatives | Glycopeptid yield(%) | OGA hydrolysis yield(%) | UDP-GlcNAc derivatives | Glycopeptide yield (%) | OGA hydrolysis yield (%) |
|---|----------------------|-------------------------|---|------------------------|--------------------------|
|  UDP-GlcNPh | 78.5 ± 1.2 | ND ^b |  UDP-GlcNGc | 56.0 ± 0.9 | 5.4 ± 0.3 |
|  UDP-GlcNTFA | 81.2 ± 1.1 | 3.0 ± 0.8 |  UDP-GlcNAz | 92.6 ± 3.2 | 96.3 ± 1.6 |
|  UDP-GlcNPr | 49.1 ± 2.5 | ND ^b |  UDP-GalNAc | 58.9 ± 0.4 | 47 ± 0.6 |
|  UDP-4-OMe-GlcNAc | 58.5 ± 1.1 | ND ^b |  UDP-4-deoxy-GlcNAz | 99.4 ± 0.8 | ND ^b |
|  UDP-6-deoxy-GlcNAc | 63.1 ± 0.9 | ND ^b |  UDP-6-N ₃ -GlcNAc | 23.8 ± 1.2 | 62.2 ± 2.4 |

ND^b: not detected

All UDP-sugars produced were characterized by capillary electrophoresis and matrix-assisted laser desorption/ionization (MALDI)-time-of-flight mass spectrometry (**Figure S3**).

The peptide substrate (YAVVPVSK) was synthesized based on the Fmoc-strategy using a Liberty Blue Peptide Synthesizer and purified by high-performance liquid chromatography (HPLC) (Liu et al., 2014) (**Figure S4**). A set of glycopeptides carrying modifications on the GlcNAc residue were subsequently prepared in a recombinant full-length hOGT-catalyzed reaction using chemoenzymatically synthesized UDP-GlcNAc derivatives (**Figure 2A**). The hOGT enzyme reactions were carried out at 37°C for 2 h in a volume of 100 µL containing 1 mM peptide, 3 mM UDP-GlcNAc analogs, and 50 µg ncOGT in buffer (50 mM Tris-HCl, pH 7.5, 10 mM Mg²⁺). The reaction was boiled, and the products were subjected to HPLC purification and yield quantification (**Table 1**). Each peak was collected and identified based on MALDI. For example, GlcNAc showed a peak at 18.6 min and was characterized as GlcNAc-peptide with $m/z = 1088.017$, while the peak at 19.7 min was characterized as a peptide with $m/z = 862.954$ (M+H) and 884.943 (M+Na) (**Figure 3A**). The retention time of the pure peptide was 19.7 min,

while the GlcNAc-peptide showed a retention time of 18.6 min because of the increased polarity of GlcNAc (**Figure 3A**). Moreover, the OGT reaction efficiency was calculated as the glycopeptide yield ($Y_a\%$). The yield was calculated with the formula $Y_a = S1/(S1+S2)$, where S1 and S2 are the integrated areas of the glycopeptide and peptide peaks, respectively (**Table 1**). The HPLC profile of the OGT and OGA reaction on the peptide are detailed in the Supporting Materials (**Figure S2**).

By utilizing this method, 10 glycopeptide derivatives (5 glycopeptides with C2-modified GlcNAc, 3 glycopeptides with C4-modified GlcNAc, and 2 glycopeptides with C6-modified GlcNAc) were produced (**Figure 2B**), purified by HPLC, and characterized by MALDI (**Figure S5**). All UDP-GlcNAc derivatives were good substrates for hOGT except for UDP-6-N₃-GlcNAc, which resulted in only 23.8% yield *in vitro* (**Table 1**). Notably, hOGT was the full-length isoform with 13.5 tetratricopeptide repeats (TPRs), which showed higher activity than sOGT (short OGT with 2.5 TPRs). For example, when sOGT was used, six UDP-GlcNAc derivatives (UDP-GlcNGc, UDP-GlcNAz, UDP-GlcNTFA, UDP-GlcNPh, UDP-6-N₃-GlcNAc, and UDP-GalNAc) used as the substrates

produced <1% yield (Ma et al., 2013). In comparison, over 49% yield was obtained when full-length hOGT was used. The crystal structures of the N-terminal domain of full-length hOGT containing the first 11.5 TPRs, showed that the conserved asparagine residues in the TPR domain directly contacted the substrates, supporting the role of the TRP domains in initial recognition and substrate specificity determination (Jinek et al., 2004). In summary, in addition to preparing glycopeptides, we found that full-length hOGT is a more efficient catalyst than the previously reported short sOGT.

OGA Substrate Specificity Assay

The glycopeptide peaks from OGT reactions were collected and lyophilized for the hOGA substrate specificity assay. The hOGA reaction was conducted overnight in a volume of 100 μ L containing the glycopeptides, $MgCl_2$ (20 mM), Tris-HCl (200 mM), and recombinant hOGA (0.1 mg). The reaction mixture was boiled and centrifuged before HPLC separation. Each peak was collected and characterized by MALDI. When the GlcNAc-peptide was treated with hOGA, efficient hydrolysis activity of hOGA and a single peptide peak were observed (Figure 3B). The hOGA hydrolysis yield (Y_b %) was calculated using the formula $Y_b = S2/(S1+S2)$, where S1 and S2 are the integrated areas of the glycopeptide and peptide peaks, respectively. The HPLC profiles of the OGT and OGA reaction on the peptide are described in detail in the Supporting Materials (Figure S2). The GlcNAz-peptide and 6-N₃-GlcNAc-peptide were well-tolerated by hOGA, and other glycopeptide derivatives significantly decreased the efficiency of hOGA, showing <10% hydrolysis yield (Table 1). The results revealed that hOGA had a relatively strict recognition for the sugar moiety in the glycopeptides, thus exhibiting limited activities for glycopeptide derivatives with C2, C4, and C6 modifications on GlcNAc.

CONCLUSION

Glycopeptides containing different GlcNAc derivatives were successfully synthesized in a recombinant full-length hOGT-catalyzed reaction, using chemoenzymatically synthesized UDP-GlcNAc derivatives. We also found that full-length hOGT is a more efficient catalyst than sOGT, as over a 49-fold yield was observed when hOGT was used. The resulting

glycopeptides were used to investigate the substrate specificity of hOGA toward the sugar moiety. hOGA was less promiscuous in tolerating glycopeptide substrates with modified GlcNAc, and changes in the C2, C4, and C6 positions of GlcNAc partially affected its recognition. Interestingly, OGT and OGA possessed different levels of tolerance to the same sugar moiety, such as GlcNPh, GlcNTFA, and 4-OMe-GlcNAc. Therefore, the acquired GlcNAc derivatives, which were well-recognized by OGT but not hydrolyzed by OGA, may increase the O-GlcNAcylation level *in vivo* when the peracetylated compound is metabolically incorporated. Indeed, our group developed an OGA-resistant probe, peracetylated 4-deoxy-N-azidoacetylglucosamine (Ac₃-4-deoxy-GlcNAz), which can be used as a potent tool for O-GlcNAcylation detection and the identification of O-GlcNAcylated proteins (Li et al., 2016). Thus, OGA-resistant GlcNAc substrates show potential as excellent probes for investigating O-GlcNAcylation and elucidating their importance in cellular events.

AUTHOR CONTRIBUTIONS

SL and JW conducted the experiments and wrote the manuscript. LZ, JG, HZ, JZ, YC, YL, and XC conducted the experiments and the sample analysis. XC and LW contributed to the manuscript revision. PW and JL designed and managed the study.

ACKNOWLEDGMENTS

We thank S. Walker from Harvard Medical School for providing the plasmid pET24b-ncOGT. We acknowledge J. Jiang for her suggestions to this project and financial support from the Molecular Basis of Disease program in Georgia State University as well as grants from the Natural Science Foundation of China (NO. 31000371), Natural Science Foundation of Tianjin (15JCYBJC29000), and Key scientific research projects of universities in Henan (19B15003).

SUPPLEMENTARY MATERIAL

The Supplementary Material for this article can be found online at: <https://www.frontiersin.org/articles/10.3389/fchem.2018.00646/full#supplementary-material>

REFERENCES

- Chen, Q., Chen, Y., Bian, C., Fujiki, R., and Yu, X. (2013). TET2 promotes histone O-GlcNAcylation during gene transcription. *Nature* 493, 561–564. doi: 10.1038/nature11742
- Chen, Y., Thon, V., Li, Y., Yu, H., Ding, L., Lau, K., et al. (2011). One-pot three-enzyme synthesis of UDP-GlcNAc derivatives. *Chem. Commun.* 47, 10815–10817. doi: 10.1039/c1cc14034e
- Elsen, N. L., Patel, S. B., Ford, R. E., Hall, D. L., Hess, F., Kandula, H., et al. (2017). Insights into activity and inhibition from the crystal structure of human O-GlcNAcase. *Nat. Chem. Biol.* 13, 613–615. doi: 10.1038/nchembio.2357
- Ferrer, C. M., Lynch, T. P., Sodi, V. L., Falcone, J. N., Schwab, L. P., Peacock, D. L., et al. (2014). O-GlcNAcylation regulates cancer metabolism and survival stress signaling via regulation of the HIF-1 pathway. *Mol. Cell.* 54, 820–831. doi: 10.1016/j.molcel.2014.04.026
- Gross, B. J., Kraybill, B. C., and Walker, S. (2005). Discovery of O-GlcNAc transferase inhibitors. *J. Am. Chem. Soc.* 127, 14588–14589. doi: 10.1021/ja0555217
- Guan, W., Cai, L., and Wang, P. G. (2010). Highly efficient synthesis of UDP-GalNAc/GlcNAc analogues with promiscuous recombinant human UDP-GalNAc pyrophosphorylase AGX1. *Chemistry* 16, 13343–13345. doi: 10.1002/chem.201002315
- Hardville, S., and Hart, G. W. (2014). Nutrient regulation of signaling, transcription, and cell physiology by O-GlcNAcylation. *Cell Metab.* 20, 208–213. doi: 10.1016/j.cmet.2014.07.014
- Jinek, M., Rehwinkel, J., Lazarus, B. D., Izaurralde, E., Hanover, J. A., and Conti, E. (2004). The superhelical TPR-repeat domain of O-linked GlcNAc transferase

- exhibits structural similarities to importin alpha. *Nat. Struct. Mol. Biol.* 11, 1001–1007. doi: 10.1038/nsmb833
- Lazarus, M. B., Nam, Y., Jiang, J., Sliz, P., and Walker, S. (2011). Structure of human O-GlcNAc transferase and its complex with a peptide substrate. *Nature* 469, 564–567. doi: 10.1038/nature09638
- Li, B., Li, H., Lu, L., and Jiang, J. (2017). Structures of human O-GlcNAcase and its complexes reveal a new substrate recognition mode. *Nat. Struct. Mol. Biol.* 24, 362–369. doi: 10.1038/nsmb.3390
- Li, J., Li, Z., Li, T., Lin, L., Zhang, Y., Guo, L., et al. (2012). Identification of a specific inhibitor of nOGA - a caspase-3 cleaved O-GlcNAcase variant during apoptosis. *Biochemistry* 77, 194–200. doi: 10.1134/S0006297912020113
- Li, J., Wang, J., Wen, L., Zhu, H., Li, S., Huang, K., et al. (2016). An OGA-resistant probe allows specific visualization and accurate identification of O-GlcNAc-modified proteins in cells. *ACS Chem. Biol.* 11, 3002–3006. doi: 10.1021/acschembio.6b00678
- Li, Y., Yu, H., Chen, Y., Lau, K., Cai, L., Cao, H., et al. (2011). Substrate promiscuity of N-acetylhexosamine 1-kinases. *Molecules* 16, 6396–6407. doi: 10.3390/molecules16086396
- Liu, X., Li, L., Wang, Y., Yan, H., Ma, X., Wang, P. G., et al. (2014). A peptide panel investigation reveals the acceptor specificity of O-GlcNAc transferase. *FASEB J.* 28, 3362–3372. doi: 10.1096/fj.13-246850
- Ma, X., Liu, P., Yan, H., Sun, H., Liu, X., Zhou, F., et al. (2013). Substrate specificity provides insights into the sugar donor recognition mechanism of O-GlcNAc transferase (OGT). *PLoS ONE* 8:e63452. doi: 10.1371/journal.pone.0063452
- Roth, C., Chan, S., Offen, W. A., Hemsworth, G. R., Willems, L. I., King, D. T., et al. (2017). Structural and functional insight into human O-GlcNAcase. *Nat. Chem. Biol.* 13, 610–612. doi: 10.1038/nchembio.2358
- Wang, J., Greenway, H., Li, S., Wei, M., Polizzi, S. J., and Wang, P. G. (2018). Facile and stereo-selective synthesis of UDP-alpha-D-xylose and UDP-beta-L-arabinose using UDP-Sugar pyrophosphorylase. *Front. Chem.* 6:163. doi: 10.3389/fchem.2018.00163
- Wells, L., Vosseller, K., and Hart, G. W. (2001). Glycosylation of nucleocytoplasmic proteins: signal transduction and O-GlcNAc. *Science* 291, 2376–2378. doi: 10.1126/science.1058714
- Wen, L., Zang, L., Huang, K., Li, S., Wang, R., and Wang, P. G. (2016a). Efficient enzymatic synthesis of L-rhamnulose and L-fuculose. *Bioorg. Med. Chem. Lett.* 26, 969–972. doi: 10.1016/j.bmcl.2015.12.051
- Wen, L., Zheng, Y., Jiang, K., Zhang, M., Kondengaden, S. M., Li, S., et al. (2016b). Two-step chemoenzymatic detection of N-Acetylneuraminic Acid-alpha(2-3)-Galactose glycans. *J. Am. Chem. Soc.* 138, 11473–11476. doi: 10.1021/jacs.6b07132
- Wu, Z., Jiang, K., Zhu, H., Ma, C., Yu, Z., Li, L., et al. (2016). Site-directed glycosylation of peptide/protein with homogeneous O-linked eukaryotic N-Glycans. *Bioconjug. Chem.* 27, 1972–1975. doi: 10.1021/acs.bioconjchem.6b00385
- Yuzwa, S. A., Shan, X., Macauley, M. S., Clark, T., Skorobogatko, Y., Vosseller, K., et al. (2012). Increasing O-GlcNAc slows neurodegeneration and stabilizes tau against aggregation. *Nat. Chem. Biol.* 8, 393–399. doi: 10.1038/nchembio.797
- Yuzwa, S. A., and Vocadlo, D. J. (2014). O-GlcNAc and neurodegeneration: biochemical mechanisms and potential roles in Alzheimer's disease and beyond. *Chem. Soc. Rev.* 43, 6839–6858. doi: 10.1039/c4cs00038b
- Zhu, Y., Shan, X., Yuzwa, S. A., and Vocadlo, D. J. (2014). The emerging link between O-GlcNAc and Alzheimer disease. *J. Biol. Chem.* 289, 34472–34481. doi: 10.1074/jbc.R114.601351

Conflict of Interest Statement: The authors declare that the research was conducted in the absence of any commercial or financial relationships that could be construed as a potential conflict of interest.

Copyright © 2019 Li, Wang, Zang, Zhu, Guo, Zhang, Wen, Chen, Li, Chen, Wang and Li. This is an open-access article distributed under the terms of the Creative Commons Attribution License (CC BY). The use, distribution or reproduction in other forums is permitted, provided the original author(s) and the copyright owner(s) are credited and that the original publication in this journal is cited, in accordance with accepted academic practice. No use, distribution or reproduction is permitted which does not comply with these terms.



Reassessing the Host Defense Peptide Landscape

Evan F. Haney¹, Suzana K. Straus² and Robert E. W. Hancock^{1*}

¹ Centre for Microbial Diseases and Immunity Research, University of British Columbia, Vancouver, BC, Canada,

² Department of Chemistry, University of British Columbia, Vancouver, BC, Canada

Current research has demonstrated that small cationic amphipathic peptides have strong potential not only as antimicrobials, but also as antibiofilm agents, immune modulators, and anti-inflammatories. Although traditionally termed antimicrobial peptides (AMPs) these additional roles have prompted a shift in terminology to use the broader term host defense peptides (HDPs) to capture the multi-functional nature of these molecules. In this review, we critically examined the role of AMPs and HDPs in infectious diseases and inflammation. It is generally accepted that HDPs are multi-faceted mediators of a wide range of biological processes, with individual activities dependent on their polypeptide sequence. In this context, we explore the concept of chemical space as it applies to HDPs and hypothesize that the various functions and activities of this class of molecule exist on independent but overlapping activity landscapes. Finally, we outline several emerging functions and roles of HDPs and highlight how an improved understanding of these processes can potentially be leveraged to more fully realize the therapeutic promise of HDPs.

Keywords: antimicrobial peptide, antibiofilm peptide, host defense peptide, chemical space, peptide therapeutics

OPEN ACCESS

Edited by:

Laszlo Otvos,
Olpe LLC, United States

Reviewed by:

Ralf Hoffmann,
Leipzig University, Germany
Maria Luisa Mangoni,
Sapienza University of Rome, Italy

*Correspondence:

Robert E. W. Hancock
bob@hancocklab.com

Specialty section:

This article was submitted to
Chemical Biology,
a section of the journal
Frontiers in Chemistry

Received: 08 November 2018

Accepted: 15 January 2019

Published: 04 February 2019

Citation:

Haney EF, Straus SK and
Hancock REW (2019) Reassessing the
Host Defense Peptide Landscape.
Front. Chem. 7:43.
doi: 10.3389/fchem.2019.00043

INTRODUCTION

Driven by the emergence of antibiotic resistance throughout the world and a dearth of antimicrobials in the drug development pipeline, we are on the precipice of returning to a pre-antibiotic age (Martens and Demain, 2017). Since their discovery in the 1980s, antimicrobial peptides (AMPs), naturally occurring polypeptide sequences (~12–50 residues) comprised of cationic and hydrophobic amino acids with direct antibacterial activity (Hancock and Sahl, 2006; Nguyen et al., 2011; Fjell et al., 2012), have long been touted as one solution to this impending medical crisis. Statements such as “promising alternative to antibiotics,” “potential to address to growing problem of antibiotic resistance” and “hold promise to be developed as novel antibiotics” appear in almost every research article describing novel AMP sequences. In fact, the vast majority of studies related to AMPs have sought to identify and characterize peptides with potent and broad spectrum antimicrobial properties. Common strategies involve searching for novel peptides from natural sources either through the analysis of increasingly-exotic biological organisms and tissue extracts (Kim et al., 2018), identifying potential AMP sequences from genomic sequence information (Rodríguez-Decuadro et al., 2018; Yang et al., 2018), or excising predicted antimicrobial sequences from larger proteins (Pane et al., 2016; Abdillahi et al., 2018). Furthermore, a large portion of the relevant scientific literature is devoted to studies aimed at selectively enhancing the antibacterial potency of synthetic peptides either by systematically altering the amino acid composition of natural AMPs (Akbari et al., 2018; Chen et al., 2018) or designing

novel sequences based on the structural and biophysical properties of known AMPs (Haney and Hancock, 2013; Kumar et al., 2018). Indeed, the prospect of finding a peptide with broad spectrum antimicrobial activity toward antibiotic resistant pathogens that plague human populations is a worthy endeavor that has captured the imagination and resources of many scientific research groups worldwide.

In spite of their tremendous promise, no peptide-based antibiotic has to-date realized regulatory approval (although several are in advanced clinical trials). There are many potential reasons for this apparent lack of success in developing this class of molecules as medicines, including low stability, toxicity, and high cost-of-goods (Haney and Hancock, 2013). However, it may be that we have already achieved the limits of antimicrobial potency for AMPs, through either natural selection by evolutionary processes or rational design, and that AMPs may never be able to achieve the same clinical outcomes as conventional antibiotics. Even more troubling is the possibility that the direct antibacterial effects of AMPs may not represent the primary biological functions of these molecules in nature and that researchers could be spending considerable effort searching for an elusive “optimal” AMP sequence that may not exist. For instance, it is well-established that the direct antibacterial activity of most AMPs is dramatically reduced under physiological conditions that would be encountered *in vivo* (Goldman et al., 1997; Bowdish et al., 2005; Starr et al., 2016). Consequently, it may be that the *in vitro* screening procedures employed to date do not effectively capture the true potential of this class of molecule since a growing amount of *in vivo* data has demonstrated the efficacy of AMPs in various animal models related to infection and inflammation, further underscoring their tremendous clinical potential. Indeed, over that past decade or so, we have begun to appreciate the other biological functions that can be inherent to amphipathic cationic peptides. These include such activities as immune modulation, including anti-infective (e.g., immune cell recruitment), anti-inflammatory, and wound healing properties, as well as antibiofilm activity. To emphasize the multifaceted nature of these cationic polypeptides, the term “Host Defense Peptide” (HDP) (Nijnik and Hancock, 2009; Takahashi et al., 2010) is now more commonly used to encompass the breadth of biological processes that are influenced by these versatile biomolecules, although the terms AMP and antibiofilm peptides are still accurate when considering only activities against planktonic and biofilm cells, respectively.

Our goal in this review is to question some of the most tightly held beliefs regarding the natural roles and functional potentials of AMPs and HDPs. We begin by critically examining the purported mechanism of action of AMPs as directly targeting the membrane of bacterial cells and highlight some of the advances that have helped many push beyond simplified models of antimicrobial activity. We then argue the need to shift the paradigm from appreciating these molecules as direct acting antibacterial compounds toward multi-faceted mediators of a wide range of biological processes. In particular, we explore the concept of chemical space (all possible polypeptide sequences of a given length) in the context of HDPs and postulate that the activity landscapes related to each biological function of HDPs

are distinct, but overlapping. Finally, we outline several emerging roles of HDPs in relation to health and disease and highlight some of the new and exciting work being done to fully realize the therapeutic promise of HDPs.

MECHANISM OF AMPs ACTIVITY—A COMPLEX QUESTION

For many years now, AMPs have largely been investigated in the context of their ability to kill bacteria by disrupting membranes ultimately leading to cell lysis and death (Hancock and Sahl, 2006; Zasloff, 2009; Kumar et al., 2018; Lázár et al., 2018). Experts in the field have often discussed at length the exact nature of the membrane perturbation, i.e., whether the peptides kill bacteria through transmembrane pore (Rapaport and Shai, 1991; Matsuzaki et al., 1998) or non-pore (Shai, 2002; Yeaman and Yount, 2003; Lee et al., 2016) mechanisms. Alternatively, the effect of bilayer integrity may be compromised upon reaching a certain threshold peptide concentration at the membrane surface (Andersson et al., 2016; Epand et al., 2016). The main models presented include the barrel-stave, carpet, detergent, toroidal pore, aggregate (Hale and Hancock, 2007), and electroporation (Lee et al., 2016) models, or combinations thereof (Kumar et al., 2018), and these have been extensively discussed in other reviews. Many detailed studies have relied on the use of a handful of biophysical methods to determine how these peptides perturb membranes (Okada and Natori, 1983; Zasloff, 1987; Lehrer et al., 1989; Arias et al., 2018; Marquette and Bechinger, 2018). Aspects considered in these studies include the structure of the peptide in the membrane, the insertion and interaction of the peptide into model lipid bilayers, lipid selectivity and/or ability to cause leakage. While all of these observations are valid within the context of the experimental setup, in the following section, we will examine how these findings may not be relevant to how HDPs actually kill bacteria outside of a culture tube. This is particularly relevant for AMPs that lack membranolytic activity. Specifically, we critically examine several mechanistic principles that are often generalized for AMPs and discuss how researchers have begun to unravel varied and complex mechanisms of action for this class of peptides.

Does the Electrostatic Attraction Between AMPs and Membranes Dictate Activity?

Most antimicrobial peptides are cationic and amphipathic with a net charge ranging from +2 to +9, due to an abundance of Arg and Lys residues within their sequence (Haney and Hancock, 2013). Given that the bacterial cytoplasmic membrane contains a high proportion of phospholipids with negatively charged headgroups [e.g., phosphatidylglycerol (PG) and cardiolipin (CL)], the initial interaction between a peptide and a bacterial cell is generally considered to be electrostatic in nature followed by an association of the hydrophobic domains of AMPs with the hydrophobic core of membranes. In reality, the path between a cationic peptide and the anionic cytoplasmic membrane is fraught with potential peptide binding targets and littered with

bacterial cell surface components that necessitate this process should be more than a simple electrostatic interaction.

For instance, Gram-negative bacteria possess an outer membrane which acts as a selective barrier and protects the cell from the action of various antibiotics. Furthermore, lipopolysaccharides (LPS) are present in high abundance on the surface of the outer membrane of Gram-negative bacteria. LPS molecules bear multiple negative charges that are typically neutralized by the presence of divalent cations (e.g., Mg^{2+} and Ca^{2+}) which in turn stabilize the outer membrane (Vaara, 1992). LPS offers an electrostatic and hydrophobic binding partner for approaching cationic amphipathic peptides (which have a higher affinity for LPS than the native divalent cations) and upon membrane binding, the peptides competitively displace the divalent cations which subsequently interferes with lipid packing and leads to increased permeability of the outer membrane thereby mediating their so-called self-promoted uptake (Hancock, 2001). Beyond this, it is unclear what the driving force is that allows peptides to transition from the Gram-negative outer membrane to the surface of the cytoplasmic membrane and beyond. Conceivably, this could involve some combination of peptide concentration gradients, Donnan potentials (created by the presence of polyanionic membrane-derived oligosaccharides in the bacterial periplasm) or the electrical potential gradient across the cytoplasmic membrane (Nikaïdo, 2003).

In Gram-positive bacteria, a thick layer of peptidoglycan surrounds the bacterial cell and provides structural support. An AMP should transit quite freely through the netlike structure of a Gram-positive cell wall to interact with the cytoplasmic membrane (Vollmer and Bertsche, 2008). However, while peptidoglycan itself lacks an explicit negative charge, teichoic acid, and lipoteichoic acids can be found interspersed throughout the peptidoglycan structure and confer a surface negative charge. These anionic molecules also provide binding sites for HDPs (Scott et al., 1999a), and these would presumably need to be circumvented to reach the cytoplasmic membrane.

Since the electrostatic attraction between a cationic AMP and the anionic bacterial cell surface is considered essential to the overall mechanism of action, several studies have examined how charge relates to activity (Dathe et al., 2001; Mihajlovic and Lazaridis, 2012) and whether this property could be manipulated to improve antibacterial potency and selectivity for bacterial cells. Results from these studies suggest that there is an optimal charge/hydrophobicity balance needed to ensure equilibrium between activity and toxicity. For example, increasing the charge of magainin 2 from +3 to +5 improved the antibacterial activity against both Gram-positive and Gram-negative bacteria, but an increase to +6 or +7 led to increased hemolytic activity and loss of antimicrobial potency (Dathe et al., 2001). It has been suggested that the loss of activity in highly cationic peptides may be due to the fact that this would result in an extremely strong interaction between the peptide and the anionic phospholipid headgroups that would prevent translocation of the peptide into the inner leaflet of the membrane (Yeaman and Yount, 2003). Alternatively, the increased charge may perturb the kinetic network, i.e., the careful balance between

peptide-bacteria interactions vs. peptide-host cell interactions (Starr et al., 2016).

In addition to overall charge on a peptide surface, the specific location of the charged residues (and by extension the hydrophobic residues) along the length of a peptide has a significant influence on antibacterial potency and toxicity (Hilpert et al., 2006; Leptihn et al., 2010; Archer et al., 2011; Yin et al., 2012; Hollmann et al., 2016). The fact that even a single amino acid change within an AMP sequence can dramatically alter the antibacterial and/or toxicity profile of a peptide would suggest that the influence of biophysical parameters such as charge and hydrophobicity are important within the context of the AMP sequence in question. Therefore, sequence manipulations aimed at improving potency may be difficult to apply broadly to all AMPs in general.

Finally, another indication that positive charge may not play the defining role in determining AMP potency is the fact that several anionic antimicrobial peptides have also been reported in the literature (Harris et al., 2009) and many of these adopt amphipathic structures and can interact with membranes, akin to the interactions that have been observed for cationic AMPs.

Do All Antimicrobial Peptides Act to Destroy Bacterial Membranes?

Since AMPs are known to interact with phospholipid bilayers, it was originally claimed that all AMPs act as membrane disrupters in keeping with early studies that demonstrated that AMPs permeabilized membranes, e.g., of vesicles. However, most of those studies relied on data obtained at concentrations far above the minimal inhibitory concentration (MIC), or under artificial assay conditions using model membranes and very high peptide:lipid ratios relative to the conditions that would occur during killing of bacterial cells (Wu et al., 1999; Wimley, 2010).

While it is true that AMPs must interact with bacterial membranes as part of their overall mechanism of action, this dogma of membrane targeting leading to lysis or cytoplasmic leakage has now been effectively refuted as summarized previously (Hancock and Sahl, 2006; Fjell et al., 2012). Indeed it is now well-understood that in addition to membrane interactions, many AMPs act on membrane-associated targets (e.g., cell wall biosynthesis, cell division, etc.) or on cytoplasmic targets (e.g., macromolecular synthesis in cells, heat shock proteins, etc.; Otvos, 2005; Hale and Hancock, 2007; Fjell et al., 2012). One of the earliest examples of this phenomenon was buforin II, a histone derived AMP from Asian toads (Park et al., 1998). Interestingly, *E. coli* cells treated with buforin II were not lysed, even at 5X the MIC, and this peptide did not perturb model membranes, clearly demonstrating that membrane perturbation does not contribute to the bactericidal effect. Instead, it was demonstrated that this peptide translocated into the bacterial cytoplasm where it readily bound DNA and RNA, implicating this interaction in the mechanism of action (Park et al., 1998). Subsequently, Wu et al. described a broad range of peptides that did not completely depolarize bacterial cells at their MIC (Wu et al., 1999). Alternatively, human α -defensin 5 has been shown to translocate into the cytoplasm of *E. coli* where it accumulates at

the cell division plate and at opposite poles of the cell, suggesting that part of the antibacterial mechanism of this AMP is due to interference with cellular division processes (Chileveru et al., 2015). Cell division targeting through QueE was also recently shown for peptide C18G, a synthetic AMP derived from platelet factor IV (Yadavalli et al., 2016). Other peptides interfere with membrane associated processes, such as binding to lipid II which is involved in cell wall and teichoic acid biosynthesis, thereby inhibiting cell wall biogenesis (Wiedemann et al., 2001; Sass et al., 2010; Schneider et al., 2010). Several more examples of AMPs that target intracellular bacterial components exist, including: PR-39 (Boman et al., 1993), indolicidin (Subbalakshmi and Sitaram, 1998), pyrrhocoricin (Kragol et al., 2001; Taniguchi et al., 2016), human β -defensin 4 (Sharma and Nagaraj, 2015), proline-rich AMPs (Scocchi et al., 2011; Li et al., 2014; Florin et al., 2017), and many others (Hale and Hancock, 2007; Shah et al., 2016).

Indeed it has been proposed that AMPs are likely to have multiple modes of action, a feature that has earned them the moniker of “dirty drugs” (Friedrich et al., 2001; Hancock and Sahl, 2006). Adding to this complexity, it has been proposed that individual AMPs elicit a unique bacterial response which was demonstrated by challenging *E. coli* with four physico-chemically related peptides: magainin 2, pleurocidin, buforin II, and a synthetic D-amino acid peptide D-LAK120-AP13 (Kozłowska et al., 2014). In this case, treatment of *E. coli* with sub-lethal concentrations of each peptide caused both metabolic and gene expression changes that were unique to each peptide, suggesting that every AMP employs a unique mechanism of action to exert their antibacterial effects. Several other studies have demonstrated that AMP treatment causes substantial changes to overall gene expression profiles (Bader et al., 2003; Tomasinsig et al., 2004; Overhage et al., 2008; Majchrzykiewicz et al., 2010; Le et al., 2016; Nagarajan et al., 2018), further demonstrating the complexity of the bacterial response to natural and synthetic AMPs.

As stated above, interactions between AMPs and biological membranes occur and these interactions play a key role in the overall mechanism of action for this class of molecules. It seems possible that some AMPs, like magainin (Matsuzaki, 1998) and/or melittin (van den Bogaart et al., 2008), exert their primary antibacterial (and/or cytotoxic) effects through a lytic mechanism of action. However, applying the concept of membrane disruption to all AMPs is likely an oversimplification of a complex and dynamic process. As work continues in the field of AMP research it will be necessary to press beyond these simplified models that are often invoked to explain the mechanistic details underpinning the biological functions of AMPs.

Do AMPs Adopt a Specific “Active” Conformation?

Another frequently-characterized feature of AMPs is their ability to fold into a variety of secondary structures including α -helices, β -structures, turns, extended structures and other permutations (Nguyen et al., 2011). It is generally accepted that most linear AMPs are unstructured in aqueous solutions

and undergo a conformational change to a folded state as they bind and insert into biological membranes. Since this membrane interaction is required for the antibacterial effects of AMPs (even if the target is intracellular, the peptide must cross bacterial membranes), in the past it was considered that this membrane bound structure represented the “active” conformation. Much has been written about peptide interactions with membranes, with some authors suggesting formal channels (barrel-stave, toroidal pore models) while others have suggested more casual interactions (carpet, detergent, and aggregate model; Lee et al., 2016). However, considering the above-described diversity of mechanisms, ultimately the most satisfying models would describe how some peptides are able to translocate across membranes without lethally permeabilizing them. This is a known feature of immunomodulatory HDPs that must translocate into cells to mediate their activities (Lau et al., 2005; Mookherjee et al., 2009) and such peptides fall into the general class of cell penetrating peptides (Sandgren et al., 2004; Zorko and Langel, 2005; Guidotti et al., 2017). That AMPs do the same is suggested by demonstrations that some peptides can accumulate in the cytoplasm of bacteria (Park et al., 1998; Powers et al., 2006) or are readily taken up by eukaryotic cells (Tomasinsig et al., 2006).

Moreover, several studies have examined how AMP sequences correlate to peptide structure and how this may be related to antibacterial potency. For instance, aurein 2.2 and 2.3 are natural cationic AMPs from the frog *Litoria aurea* (Rozek et al., 2000). They are both 16 amino acid residues in length, have a net +2 charge, and an amidated C-terminus. Circular dichroism and NMR studies have shown that both peptides adopt a continuous α -helical structure in a membrane or membrane-mimetic environment (Pan et al., 2007; Cheng et al., 2009, 2010, 2011). This structure is only present when the peptides interact with the membrane, hence it could be assumed to be important for function. However, an analog of aurein 2.3 with a carboxylated C-terminus also adopts the same structure as the natural form, but does not have any antimicrobial activity (Pan et al., 2007).

The example cited above suggests that AMPs do not necessarily adopt a specific “active” conformation, i.e., there is no direct correlation between the amount or type of secondary structure and any quantifiable biological activity such as MIC. Indeed, short polypeptides are notorious for their conformational flexibility and several examples of natural and synthetic AMPs with a high degree of structural plasticity have been reported in the literature including: 1018 (Wieczorek et al., 2010), indolicidin (Nagpal et al., 2009), HHC-36 (Nichols et al., 2013), Gad-2 (McDonald et al., 2015) etc. It is this structural plasticity that makes peptides natural biological messengers (Henninot et al., 2018) and this flexibility in structure likely ensures that interactions between AMPs and their targets are malleable, enabling them to interact with a variety of binding targets including not only membranes, but also DNA, RNA, and certain proteins. These interactions, in turn, ensure that AMPs and HDPs are active against a broad range of microorganisms (including their biofilm growth states) while also being capable of causing pleiotropic effects in the host, all of which are essential

to innate host defense processes (Hancock and Sahl, 2006, 2013).

Are Bacteria Able to Develop Resistance to AMPs?

As natural molecules involved in host defense, HDPs have co-evolved for millions of years alongside bacteria and it has been frequently argued that bacteria are virtually incapable of developing resistance to AMPs. This is often touted as one of the attractive features of developing synthetic AMPs as alternatives to antibiotics. Unfortunately, bacteria are quite resourceful and indeed several resistance mechanisms to AMPs have been reported (Nizet, 2006; Bechinger and Gorr, 2017). Examples include remodeling of the membrane to reduce the overall negative charge, blocking the anionic groups in LPS by attaching an aminoarabinose group or decorating TA polymers with D-alanine moieties to counteract the negative charge arising from the phosphate groups in the TA monomers. Furthermore, AMPs may be degraded by the action of bacterial proteases (Sieprawska-Lupa et al., 2004; Lai et al., 2007) or they may simply be expelled from the cell following upregulation of bacterial efflux systems (Joo et al., 2016). Alternatively, the ability of peptides to induce resistance regulons in *Pseudomonas* to some extent dictated their activity against this bacterium (McPhee et al., 2003; Fernández et al., 2012). Regardless of which resistance mechanism is invoked by a particular bacterial species, it is important to consider these resistance mechanisms as we continue the search for novel AMP sequences with ever increasing antibacterial potency. At best, the various resistance mechanisms described for AMPs indicate that any new peptide-based antibiotic, once introduced in the clinic, would be prone to similar patterns of resistance as those observed for conventional antibiotics (Blair et al., 2015). In this scenario, AMPs could be viewed as merely stemming the rising tide of antibiotic resistance rather than acting as a miracle drug that will solve all our problems.

Are Antibiofilm Peptides Distinct From AMPs?

The development of antibiofilm peptides and their potential to address the issues of biofilm-associated infections has been reviewed elsewhere (Batoni et al., 2016; de la Fuente-Núñez et al., 2016; Pletzer and Hancock, 2016) and hence, we will only briefly discuss some of their properties here. This class of peptide acts against biofilms formed by multiple species of bacteria, including the most resistant organisms in our society termed the ESKAPE pathogens (*Enterococcus faecium*, *S. aureus*, *Klebsiella pneumoniae*, *Acinetobacter baumannii*, *Pseudomonas aeruginosa*, *Enterobacter cloacae*) and other clinically relevant bacteria (de la Fuente-Núñez et al., 2014b). As mentioned above, structure activity relationship studies showed no direct overlap between antibiofilm and antimicrobial (vs. planktonic bacteria) activities. Thus peptides are able to inhibit biofilms formed by *Burkholderia cenocepacia* which is normally resistant to the effects of AMPs (Loutet and Valvano, 2011) and it is also possible to isolate peptides with excellent antibiofilm activity but poor activity against planktonic bacteria and vice versa (de la Fuente-Núñez et al., 2012). This suggests that the mechanism of action employed by

antibiofilm peptides must be distinct from those employed by AMPs.

Recent work by our group has implicated the widespread bacterial stringent response as a common target for the antibiofilm activity of HDPs. When bacteria are subject to amino-acid starvation, fatty acid limitation, iron limitation, heat shock and other stressors (Crosse et al., 2000; Potrykus and Cashel, 2008), a stringent response is triggered through up-regulation of the two signaling nucleotides: guanosine tetraphosphate (ppGpp) and pentaphosphate (pppGpp) [collectively known as (p)ppGpp]. These signals cause the bacteria to divert nutrients from growth and division processes in order to promote survival, ultimately resulting in biofilm formation (Potrykus and Cashel, 2008; Wolz et al., 2010). In many bacterial species, ppGpp is required for biofilm growth and mutants lacking the enzymes responsible for generating (p)ppGpp are unable to elicit a stringent response and therefore do not form biofilms (Åberg et al., 2006; He et al., 2012; de la Fuente-Núñez et al., 2014b).

In this regard, the synthetic HDP (also termed Innate Defense Regulator or IDR) peptide IDR-1018 (de la Fuente-Núñez et al., 2014b), and several D-enantiomeric peptides, including DJK-5 (de la Fuente-Núñez et al., 2015), have been shown deplete (p)ppGpp from cells *in vivo*, as well as to directly interact with (p)ppGpp *in vitro*, by preferentially binding to it as compared to other nucleotides (e.g., GTP). In an *in vivo* mouse abscess model for which pathology (cutaneous lesion formation) is dependent on the stringent response, both peptides suppressed lesion formation by either *Staphylococcus aureus* or *Pseudomonas aeruginosa* (Mansour et al., 2016), and for the latter a specific role of the stringent response and suppression of the expression of the bifunctional (p)ppGpp metabolizing enzyme, SpoT, was indicated (Pletzer et al., 2017). A study showed that an analog of 1018, with its amino acid sequence reversed (Andresen et al., 2016), was equally able to co-precipitate ppGpp in a test tube and still exhibited inhibitory effects on *P. aeruginosa* biofilms. Similarly, the D-analog of this reversed sequence also depleted (p)ppGpp from cells (de la Fuente-Núñez et al., 2015). It is worth mentioning that Andresen et al. argued that since the reversed 1018 peptide sequence exhibited similar ppGpp and antibiofilm activities compared to the native 1018 peptide, that this could not explain the specificity of the mechanism of action or the involvement of the stringent response. We have recently addressed this critique in some detail (Pletzer et al., 2017) and we contend that binding of phosphorylated nucleotides may be a common feature of many cationic HDPs and represents a molecular interaction that could be exploited if we could better understand the specific peptide requirements for (p)ppGpp binding. Nevertheless, the implication of this molecular mechanism for antibiofilm peptides is that they must be able to translocate across the membrane into bacteria in order to act on this intracellular nucleotide.

Since the effect of antibiofilm peptide activity in mice is to inhibit the formation of necrotic lesions, it is worth mentioning that DJK-5 strongly suppressed the production of alpha-type phenol soluble modulins (Mansour et al., 2016), which are stringently regulated cytotoxins that are also involved in biofilm structuring (Periasamy et al., 2012). Evidently, HDPs that exhibit

antibiofilm activities can mediate a range of biological functions and exert their activities through a variety of mechanisms; indeed peptide 1018 also possesses potent immunomodulatory functions and works in a wide range of *in vivo* animal models of infection and inflammation (Mansour et al., 2015).

To this point, we have examined several of the commonly held beliefs regarding the antibacterial functions of AMPs and have discussed how the prevailing view of these molecules has shifted from being simple membrane destroyers to biomolecules that exert their antimicrobial effects by targeting a plethora of bacterial components using a variety of mechanisms. Indeed, several features of AMPs have emerged over the years as contributing factors to the observed antibacterial potency including charge, hydrophobicity, and structure. However, we should be cautious about extrapolating the observed effects of a single peptide to all AMPs in general as this oversimplifies many of these processes and fails to appreciate that each individual peptide sequence mediates a variety of functions independently. This multifaceted nature of AMPs and HDPs is reflected in the fact that these molecules have biological functions that extend beyond bacterial cells. In the following sections, we will examine some of the other activities that have been observed for HDPs *in vitro* and *in vivo* and we will further examine how an appreciation of these additional functions is shaping the future clinical and therapeutic applications of these biomolecules.

ACTIVITY LANDSCAPES OF HOST DEFENSE PEPTIDES

Beyond questioning tightly-held beliefs about the bacteriostatic and bactericidal nature of AMPs, one has to consider that many HDPs influence a wide range of biological functions *in vivo*. Other types of activities, in addition to various forms of immune modulation (Hancock et al., 2016) and antibiofilm activity (Pletzer and Hancock, 2016) are increasingly being appreciated for HDPs and include (but are not limited to): antiviral (Gwyer Findlay et al., 2013), antifungal (Weerden et al., 2013) antiparasitic (Mor, 2009), anticancer (Gaspar et al., 2013), wound healing (Mangoni et al., 2016), adjuvanticity for vaccines (Nicholls et al., 2010), and more recently they have been proposed as biomarkers for certain diseases (Silva et al., 2018). Each of these have been extensively reviewed elsewhere (see review articles referenced above) and these “alternative” activities of HDPs are rapidly gaining prominence as more investigators examine these diverse biological effects. These broad activity classes also present tremendous opportunities for researchers to identify and optimize natural and synthetic peptide sequences that are tailored for a specific biological function. However, the question remains, what represents an “optimal” HDP sequence?

Since their discovery in insects (Steiner et al., 1981), mammals (Ganz et al., 1985; Selsted et al., 1985a,b) and frogs (Zasloff, 1987), the majority of research endeavors in the HDP field have been focused on identifying, characterizing and optimizing peptide sequences for their direct antibacterial activity while limiting toxicity toward eukaryotic cells (often assessed as hemolysis of red blood cells). Indeed, up until the last decade or so,

the holy grail of AMP research was a peptide with potent activity against a wide assortment of bacterial pathogens *in vitro*, while exhibiting no toxicity toward the cells of the host. In general, the scientific community has had remarkable success in searching for antimicrobial HDP sequences from natural sources, as evidenced by the current tally of nearly 3,000 sequences deposited in the Antimicrobial Peptide Database (APD, <http://aps.unmc.edu/AP/main.php>) (Wang et al., 2015a). Many more studies have sought to manipulate the biophysical characteristics of these natural HDP sequences to optimize synthetic peptides for their antibacterial effects (reviewed in Fjell et al., 2012). Optimization strategies such as these typically manipulate a few biophysical traits of a given peptide and evaluate the effects of substituting specific amino acids at various points within the parent sequence. Normally, these parameters involve some combination of cationic charge and hydrophobicity and a small library of ~5–10 peptides is generated based on a starting peptide scaffold. In most published examples, some derivatives exhibit moderately enhanced antimicrobial potency relative to the parent sequence, or perhaps reduced toxicity, and this is then used to justify the design approach. It is difficult to estimate how many synthetic peptides have been evaluated in studies such as these, although manually-curated databases of published HDPs count between 11,000 and 17,000 entries (Fan et al., 2016; Pirtskhalava et al., 2016). Based on our own experience (and the number of synthetic peptides in our laboratory freezers), as well as the fact that the search term “Antimicrobial Peptide” yields more than 300,000 hits in PubMed, we would venture to guess that the actual number of peptides that have been created and tested in labs is substantially higher.

In principle, the possible chemical space of HDPs can be represented mathematically by the equation 20^n , which encompasses all possible permutations and combinations of the 20 naturally occurring amino acids for a peptide of length n (the problem becomes exceedingly complex if we start to consider the 700 or so non-natural amino acids, enantiomers, and peptidomimetic backbones). Since the primary structure of a peptide and how these fold in three-dimensions dictates the biological activity of any given peptide (Fjell et al., 2012), if the activities of all the peptides within this chemical space could be evaluated, it would be possible to unequivocally identify the best HDP for any given type of activity. Unfortunately, this scenario is virtually impossible as this chemical space becomes overwhelmingly large rather quickly as even a chemical space limited to peptides of 10 residues in length would include over 10 trillion sequences (Table 1). It may be possible to limit the chemical space of HDPs by focusing on specific amino acids generally considered important for HDP function such as cationic (Arg and Lys) and hydrophobic (Gly, Ala, Val, Ile, Leu, Phe, Tyr, and Trp) residues (Table 1). However, it should be noted that all 20 amino acids are represented within HDP sequences deposited in the APD (Wang et al., 2015a) and such a strategy might remove potentially active sequences from the overall chemical space.

With such large numbers encompassing the possible chemical space of HDPs, it seems likely that the activities of individual peptides from within this chemical space would also be quite

TABLE 1 | Number of possible peptide sequences encompassing the chemical space of peptides of a given length (*n*).

| Peptide length (<i>n</i>) | Number of peptides in the chemical space (20 ^{<i>n</i>}) | Chemical space limited to cationic (2) and hydrophobic (8) residues ((2+8) ^{<i>n</i>}) |
|-----------------------------|--|--|
| 2 | 400 | 100 |
| 3 | 8,000 | 1,000 |
| 4 | 160,000 | 10,000 |
| 5 | 3,200,000 | 100,000 |
| 6 | 64,000,000 | 1,000,000 |
| 7 | 1,280,000,000 | 10,000,000 |
| 8 | 25,600,000,000 | 100,000,000 |
| 9 | 512,000,000,000 | 1,000,000,000 |
| 10 | 10,240,000,000,000 | 10,000,000,000 |
| 20 | 1.05 × 10 ²⁶ | 1 × 10 ²⁰ |
| 30 | 1.07 × 10 ³⁹ | 1 × 10 ³⁰ |

varied. An analogy that could be used to describe the activity landscape of this chemical space would be to envision this as a mountain range filled with peaks and valleys (**Figure 1**). Some peptides within the chemical space will have high activity (the peaks) while others will have low activity (the valleys). As we move around this chemical space by manipulating the primary amino acid sequence of a peptide and record the biological activities, this vast chemical space can be mapped with the ultimate goal of identifying the highest peak that represents a truly “optimal” sequence (e.g., left panel, **Figure 1**).

Such an approach might be more feasible if the activity landscape for each individual type of HDP activity were identical. However, there is ample evidence that these activity landscapes are independently defined for each biological function of HDPs. For instance, LL-37 possesses relatively weak direct antibacterial activity but inhibits *P. aeruginosa* biofilms at sub-inhibitory concentrations (Overhage et al., 2008). Selective antibiofilm activity by LL-37 has also been observed against *Aggregatibacter actinomycetemcomitans* which causes oral biofilms and can contribute to periodontal disease (Sol et al., 2013). In addition, several synthetic peptides have been identified with sub-inhibitory effects on bacterial biofilms including truncated variants of LL-37 (Luo et al., 2017) or the synthetic peptide WLBU2 (Lin et al., 2018). With respect to immunomodulatory activity, a synthetic HDP, IDR-1, offered protection in murine infection models against both Gram-positive or Gram-negative pathogens, despite the fact that IDR-1 exhibited no direct antibacterial effects *in vitro* (Scott et al., 2007). The selective modulation of the immune response by IDR-1 was found to be responsible for the protective effects, indicating that the antibacterial and immunomodulatory properties of HDPs were independently defined.

More recently, we sought to define the sequence requirements of two synthetic HDPs, IDR-1002 and IDR-HH2, to understand which residues contributed to the antibiofilm and immunomodulatory properties of these peptides (Haney et al., 2015). Using SPOT-synthesized peptide arrays, peptide

libraries consisting of single amino acid substitution variants of the parent sequence were generated by replacing each residue with one of nine amino acids (R, K, D, G, A, I, L, V, or W). The antibiofilm and immunomodulatory (chemokine induction and anti-inflammatory) properties of each peptide variant were measured *in vitro* and plotted as substitution matrices to identify which residues contributed to each individual activity type. Interestingly, substantial overlap was observed between the activity profiles of the two peptides but there were also distinct residues that, when positionally substituted, appeared to preferentially improve one activity over another. These results imply that the activity landscapes for each biological function of HDPs within the chemical space are overlapping but distinct from each other (**Figure 1**). If these activity landscapes could be adequately defined for each activity type, it would, in principle, be possible to simultaneously optimize synthetic peptides for multiple activities, while avoiding potentially harmful sequences that are toxic or exert undesired effects. Therein lies the challenge for researchers working in the HDP field: how can we adequately define the activity landscape of the HDP chemical space?

Several approaches have been used to try and sample the chemical space of HDPs and get a glimpse into these activity landscapes, particularly for the antibacterial properties of HDPs. Early approaches involved screening of combinatorial peptide libraries to identify novel sequences with antibacterial activity (Blondelle and Houghten, 1996; Blondelle and Lohner, 2000) but these were effectively limited by the cost of such methods and the extreme numbers of variants such that only 6-mer sequences were considered.

Computational approaches have also been employed to design and optimize novel peptide sequences with enhanced antibacterial potency. Early attempts involved modeling AMPs as a language and using natural AMPs sequences to define a set of “grammars” that described the language (Loose et al., 2006) and the implementation of similar grammatical approaches continues to identify novel AMP sequences (Nagarajan et al., 2018; Porto et al., 2018). Other computational approaches have sought to establish quantitative structure activity relationships (QSAR) that model the activity of test peptides based on the chemical properties of AMPs using hundreds or thousands of so-called “descriptors” based on the primary structure and the physicochemical interrelationships of individual amino acids along the peptide chain. Artificial intelligence strategies (neural networks) were used to create models that quite accurately predicted the antibacterial activity of virtual peptides and ultimately identified novel 9-mer AMPs with enhanced antibacterial potency *in vitro* that were also effective in an *in vivo* model (Cherkasov et al., 2009). The emergence of machine learning methods to predict novel AMP sequences has proven quite popular and has made great strides in identifying many unexplored AMP sequences (Torrent et al., 2011; Maccari et al., 2013; Lee et al., 2017; Yoshida et al., 2018). Moving forward, an improved understanding of the mechanistic details of AMP activity coupled with the application of increasingly sophisticated computational algorithms will surely lead to more exciting outcomes from this line of inquiry.

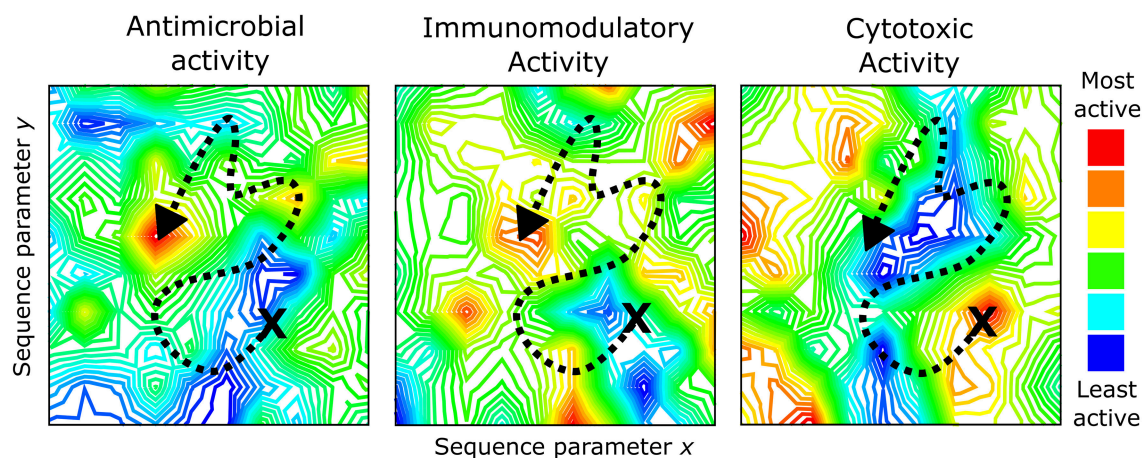


FIGURE 1 | The activity landscapes for HDPs are complex (represented as topographical maps) and encompass a variety of biophysical characteristics such as charge, hydrophobicity, amphipathicity, folding propensity, etc. When optimizing synthetic peptides by moving around the chemical space of an activity of interest (represented by the dashed line), it is necessary to consider how this sequence alteration may impact other peptide properties and/or activities. This could result in a convergence of activities within an HDP sequence (e.g., antimicrobial and immunomodulatory activities above) or a reduction in one activity type (e.g., cytotoxicity landscape above). Topographical maps were generated by Contour Map Creator (<http://contourmapcreator.ugr8.ch/>), and the maps shown are only illustrative and actually correspond to various locations near Vancouver, Canada.

Directed evolution methods have also been adapted to allow a specific biological interaction or biological activity to guide the discovery of novel peptide sequences. For instance, a phage display approach was used to identify peptides capable of binding to the cell surface of *E. coli* resulting in a novel antibacterial peptide sequence with activity against both *E. coli* and *P. aeruginosa*, although the resultant peptide was unfortunately only moderately active and did not inhibit other tested bacteria (Rao et al., 2013). A similar strategy was employed to identify AMPs with selective activity against *Listeria monocytogenes* (Flachbartova et al., 2016). Furthermore, phage display has successfully identified peptides with antiviral (Ojeda et al., 2016) and antifungal activity (de Oliveira et al., 2016) demonstrating the utility of such a technique to explore other activity landscapes within the chemical space of HDPs.

Recently, an elegant high-throughput synthetic biology approach was described wherein ~800,000 random 20mer peptide sequences were displayed on the surface of a bacterial cell as part of a fusion protein coupled to the outer membrane protein OmpA (Tucker et al., 2018). Pools of transformed bacterial cells before and after induction of the OmpA-peptide fusion constructs were sequenced and nearly 8,000 peptide sequences were identified as “hits” with potential antimicrobial activity. Of the 22 peptide sequences that were synthesized to validate the methodology, only two exhibited antimicrobial activity when evaluated in the standard MIC assay using Mueller-Hinton broth but 18 (~80%) exhibited bactericidal activity when cells were treated in a simple tris-based buffer (10 mM Tris, 25 mM NaCl). It should be mentioned that the majority of these validation sequences were chosen based on opposite physico-chemical characteristics compared to classical AMPs (i.e., low hydrophobicity and neutral to negative charge) in an effort to sample unexplored regions of the peptide chemical space, while

the two that exhibited the most potent activity conformed to properties of known AMPs. In fact, no particular bias toward hydrophobicity, charge, or enrichment of specific amino acids was observed for the ~8,000 “hit” sequences (Tucker et al., 2018), suggesting that the chemical composition of active antibacterial HDPs is likely more diverse than originally thought.

The examples described above primarily focused on sampling the activity landscape that defines the antibacterial properties of HDPs. However, the multifaceted nature of HDPs and their wide range of biological activities suggest that independent activity landscapes could be defined for every biological function of HDPs. In the following section, we examine some of these emerging roles of HDPs, beyond their direct antibacterial effects, that represent the next wave of research that could propel these molecules to clinical significance.

HDPs IN HEALTH AND DISEASE

HDPs as Modulators of Microbial Communities

The drive to target pathogenic bacteria in the face of rising antibiotic resistance has spurred the lion’s share of research into natural and synthetic HDPs. However, the interactions between bacterial cells and HDPs, involving the polycationic amphipathic peptides associating with polyanionic and hydrophobic surfaces, would not be limited to pathogenic bacteria, so it seems likely that an AMP would have similar antibacterial effects on commensal bacteria when present at sufficiently high concentrations. Inevitably, the disruption of the natural microbiota could lead to the expansion of opportunistic pathogens, such as *Clostridium difficile* infections that often follow antibiotic therapy (Kelly and LaMont, 2008). Fortunately, natural HDPs are rarely found at concentrations high enough to sterilize the environment in their

immediate vicinity (Hancock et al., 2016), but this raises the question as to the functions of HDPs within the body. Several pieces of evidence have emerged that natural HDPs may in fact help to shape microbial communities within the host to promote a healthy microbiota, rather than specifically removing pathogenic bacterial species.

Compelling evidence for this idea came from analysis of the microbial communities of cnidarians. Using seven different species of *Hydra* that had been cultivated in the lab under identical conditions for more than three decades, sequencing of the associated microbial community revealed that each species had a distinct microbial community associated with them (Franzenburg et al., 2013). Furthermore, even when co-cultured with another *Hydra* species, the microbial community differences between *Hydra* species did not change, demonstrating that some host-derived factor was dictating the associated bacterial community composition. Arminins are the most highly expressed HDPs in *Hydra* (Augustin et al., 2009) and are only found within the *Hydra* genus. Intriguingly, several orthologs of arminin peptides were found amongst the various *Hydra* species studied and their expression patterns varied depending on the species being evaluated (Franzenburg et al., 2013). Recolonization of germ-free arminin-deficient *Hydra* (with ~50% reduced arminin levels) by donor polyps from other *Hydra* species, revealed that the arminin-deficient *Hydra* were unable to reshape their microbial community into one that resembled their native microbiota, resulting in a distinct microbial community composition. Indeed, the diversity of natural HDP sequences and structures observed for most animals, and even in different body compartments (Nguyen et al., 2011; Mylonakis et al., 2016), might result from species-specific HDPs that have co-evolved to select specific microbial communities beneficial to that specific host, while possibly limiting other species.

The spatial expression pattern of HDPs throughout the body is also known to be tissue and cell type specific and this could well play a role in defining variations in local microbial communities within the same organism. For instance, analysis of HDP expression patterns in the bovine udder revealed differential expression levels of various peptides including the lingual antimicrobial peptide, tracheal antimicrobial peptide, and bovine neutrophil β -defensins 4 and 10 (Tetens et al., 2010). Expression of most of these was confined to the lymph node while *DEFB1* (the β -defensin-1 gene) expression occurred primarily at distal regions of the mammary gland. Furthermore, bovine psoriasin (also known as S100A7) expression was found to be strongly expressed in the streak canal (udder entrance) and the authors suggest that this peptide may prevent the development of coliform mastitis because of its strong antibacterial potency and proximity to the region of the udder that would be exposed to the most pathogens (Tetens et al., 2010). Alternatively, or perhaps in addition, since psoriasin is anti-inflammatory it might serve to prevent inflammation in this environmentally exposed tissue.

In mammals, the role of natural HDPs in maintaining homeostasis within the gut is becoming increasingly appreciated (Bevins and Salzman, 2011; Muniz et al., 2012; Ostaff et al., 2013). For instance, the role of natural HDPs on the host microbiome was evaluated in mice genetically engineered to express human

defensin 5 (DEFA5) or lacking the matrix metalloprotease 7 enzyme (MMP7) required to activate the endogenous mouse α -defensins. In both cases, a distinct shift in the composition of the bacterial community was observed, indicating that α -defensins play an important role in shaping the microbiota of the small intestine (Salzman et al., 2010). Specifically, MMP7 deficient mice had low proportions and abundance of *Bacteroides* and mouse intestinal *Bacteroides* (MIB) groups while DEFA5-transgenic mice lacked segmented filamentous bacteria which directly contact the epithelium in small intestines of several animals. In diabetes-prone rats, cathelin-related antimicrobial peptide (CRAMP) expression from β -cells was decreased, suggesting a potential role of this peptide in type 1 diabetes (Pound et al., 2015). At the same time, administration of the human CRAMP homolog, LL-37, to diabetes-prone rats shifted the microbiota toward a composition seen in diabetes-resistant mice (Pound et al., 2015), suggesting that this HDP also plays a role in maintaining gut homeostasis.

As the role of natural HDPs in maintaining homeostasis has become appreciated, their potential to treat microbial dysbiosis has also been considered. HIF-1 α is a transcription factor that has been shown to influence the expression of CRAMP in murine myeloid cells (Peyssonnaud et al., 2005). The commensal bacterium *Bacteroides thetaiotamicron* has been shown to activate HIF-1 α and promote cathelicidin production in the gut of mice previously exposed to antibiotics which in turn prevented invasive colonization by *Candida albicans* (Fan et al., 2015). This demonstrated that modulation of the mucosal immune effectors might represent a viable therapeutic approach for preventing fungal infections following a course of antibiotic treatment. In this regard, protection against murine *Candida albicans* infections has also been demonstrated using a synthetic immunomodulatory peptide, IDR-1018 (Freitas et al., 2017).

Several HDPs are also produced by epithelial cells within the oral mucosa and the ease of accessibility to this ecological niche within the body has prompted several studies aimed at understanding the relationship of HDPs to oral health. Salivary levels of various HDPs are known to be highly variable within the human population (Tao et al., 2005) and this may be reflective of the diverse oral microbiome composition amongst different individuals (Kilian et al., 2016). Interestingly, low salivary levels of α -defensins (Dale et al., 2006), HNPs 1-3 (Tao et al., 2005), and LL-37 (Davidopoulou et al., 2012) have each been associated with increased levels of caries in children. Patients with morbus Kostmann syndrome, a severe congenital neutropenic disease, also exhibit low LL-37 expression from neutrophils and none of this HDP can be detected in their plasma or saliva (Pütsep et al., 2002). Of note, all patients with morbus Kostmann experience severe periodontal disease, which is consistent with the suggestion that low LL-37 levels in the saliva could contribute to this disease phenotype (Pütsep et al., 2002).

A synthetic peptide C16G2 was developed that was able to specifically target and kill a cariogenic pathogen, *Streptococcus mutans*, within an oral microbial community (Guo et al., 2015). Not surprisingly, when treated with C16G2, the overall microbial community exhibited a dramatic shift possibly due to killing of certain microflora organisms by the peptide or to a reduction

in bacterial species that were dependent on *S. mutans* for their maintenance. Importantly, this study demonstrates the possibility of using synthetic peptides to shape and modulate natural microbial communities. Alternatively, synthetic HDPs may prove useful for preventing infections associated with microbes present in complex dental plaque biofilms, such as peptide 1018 that significantly inhibited mixed biofilms formed by natural salivary microflora (Wang et al., 2015b).

The mechanisms by which HDPs maintain this microbial balance within the host are not completely understood, although it is likely that these mechanisms will be dependent on the specific HDP that is expressed at (or delivered to) a given epithelial surface, as well as the type of effector cells in the immediate vicinity that can be influenced by the pleiotropic effects of these molecules. Indeed, it is tempting to speculate that an activity landscape defining the homeostatic activity of HDPs could be exploited to develop prophylactic options to maintain a healthy microbial balance. As our understanding of these processes improves, opportunities to use HDPs as promoters of healthy microflora will surely emerge.

Diseases Associated With Altered HDP Expression or Activity

Due to their significant role in innate immunity and various inflammatory processes, it is perhaps unsurprising that many diseases and chronic inflammatory conditions have been associated with a dysregulation of the natural HDP response, particularly at epithelial surfaces where natural peptides are present in high abundance or can be induced in response to various environmental stimuli. These include conditions associated with the skin, gut, lungs and several autoimmune disorders (Hancock et al., 2016). Furthermore, there is increasing evidence that natural HDPs can influence tumorigenesis, either positively or negatively depending on the peptide in question and the tissue affected. Many of these topics have been reviewed in detail by others and we will only briefly highlight some of the work that has been described pertaining to several of these conditions.

Skin Disorders

The skin is the largest organ in the human body. It is comprised of several different cell types that are organized into a complex architecture that allows skin to perform a wide range of biological functions. Since skin is constantly exposed to bacteria within the environment, one of the main functions of skin is to protect against invading pathogens while maintaining a healthy skin-associated microbiota. Several HDPs have been implicated in skin health and it is not surprising that a dysregulation in these HDP levels can contribute to a variety of skin disorders (Schauber and Gallo, 2008; Marcinkiewicz and Majewski, 2016).

Psoriasis is a relatively common autoimmune disorder characterized by inflamed skin resulting in abnormal skin patches that are itchy, scaly and inflamed. Psoriatic skin is characterized by overexpression of several HDPs and antimicrobial proteins and it is generally thought that the presence of HDPs exacerbates psoriatic lesions (Morizane and Gallo, 2012). Indeed, high β -defensin gene copy number has been associated with increased

risk for psoriasis (Hollox et al., 2008) and the human cathelicidin LL-37 is also overexpressed in psoriatic skin (Lande et al., 2007, 2014). Intriguingly, activation of both the innate and adaptive immune response has been implicated in the pathogenesis of psoriasis. For instance, LL-37 has been shown to activate plasmacytoid dendritic cells by breaking tolerance to self-DNA (Lande et al., 2007), while it was demonstrated that LL-37 could also serve as an autoantigen for T-cells (Lande et al., 2014). However, offsetting this is the potent anti-inflammatory activity of LL-37 (Bowdish et al., 2005) which has been clinically tested as a method for counteracting ulcerative lesions (Grönberg et al., 2014). Patients with cutaneous lupus erythematosus also have increased expression of several HDPs which has been proposed to explain why they seldom develop skin infections (Kreuter et al., 2011), although it is unclear how HDP expression contributes to the pathogenesis of this disease in general.

Atopic dermatitis (AD, known colloquially as eczema) is another common inflammatory condition characterized by dry, red and itchy skin. In contrast to psoriasis, however, AD is associated with reduced HDP levels and it has been suggested that impairment of HDP production in AD skin contributes to higher incidence of skin infections, particularly *S. aureus* infections (Marcinkiewicz and Majewski, 2016).

In addition to these inflammatory disorders, a dysregulation of HDP production in chronic wounds has been implicated in a failure of these lesions to heal properly (Haney et al., 2018b). Compounding this issue is that chronic wounds are often colonized by bacteria growing in biofilms (James et al., 2008) that are intrinsically resistant to conventional antibiotics (Lopez et al., 2010) and whose presence may exacerbate inflammation in the wound bed (Zhao et al., 2013). The therapeutic use of natural and synthetic HDPs to promote wound closure while also targeting the bacteria in the biofilm growth state may therefore represent an underexplored strategy to treat chronic wounds (Haney et al., 2018b), and proof of principle has indeed been achieved for venous leg ulcers (Grönberg et al., 2014). Similarly, synthetic peptides have shown efficacy in murine cutaneous abscess infections (Mansour et al., 2016; Pletzer et al., 2017) and sterile skin inflammation mouse models (Wu et al., 2017a).

Inflammatory Bowel Diseases

The gastrointestinal tract in humans is home to a large and diverse community of bacteria and other microbes. The ability of the epithelial cells lining the intestinal tract to contain these bacteria is due to the presence of a complex layer of mucus and proteins, including a wide assortment of HDPs (Wehkamp et al., 2007). The term inflammatory bowel disease (IBD) encompasses a range of inflammatory conditions of the intestinal tract. The two most common IBDs are ulcerative colitis, which largely affects the colon, and Crohn's disease, which can affect the entire gastrointestinal tract (Geboes et al., 2018). The exact causes of these conditions are currently unknown but they are likely to involve a combination of genetic, immune and environmental factors. Various HDPs have been implicated in these diseases (Holani et al., 2018), consistent with the potentially important role that these molecules play in regulating overall gut health. For instance, expression of many HDPs is high during colitis,

particularly HBD2 and HBD3, and some of these may serve as biomarkers of disease (Wehkamp et al., 2007; Ho et al., 2013). Interestingly, the opposite phenomenon occurs in Crohn's disease, as the levels of several HDPs, including β -defensins and LL-37, are substantially diminished (Wehkamp et al., 2007), which may lead to disruption of the barrier function of the gut and allow bacteria to reach the epithelial cell surface where they elicit an inflammatory response.

Lung Disorders

As with other airway epithelial surfaces, the lungs are constantly exposed to bacteria and other molecules that are carried into the lungs with each inhaled breath. Fortunately, our lungs are well-adapted to withstand this constant exposure to potential pathogens and respiratory infections are kept at bay through phagocytes and the mucociliary response. Unfortunately, respiratory infections are relatively common (Vos et al., 2015) and there is evidence that dysregulation of natural HDPs within the lungs can contribute to an increased susceptibility to respiratory infections (Hiemstra et al., 2016). Lung tissue is known to express several HDPs including α -defensins, β -defensins, and LL-37 (Hiemstra et al., 2016), and their expression is often upregulated in response to pathogen exposure, e.g., β -defensin 2 induction in lung cells exposed to *P. aeruginosa* (Harder et al., 2000). Furthermore, CRAMP-deficient mice have been shown to have increased susceptibility to lung infections caused by *Klebsiella pneumonia* (Kovach et al., 2012) implicating a key role for natural HDPs in maintaining healthy lung function.

In addition to preventing respiratory infections, several other inflammatory conditions of the lungs have been associated with a dysregulation of HDP function including: cystic fibrosis (CF), chronic obstructive pulmonary disease (COPD), and asthma. As with the other inflammatory conditions described above, both high and low expression of natural HDPs within the lungs can contribute to various disease pathologies.

CF is an autosomal recessive genetic disorder caused by mutations in the CF transmembrane conductance regulator protein (*CFTR*) gene which regulates anion transport in the airway and other epithelial surfaces (Elborn, 2016). Patients with this disease get mucus buildup within the lungs and have difficulty clearing bacteria which contributes to persistent respiratory infections and chronic inflammation (Elborn, 2016). A direct consequence of this *CFTR* defect is that the salt concentration within the lungs of CF patients is higher than in healthy individuals (Smith et al., 1996) and this high salt concentration has been shown to inhibit the antibacterial activity of natural HDPs like HNP1 (Turner et al., 1998) possibly contributing to increased susceptibility to bacterial infections. Interestingly, in *in vitro* models, IDR-1018 was able to reduce the exaggerated inflammatory response of *CFTR*-mutated human airway epithelial cells to bacterial inflammatory agonists, largely by correcting defective autophagosomal clearance (Mayer et al., 2013).

COPD is a progressive lung disease that affects nearly 10% of the population and is particularly prevalent in smokers

(Cosio et al., 2009). Patients with COPD have limited and progressively deteriorating lung function and exhibit abnormal inflammatory responses within the small airways and alveoli in their lungs (Cosio et al., 2009). The role of HDPs in COPD has been recognized for some time and the expression of many natural HDPs is often dysregulated in patients afflicted with this condition, which causes patients to have increased lung inflammation and leaves them prone to bacterial infections (Hiemstra et al., 2016). In addition to altered HDP expression, the enzymatic activity of peptidylarginine deiminases (PADIs) has recently been shown to influence the function of natural HDPs in the lungs of smokers with COPD. PADIs are enzymes that postrationally modify cationic peptidylarginine residues to peptidylcitrulline which blocks their associated cationic charge (Wang and Wang, 2013). Interestingly, the levels of PADI2 are elevated in the lungs of smokers (Makrygiannakis et al., 2008) and recombinant human PADI2 has been shown to citrullinate the Arg residues in LL-37 *in vitro* (Kilsgård et al., 2012). Citrullinated LL-37 exhibits reduced antibacterial activity *in vitro* compared to LL-37 and is more susceptible to protease degradation (Kilsgård et al., 2012), suggesting that this form of the peptide would be less effective and more rapidly cleared from the lungs of COPD patients. More recent work has demonstrated that citrullination of LL-37 also suppressed the immunomodulatory function of this peptide by reducing its anti-inflammatory ability to neutralize the pro-inflammatory activity of bacterial LPS (Koziel et al., 2014), further implicating this process as a contributing factor to COPD progression.

Asthma is the most common inflammatory condition of the lung and, when triggered by dust or allergens, leads to airway inflammation and airflow obstruction (Holgate et al., 2015). The exact cause of asthma is thought to involve a range of environmental and genetic factors; however, one of the features of this disease is an altered innate immune response (Holgate et al., 2015). Allergic airway inflammation has been shown to suppress innate host defenses in mouse models of asthma, including reducing levels of the mouse cathelicidin CRAMP (Beisswenger et al., 2006). Steroid treatment by glucocorticoids is a common treatment for asthma. However, steroid treatment in a murine model of asthma reduced the levels of pulmonary HDPs and led to increased susceptibility to infections by *P. aeruginosa* (Wang et al., 2013).

Recently, the use of synthetic HDPs was explored as a potential treatment option to overcome the reduced levels of natural HDPs seen in asthmatic lungs. Impressively, subcutaneous administration of IDR-1002 reduced airway hyper-responsiveness in a murine model of house dust mite (HDM) induced allergic asthma (Piyadasa et al., 2018). Mechanistic studies revealed that the peptide suppressed the production of interleukin (IL)-33 in murine lungs and human primary bronchial epithelial cells. Since the levels of IL-33 are often elevated in patients with asthma and disease severity is linked with the levels of this chemokine (Préfontaine et al., 2009), the use of peptide based therapeutics to suppress this key effector molecule represents a potentially unexplored treatment option for asthma. Notably, IDR and HDP peptides have demonstrated activity in a variety of lung infection models including *M.*

tuberculosis (Rivas-Santiago et al., 2013a,b) as well as acute and chronic *P. aeruginosa* infection models (Wuerth et al., 2017, 2018), demonstrating anti-inflammatory and/or anti-infective activity.

Cancer

The role of natural HDPs in tumorigenesis is complex and not fully understood (for recent reviews, see Droin et al., 2009; Wu et al., 2010; Jin and Weinberg, 2018). Nevertheless, several studies have shown that natural HDPs are dysregulated in various cancers and whether they are purported to promote or prevent cancer progression appears to depend on the type of cancer and which peptide is being considered. For instance, the human cathelicidin LL-37 is expressed in lung (von Haussen et al., 2008), breast (Heilborn et al., 2005), and ovarian (Coffelt et al., 2008) cancers. It has been shown to have angiogenic properties (Salvado et al., 2013) and can serve as a growth factor (Heilborn et al., 2005; von Haussen et al., 2008), two functions which could promote tumor growth *in vivo*. On the other hand, LL-37 has also been shown to kill Jurkat T leukemia cells by inducing apoptosis (Mader et al., 2009) and peptide fragments derived from LL-37 have been identified with direct anticancer activity against several cancer cell lines (Kuroda et al., 2015).

HBD-1 appears to have largely antitumor effects since this peptide is toxic toward late stage prostate cancer cell lines (Bullard et al., 2008), while hBD-1 expression is suppressed in malignant prostate tissue (Donald et al., 2003). Furthermore, four common defensin haplotypes are associated with the increased risk of prostate cancer and high copy numbers of the defensin gene cluster are less observed in prostate cancer patient samples (Huse et al., 2008). Conversely, hBD-3 appears to be carcinogenic as it is highly expressed in cervical cancer (Xu et al., 2016) and carcinomas of the head and neck (Mburu et al., 2011) and has been shown to promote cervical cancer growth in mouse models (Xu et al., 2016).

Based on these examples, it is attractive to speculate that the peptide activity landscape that promotes tumorigenesis is independent of peptides with anticancer properties and it therefore may be possible to specifically enhance the anticancer properties of a peptide as novel chemotherapeutics. In fact, this anticancer activity of HDPs has spurred significant interest into this class of molecules (Gaspar et al., 2013; Felício et al., 2017) as researchers seek to identify and optimize peptides for their direct anticancer effects (Hilchie et al., 2016; Arias et al., 2017).

Biofilm-Associated Infections

While this category is not *per se* a specific disease type, biofilms form locally and can be associated with a variety of pathological circumstances (including some of those described above). The seminal observation that the human cathelicidin LL-37 inhibited biofilm growth at sub-inhibitory concentrations (Overhage et al., 2008) revealed that HDPs could potentially be exploited as novel antibiofilm agents. Many more antibiofilm peptides have since been identified from screening available synthetic peptide libraries for biofilm specific activity (de la Fuente-Núñez et al., 2014a,b; Reffuveille et al., 2014) or using activity-guided design strategies to optimize known antibiofilm peptide sequences

(Haney et al., 2015). Indeed, the antibiofilm activity of newly described HDP sequences is now often reported in addition to the standard MIC values.

The reason for the preferential activity of some peptides against biofilms (Overhage et al., 2008; de la Fuente-Núñez et al., 2014b, 2015) is likely related to differing abilities to target the physiological underpinnings of biofilms as a stress-coping state, such as attacking the (p)ppGpp nucleotide signals that mediate the stringent stress response (Potrykus and Cashel, 2008). This suggests that the mechanism of action (and by extension, the activity landscape) of HDPs with antibiofilm activity is independent from the cellular functions that target planktonic bacterial cells. Given that overall HDPs are seen as “dirty drugs” (Hancock and Sahl, 2006), it is probable that multiple mechanisms of action occur downstream of the stress response, likely dependent on the environment of the HDP and the composition of the biofilm itself. Whether or not these mechanisms are truly independent or interdependent remains to be determined.

In an effort to begin to appreciate the range of HDP sequences with antibiofilm activity, an online database has been established to collect information on peptide sequences with documented activity specifically directed toward bacterial biofilms (Luca et al., 2015). In addition, a computational approach using QSAR modeling was recently used to identify novel antibiofilm specific peptides with therapeutic potential (Haney et al., 2018a). Using antibiofilm activity data derived from a SPOT-synthesized peptide arrays consisting of singly-substituted variants of 1018, a QSAR model was generated to describe this antibiofilm activity. The resulting model, which identified the seven most important molecular descriptors from a starting list of ~2,500 descriptors, was able to accurately predict 85% of the antibiofilm peptides within the training set. This QSAR model was subsequently used to predict potential antibiofilm peptides *in silico* from a virtual library consisting of 100,000 peptides and a subset were synthesized to evaluate and confirm their antibiofilm activity *in vitro* and *in vivo* (Haney et al., 2018a).

As more diverse antibiofilm peptide sequences are reported with greater potency, the activity landscape of antibiofilm specific peptides will begin to materialize. As details regarding their mechanism of action and overlapping activity landscapes with other biological functions are appreciated, multifunctional peptides capable of exerting an array of biological effects are sure to emerge as promising drug candidates to treat biofilm-associated infections.

EMERGING CONCEPTS IN HDP RESEARCH

In this review, we have highlighted several biological functions that have been reported for natural and synthetic HDPs. The breadth and diversity of these activities is vast (**Figure 2**) and new peptide sequences and biological functions are continuously being reported in the literature. Indeed, the majority of new studies continue to focus on the antibacterial effects of HDPs with an emphasis on membrane-active peptide sequences. However,

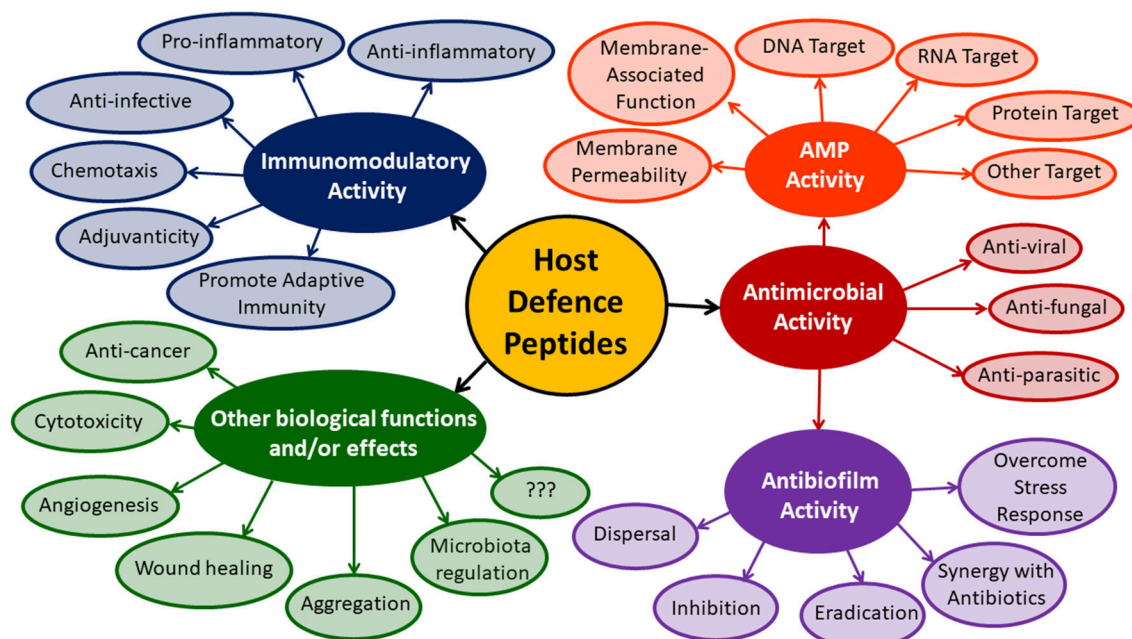


FIGURE 2 | Diversity of biological functions described for HDPs.

the plethora of other activities described for HDPs deserves increased appreciation and detailed mechanistic studies that push beyond the idea of “membrane busters” will be necessary to finally unlock the therapeutic potential of these biomolecules. In an ideal world, synthetic HDPs could be designed to maximize a desired biological function provided sufficient data existed to accurately define the activity landscape of all possible activities of interest. At the moment, defining these activity landscapes and accurately mapping their chemical space is a daunting challenge, but with new sophisticated screening and modeling techniques, it is something that can likely be overcome.

An important consideration that is often overlooked in many optimization studies is whether the assay conditions used to measure a biological property of an HDP accurately capture the behavior of the peptide that would occur *in vivo*. For instance, measuring the MIC of a peptide in phosphate buffer or nutrient limiting conditions will often yield values that appear more potent than MICs recorded in rich media or in the presence of high salt (Mahlapuu et al., 2016). Furthermore, the presence of host cells can also interfere with the observed potency of AMPs. For instance, preincubation of several AMPs with red blood cells (RBCs) drastically reduced their antibacterial efficacy against *E. coli* and *S. aureus* *in vitro* (Starr et al., 2016). However, when added to a cell suspension containing both RBCs and bacteria, the inhibition of antimicrobial activity was not observed (Savini et al., 2017), highlighting the influence of experimental setup on the observed biological activities. In practice, the optimization of an HDP actually enhances peptide sequences for a very specific functional assay. The more faithfully that an experimental setup represents conditions that would be encountered *in vivo*, the greater the likelihood that the

optimized synthetic HDPs would retain their biological functions *in vivo*.

It is also presently unclear whether a peptide should or could be simultaneously optimized for multiple biological functions or if a specific biological activity should be the driving force that guides the optimization strategy. For instance, the antibacterial and antibiofilm properties of HDPs appear to be independent of one another (Overhage et al., 2008; de la Fuente-Núñez et al., 2014b; Haney et al., 2018a) and they are likely defined by distinct activity landscapes. This is also probably the case for AMPs and immunomodulatory functions (Scott et al., 2007) as well as antibiofilm, chemokine induction and anti-inflammatory activities (Haney et al., 2015). Perhaps ultimately the best candidate peptide will be one that has the best compromise of a mixture of activities. Furthermore, HDPs like LL-37 exert their pleiotropic effects on the host through binding to various receptors or intracellular targets, as well as interacting with the cell membrane (Verjans et al., 2016). Presumably, each of these functions occurs because of a specific interaction between LL-37 and a particular biomolecule but whether the enhancement of a unique HDP interaction could be teased apart to target a specific immune cell or signaling pathway of interest remains to be elucidated.

A long recognized (Scott et al., 1999b) but increasingly appreciated (Lewies et al., 2018) ability of HDPs to synergize with conventional antibiotics holds promise as a means to overcome specific bacterial resistance mechanisms or restore the antibacterial potency of previously effective antibiotics. Several AMPs have been shown to synergize with conventional antibiotics *in vitro* (Choi and Lee, 2012; Mataraci and Dosler, 2012; Hwang et al., 2013; Gier et al., 2016; Wu et al., 2017b)

and these protective effects have been demonstrated in *in vivo* infection models (Otvos et al., 2018) providing an exciting path forward for the development of AMPs as adjunctive therapies for conventional antibiotics. This combination approach can be applied to bacteria growing within biofilms as antibiofilm peptides have been shown to synergize with conventional antibiotics to prevent and eradicate biofilms *in vitro* (Dosler and Karaaslan, 2014; Reffuveille et al., 2014; de la Fuente-Núñez et al., 2015). Recent studies *in vivo* revealed that this synergy can be extended to hard-to-treat cutaneous abscesses in mice and that peptides could be used in combination with an array of antibiotics to effectively reduce the size of abscesses caused by all of the ESKAPE pathogens (Pletzer et al., 2018). The mechanism of antimicrobial synergy was proposed to involve promoting antibiotic penetration and disruption of the stringent response. Thus, future design studies could be aimed at promoting specific aspects of this synergistic relationship to further enhance the effectiveness of drug combinations.

Enhancing endogenous expression of natural HDPs as a therapeutic approach has also been a topic of considerable interest in recent years. Much of this work has stemmed from the observation that transcription of the *CAMP* gene is regulated by the vitamin D receptor (Gombart et al., 2005; Liu et al., 2006) and it has been shown that vitamin D levels directly correlate with LL-37 levels in healthy individuals (Bhan et al., 2011; Dixon et al., 2012). Clinical trials have examined the effects of supplementing patients suffering from a variety of inflammatory disorders with vitamin D in an effort to enhance LL-37 levels and promote innate immune functions associated with this peptide. The benefits of such a therapeutic approach have been seen in several diseases including: CF (Grossmann et al., 2012), atopic dermatitis (Hata et al., 2008), cirrhosis (Zhang et al., 2016), tuberculosis (Coussens et al., 2012), and Crohn's disease (Raftery et al., 2015). The success of vitamin D as an inducer of a natural HDP (although it should be mentioned that this vitamin has many other immunomodulatory properties), has spurred research looking to identify other compounds capable of the same effect. For instance, butyrate and other short chain fatty acids are well-known inducers of LL-37 expression (Schauber et al., 2003; Jiang et al., 2013). Proteins and biomolecules produced by commensal bacteria have also been shown to modulate expression of HDP levels in the host. For example, a bacterial lipoprotein from the commensal bacterium *Fusobacterium nucleatum* called FAD-I (Fusobacterium Associated Defensin Inducer) was recently shown to activate hBD-2 expression in oral epithelial cells (Ghosh et al., 2018). Since *F. nucleatum* is resistant to direct killing by hBD-2, it was speculated that this may represent a co-evolution of a commensal organism with the human host to outcompete bacteria that would be susceptible to this HDP.

Finally, there are several perceived limitations to the development of HDPs as viable therapeutics that warrant some discussion. The most often cited issues associated with peptide drugs include high production costs, low stability and bioavailability *in vivo* as well as the potential to induce an immunogenic response (Marr et al., 2006; Vlieghe et al., 2010). Issues associated with production costs are likely unfounded

as these can be addressed by optimizing large scale synthesis procedures (Bray, 2003). With regards to bioavailability, peptides appear to have unusual pharmacokinetics when delivered systemically, with a rapid initial distribution blood followed by moderate stable levels appearing in various tissues for up to 4 (Bolouri et al., 2014) or 6 h (Brunetti et al., 2016). These concentrations may be too low to achieve direct antibacterial activity (Roversi et al., 2014) but they could prove useful in situations where these levels are sufficient (e.g., as immune modulators), or certain peptides may delivered locally to achieve high concentrations in the affected tissue (e.g., for skin or lung infections). In general, small therapeutic peptides are considered to be non-immunogenic (McGregor, 2008); however, detailed studies on the ability of synthetic HDPs to elicit an immunogenic response are largely lacking. In our experience, generating antibodies against synthetic HDPs is difficult, suggesting that HDPs may occupy an immunological "blindspot" (perhaps mediated by clonal T-cell deletion during development) with regards to adaptive immunity. Synthetic HDPs also have potential issues associated with toxicity mediated in part by a tendency to aggregate in the presence of specific anions and body fluids (Haney et al., 2017) or through non-specific interactions with host cells that cause cell lysis. Formulating peptides with various delivery vectors such as liposomes (Yang et al., 2011; Allen and Cullis, 2013), nanoparticles (d'Angelo et al., 2015; Nordström and Malmsten, 2017; Wadhwani et al., 2017) or covalently attaching them to bio-compatible polymers (Sahariah et al., 2015; Pranantyo et al., 2016; Kumar et al., 2017) can potentially mitigate some of these effects while retaining the desired biological functions, but further studies will be required to define how a given peptide-drug formulation combination impacts the pharmacokinetics, pharmacodynamics, and activity profile of a given therapeutic peptide.

CONCLUDING REMARKS

Faced with the prospect of a world without effective antibiotics, it is imperative that we continue the search for new anti-infective strategies and especially alternatives to conventional antibiotics. AMPs and HDPs have been championed as candidate drugs that could fill the void created by the rise of antibiotic resistance, largely by considering them as a new wave of antibiotics. Unfortunately, even after nearly 40 years of work since their discovery, we have yet to see this promise fulfilled. It could be argued that the writing is on the wall for AMPs and that we will never make these compounds into viable drugs. However, we maintain that HDPs overall still have tremendous potential as therapeutic options for bacterial infections but we have been focusing our efforts on mapping the wrong activity landscape related to anti-infective activity. The multifaceted nature of HDPs and their ability to influence a wide range of biological processes opens the door to expanding our understanding of other activity landscapes within the chemical space of HDPs. As our understanding of these other activity types improves, and the mechanistic details underpinning

these other processes are laid bare, this will undoubtedly lead to the development of HDP based drugs that are effective against infectious diseases as well as inflammatory conditions. Indeed, the antibacterial mountain of HDPs has probably been conquered, but the exploration of the peaks and valleys that make up the entire chemical landscape of HDPs has only just begun.

AUTHOR CONTRIBUTIONS

EH and SS wrote the first draft of the manuscript. All authors contributed to manuscript revision, approved the

final version and contributed to the conception of this work.

ACKNOWLEDGMENTS

Our research is currently supported by a grant from the Canadian Institutes for Health Research (CIHR) FDN-154287 to RH, and the National Sciences and Engineering Research Council of Canada through a Discovery Grant to SS. EH has been supported by a postdoctoral fellowship from the CIHR. RH holds a Canada Research Chair in Health and Genomics and a UBC Killam Professorship.

REFERENCES

- Åberg, A., Shingler, V., and Balsalobre, C. (2006). (p)ppGpp regulates type 1 fimbriation of *Escherichia coli* by modulating the expression of the site-specific recombinase FimB. *Mol. Microbiol.* 60, 1520–1533. doi: 10.1111/j.1365-2958.2006.05191.x
- Abdillahi, S. M., Maaß, T., Kasetty, G., Strömstedt, A. A., Baumgarten, M., Tati, R., et al. (2018). Collagen VI contains multiple host defense peptides with potent *in vivo* activity. *J. Immunol.* 201, 1007–1020. doi: 10.4049/jimmunol.1700602
- Akbari, R., Hakemi Vala, M., Hashemi, A., Aghazadeh, H., Sabatier, J.-M., and Pooshang Bagheri, K. (2018). Action mechanism of melittin-derived antimicrobial peptides, MDP1 and MDP2, de novo designed against multidrug resistant bacteria. *Amino Acids* doi: 10.1007/s00726-018-2596-5
- Allen, T. M., and Cullis, P. R. (2013). Liposomal drug delivery systems: From concept to clinical applications. *Adv. Drug Deliv. Rev.* 65, 36–48. doi: 10.1016/j.addr.2012.09.037
- Andersson, D. I., Hughes, D., and Kubicek-Sutherland, J. Z. (2016). Mechanisms and consequences of bacterial resistance to antimicrobial peptides. *Drug Resist. Updat.* 26, 43–57. doi: 10.1016/j.drup.2016.04.002
- Andresen, L., Tenson, T., and Haurlyuk, V. (2016). Cationic bactericidal peptide 1018 does not specifically target the stringent response alarmone (p)ppGpp. *Sci. Rep.* 6:36549. doi: 10.1038/srep36549
- Archer, N. K., Mazaitis, M. J., Costerton, J. W., Leid, J. G., Powers, M. E., and Shirliff, M. E. (2011). *Staphylococcus aureus* biofilms: properties, regulation and roles in human disease. *Virulence* 2, 445–459. doi: 10.4161/viru.2.5.17724
- Arias, M., Hilchie, A. L., Haney, E. F., Bolscher, J. G. M., Hyndman, M. E., Hancock, R. E. W., et al. (2017). Anticancer activities of bovine and human lactoferricin-derived peptides. *Biochem. Cell Biol.* 95, 91–98. doi: 10.1139/bcb-2016-0175
- Arias, M., Piga, K. B., Hyndman, E. M., and Vogel, H. J. (2018). Improving the activity of Trp-rich antimicrobial peptides by Arg/Lys substitutions and changes in the length of cationic residues. *Biomolecules* 8:E19. doi: 10.3390/biom8020019
- Augustin, R., Anton-Erxleben, F., Jungnickel, S., Hemmrich, G., Spudy, B., Podschun, R., et al. (2009). Activity of the novel peptide Arminin against multidrug-resistant human pathogens shows the considerable potential of phylogenetically ancient organisms as drug sources. *Antimicrob. Agents Chemother.* 53, 5245–5250. doi: 10.1128/AAC.00826-09
- Bader, M. W., Navarre, W. W., Shiau, W., Nikaido, H., Frye, J. G., McClelland, M., et al. (2003). Regulation of *Salmonella typhimurium* virulence gene expression by cationic antimicrobial peptides. *Mol. Microbiol.* 50, 219–230. doi: 10.1046/j.1365-2958.2003.03675.x
- Batoni, G., Maisetta, G., and Esin, S. (2016). Antimicrobial peptides and their interaction with biofilms of medically relevant bacteria. *Biochim. Biophys. Acta* 1858, 1044–1060. doi: 10.1016/j.bbame.2015.10.013
- Bechinger, B., and Gorr, S.-U. (2017). Antimicrobial peptides: Mechanisms of action and resistance. *J. Dent. Res.* 96, 254–260. doi: 10.1177/0022034516679973
- Beisswenger, C., Kandler, K., Hess, C., Garn, H., Felgentreff, K., Wegmann, M., et al. (2006). Allergic airway inflammation inhibits pulmonary antibacterial host defense. *J. Immunol.* 177, 1833–1837. doi: 10.4049/jimmunol.177.3.1833
- Bevins, C. L., and Salzman, N. H. (2011). Paneth cells, antimicrobial peptides and maintenance of intestinal homeostasis. *Nat. Rev. Microbiol.* 9, 356–368. doi: 10.1038/nrmicro2546
- Bhan, I., Camargo, C. A., Wenger, J., Ricciardi, C., Ye, J., Borregaard, N., et al. (2011). Circulating levels of 25-hydroxyvitamin D and human cathelicidin in healthy adults. *J. Allergy Clin. Immunol.* 127, 1302–1304.e1. doi: 10.1016/j.jaci.2010.12.1097
- Blair, J. M. A., Webber, M. A., Baylay, A. J., Ogbolu, D. O., and Piddock, L. J. V. (2015). Molecular mechanisms of antibiotic resistance. *Nat. Rev. Microbiol.* 13, 42–51. doi: 10.1038/nrmicro3380
- Blondelle, S. E., and Houghten, R. A. (1996). Novel antimicrobial compounds identified using synthetic combinatorial library technology. *Trends Biotechnol.* 14, 60–65. doi: 10.1016/0167-7799(96)80922-X
- Blondelle, S. E., and Lohner, K. (2000). Combinatorial libraries: A tool to design antimicrobial and antifungal peptide analogues having lytic specificities for structure–activity relationship studies. *Pept. Sci.* 55, 74–87. doi: 10.1002/1097-0282(2000)55:1<74::AID-BIP70>3.0.CO;2-S
- Bolouri, H., Sävman, K., Wang, W., Thomas, A., Maurer, N., Dullaghan, E., et al. (2014). Innate defense regulator peptide 1018 protects against perinatal brain injury. *Ann. Neurol.* 75, 395–410. doi: 10.1002/ana.24087
- Boman, H. G., Agerberth, B., and Boman, A. (1993). Mechanisms of action on *Escherichia coli* of cecropin P1 and PR-39, two antibacterial peptides from pig intestine. *Infect. Immun.* 61, 2978–2984.
- Bowdish, D. M. E., Davidson, D. J., Lau, Y. E., Lee, K., Scott, M. G., and Hancock, R. E. W. (2005). Impact of LL-37 on anti-infective immunity. *J. Leukoc. Biol.* 77, 451–459. doi: 10.1189/jlb.0704380
- Bray, B. L. (2003). Large-scale manufacture of peptide therapeutics by chemical synthesis. *Nat. Rev. Drug Discov.* 2, 587–593. doi: 10.1038/nrd1133
- Brunetti, J., Falciani, C., Roscia, G., Pollini, S., Bindi, S., Scali, S., et al. (2016). *In vitro* and *in vivo* efficacy, toxicity, bio-distribution and resistance selection of a novel antibacterial drug candidate. *Sci. Rep.* 6:26077. doi: 10.1038/srep26077
- Bullard, R. S., Gibson, W., Bose, S. K., Belgrave, J. K., Eaddy, A. C., Wright, C. J., et al. (2008). Functional analysis of the host defense peptide human beta defensin-1: New insight into its potential role in cancer. *Mol. Immunol.* 45, 839–848. doi: 10.1016/j.molimm.2006.11.026
- Chen, X., Zhang, L., Wu, Y., Wang, L., Ma, C., Xi, X., et al. (2018). Evaluation of the bioactivity of a mastoparan peptide from wasp venom and of its analogues designed through targeted engineering. *Int. J. Biol. Sci.* 14, 599–607. doi: 10.7150/ijbs.23419
- Cheng, J. T. J., Hale, J. D., Elliot, M., Hancock, R. E. W., and Straus, S. K. (2009). Effect of membrane composition on antimicrobial peptides aurein 2.2 and 2.3 from Australian southern bell frogs. *Biophys. J.* 96, 552–565. doi: 10.1016/j.bpj.2008.10.012
- Cheng, J. T. J., Hale, J. D., Elliott, M., Hancock, R. E. W., and Straus, S. K. (2011). The importance of bacterial membrane composition in the structure and function of aurein 2.2 and selected variants. *Biochim. Biophys. Acta* 1808, 622–633. doi: 10.1016/j.bbame.2010.11.025
- Cheng, J. T. J., Hale, J. D., Kindrachuk, J., Jensen, H., Elliott, M., Hancock, R. E. W., et al. (2010). Importance of residue 13 and the C-terminus for the structure

- and activity of the antimicrobial peptide aurein 2.2. *Biophys. J.* 99, 2926–2935. doi: 10.1016/j.bpj.2010.08.077
- Cherkasov, A., Hilpert, K., Jenssen, H., Fjell, C. D., Waldbrook, M., Mullaly, S. C., et al. (2009). Use of artificial intelligence in the design of small peptide antibiotics effective against a broad spectrum of highly antibiotic-resistant superbugs. *ACS Chem. Biol.* 4, 65–74. doi: 10.1021/cb800240j
- Chileveru, H. R., Lim, S. A., Chairatana, P., Wommack, A. J., Chiang, I.-L., and Nolan, E. M. (2015). Visualizing attack of *Escherichia coli* by the antimicrobial peptide human defensin 5. *Biochemistry* 54, 1767–1777. doi: 10.1021/bi501483q
- Choi, H., and Lee, D. G. (2012). Synergistic effect of antimicrobial peptide arenicin-1 in combination with antibiotics against pathogenic bacteria. *Res. Microbiol.* 163, 479–486. doi: 10.1016/j.resmic.2012.06.001
- Coffelt, S. B., Waterman, R. S., Florez, L., Bentrup, K. H., zu, Zwezdaryk, K. J., Tomchuck, S. L., et al. (2008). Ovarian cancers overexpress the antimicrobial protein hCAP-18 and its derivative LL-37 increases ovarian cancer cell proliferation and invasion. *Int. J. Cancer* 122, 1030–1039. doi: 10.1002/ijc.23186
- Cosio, M. G., Saetta, M., and Agusti, A. (2009). Immunologic aspects of chronic obstructive pulmonary disease. *N. Engl. J. Med.* 360, 2445–2454. doi: 10.1056/NEJMra0804752
- Coussens, A. K., Wilkinson, R. J., Hanifa, Y., Nikolayevskyy, V., Elkington, P. T., Islam, K., et al. (2012). Vitamin D accelerates resolution of inflammatory responses during tuberculosis treatment. *Proc. Natl. Acad. Sci. U. S. A.* 109, 15449–15454. doi: 10.1073/pnas.1200072109
- Crosse, A. M., Greenway, D. L., and England, R. R. (2000). Accumulation of ppGpp and ppGp in *Staphylococcus aureus* 8325-4 following nutrient starvation. *Lett. Appl. Microbiol.* 31, 332–337. doi: 10.1046/j.1472-765x.2000.00822.x
- Dale, B. A., Tao, R., Kimball, J. R., and Jurevic, R. J. (2006). Oral antimicrobial peptides and biological control of caries. *BMC Oral Health* 6:S13. doi: 10.1186/1472-6831-6-S1-S13
- d'Angelo, I., Casciaro, B., Miro, A., Quaglia, F., Mangoni, M. L., and Ungaro, F. (2015). Overcoming barriers in *Pseudomonas aeruginosa* lung infections: engineered nanoparticles for local delivery of a cationic antimicrobial peptide. *Colloids Surf. B Biointerfaces* 135, 717–725. doi: 10.1016/j.colsurf.2015.08.027
- Dathe, M., Nikolenko, H., Meyer, J., Beyermann, M., and Bienert, M. (2001). Optimization of the antimicrobial activity of magainin peptides by modification of charge. *FEBS Lett.* 501, 146–150. doi: 10.1016/S0014-5793(01)02648-5
- Davidopoulou, S., Diza, E., Meneses, G., and Kalfas, S. (2012). Salivary concentration of the antimicrobial peptide LL-37 in children. *Arch. Oral Biol.* 57, 865–869. doi: 10.1016/j.archoralbio.2012.01.008
- de la Fuente-Núñez, C., Cardoso, M. H., de Souza Cândido, E., Franco, O. L., and Hancock, R. E. W. (2016). Synthetic antibiofilm peptides. *Biochim. Biophys. Acta* 1858, 1061–1069. doi: 10.1016/j.bbamem.2015.12.015
- de la Fuente-Núñez, C., Korolik, V., Bains, M., Nguyen, U., Breidenstein, E. B., Horsman, S., et al. (2012). Inhibition of bacterial biofilm formation and swarming motility by a small synthetic cationic peptide. *Antimicrob. Agents Chemother.* 56, 2696–2704. doi: 10.1128/AAC.00064-12
- de la Fuente-Núñez, C., Mansour, S. C., Wang, Z., Jiang, L., Breidenstein, E. B. M., Elliott, M., et al. (2014a). Anti-biofilm and immunomodulatory activities of peptides that inhibit biofilms formed by pathogens isolated from Cystic Fibrosis patients. *Antibiot.* 3, 509–526. doi: 10.3390/antibiotics3040509
- de la Fuente-Núñez, C., Reffuveille, F., Haney, E. F., Straus, S. K., and Hancock, R. E. W. (2014b). Broad-spectrum anti-biofilm peptide that targets a cellular stress response. *PLoS Pathog.* 10:e1004152. doi: 10.1371/journal.ppat.1004152
- de la Fuente-Núñez, C., Reffuveille, F., Mansour, S. C., Reckseidler-Zenteno, S. L., Hernández, D., Brackman, G., et al. (2015). D-enantiomeric peptides that eradicate wild-type and multidrug-resistant biofilms and protect against lethal *Pseudomonas aeruginosa* infections. *Chem. Biol.* 22, 196–205. doi: 10.1016/j.chembiol.2015.01.002
- de Oliveira, H. C., Michaloski, J. S., da Silva, J. F., Scorzoni, L., de Paula e Silva, A. C. A., Marcos, C. M., et al. (2016). Peptides derived from a phage display library inhibit adhesion and protect the host against infection by *Paracoccidioides brasiliensis* and *Paracoccidioides lutzii*. *Front. Pharmacol.* 7:509. doi: 10.3389/fphar.2016.00509
- Dixon, B. M., Barker, T., McKinnon, T., Cuomo, J., Frei, B., Borregaard, N., et al. (2012). Positive correlation between circulating cathelicidin antimicrobial peptide (hCAP18/LL-37) and 25-hydroxyvitamin D levels in healthy adults. *BMC Res. Notes* 5:575. doi: 10.1186/1756-0500-5-575
- Donald, C. D., Sun, C. Q., Lim, S. D., Macoska, J., Cohen, C., Amin, M. B., et al. (2003). Cancer-specific loss of beta-defensin 1 in renal and prostatic carcinomas. *Lab. Invest. J. Tech. Methods Pathol.* 83, 501–505. doi: 10.1097/01.LAB.0000063929.61760.F6
- Dosler, S., and Karaaslan, E. (2014). Inhibition and destruction of *Pseudomonas aeruginosa* biofilms by antibiotics and antimicrobial peptides. *Peptides* 62, 32–37. doi: 10.1016/j.peptides.2014.09.021
- Droin, N., Hendra, J.-B., Ducoroy, P., and Solary, E. (2009). Human defensins as cancer biomarkers and antitumour molecules. *J. Proteomics* 72, 918–927. doi: 10.1016/j.jprot.2009.01.002
- Elborn, J. S. (2016). Cystic fibrosis. *Lancet* 388, 2519–2531. doi: 10.1016/S0140-6736(16)00576-6
- Epand, R. M., Walker, C., Epand, R. F., and Magarvey, N. A. (2016). Molecular mechanisms of membrane targeting antibiotics. *Biochim. Biophys. Acta* 1858, 980–987. doi: 10.1016/j.bbamem.2015.10.018
- Fan, D., Coughlin, L. A., Neubauer, M. M., Kim, J., Kim, M. S., Zhan, X., et al. (2015). Activation of HIF-1 α and LL-37 by commensal bacteria inhibits *Candida albicans* colonization. *Nat. Med.* 21, 808–814. doi: 10.1038/nm.3871
- Fan, L., Sun, J., Zhou, M., Zhou, J., Lao, X., Zheng, H., et al. (2016). DRAMP: a comprehensive data repository of antimicrobial peptides. *Sci. Rep.* 6:24482. doi: 10.1038/srep24482
- Felício, M. R., Silva, O. N., Gonçalves, S., Santos, N. C., and Franco, O. L. (2017). Peptides with dual antimicrobial and anticancer activities. *Front. Chem.* 5:5. doi: 10.3389/fchem.2017.00005
- Fernández, L., Jenssen, H., Bains, M., Wiegand, I., Gooderham, W. J., and Hancock, R. E. W. (2012). The two-component system CprRS senses cationic peptides and triggers adaptive resistance in *Pseudomonas aeruginosa* independently of ParRS. *Antimicrob. Agents Chemother.* 56, 6212–6222. doi: 10.1128/AAC.01530-12
- Fjell, C. D., Hiss, J. A., Hancock, R. E. W., and Schneider, G. (2012). Designing antimicrobial peptides: form follows function. *Nat. Rev. Drug Discov.* 11, 37–51. doi: 10.1038/nrd3591
- Flachbartova, Z., Pulzova, L., Bencurova, E., Potocnakova, L., Comor, L., Bednarikova, Z., et al. (2016). Inhibition of multidrug resistant *Listeria monocytogenes* by peptides isolated from combinatorial phage display libraries. *Microbiol. Res.* 188–189, 34–41. doi: 10.1016/j.micres.2016.04.010
- Florin, T., Maracci, C., Graf, M., Karki, P., Klepacki, D., Berninghausen, O., et al. (2017). An antimicrobial peptide that inhibits translation by trapping release factors on the ribosome. *Nat. Struct. Mol. Biol.* 24, 752–757. doi: 10.1038/nsmb.3439
- Franzenburg, S., Walter, J., Künzel, S., Wang, J., Baines, J. F., Bosch, T. C. G., et al. (2013). Distinct antimicrobial peptide expression determines host species-specific bacterial associations. *Proc. Natl. Acad. Sci. U. S. A.* 110, E3730–E3738. doi: 10.1073/pnas.1304960110
- Freitas, C. G., Lima, S. M. F., Freire, M. S., Cantuária, A. P. C., Júnior, N. G. O., Santos, T. S., et al. (2017). An immunomodulatory peptide confers protection in an experimental candidemia murine model. *Antimicrob. Agents Chemother.* 61:e02518–16. doi: 10.1128/AAC.02518-16
- Friedrich, C. L., Rozek, A., Patrzykat, A., and Hancock, R. E. W. (2001). Structure and mechanism of action of an indolicidin peptide derivative with improved activity against gram-positive bacteria. *J. Biol. Chem.* 276, 24015–24022. doi: 10.1074/jbc.M009691200
- Ganz, T., Selsted, M. E., Szklarek, D., Harwig, S. S., Daher, K., Bainton, D. F., et al. (1985). Defensins. Natural peptide antibiotics of human neutrophils. *J. Clin. Invest.* 76, 1427–1435. doi: 10.1172/JCI112120
- Gaspar, D., Veiga, A. S., and Castanho, M. A. R. B. (2013). From antimicrobial to anticancer peptides. A review. *Antimicrob. Resist. Chemother.* 4:294. doi: 10.3389/fmicb.2013.00294
- Geboes, K., Dewit, O., Moreels, T. G., Faa, G., and Jouret-Mourin, A. (2018). “Inflammatory Bowel Diseases,” in *Colitis*, eds A. Jouret-Mourin, G. Faa, and K. Geboes (Cham: Springer), 107–140.
- Ghosh, S. K., Feng, Z., Fujioka, H., Lux, R., McCormick, T. S., and Weinberg, A. (2018). Conceptual perspectives: Bacterial antimicrobial peptide induction as a novel strategy for symbiosis with the human host. *Front. Microbiol.* 9:302. doi: 10.3389/fmicb.2018.00302
- Gier, M. G., de, Albada, H. B., Josten, M., Willems, R., Leavis, H., and Mansveld, R., van, et al. (2016). Synergistic activity of a short lipidated antimicrobial peptide (lipoAMP) and colistin or tobramycin against

- Pseudomonas aeruginosa* from cystic fibrosis patients. *MedChemComm* 7, 148–156. doi: 10.1039/C5MD00373C
- Goldman, M. J., Anderson, G. M., Stolzenberg, E. D., Kari, U. P., Zasloff, M., and Wilson, J. M. (1997). Human β -defensin-1 is a salt-sensitive antibiotic in lung that is inactivated in cystic fibrosis. *Cell* 88, 553–560. doi: 10.1016/S0092-8674(00)81895-4
- Gombart, A. F., Borregaard, N., and Koeffler, H. P. (2005). Human cathelicidin antimicrobial peptide (CAMP) gene is a direct target of the vitamin D receptor and is strongly up-regulated in myeloid cells by 1,25-dihydroxyvitamin D₃. *FASEB J.* 19, 1067–1077. doi: 10.1096/fj.04-3284com
- Grönberg, A., Mahlapuu, M., Stähle, M., Whately-Smith, C., and Rollman, O. (2014). Treatment with LL-37 is safe and effective in enhancing healing of hard-to-heal venous leg ulcers: a randomized, placebo-controlled clinical trial. *Wound Repair Regen.* 22, 613–621. doi: 10.1111/wrr.12211
- Grossmann, R. E., Zughaier, S. M., Liu, S., Lyles, R. H., and Tangpricha, V. (2012). Impact of vitamin D supplementation on markers of inflammation in adults with cystic fibrosis hospitalized for a pulmonary exacerbation. *Eur. J. Clin. Nutr.* 66, 1072–1074. doi: 10.1038/ejcn.2012.82
- Guidotti, G., Brambilla, L., and Rossi, D. (2017). Cell-penetrating peptides: From basic research to clinics. *Trends Pharmacol. Sci.* 38, 406–424. doi: 10.1016/j.tips.2017.01.003
- Guo, L., McLean, J. S., Yang, Y., Eckert, R., Kaplan, C. W., Kyme, P., et al. (2015). Precision-guided antimicrobial peptide as a targeted modulator of human microbial ecology. *Proc. Natl. Acad. Sci. U. S. A.* 112, 7569–7574. doi: 10.1073/pnas.1506207112
- Gwyer Findlay, E., Currie, S. M., and Davidson, D. J. (2013). Cationic host defence peptides: potential as antiviral therapeutics. *BioDrugs* 27, 479–493. doi: 10.1007/s40259-013-0039-0
- Hale, J. D., and Hancock, R. E. (2007). Alternative mechanisms of action of cationic antimicrobial peptides on bacteria. *Expert Rev. Anti Infect. Ther.* 5, 951–959. doi: 10.1586/14787210.5.6.951
- Hancock, R. E. (2001). Cationic peptides: effectors in innate immunity and novel antimicrobials. *Lancet Infect. Dis.* 1, 156–164. doi: 10.1016/S1473-3099(01)00092-5
- Hancock, R. E., and Sahl, H.-G. (2013). New strategies and compounds for anti-infective treatment. *Curr. Opin. Microbiol.* 16, 519–521. doi: 10.1016/j.mib.2013.08.004
- Hancock, R. E. W., Haney, E. F., and Gill, E. E. (2016). The immunology of host defence peptides: beyond antimicrobial activity. *Nat. Rev. Immunol.* 16, 321–334. doi: 10.1038/nri.2016.29
- Hancock, R. E. W., and Sahl, H.-G. (2006). Antimicrobial and host-defense peptides as new anti-infective therapeutic strategies. *Nat. Biotechnol.* 24, 1551–1557. doi: 10.1038/nbt1267
- Haney, E. F., Brito-Sánchez, Y., Trimble, M. J., Mansour, S. C., Cherkasov, A., and Hancock, R. E. W. (2018a). Computer-aided discovery of peptides that specifically attack bacterial biofilms. *Sci. Rep.* 8:1871. doi: 10.1038/s41598-018-19669-4
- Haney, E. F., and Hancock, R. E. W. (2013). Peptide design for antimicrobial and immunomodulatory applications. *Biopolymers* 100, 572–583. doi: 10.1002/bip.22250
- Haney, E. F., Mansour, S. C., Hilchie, A. L., de la Fuente-Núñez, C., and Hancock, R. E. W. (2015). High throughput screening methods for assessing antibiofilm and immunomodulatory activities of synthetic peptides. *Peptides* 71, 276–285. doi: 10.1016/j.peptides.2015.03.015
- Haney, E. F., Pletzer, D., and Hancock, R. E. W. (2018b). “Impact of host defense peptides on chronic wounds and infections,” in *SpringerLink Recent Clinical Techniques, Results, and Research in Wounds*, ed M. A. Shiffman (Cham: Springer), 1–17.
- Haney, E. F., Wu, B., Lee, K., Hilchie, A. L., and Hancock, R. E. W. (2017). Aggregation and its influence on the immunomodulatory activity of synthetic innate defense regulator peptides. *Cell Chem. Biol.* 24, 969–980.e4. doi: 10.1016/j.chembiol.2017.07.010
- Harder, J., Meyer-Hoffert, U., Teran, L. M., Schwichtenberg, L., Bartels, J., Maune, S., et al. (2000). Mucoid *Pseudomonas aeruginosa*, TNF- α , and IL-1 β , but not IL-6, induce human β -defensin-2 in respiratory epithelia. *Am. J. Respir. Cell Mol. Biol.* 22, 714–721. doi: 10.1165/ajrcmb.22.6.4023
- Harris, F., Dennison, S. R., and Phoenix, D. A. (2009). Anionic antimicrobial peptides from eukaryotic organisms. *Curr. Protein Pept. Sci.* 10, 585–606. doi: 10.2174/138920309789630589
- Hata, T. R., Kotol, P., Jackson, M., Nguyen, M., Paik, A., Udall, D., et al. (2008). Administration of oral vitamin D induces cathelicidin production in atopic individuals. *J. Allergy Clin. Immunol.* 122, 829–831. doi: 10.1016/j.jaci.2008.08.020
- He, H., Cooper, J. N., Mishra, A., and Raskin, D. M. (2012). Stringent response regulation of biofilm formation in *Vibrio cholerae*. *J. Bacteriol.* 194, 2962–2972. doi: 10.1128/JB.00014-12
- Heilborn, J. D., Nilsson, M. F., Jimenez, C. I. C., Sandstedt, B., Borregaard, N., Tham, E., et al. (2005). Antimicrobial protein hCAP18/LL-37 is highly expressed in breast cancer and is a putative growth factor for epithelial cells. *Int. J. Cancer* 114, 713–719. doi: 10.1002/ijc.20795
- Henninot, A., Collins, J. C., and Nuss, J. M. (2018). The current state of peptide drug discovery: back to the future? *J. Med. Chem.* 61, 1382–1414. doi: 10.1021/acs.jmedchem.7b00318
- Hiemstra, P. S., Amatngalim, G. D., van der Does, A. M., and Taube, C. (2016). Antimicrobial peptides and innate lung defenses: role in infectious and noninfectious lung diseases and therapeutic applications. *Chest* 149, 545–551. doi: 10.1378/chest.15-1353
- Hilchie, A. L., Sharon, A. J., Haney, E. F., Hoskin, D. W., Bally, M. B., Franco, O. L., et al. (2016). Mastoparan is a membranolytic anti-cancer peptide that works synergistically with gemcitabine in a mouse model of mammary carcinoma. *Biochim. Biophys. Acta* 1858, 3195–3204. doi: 10.1016/j.bbame.2016.09.021
- Hilpert, K., Elliott, M. R., Volkmer-Engert, R., Henklein, P., Donini, O., Zhou, Q., et al. (2006). Sequence requirements and an optimization strategy for short antimicrobial peptides. *Chem. Biol.* 13, 1101–1107. doi: 10.1016/j.chembiol.2006.08.014
- Ho, S., Pothoulakis, C., and Koon, H. W. (2013). Antimicrobial peptides and colitis. *Curr. Pharm. Des.* 19, 40–47. doi: 10.2174/1381612811306010040
- Holani, R., Marin, M. S., Kastelic, J. P., and Cobo, E. R. (2018). “Chapter 7 - Host defense peptides as innate immunomodulators in the pathogenesis of colitis,” in *Antimicrobial Peptides in Gastrointestinal Diseases*, ed C. H. Cho (Cambridge: Academic Press), 133–164.
- Holgate, S. T., Wenzel, S., Postma, D. S., Weiss, S. T., Renz, H., and Sly, P. D. (2015). Asthma. *Nat. Rev. Dis. Primer* 1:15025. doi: 10.1016/B978-0-12-415847-4.00096-3
- Hollmann, A., Martínez, M., Noguera, M. E., Augusto, M. T., Disalvo, A., Santos, N. C., et al. (2016). Role of amphipathicity and hydrophobicity in the balance between hemolysis and peptide-membrane interactions of three related antimicrobial peptides. *Colloids Surf. B Biointerfaces* 141, 528–536. doi: 10.1016/j.colsurfb.2016.02.003
- Hollox, E. J., Huffmeier, U., Zeeuwen, P. L. J. M., Palla, R., Lascorz, J., Rodijk-Olthuis, D., et al. (2008). Psoriasis is associated with increased β -defensin genomic copy number. *Nat. Genet.* 40, 23–25. doi: 10.1038/ng.2007.48
- Huse, K., Taudien, S., Groth, M., Rosenstiel, P., Szafranski, K., Hiller, M., et al. (2008). Genetic variants of the copy number polymorphic β -defensin locus are associated with sporadic prostate cancer. *Tumour Biol. J. Int. Soc. Oncodevelopmental Biol. Med.* 29, 83–92. doi: 10.1159/000135688
- Hwang, I., Hwang, J.-S., Hwang, J. H., Choi, H., Lee, E., Kim, Y., et al. (2013). Synergistic effect and antibiofilm activity between the antimicrobial peptide coprisin and conventional antibiotics against opportunistic bacteria. *Curr. Microbiol.* 66, 56–60. doi: 10.1007/s00284-012-0239-8
- James, G. A., Swogger, E., Wolcott, R., Pulcini, E., deLancey, S. and Sestrich, J., et al. (2008). Biofilms in chronic wounds. *Wound Repair Regen.* 16, 37–44. doi: 10.1111/j.1524-475X.2007.00321.x
- Jiang, W., Sunkara, L. T., Zeng, X., Deng, Z., Myers, S. M., and Zhang, G. (2013). Differential regulation of human cathelicidin LL-37 by free fatty acids and their analogs. *Peptides* 50, 129–138. doi: 10.1016/j.peptides.2013.10.008
- Jin, G., and Weinberg, A. (2018). Human antimicrobial peptides and cancer. *Semin. Cell Dev. Biol.* doi: 10.1016/j.semcdb.2018.04.006. [Epub ahead of print].
- Joo, H.-S., Fu, C.-I., and Otto, M. (2016). Bacterial strategies of resistance to antimicrobial peptides. *Philos. Trans. R. Soc. B* 371:20150292. doi: 10.1098/rstb.2015.0292
- Kelly, C. P., and LaMont, J. T. (2008). *Clostridium difficile* — More difficult than ever. *N. Engl. J. Med.* 359, 1932–1940. doi: 10.1056/NEJMra0707500

- Kilian, M., Chapple, I. L. C., Hannig, M., Marsh, P. D., Meuric, V., Pedersen, A. M. L., et al. (2016). The oral microbiome – an update for oral healthcare professionals. *Br. Dent. J.* 221, 657–666. doi: 10.1038/sj.bdj.2016.865
- Kilsgård, O., Andersson, P., Malmsten, M., Nordin, S. L., Linge, H. M., Eliasson, M., et al. (2012). Peptidylarginine deiminase present in the airways during tobacco smoking and inflammation can citrullinate the host defense peptide LL-37, resulting in altered activities. *Am. J. Respir. Cell Mol. Biol.* 46, 240–248. doi: 10.1165/rcmb.2010-0500OC
- Kim, C.-H., Go, H.-J., Oh, H. Y., Park, J. B., Lee, T. K., Seo, J.-K., et al. (2018). Identification of a novel antimicrobial peptide from the sea star *Patiria pectinifera*. *Dev. Comp. Immunol.* 86, 203–213. doi: 10.1016/j.dci.2018.05.002
- Kovach, M. A., Ballinger, M. N., Newstead, M. W., Zeng, X., Bhan, U., Yu, F., et al. (2012). Cathelicidin-related antimicrobial peptide is required for effective lung mucosal immunity in Gram-negative bacterial pneumonia. *J. Immunol.* 189, 304–311. doi: 10.4049/jimmunol.1103196
- Koziej, J., Bryzek, D., Sroka, A., Maresz, K., Glowczyk, I., Bielecka, E., et al. (2014). Citrullination alters immunomodulatory function of LL-37 essential for prevention of endotoxin-induced sepsis. *J. Immunol.* 192, 5363–5372. doi: 10.4049/jimmunol.1303062
- Kozłowska, J., Vermeer, L. S., Rogers, G. B., Rehnuma, N., Amos, S.-B. T. A., Koller, G., et al. (2014). Combined systems approaches reveal highly plastic responses to antimicrobial peptide challenge in *Escherichia coli*. *PLoS Pathog.* 10:e1004104. doi: 10.1371/journal.ppat.1004104
- Kragol, G., Lovas, S., Varadi, G., Condie, B. A., Hoffmann, R., and Otvos, L. (2001). The antibacterial peptide pyrrolicorin inhibits the ATPase actions of DnaK and prevents chaperone-assisted protein folding. *Biochemistry* 40, 3016–3026. doi: 10.1021/bi002656a
- Kreuter, A., Jaouhar, M., Skrygan, M., Tigges, C., Stücker, M., Altmeyer, P., et al. (2011). Expression of antimicrobial peptides in different subtypes of cutaneous lupus erythematosus. *J. Am. Acad. Dermatol.* 65, 125–133. doi: 10.1016/j.jaad.2010.12.012
- Kumar, P., Kizhakkedathu, J. N., and Straus, S. K. (2018). Antimicrobial peptides: diversity, mechanism of action and strategies to improve the activity and biocompatibility *in vivo*. *Biomolecules* 8:E4. doi: 10.3390/biom8010004
- Kumar, P., Takayesu, A., Abbasi, U., Kalathottukaren, M. T., Abbina, S., Kizhakkedathu, J. N., et al. (2017). Antimicrobial peptide–polymer conjugates with high activity: Influence of polymer molecular weight and peptide sequence on antimicrobial activity, proteolysis, and biocompatibility. *ACS Appl. Mater. Inter.* 9, 37575–37586. doi: 10.1021/acsami.7b09471
- Kuroda, K., Okumura, K., Isogai, H., and Isogai, E. (2015). The human cathelicidin antimicrobial peptide LL-37 and mimics are potential anticancer drugs. *Front. Oncol.* 5:144. doi: 10.3389/fonc.2015.00144
- Lai, Y., Villaruz, A. E., Li, M., Cha, D. J., Sturdevant, D. E., and Otto, M. (2007). The human anionic antimicrobial peptide dermcidin induces proteolytic defence mechanisms in staphylococci. *Mol. Microbiol.* 63, 497–506. doi: 10.1111/j.1365-2958.2006.05540.x
- Lande, R., Botti, E., Jandus, C., Dojcinovic, D., Fanelli, G., Conrad, C., et al. (2014). The antimicrobial peptide LL37 is a T-cell autoantigen in psoriasis. *Nat. Commun.* 5:5621. doi: 10.1038/ncomms5621
- Lande, R., Gregorio, J., Facchinetti, V., Chatterjee, B., Wang, Y.-H., Homey, B., et al. (2007). Plasmacytoid dendritic cells sense self-DNA coupled with antimicrobial peptide. *Nature* 449, 564–569. doi: 10.1038/nature06116
- Lau, Y. E., Rozek, A., Scott, M. G., Goosney, D. L., Davidson, D. J., and Hancock, R. E. W. (2005). Interaction and cellular localization of the human host defense peptide LL-37 with lung epithelial cells. *Infect. Immun.* 73, 583–591. doi: 10.1128/IAI.73.1.583-591.2005
- Lázár, V., Martins, A., Spohn, R., Daruka, L., Grézel, G., Fekete, G., et al. (2018). Collateral sensitivity to antimicrobial peptides. *Nat. Microbiol.* 3, 718–731. doi: 10.1038/s41564-018-0164-0
- Le, C.-F., Gudimella, R., Razali, R., Manikam, R., and Sekaran, S. D. (2016). Transcriptome analysis of *Streptococcus pneumoniae* treated with the designed antimicrobial peptides, DM3. *Sci. Rep.* 6:26828. doi: 10.1038/srep26828
- Lee, E. Y., Lee, M. W., Fulan, B. M., Ferguson, A. L., and Wong, G. C. L. (2017). What can machine learning do for antimicrobial peptides, and what can antimicrobial peptides do for machine learning? *Interface Focus* 7:20160153. doi: 10.1098/rsfs.2016.0153
- Lee, T.-H., Hall, K. N., and Aguilar, M.-I. (2016). Antimicrobial peptide structure and mechanism of action: a focus on the role of membrane structure. *Curr. Top. Med. Chem.* 16, 25–39. doi: 10.2174/1568026615666150703121700
- Lehrer, R. I., Barton, A., Daher, K. A., Harwig, S. S., Ganz, T., and Selsted, M. E. (1989). Interaction of human defensins with *Escherichia coli*. Mechanism of bactericidal activity. *J. Clin. Invest.* 84, 553–561. doi: 10.1172/JCI114198
- Leptihn, S., Har, J. Y., Wohland, T., and Ding, J. L. (2010). Correlation of charge, hydrophobicity, and structure with antimicrobial activity of S1 and MIRIAM peptides. *Biochemistry* 49, 9161–9170. doi: 10.1021/bi1011578
- Lewies, A., Du Plessis, L. H., and Wentzel, J. F. (2018). Antimicrobial peptides: the Achilles' heel of antibiotic resistance? *Probiotics Antimicrob. Proteins* doi: 10.1007/s12602-018-9465-0. [Epub ahead of print].
- Li, W., Tailhades, J., O'Brien-Simpson, N. M., Separovic, F., Otvos, L., Hossain, M. A., et al. (2014). Proline-rich antimicrobial peptides: potential therapeutics against antibiotic-resistant bacteria. *Amino Acids* 46, 2287–2294. doi: 10.1007/s00726-014-1820-1
- Lin, Q., Deslouches, B., Montelaro, R. C., and Di, Y. P. (2018). Prevention of ESKAPE pathogen biofilm formation by antimicrobial peptides WLB2 and LL37. *Int. J. Antimicrob. Agents* 52, 667–672. doi: 10.1016/j.ijantimicag.2018.04.019
- Liu, P. T., Stenger, S., Li, H., Wenzel, L., Tan, B. H., Krutzik, S. R., et al. (2006). Toll-like receptor triggering of a vitamin D-mediated human antimicrobial response. *Science* 311, 1770–1773. doi: 10.1126/science.1123933
- Loose, C., Jensen, K., Rigoutsos, I., and Stephanopoulos, G. (2006). A linguistic model for the rational design of antimicrobial peptides. *Nature* 443, 867–869. doi: 10.1038/nature05233
- Lopez, D., Vlamakis, H., and Kolter, R. (2010). Biofilms. *Cold Spring Harb. Perspect. Biol.* 2:a000398. doi: 10.1101/cshperspect.a000398
- Loutet, S. A., and Valvano, M. A. (2011). Extreme antimicrobial peptide and polymyxin B resistance in the genus *Burkholderia*. *Front. Microbiol.* 2:159. doi: 10.3389/fmicb.2011.00159
- Luca, M. D., Maccari, G., Maisetta, G., and Batoni, G. (2015). BaAMPs: the database of biofilm-active antimicrobial peptides. *Biofouling* 31, 193–199. doi: 10.1080/08927014.2015.1021340
- Luo, Y., McLean, D. T. F., Linden, G. J., McAuley, D. F., McMullan, R., and Lundy, F. T. (2017). The naturally occurring host defense peptide, LL-37, and its truncated mimetics KE-18 and KR-12 have selected biocidal and antibiofilm activities against *Candida albicans*, *Staphylococcus aureus*, and *Escherichia coli* *in vitro*. *Front. Microbiol.* 8:544. doi: 10.3389/fmicb.2017.00544
- Maccari, G., Luca, M. D., Nifosi, R., Cardarelli, F., Signore, G., Boccardi, C., et al. (2013). Antimicrobial peptides design by evolutionary multiobjective optimization. *PLoS Comput. Biol.* 9:e1003212. doi: 10.1371/journal.pcbi.1003212
- Mader, J. S., Mookherjee, N., Hancock, R. E. W., and Bleackley, R. C. (2009). The human host defense peptide LL-37 induces apoptosis in a calpain- and apoptosis-inducing factor-dependent manner involving Bax activity. *Mol. Cancer Res.* 7, 689–702. doi: 10.1158/1541-7786.MCR-08-0274
- Mahlapuu, M., Håkansson, J., Ringstad, L., and Björn, C. (2016). Antimicrobial peptides: An emerging category of therapeutic agents. *Front. Cell. Infect. Microbiol.* 6:194. doi: 10.3389/fcimb.2016.00194
- Majchrzykiewicz, J. A., Kuipers, O. P., and Bijlsma, J. J. E. (2010). Generic and specific adaptive responses of *Streptococcus pneumoniae* to challenge with three distinct antimicrobial peptides, Bacitracin, LL-37, and Nisin. *Antimicrob. Agents Chemother.* 54, 440–451. doi: 10.1128/AAC.00769-09
- Makrygiannakis, D., Hermansson, M., Ulfgrén, A.-K., Nicholas, A. P., Zendman, A. J. W., Eklund, A., et al. (2008). Smoking increases peptidylarginine deiminase 2 enzyme expression in human lungs and increases citrullination in BAL cells. *Ann. Rheum. Dis.* 67, 1488–1492. doi: 10.1136/ard.2007.075192
- Mangoni, M. L., McDermott, A. M., and Zasloff, M. (2016). Antimicrobial peptides and wound healing: biological and therapeutic considerations. *Exp. Dermatol.* 25, 167–173. doi: 10.1111/exd.12929
- Mansour, S. C., de la Fuente-Núñez, C., and Hancock, R. E. W. (2015). Peptide IDR-1018: modulating the immune system and targeting bacterial biofilms to treat antibiotic-resistant bacterial infections. *J. Pept. Sci.* 21, 323–329. doi: 10.1002/psc.2708
- Mansour, S. C., Pletzer, D., de la Fuente-Núñez, C., Kim, P., Cheung, G. Y. C., Joo, H. S., et al. (2016). Bacterial abscess formation is controlled by the stringent

- stress response and can be targeted therapeutically. *EBio Med.* 12, 219–226. doi: 10.1016/j.ebiom.2016.09.015
- Marcinkiewicz, M., and Majewski, S. (2016). The role of antimicrobial peptides in chronic inflammatory skin diseases. *Adv. Dermatol. Allergol. Dermatol. Alergol.* 33, 6–12. doi: 10.5114/pdia.2015.48066
- Marquette, A., and Bechinger, B. (2018). Biophysical investigations elucidating the mechanisms of action of antimicrobial peptides and their synergism. *Biomolecules* 8:E18. doi: 10.3390/biom8020018
- Marr, A. K., Gooderham, W. J., and Hancock, R. E. W. (2006). Antibacterial peptides for therapeutic use: obstacles and realistic outlook. *Curr. Opin. Pharmacol.* 6, 468–472. doi: 10.1016/j.coph.2006.04.006
- Martens, E., and Demain, A. L. (2017). The antibiotic resistance crisis, with a focus on the United States. *J. Antibiot.* 70, 520–526. doi: 10.1038/ja.2017.30
- Mataraci, E., and Dosler, S. (2012). *In vitro* activities of antibiotics and antimicrobial cationic peptides alone and in combination against methicillin-resistant *Staphylococcus aureus* biofilms. *Antimicrob. Agents Chemother.* 56, 6366–6371. doi: 10.1128/AAC.01180-12
- Matsuzaki, K. (1998). Magainins as paradigm for the mode of action of pore forming polypeptides. *Biochim. Biophys. Acta* 1376, 391–400. doi: 10.1016/S0304-4157(98)00014-8
- Matsuzaki, K., Sugishita, K., Ishibe, N., Ueha, M., Nakata, S., Miyajima, K., et al. (1998). Relationship of membrane curvature to the formation of pores by magainin 2. *Biochemistry* 37, 11856–11863. doi: 10.1021/bi980539y
- Mayer, M. L., Blohmke, C. J., Falsafi, R., Fjell, C. D., Madera, L., Turvey, S. E., et al. (2013). Rescue of dysfunctional autophagy attenuates hyperinflammatory responses from cystic fibrosis cells. *J. Immunol.* 190, 1227–1238. doi: 10.4049/jimmunol.1201404
- Mburu, Y. K., Abe, K., Ferris, L. K., Sarkar, S. N., and Ferris, R. L. (2011). Human β -defensin 3 promotes NF- κ B-mediated CCR7 expression and anti-apoptotic signals in squamous cell carcinoma of the head and neck. *Carcinogenesis* 32, 168–174. doi: 10.1093/carcin/bgq236
- McDonald, M., Mannion, M., Pike, D., Lewis, K., Flynn, A., Brannan, A. M., et al. (2015). Structure–function relationships in histidine-rich antimicrobial peptides from Atlantic cod. *Biochim. Biophys. Acta* 1848, 1451–1461. doi: 10.1016/j.bbame.2015.03.030
- McGregor, D. P. (2008). Discovering and improving novel peptide therapeutics. *Curr. Opin. Pharmacol.* 8, 616–619. doi: 10.1016/j.coph.2008.06.002
- McPhee, J. B., Lewenza, S., and Hancock, R. E. W. (2003). Cationic antimicrobial peptides activate a two-component regulatory system, PmrA–PmrB, that regulates resistance to polymyxin B and cationic antimicrobial peptides in *Pseudomonas aeruginosa*. *Mol. Microbiol.* 50, 205–217. doi: 10.1046/j.1365-2958.2003.03673.x
- Mihajlovic, M., and Lazaridis, T. (2012). Charge distribution and imperfect amphipathicity affect pore formation by antimicrobial peptides. *Biochim. Biophys. Acta* 1818, 1274–1283. doi: 10.1016/j.bbame.2012.01.016
- Mookherjee, N., Lippert, D. N., Hamill, P., Falsafi, R., Nijnik, A., Kindrachuk, J., et al. (2009). Intracellular receptor for human host defense peptide LL-37 in monocytes. *J. Immunol.* 183, 2688–2696. doi: 10.4049/jimmunol.0802586
- Mor, A. (2009). Multifunctional host defense peptides: antiparasitic activities. *FEBS J.* 276, 6474–6482. doi: 10.1111/j.1742-4658.2009.07358.x
- Morizane, S., and Gallo, R. L. (2012). Antimicrobial peptides in the pathogenesis of psoriasis. *J. Dermatol.* 39, 225–230. doi: 10.1111/j.1346-8138.2011.01483.x
- Muniz, L. R., Knosp, C., and Yeretssian, G. (2012). Intestinal antimicrobial peptides during homeostasis, infection, and disease. *Front. Immunol.* 3:310. doi: 10.3389/fimmu.2012.00310
- Mylonakis, E., Podsiadlowski, L., Muhammed, M., and Vilcinskis, A. (2016). Diversity, evolution and medical applications of insect antimicrobial peptides. *Philos. Trans. R. Soc. Lond. B. Biol. Sci.* 371:20150290. doi: 10.1098/rstb.2015.0290
- Nagarajan, D., Nagarajan, T., Roy, N., Kulkarni, O., Ravichandran, S., Mishra, M., et al. (2018). Computational antimicrobial peptide design and evaluation against multidrug-resistant clinical isolates of bacteria. *J. Biol. Chem.* 293, 3492–3509. doi: 10.1074/jbc.M117.805499
- Nagpal, S., Kaur, K. J., Jain, D., and Salunke, D. M. (2009). Plasticity in structure and interactions is critical for the action of indolicidin, an antibacterial peptide of innate immune origin. *Protein Sci.* 11, 2158–2167. doi: 10.1110/ps.0211602
- Nguyen, L. T., Haney, E. F., and Vogel, H. J. (2011). The expanding scope of antimicrobial peptide structures and their modes of action. *Trends Biotechnol.* 29, 464–472. doi: 10.1016/j.tibtech.2011.05.001
- Nicholls, E. F., Madera, L., and Hancock, R. E. W. (2010). Immunomodulators as adjuvants for vaccines and antimicrobial therapy. *Ann. N. Y. Acad. Sci.* 1213, 46–61. doi: 10.1111/j.1749-6632.2010.05787.x
- Nichols, M., Kuljanin, M., Nategholeslam, M., Hoang, T., Vafaei, S., Tomberli, B., et al. (2013). Dynamic turn conformation of a short tryptophan-rich cationic antimicrobial peptide and its interaction with phospholipid membranes. *J. Phys. Chem. B* 117, 14697–14708. doi: 10.1021/jp4096985
- Nijnik, A., and Hancock, R. (2009). Host defence peptides: antimicrobial and immunomodulatory activity and potential applications for tackling antibiotic-resistant infections. *Emerg. Health Threats J.* 2:e1. doi: 10.3402/ehth.v2i0.7078
- Nikaido, H. (2003). Molecular basis of bacterial outer membrane permeability revisited. *Microbiol. Mol. Biol. Rev.* 67, 593–656. doi: 10.1128/MMBR.67.4.593-656.2003
- Nizet, V. (2006). Antimicrobial peptide resistance mechanisms of human bacterial pathogens. *Curr. Issues Mol. Biol.* 8, 11–26.
- Nordström, R., and Malmsten, M. (2017). Delivery systems for antimicrobial peptides. *Adv. Colloid Interface Sci.* 242, 17–34. doi: 10.1016/j.cis.2017.01.005
- Ojeda, N., Cárdenas, C., Guzmán, F., and Marshall, S. H. (2016). Chemical synthesis and *in vitro* evaluation of a phage display-derived peptide active against infectious salmon anemia virus. *Appl. Env. Microbiol.* 82, 2563–2571. doi: 10.1128/AEM.00184-16
- Okada, M., and Natori, S. (1983). Purification and characterization of an antibacterial protein from haemolymph of *Sarcophaga peregrina* (flesh-fly) larvae. *Biochem. J.* 211, 727–734. doi: 10.1042/bj2110727
- Ostaff, M. J., Stange, E. F., and Wehkamp, J. (2013). Antimicrobial peptides and gut microbiota in homeostasis and pathology. *EMBO Mol. Med.* 5, 1465–1483. doi: 10.1002/emmm.201201773
- Otvos L. Jr., Ostorhazi, E., Szabo, D., Zumbun, S. D., and Miller, L. L., Halasohoris, S. A., et al. (2018). Synergy between proline-rich antimicrobial peptides and small molecule antibiotics against selected Gram-negative pathogens *in vitro* and *in vivo*. *Front. Chem.* 6:309. doi: 10.3389/fchem.2018.00309
- Otvos, L. (2005). Antibacterial peptides and proteins with multiple cellular targets. *J. Pept. Sci.* 11, 697–706. doi: 10.1002/psc.698
- Overhage, J., Campisano, A., Bains, M., Torfs, E. C. W., Rehm, B. H. A., and Hancock, R. E. W. (2008). Human host defense peptide LL-37 prevents bacterial biofilm formation. *Infect. Immun.* 76, 4176–4182. doi: 10.1128/IAI.00318-08
- Pan, Y.-L., Cheng, J. T.-J., Hale, J., Pan, J., Hancock, R. E. W., and Straus, S. K. (2007). Characterization of the structure and membrane interaction of the antimicrobial peptides aurein 2.2 and 2.3 from Australian southern bell frogs. *Biophys. J.* 92, 2854–2864. doi: 10.1529/biophysj.106.097238
- Pane, K., Sgambati, V., Zanfardino, A., Smaldone, G., Cafaro, V., Angrisano, T., et al. (2016). A new cryptic cationic antimicrobial peptide from human apolipoprotein E with antibacterial activity and immunomodulatory effects on human cells. *FEBS J.* 283, 2115–2131. doi: 10.1111/febs.13725
- Park, C. B., Kim, H. S., and Kim, S. C. (1998). Mechanism of action of the antimicrobial peptide buforin II: buforin II kills microorganisms by penetrating the cell membrane and inhibiting cellular functions. *Biochem. Biophys. Res. Commun.* 244, 253–257. doi: 10.1006/bbrc.1998.8159
- Periasamy, S., Chatterjee, S. S., Cheung, G. Y. C., and Otto, M. (2012). Phenol-soluble modulins in staphylococci: what are they originally for? *Commun. Integr. Biol.* 5, 275–277. doi: 10.4161/cib.19420
- Peyssonnaud, C., Datta, V., Cramer, T., Doedens, A., Theodorakis, E. A., Gallo, R. L., et al. (2005). HIF-1 α expression regulates the bactericidal capacity of phagocytes. *J. Clin. Invest.* 115, 1806–1815. doi: 10.1172/JCI23865
- Pirtskhalava, M., Gabrielian, A., Cruz, P., Griggs, H. L., Squires, R. B., Hurt, D. E., et al. (2016). DBAASP v.2: an enhanced database of structure and antimicrobial/cytotoxic activity of natural and synthetic peptides. *Nucleic Acids Res.* 44, D1104–D1112. doi: 10.1093/nar/gkv1174
- Piyadasa, H., Hemshekhkar, M., Altieri, A., Basu, S., van der Does, A. M., Halayko, A. J., et al. (2018). Immunomodulatory innate defence regulator (IDR) peptide alleviates airway inflammation and hyper-responsiveness. *Thorax* 73, 908–917. doi: 10.1136/thoraxjnl-2017-210739
- Pletzer, D., and Hancock, R. E. W. (2016). Antibiofilm peptides: potential as broad-spectrum agents. *J. Bacteriol.* 198, 2572–2578. doi: 10.1128/JB.00017-16

- Pletzer, D., Mansour, S. C., and Hancock, R. E. W. (2018). Synergy between conventional antibiotics and anti-biofilm peptides in a murine, sub-cutaneous abscess model caused by recalcitrant ESKAPE pathogens. *PLoS Pathog.* 14:e1007084. doi: 10.1371/journal.ppat.1007084
- Pletzer, D., Wolfmeier, H., Bains, M., and Hancock, R. E. W. (2017). Synthetic peptides to target stringent response-controlled virulence in a *Pseudomonas aeruginosa* murine cutaneous infection model. *Front. Microbiol.* 8:1867. doi: 10.3389/fmicb.2017.01867
- Porto, W. F., Fensterseifer, I. C. M., Ribeiro, S. M., and Franco, O. L. (2018). Joker: An algorithm to insert patterns into sequences for designing antimicrobial peptides. *Biochim. Biophys. Acta* 1862, 2043–2052. doi: 10.1016/j.bbagen.2018.06.011
- Potrykus, K., and Cashel, M. (2008). (p)ppGpp: Still magical? *Annu. Rev. Microbiol.* 62, 35–51. doi: 10.1146/annurev.micro.62.081307.162903
- Pound, L. D., Patrick, C., Eberhard, C. E., Mottawea, W., Wang, G.-S., Abujamel, T., et al. (2015). Cathelicidin antimicrobial peptide: a novel regulator of islet function, islet regeneration and selected gut bacteria. *Diabetes* 64, 4135–4147. doi: 10.2337/db15-0788
- Powers, J. P., Martin, M. M., Goosney, D. L., and Hancock, R. E. W. (2006). The antimicrobial peptide polyphemusin localizes to the cytoplasm of *Escherichia coli* following treatment. *Antimicrob. Agents Chemother.* 50, 1522–1524. doi: 10.1128/AAC.50.4.1522-1524.2006
- Pranantyo, D., Xu, L. Q., Kang, E.-T., Mya, M. K., and Chan-Park, M. B. (2016). Conjugation of polyphosphoester and antimicrobial peptide for enhanced bactericidal activity and biocompatibility. *Biomacromolecules* 17, 4037–4044. doi: 10.1021/acs.biomac.6b01452
- Préfontaine, D., Lajoie-Kadoch, S., Foley, S., Audusseau, S., Olivenstein, R., Halayko, A. J., et al. (2009). Increased expression of IL-33 in severe asthma: evidence of expression by airway smooth muscle cells. *J. Immunol.* 183, 5094–5103. doi: 10.4049/jimmunol.0802387
- Pütsep, K., Carlsson, G., Boman, H. G., and Andersson, M. (2002). Deficiency of antibacterial peptides in patients with morbus Kostmann: an observation study. *Lancet* 360, 1144–1149. doi: 10.1016/S0140-6736(02)11201-3
- Raftery, T., Martineau, A. R., Greiller, C. L., Ghosh, S., McNamara, D., Bennett, K., et al. (2015). Effects of vitamin D supplementation on intestinal permeability, cathelicidin and disease markers in Crohn's disease: results from a randomised double-blind placebo-controlled study. *United Eur. Gastroenterol. J.* 3, 294–302. doi: 10.1177/2050640615572176
- Rao, S. S., Mohan, K. V. K., and Atreya, C. D. (2013). A peptide derived from phage display library exhibits antibacterial activity against *E. coli* and *Pseudomonas aeruginosa*. *PLoS ONE* 8:e56081. doi: 10.1371/journal.pone.0056081
- Rapaport, D., and Shai, Y. (1991). Interaction of fluorescently labeled pardaxin and its analogues with lipid bilayers. *J. Biol. Chem.* 266, 23769–23775.
- Reffuveille, F., Fuente-Núñez, C., de la, Mansour, S., and Hancock, R. E. W. (2014). A broad-spectrum antibiofilm peptide enhances antibiotic action against bacterial biofilms. *Antimicrob. Agents Chemother.* 58, 5363–5371. doi: 10.1128/AAC.03163-14
- Rivas-Santiago, B., Castañeda-Delgado, J. E., Santiago, C. E. R., Waldbrook, M., González-Curiel, I., León-Contreras, J. C., et al. (2013a). Ability of innate defence regulator peptides IDR-1002, IDR-HH2 and IDR-1018 to protect against *Mycobacterium tuberculosis* infections in animal models. *PLoS ONE* 8:e59119. doi: 10.1371/journal.pone.0059119
- Rivas-Santiago, B., Rivas Santiago, C. E., Castañeda-Delgado, J. E., León-Contreras, J. C., Hancock, R. E. W., and Hernandez-Pando, R. (2013b). Activity of LL-37, CRAMP and antimicrobial peptide-derived compounds E2, E6 and CP26 against *Mycobacterium tuberculosis*. *Int. J. Antimicrob. Agents* 41, 143–148. doi: 10.1016/j.ijantimicag.2012.09.015
- Rodríguez-Decuadro, S., Barraco-Vega, M., Dans, P. D., Pandolfi, V., Benko-Iseppon, A. M., and Cecchetto, G. (2018). Antimicrobial and structural insights of a new snakine-like peptide isolated from *Peltophorum dubium* (Fabaceae). *Amino Acids* 50, 1245–1259. doi: 10.1007/s00726-018-2598-3
- Roversi, D., Luca, V., Aureli, S., Park, Y., Mangoni, M. L., and Stella, L. (2014). How many antimicrobial peptide molecules kill a bacterium? The case of PMAP-23. *ACS Chem. Biol.* 9, 2003–2007. doi: 10.1021/cb500426r
- Rozek, T., Wegener, K. L., Bowie, J. H., Olver, I. N., Carver, J. A., Wallace, J. C., et al. (2000). The antibiotic and anticancer active aurein peptides from the Australian Bell Frogs *Litoria aurea* and *Litoria raniformis*. *Eur. J. Biochem.* 267, 5330–5341. doi: 10.1046/j.1432-1327.2000.01536.x
- Sahariah, P., Sørensen, K. K., Hjalmsdóttir, M. Á., Sigurjónsson, Ó. E., Jensen, K. J., Másson, M., et al. (2015). Antimicrobial peptide shows enhanced activity and reduced toxicity upon grafting to chitosan polymers. *Chem. Commun.* 51, 11611–11614. doi: 10.1039/C5CC04010H
- Salvado, M. D., Gennaro, A. D., Lindbom, L., Agerberth, B., and Haeggström, J. Z. (2013). Cathelicidin LL-37 induces angiogenesis via PGE2–EP3 signaling in endothelial cells, *in vivo* inhibition by a aspirin. *Arterioscler. Thromb. Vasc. Biol.* 33, 1965–1972. doi: 10.1161/ATVBAHA.113.301851
- Salzman, N. H., Hung, K., Haribhai, D., Chu, H., Karlsson-Sjöberg, J., Amir, E., et al. (2010). Enteric defensins are essential regulators of intestinal microbial ecology. *Nat. Immunol.* 11, 76–83. doi: 10.1038/ni.1825
- Sandgren, S., Wittrup, A., Cheng, F., Jönsson, M., Eklund, E., Busch, S., et al. (2004). The human antimicrobial peptide LL-37 transfers extracellular DNA plasmid to the nuclear compartment of mammalian cells via lipid rafts and proteoglycan-dependent endocytosis. *J. Biol. Chem.* 279, 17951–17956. doi: 10.1074/jbc.M311440200
- Sass, V., Schneider, T., Wilmes, M., Körner, C., Tossi, A., Novikova, N., et al. (2010). Human β -defensin 3 inhibits cell wall biosynthesis in *Staphylococci*. *Infect. Immun.* 78, 2793–2800. doi: 10.1128/IAI.00688-09
- Savini, F., Luca, V., Bocedi, A., Massoud, R., Park, Y., Mangoni, M. L., et al. (2017). Cell-density dependence of host-defense peptide activity and selectivity in the presence of host cells. *ACS Chem. Biol.* 12, 52–56. doi: 10.1021/acscchembio.6b00910
- Schauber, J., and Gallo, R. L. (2008). Antimicrobial peptides and the skin immune defense system. *J. Allergy Clin. Immunol.* 122, 261–266. doi: 10.1016/j.jaci.2008.03.027
- Schauber, J., Svanholm, C., Termén, S., Iffland, K., Menzel, T., Scheppach, W., et al. (2003). Expression of the cathelicidin LL-37 is modulated by short chain fatty acids in colonocytes: relevance of signalling pathways. *Gut* 52, 735–741. doi: 10.1136/gut.52.5.735
- Schneider, T., Kruse, T., Wimmer, R., Wiedemann, I., Sass, V., Pag, U., et al. (2010). Plectasin, a fungal defensin, targets the bacterial cell wall precursor lipid II. *Science* 328, 1168–1172. doi: 10.1126/science.1185723
- Scocchi, M., Tossi, A., and Gennaro, R. (2011). Proline-rich antimicrobial peptides: converging to a non-lytic mechanism of action. *Cell. Mol. Life Sci.* 68, 2317–2330. doi: 10.1007/s00018-011-0721-7
- Scott, M. G., Dullaghan, E., Mookherjee, N., Glavas, N., Waldbrook, M., Thompson, A., et al. (2007). An anti-infective peptide that selectively modulates the innate immune response. *Nat. Biotechnol.* 25, 465–472. doi: 10.1038/nbt1288
- Scott, M. G., Gold, M. R., and Hancock, R. E. W. (1999a). Interaction of cationic peptides with lipoteichoic acid and Gram-positive bacteria. *Infect. Immun.* 67, 6445–6453.
- Scott, M. G., Yan, H., and Hancock, R. E. (1999b). Biological properties of structurally related alpha-helical cationic antimicrobial peptides. *Infect. Immun.* 67, 2005–2009.
- Selsted, M. E., Brown, D. M., DeLange, R. J., Harwig, S. S., and Lehrer, R. I. (1985a). Primary structures of six antimicrobial peptides of rabbit peritoneal neutrophils. *J. Biol. Chem.* 260, 4579–4584.
- Selsted, M. E., Harwig, S. S., Ganz, T., Schilling, J. W., and Lehrer, R. I. (1985b). Primary structures of three human neutrophil defensins. *J. Clin. Invest.* 76, 1436–1439. doi: 10.1172/JCI112121
- Shah, P., Hsiao, F. S.-H., Ho, Y.-H., and Chen, C.-S. (2016). The proteome targets of intracellular targeting antimicrobial peptides. *Prpteomics* 16, 1225–1237. doi: 10.1002/pmic.201500380
- Shai, Y. (2002). Mode of action of membrane active antimicrobial peptides. *Biopolymers* 66, 236–248. doi: 10.1002/bip.10260
- Sharma, H., and Nagaraj, R. (2015). Human β -defensin 4 with non-native disulfide bridges exhibit antimicrobial activity. *PLoS ONE* 10:e0119525. doi: 10.1371/journal.pone.0119525
- Sieprawska-Lupa, M., Mydel, P., Krawczyk, K., Wójcik, K., Puklo, M., Lupa, B., et al. (2004). Degradation of human antimicrobial peptide LL-37 by *Staphylococcus aureus*-derived proteinases. *Antimicrob. Agents Chemother.* 48, 4673–4679. doi: 10.1128/AAC.48.12.4673-4679.2004
- Silva, O. N., Porto, W. F., Ribeiro, S. M., Batista, I., and Franco, O. L. (2018). Host-defense peptides and their potential use as biomarkers in human diseases. *Drug Discov. Today*. 23, 1666–1671. doi: 10.1016/j.drudis.2018.05.024

- Smith, J. J., Travis, S. M., Greenberg, E. P., and Welsh, M. J. (1996). Cystic fibrosis airway epithelia fail to kill bacteria because of abnormal airway surface fluid. *Cell* 85, 229–236. doi: 10.1016/S0092-8674(00)81099-5
- Sol, A., Ginesin, O., Chaushu, S., Karra, L., Copenhagen-Glazer, S., Ginsburg, I., et al. (2013). LL-37 opsonizes and inhibits biofilm formation of *Aggregatibacter actinomycetemcomitans* at subbactericidal concentrations. *Infect. Immun.* 81, 3577–3585. doi: 10.1128/IAI.01288-12
- Starr, C. G., He, J., and Wimley, W. C. (2016). Host cell interactions are a significant barrier to the clinical utility of peptide antibiotics. *ACS Chem. Biol.* 11, 3391–3399. doi: 10.1021/acscchembio.6b00843
- Steiner, H., Hultmark, D., Engström, Å., Bennich, H., and Boman, H. G. (1981). Sequence and specificity of two antibacterial proteins involved in insect immunity. *Nature* 292, 246–248. doi: 10.1038/292246a0
- Subbalakshmi, C., and Sitarum, N. (1998). Mechanism of antimicrobial action of indolicidin. *FEMS Microbiol. Lett.* 160, 91–96. doi: 10.1111/j.1574-6968.1998.tb12896.x
- Takahashi, D., Shukla, S. K., Prakash, O., and Zhang, G. (2010). Structural determinants of host defense peptides for antimicrobial activity and target cell selectivity. *Biochimie* 92, 1236–1241. doi: 10.1016/j.biochi.2010.02.023
- Taniguchi, M., Ochiai, A., Kondo, H., Fukuda, S., Ishiyama, Y., Saitoh, E., et al. (2016). Pyrrhocoricin, a proline-rich antimicrobial peptide derived from insect, inhibits the translation process in the cell-free *Escherichia coli* protein synthesis system. *J. Biosci. Bioeng.* 121, 591–598. doi: 10.1016/j.jbiosc.2015.09.002
- Tao, R., Jurevic, R. J., Coulton, K. K., Tsutsui, M. T., Roberts, M. C., Kimball, J. R., et al. (2005). Salivary antimicrobial peptide expression and dental caries experience in children. *Antimicrob. Agents Chemother.* 49, 3883–3888. doi: 10.1128/AAC.49.9.3883-3888.2005
- Tetens, J., Friedrich, J. J., Hartmann, A., Schwerin, M., Kalm, E., and Thaller, G. (2010). The spatial expression pattern of antimicrobial peptides across the healthy bovine udder. *J. Dairy Sci.* 93, 775–783. doi: 10.3168/jds.2009-2729
- Tomasinsig, L., Scocchi, M., Mettullo, R., and Zanetti, M. (2004). Genome-wide transcriptional profiling of the *Escherichia coli* response to a proline-rich antimicrobial peptide. *Antimicrob. Agents Chemother.* 48, 3260–3267. doi: 10.1128/AAC.48.9.3260-3267.2004
- Tomasinsig, L., Skerlavaj, B., Papo, N., Giabbai, B., Shai, Y., and Zanetti, M. (2006). Mechanistic and functional studies of the interaction of a proline-rich antimicrobial peptide with mammalian cells. *J. Biol. Chem.* 281, 383–391. doi: 10.1074/jbc.M510354200
- Torrent, M., Andreu, D., Nogues, V. M., and Boix, E. (2011). Connecting peptide physicochemical and antimicrobial properties by a rational prediction model. *PLoS ONE* 6:e16968. doi: 10.1371/journal.pone.0016968
- Tucker, A. T., Leonard, S. P., DuBois, C. D., Knauf, G. A., Cunningham, A. L., Wilke, C. O., et al. (2018). Discovery of next-generation antimicrobials through bacterial self-screening of surface-displayed peptide libraries. *Cell* 172, 618–628.e13. doi: 10.1016/j.cell.2017.12.009
- Turner, J., Cho, Y., Dinh, N. N., Waring, A. J., and Lehrer, R. I. (1998). Activities of LL-37, a cathelin-associated antimicrobial peptide of human neutrophils. *Antimicrob. Agents Chemother.* 42, 2206–2214. doi: 10.1128/AAC.42.9.2206
- Vaara, M. (1992). Agents that increase the permeability of the outer membrane. *Microbiol. Rev.* 56, 395–411.
- van den Bogaart, G., Guzmán, J. V., Mika, J. T., and Poolman, B. (2008). On the mechanism of pore formation by melittin. *J. Biol. Chem.* 283, 33854–33857. doi: 10.1074/jbc.M805171200
- Verjans, E.-T., Zels, S., Luyten, W., Landuyt, B., and Schoofs, L. (2016). Molecular mechanisms of LL-37-induced receptor activation: an overview. *Peptides* 85, 16–26. doi: 10.1016/j.peptides.2016.09.002
- Vlieghe, P., Lisowski, V., Martinez, J., and Khrestchatsky, M. (2010). Synthetic therapeutic peptides: science and market. *Drug Discov. Today* 15, 40–56. doi: 10.1016/j.drudis.2009.10.009
- Vollmer, W., and Bertsche, U. (2008). Murein (peptidoglycan) structure, architecture and biosynthesis in *Escherichia coli*. *Biochim. Biophys. Acta* 1778, 1714–1734. doi: 10.1016/j.bbame.2007.06.007
- von Haussen, J., Koczulla, R., Shaykhiev, R., Herr, C., Pinkenburg, O., Reimer, D., et al. (2008). The host defence peptide LL-37/hCAP-18 is a growth factor for lung cancer cells. *Lung Cancer* 59, 12–23. doi: 10.1016/j.lungcan.2007.07.014
- Vos, T., Barber, R. M., Bell, B., Bertozzi-Villa, A., Biryukov, S., Bolliger, I., et al. (2015). Global, regional, and national incidence, prevalence, and years lived with disability for 301 acute and chronic diseases and injuries in 188 countries, 1990–2013: a systematic analysis for the Global Burden of Disease Study 2013. *Lancet* 386, 743–800. doi: 10.1016/S0140-6736(15)60692-4
- Wadhvani, P., Heidenreich, N., Podeyn, B., Bürck, J., and Ulrich, A. S. (2017). Antibiotic gold: tethering of antimicrobial peptides to gold nanoparticles maintains conformational flexibility of peptides and improves trypsin susceptibility. *Biomater. Sci.* 5, 817–827. doi: 10.1039/C7BM00069C
- Wang, G., Li, X., and Wang, Z. (2015a). APD3: the antimicrobial peptide database as a tool for research and education. *Nucleic Acids Res.* 44:D1087–93. doi: 10.1093/nar/gkv1278
- Wang, P., Wang, X., Yang, X., Liu, Z., Wu, M., and Li, G. (2013). Budesonide suppresses pulmonary antibacterial host defense by down-regulating cathelicidin-related antimicrobial peptide in allergic inflammation mice and in lung epithelial cells. *BMC Immunol.* 14:7. doi: 10.1186/1471-2172-14-7
- Wang, S., and Wang, Y. (2013). Peptidylarginine deiminases in citrullination, gene regulation, health and pathogenesis. *Biochim. Biophys. Acta* 1829, 1126–1135. doi: 10.1016/j.bbagr.2013.07.003
- Wang, Z., Fuente-Núñez, C., de la, Shen, Y., Haapasalo, M., and Hancock, R. E. W. (2015b). Treatment of oral multispecies biofilms by an anti-biofilm peptide. *PLoS ONE* 10:e0132512. doi: 10.1371/journal.pone.0132512
- Weerden, N. L., van der, Bleackley, M. R., and Anderson, M. A. (2013). Properties and mechanisms of action of naturally occurring antifungal peptides. *Cell. Mol. Life Sci.* 70, 3545–3570. doi: 10.1007/s00018-013-1260-1
- Wehkamp, J., Schmid, M., and Stange, E. F. (2007). Defensins and other antimicrobial peptides in inflammatory bowel disease. *Curr. Opin. Gastroenterol.* 23, 370–378. doi: 10.1097/MOG.0b013e328136c580
- Wieczorek, M., Jessen, H., Kindrachuk, J., Scott, W. R., Elliott, M., Hilpert, K., et al. (2010). Structural studies of a peptide with immune modulating and direct antimicrobial activity. *Chem. Biol.* 17, 970–980. doi: 10.1016/j.chembiol.2010.07.007
- Wiedemann, I., Breukink, E., van Kraaij, C., Kuipers, O. P., Bierbaum, G., de Kruijff, B., et al. (2001). Specific binding of nisin to the peptidoglycan precursor lipid II combines pore formation and inhibition of cell wall biosynthesis for potent antibiotic activity. *J. Biol. Chem.* 276, 1772–1779. doi: 10.1074/jbc.M006770200
- Wimley, W. C. (2010). Describing the mechanism of antimicrobial peptide action with the interfacial activity model. *ACS Chem. Biol.* 5, 905–917. doi: 10.1021/cb1001558
- Wolz, C., Geiger, T., and Goerke, C. (2010). The synthesis and function of the alarmone (p)ppGpp in firmicutes. *Int. J. Med. Microbiol.* 300, 142–147. doi: 10.1016/j.ijmm.2009.08.017
- Wu, B. C., Lee, A. H.-Y., and Hancock, R. E. W. (2017a). Mechanisms of the innate defense regulator peptide-1002 anti-inflammatory activity in a sterile inflammation mouse model. *J. Immunol.* 199, 3592–3603. doi: 10.4049/jimmunol.1700985
- Wu, M., Maier, E., Benz, R., and Hancock, R. E. W. (1999). Mechanism of interaction of different classes of cationic antimicrobial peptides with planar bilayers and with the cytoplasmic membrane of *Escherichia coli*. *Biochemistry* 38, 7235–7242. doi: 10.1021/bi9826299
- Wu, W. K. K., Wang, G., Coffelt, S. B., Betancourt, A. M., Lee, C. W., Fan, D., et al. (2010). Emerging roles of the host defense peptide LL-37 in human cancer and its potential therapeutic applications. *Int. J. Cancer* 127, 1741–1747. doi: 10.1002/ijc.25489
- Wu, X., Li, Z., Li, X., Tian, Y., Fan, Y., Yu, C., et al. (2017b). Synergistic effects of antimicrobial peptide DP7 combined with antibiotics against multidrug-resistant bacteria. *Drug Des. Devel. Ther.* 11, 939–946. doi: 10.2147/DDDT.S107195
- Wuerth, K., Lee, A. H. Y., Falsafi, R., Gill, E. E., and Hancock, R. E. W. (2018). Characterization of host responses during *Pseudomonas aeruginosa* acute lung infection in the lungs and blood and after treatment with the synthetic immunomodulatory peptide IDR-1002. *Infect. Immun.* 87:e00661-18. doi: 10.1128/IAI.00661-18
- Wuerth, K. C., Falsafi, R., and Hancock, R. E. W. (2017). Synthetic host defense peptide IDR-1002 reduces inflammation in *Pseudomonas aeruginosa* lung infection. *PLoS ONE* 12:e0187565. doi: 10.1371/journal.pone.0187565
- Xu, D., Zhang, B., Liao, C., Zhang, W., Wang, W., Chang, Y., et al. (2016). Human beta-defensin 3 contributes to the carcinogenesis of cervical

- cancer via activation of NF- κ B signaling. *Oncotarget* 7, 75902–75913. doi: 10.18632/oncotarget.12426
- Yadavalli, S. S., Carey, J. N., Leibman, R. S., Chen, A. I., Stern, A. M., Roggiani, M., et al. (2016). Antimicrobial peptides trigger a division block in *Escherichia coli* through stimulation of a signalling system. *Nat. Commun.* 7:12340. doi: 10.1038/ncomms12340
- Yang, K., Gitter, B., Rüger, R., Wieland, G. D., Chen, M., Liu, X., et al. (2011). Antimicrobial peptide-modified liposomes for bacteria targeted delivery of temoporfin in photodynamic antimicrobial chemotherapy. *Photochem. Photobiol. Sci.* 10, 1593–1601. doi: 10.1039/c1pp05100h
- Yang, L.-L., Zhan, M.-Y., Zhuo, Y.-L., Pan, Y.-M., Xu, Y., Zhou, X.-H., et al. (2018). Antimicrobial activities of a proline-rich proprotein from *Spodoptera litura*. *Dev. Comp. Immunol.* 87, 137–146. doi: 10.1016/j.dci.2018.06.011
- Yeaman, M. R., and Yount, N. Y. (2003). Mechanisms of antimicrobial peptide action and resistance. *Pharmacol. Rev.* 55, 27–55. doi: 10.1124/pr.55.1.2
- Yin, L. M., Edwards, M. A., Li, J., Yip, C. M., and Deber, C. M. (2012). Roles of hydrophobicity and charge distribution of cationic antimicrobial peptides in peptide-membrane interactions. *J. Biol. Chem.* 287, 7738–7745. doi: 10.1074/jbc.M111.303602
- Yoshida, M., Hinkley, T., Tsuda, S., Abul-Haija, Y. M., McBurney, R. T., Kulikov, V., et al. (2018). Using evolutionary algorithms and machine learning to explore sequence space for the discovery of antimicrobial peptides. *Chem* 4, 533–543. doi: 10.1016/j.chempr.2018.01.005
- Zasloff, M. (1987). Magainins, a class of antimicrobial peptides from *Xenopus* skin: isolation, characterization of two active forms, and partial cDNA sequence of a precursor. *Proc. Natl. Acad. Sci. U. S. A.* 84, 5449–5453. doi: 10.1073/pnas.84.15.5449
- Zasloff, M. (2009). Mysteries that still remain. *Biochim. Biophys. Acta* 1788, 1693–1694. doi: 10.1016/j.bbame.2009.04.011
- Zhang, C., Zhao, L., Ding, Y., Sheng, Q., Bai, H., An, Z., et al. (2016). Enhanced LL-37 expression following vitamin D supplementation in patients with cirrhosis and spontaneous bacterial peritonitis. *Liver Int.* 36, 68–75. doi: 10.1111/liv.12888
- Zhao, G., Usui, M. L., Lippman, S. I., James, G. A., Stewart, P. S., Fleckman, P., et al. (2013). Biofilms and inflammation in chronic wounds. *Adv. Wound Care* 2, 389–399. doi: 10.1089/wound.2012.0381
- Zorko, M., and Langel, Ü. (2005). Cell-penetrating peptides: mechanism and kinetics of cargo delivery. *Adv. Drug Deliv. Rev.* 57, 529–545. doi: 10.1016/j.addr.2004.10.010

Conflict of Interest Statement: HDPs, including some of those described here but published as open source articles, have been filed for patent protection by RH and EH and assigned to their employer the University of British Columbia, and licensed to ABT Innovations Inc., Victoria, Canada, in which the University of British Columbia, EH and RH own shares.

The remaining author declares that the research was conducted in the absence of any commercial or financial relationships that could be construed as a potential conflict of interest.

Copyright © 2019 Haney, Straus and Hancock. This is an open-access article distributed under the terms of the Creative Commons Attribution License (CC BY). The use, distribution or reproduction in other forums is permitted, provided the original author(s) and the copyright owner(s) are credited and that the original publication in this journal is cited, in accordance with accepted academic practice. No use, distribution or reproduction is permitted which does not comply with these terms.



Three Decades of Amyloid Beta Synthesis: Challenges and Advances

Johanes K. Kasim¹, Iman Kavianinia^{1,2,3}, Paul W. R. Harris^{1,2,3} and Margaret A. Brimble^{1,2,3*}

¹ School of Biological Sciences, The University of Auckland, Auckland, New Zealand, ² Maurice Wilkins Centre for Molecular Biodiscovery, The University of Auckland, Auckland, New Zealand, ³ School of Chemical Sciences, The University of Auckland, Auckland, New Zealand

Aggregation of the pathological amyloid beta (A β) isoform A β _{1–42} into senile plaques is a neuropathological hallmark of Alzheimer's disease (AD). The biochemical significance of this phenomenon therefore necessitates the need for ready access to A β _{1–42} for research purposes. Chemical synthesis of the peptide, however, is technically difficult to perform given its propensity to aggregate both on resin during solid phase peptide synthesis and in solution during characterization. This review presents a chronological summary of key publications in the field of A β _{1–42} synthesis, dating back from its maiden synthesis by Burdick et al. Challenges associated with the preparation of A β _{1–42} were identified, and the solutions designed over the course of time critically discussed herein. Ultimately, the intention of this review is to provide readers with an insight into the progress that has been made in the last three decades, and how this has advanced broader research in AD.

Keywords: Alzheimer's disease, dementia, neurodegenerative disorders, difficult peptide sequences, amyloid beta, peptide chemistry, solid phase peptide synthesis

OPEN ACCESS

Edited by:

Julio A. Camarero,
University of Southern California,
United States

Reviewed by:

Fernando Albericio,
University of KwaZulu-Natal,
South Africa
Max Julian Cryle,
Monash University, Australia

*Correspondence:

Margaret A. Brimble
m.brimble@auckland.ac.nz

Specialty section:

This article was submitted to
Chemical Biology,
a section of the journal
Frontiers in Chemistry

Received: 07 May 2019

Accepted: 19 June 2019

Published: 02 July 2019

Citation:

Kasim JK, Kavianinia I, Harris PWR
and Brimble MA (2019) Three
Decades of Amyloid Beta Synthesis:
Challenges and Advances.
Front. Chem. 7:472.
doi: 10.3389/fchem.2019.00472

INTRODUCTION

Alzheimer's disease (AD) is a degenerative disorder of the brain that was named after the German psychiatrist Alois Alzheimer, who in 1906 delivered a lecture at the 37th Conference of South-West German Psychiatrists in Tübingen, detailing his observations on a novel form of dementia that had befallen a 51-year-old Frankfurt woman by the name of Auguste Deter (Maurer et al., 1997). According to the latest World Health Organization (WHO) report, AD contributes to over two-thirds of dementia cases worldwide, as according to the latest World Health Organization (WHO) report (World Health Organization, 2019). On a histopathological level, the disease is characterized by two hallmarks: senile plaques and tangles (Scheltens et al., 2016). The former is composed of extraneuronal deposits of amyloid beta (A β) peptide, while the latter arises from intracellular interactions between hyperphosphorylated tau, a microtubule-associated protein that would normally facilitate cytoskeletal transport within the axonal network. Clinically, AD patients present with a progressive loss of cognitive function; this is because the hippocampus, which is the brain region associated with learning and memory processes, is one of the first affected structures in the course of disease progression (Halliday, 2017).

Research endeavors in AD over the last few decades have predominantly focussed on A β peptide, which was proposed by Hardy and Higgins in their "amyloid cascade hypothesis" to be a central figure in the overall disease mechanism (Hardy and Higgins, 1992). While this hypothesis has come under substantial criticism recently (Herrup, 2015), in light of a number of high-profile failures in clinical trials for novel AD drugs (Cummings et al., 2018), the role of A β peptide in

the disease, regardless of its actual extent, remains pivotal toward understanding the complex underlying architecture of AD.

A β peptide was first isolated in 1984 from a larger precursor molecule named amyloid precursor protein (APP) (Glenner and Wong, 1984). It is understood that APP is processed by the secretase family of enzymes via two main pathways: non-amyloidogenic and amyloidogenic (Figure 1; Thinakaran and Koo, 2008).

In the former pathway, α -secretase cleaves APP between residues Lys16 and Leu17 in the A β encoding region. This cleavage, which generates two fragments—soluble APP alpha (sAPP α) and C83, an 83-residue long C-terminus fragment, effectively disables formation of intact A β peptide, hence the designated term “non-amyloidogenic.” γ -secretase then subsequently cleaves C83 to yield p3 and APP intracellular domain (AICD). In contrast, β -secretase commences APP cleavage in the latter pathway, generating soluble APP beta (sAPP β) and C99, which contains the intact N-terminus of A β peptide. γ -secretase again completes this process, in this instance cleaving C99 to afford A β peptide of between 38 and 43 residues in length, and AICD. Most of the A β peptides produced are 40 residues in length, with the longer 42-residue variant making up a smaller proportion (Zhang et al., 2011). Despite accounting for a lesser percentage, the latter is understood to be more pathogenic compared to the former (Qiu et al., 2015).

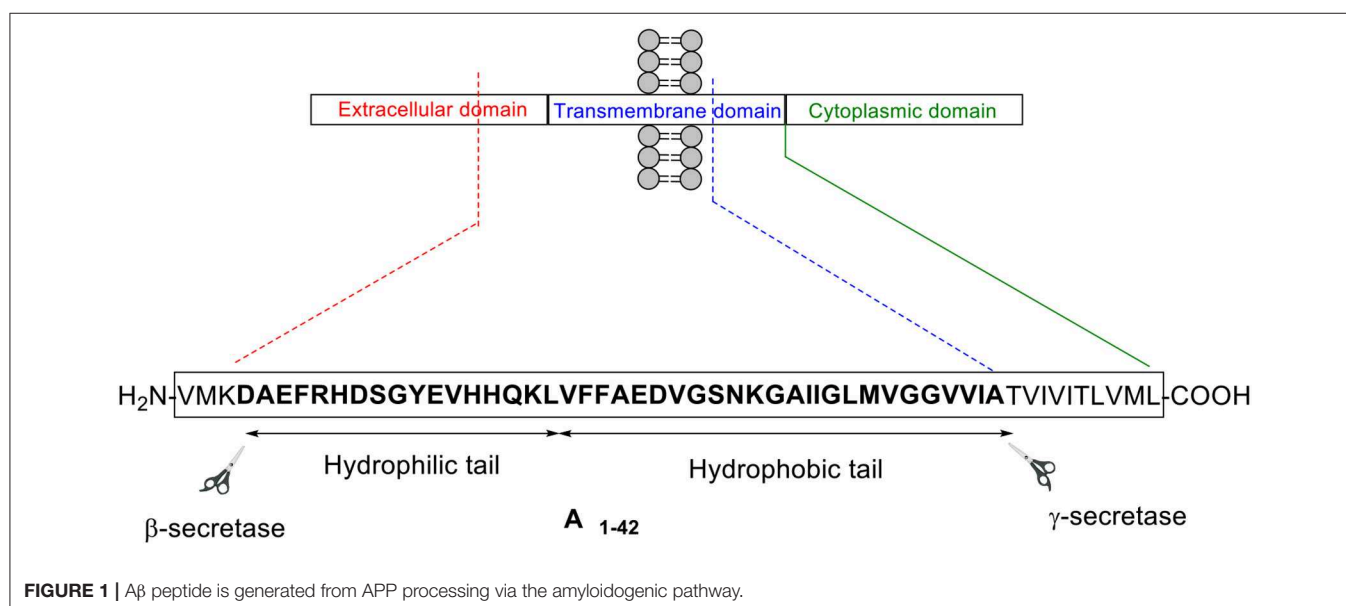
Thus, given the potentially greater significance of A β_{1-42} in AD neuropathology, it would be most desirable to possess a ready means of access to this biologically relevant peptide in ample quantities, and perhaps more importantly, with purity levels that mirror the endogenous peptide. Indeed, chemical synthesis of A β peptide has been attempted by numerous research groups globally, predominantly employing 9-fluorenylmethoxycarbonyl (Fmoc)/*tert*-butyl (*t*Bu) solid phase peptide synthesis (SPPS) strategy, which was first introduced by Atherton et al. (1978). These past endeavors, however, have in general focussed on

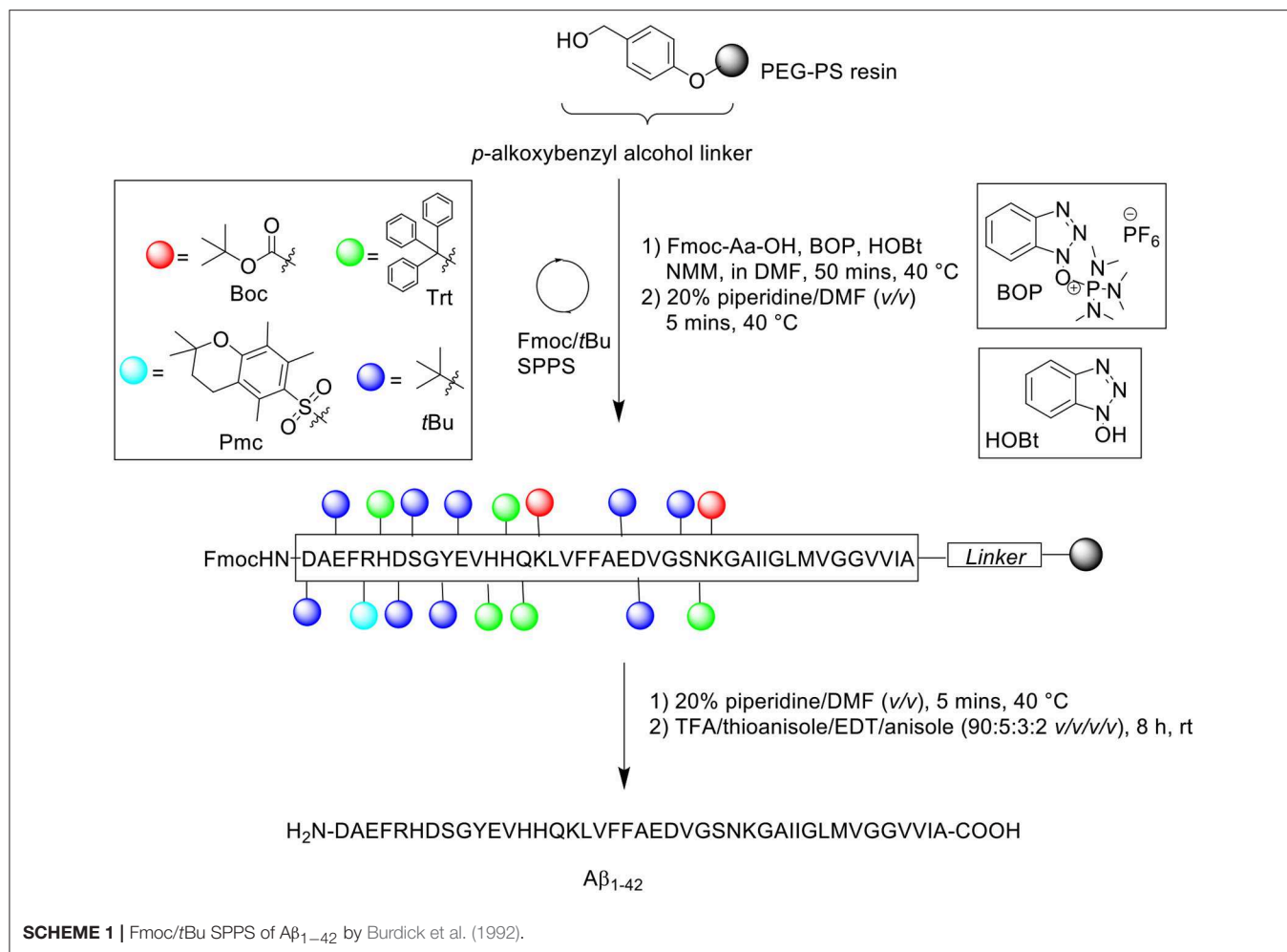
fragments of the peptide with established bioactivity (Wang et al., 2014), or the shorter A β_{1-40} variant (Choi et al., 2012).

While chemical syntheses of A β_{1-42} fragments are beneficial to the peptide research community, in that they have provided valuable structure-activity relationship (SAR) information with regards to key residues in the peptide that are involved in its aggregation and neurotoxicity properties, such data should be treated with care as these residues might behave in a distinct fashion when considered in context of the “full-length” A β_{1-42} peptide. The development of methodologies that enable preparation of A β_{1-42} in an efficient manner is therefore still very much in demand.

Routine preparation of A β_{1-42} is not typically undertaken owing to the “A β_{1-42} problem,” which is largely attributed to its propensity to aggregate both on resin during SPPS, as well as in solution. On-resin aggregation renders the free N-terminus inaccessible for coupling of subsequent amino acids in the sequence, resulting in either a truncated synthesis or an especially low crude recovery (Paradís-Bas et al., 2016). With regards to its characterization, purification of the peptide under conventional reverse phase-high performance liquid chromatography (RP-HPLC) conditions (acidic mobile phases, room temperature) yields an asymmetric, broad, and unresolved chromatographic peak, which is indicative of peptide aggregation. Thus, novel or improved protocols for preparation of this amyloidogenic peptide should be able to effectively mitigate these established issues, so as to afford the desired product in acceptable quantity and purity for further biological studies.

In this review, key publications concerning A β_{1-42} synthesis are critically discussed, providing readers with an insight into strategies that have been developed to overcome challenges associated with preparation of this “difficult peptide sequence.” For each publication reviewed herein, the synthetic protocol employed will be described in detail, and where the information was available, the overall yield and purity of the final product will





be stated accordingly, as well as any related assays performed to provide satisfactory proof of bioequivalence.

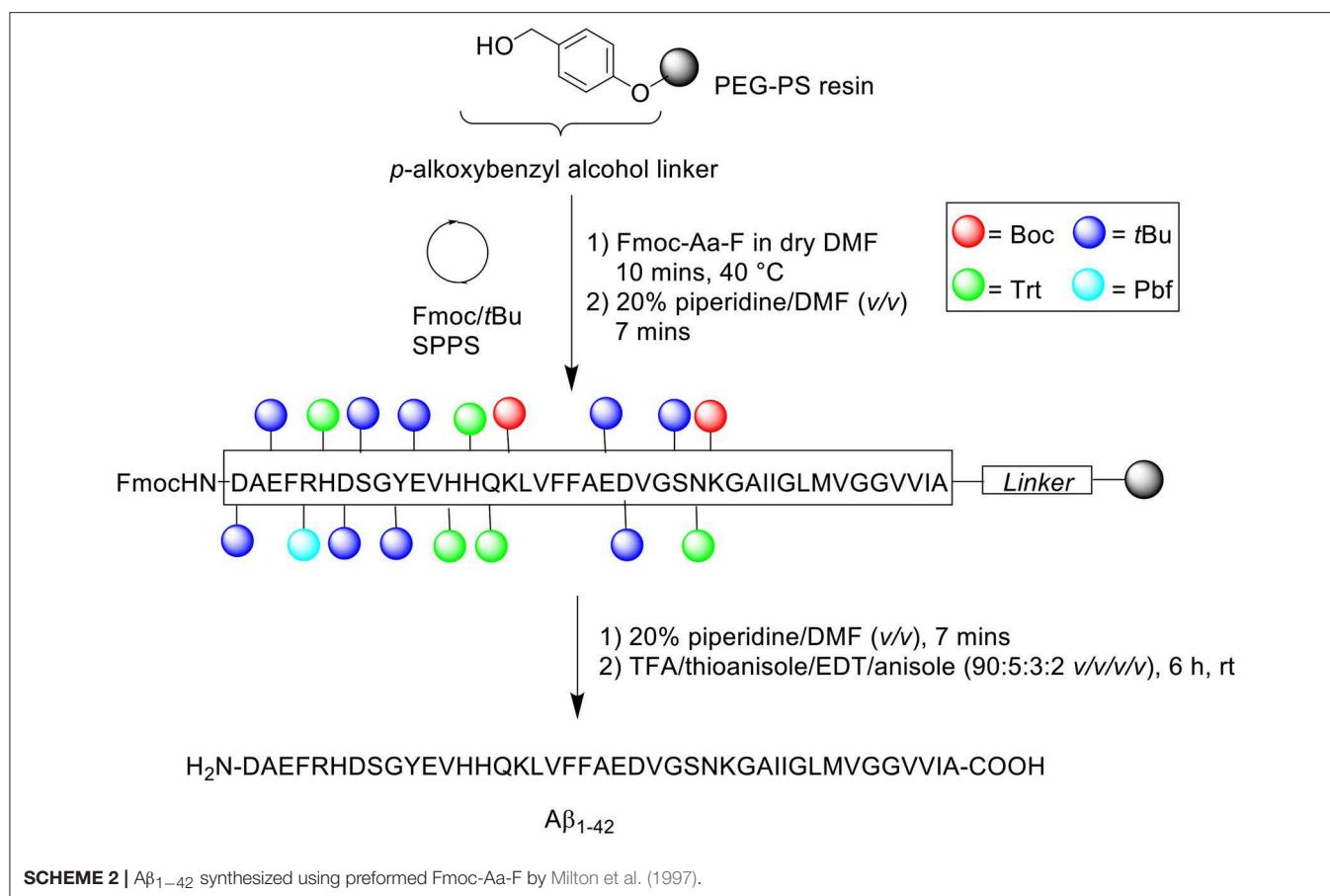
BURDICK ET AL. (1992)

Burdick et al. is credited with the first reported synthesis of A β_{1-42} in 1992, utilizing continuous flow SPPS on a custom built synthesizer, which consisted of a Chontrol 4 outlet timer (Fisher Scientific), a back pressure regulator (Western Analytical), an FMI pump (Fluid Metering Inc.), and slider valves (Rainin). These elements were connected to a pressurized nitrogen gas source to actuate the valves. Furthermore, the synthesizer was fitted with a 5 ml sample loop (Rainin), and Omni columns and fittings (Omnifit).

Peptide synthesis commenced on poly(ethylene) glycol-polystyrene (PEG-PS) resin (*loading not stated*), which was functionalized with a *p*-alkoxybenzyl alcohol linker (**Scheme 1**). The reactive side chains were protected as follows: arginine (Arg) residue was protected by 2,2,5,7,8-pentamethylchroman-6-sulfonyl (Pmc); asparagine (Asn), glutamine (Gln), and histidine (His) residues were protected by trityl; lysine (Lys) was protected by Boc; aspartic acid (Asp), glutamic acid (Glu), serine (Ser),

tyrosine (Tyr), and threonine (Thr) residues were protected by *t*Bu (Burdick et al., 1992).

The reaction column was first immersed in a one-liter water bath at 40°C, washed with DMF at a flow rate of 5 mL/min for 1 min, and allowed to equilibrate gradually to room temperature as the reaction cycle progresses over time. Fmoc removal was achieved using 20% piperidine in DMF (v/v) for 5 min. Fmoc-amino acid couplings were afforded using Fmoc-Aa-OH (4 eq.), hydroxybenzotriazole (HOBT, 4 eq.), (benzotriazol-1-yloxy)tris(dimethylamino)phosphonium hexafluorophosphate (BOP, 4 eq.) in 5% *N*-methylmorpholine (NMM) in *N,N'*-dimethylformamide (DMF) (v/v) for 20 min, and repeated for a further 30 min with fresh reagents. A qualitative ninhydrin test was performed after each completed coupling cycle; coupling of Val12, His13, Val18, and Phe19 were reported by the authors to be incomplete, and consequently repeated. The completed peptide chain was cleaved from the resin using trifluoroacetic acid (TFA)/thioanisole/1,2-ethanedithiol (EDT)/anisole (90:5:3:2 v/v/v/v) at room temperature for 8 h. Crude peptides were dissolved in 88% formic acid (v/v) prior to purification on RP-HPLC using Vydac (Hesperia, CA) 214TP C4 column (10 μ m, 2.2 \times 2.5 cm, 300Å) at flow rate of 8 mL/min. A linear gradient



between 0.1% TFA in water and 0.1% TFA in acetonitrile was employed over 55 min. Peak fractions were collected manually, lyophilized, and stored dry at -20°C until required. Peptide samples were characterized by electrospray ionization mass spectrometry (ESI-MS), amino acid sequencing by automated Edman degradation, and microscopy imaging. Additional assays were also undertaken to investigate the effects of pH and peptide concentration on peptide assembly. The results obtained show minimal to no sedimentation (as determined by γ -counting) at slightly basic pH and low peptide concentration, which suggested the need to employ basic buffers for purification of this peptide. No further bio-testing was attempted by the group.

A follow-up to this work was undertaken by Milton et al. (1997). The group utilized preformed Fmoc-aminoacyl fluorides (Fmoc-Aa-F) (Scheme 2) to facilitate the efficient synthesis of A β _{1–42} (Milton et al., 1997).

Previous studies have established the advantage conferred by using Fmoc-Aa-F building blocks over standard coupling reagents (Carpino et al., 1990; Wenschuh et al., 1995). Fmoc-Aa-F was prepared using two methods: dimethylaminosulfur trifluoride (DAST) and cyanuric fluoride. DAST was employed for the preparation of Fmoc-Aa-F of protected Ser, Val, Gly, Asn, Glu, and Met residues, while cyanuric fluoride was used to prepare Fmoc-Aa-F of protected Ala, Gln, Leu, Asp, Ile, Phe, Lys, and Tyr residues. Peptide synthesis commenced on a

PEG-PS support (*loading not stated*), which was functionalized with a *p*-alkoxybenzyl ester to form an acid labile linker. For comparative purposes, three activation protocols were trialed: (1) BOP/HOBt/NMM – Fmoc-Aa-OH (4 eq.), BOP (4 eq.), HOBt (4 eq.) and NMM in DMF for 2 h at 40°C , (2) Preformed Fmoc-aminoacyl-fluorides – Fmoc-Aa-F (4 eq.) in dry DMF for 10 min at either 22 or 40°C , and (3) 1-[bis(dimethylamino)methylene]-1*H*-1,2,3-triazolo[4,5-*b*]pyridinium 3-oxide hexafluorophosphate (HATU)/*N,N*-diisopropylethylamine (DIPEA) – Fmoc-Aa-OH (4 eq.), HATU (4 eq.), DIPEA (8 eq.) in DMF for 1 h at 40°C . Fmoc removal was afforded using 20% piperidine in DMF (v/v) for 7 min at 40 or 55°C . The completed peptide chain was cleaved from the resin with TFA/thioanisole/EDT/anisole (90:5:3:2 v/v/v/v) at room temperature for 6 h. The TFA was then evaporated, and the remaining filtrate precipitated in cold diethyl ether, and stored overnight at -20°C . The frozen precipitate was sequentially washed with ether and allowed to dry *in vacuo*.

The crude peptide was purified by RP-HPLC using Vydac (Hesperia, CA) 214TP C4 column (10 μm , 2.2×2.5 cm, 300Å) at a flow rate of 8 mL/min using a linear gradient of 5–95% B over 60 min, where solvent B was 0.1% TFA in acetonitrile, whereas solvent A was 0.1% TFA in water. Fractions collected were immediately lyophilized, prior to analysis using a C4 column at a flow rate of 1 mL/min. ESI-MS to determine presence of

the desired product was undertaken by an external company (Peptidogenic Research, Livermore, CA). In the resulting HPLC spectrum, the major peak of A β _{1–42} synthesized with BOP/HOBt/NMM at 40°C for both acylation and deprotection steps was shown to not correspond to the desired product, which was identified to elute slightly later in time. Increasing Fmoc removal temperature to 55°C also yielded an identical spectrum. However, an increase in yield of the desired, but not major product, was noted, most likely due to a more “complete” removal of the temporary Fmoc protecting group. In contrast, the major peak of A β _{1–42} prepared using preformed Fmoc-Aa-F,

carrying out the acylation and deprotection steps at 40 and 55°C, respectively, was shown to correspond to the desired product, thereby facilitating an easier purification process (Table 1). No further bio-testing was attempted by the group.

HENDRIX ET AL. (1992)

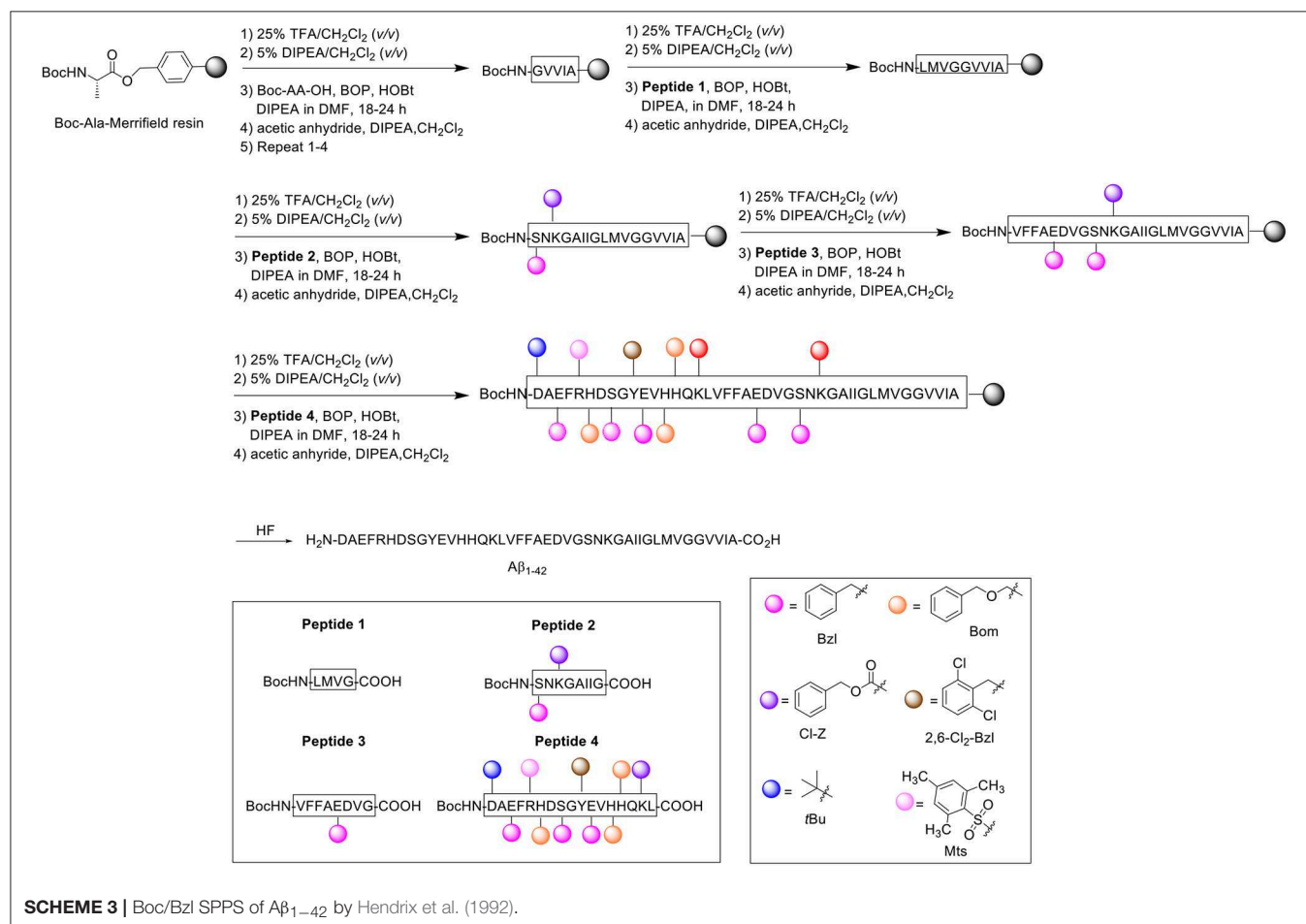
During pioneering syntheses of A β _{1–42} by the Glabe laboratory, Hendrix et al. at the Massachusetts Institute of Technology, US also published their synthesis of the peptide (Scheme 3; Hendrix et al., 1992).

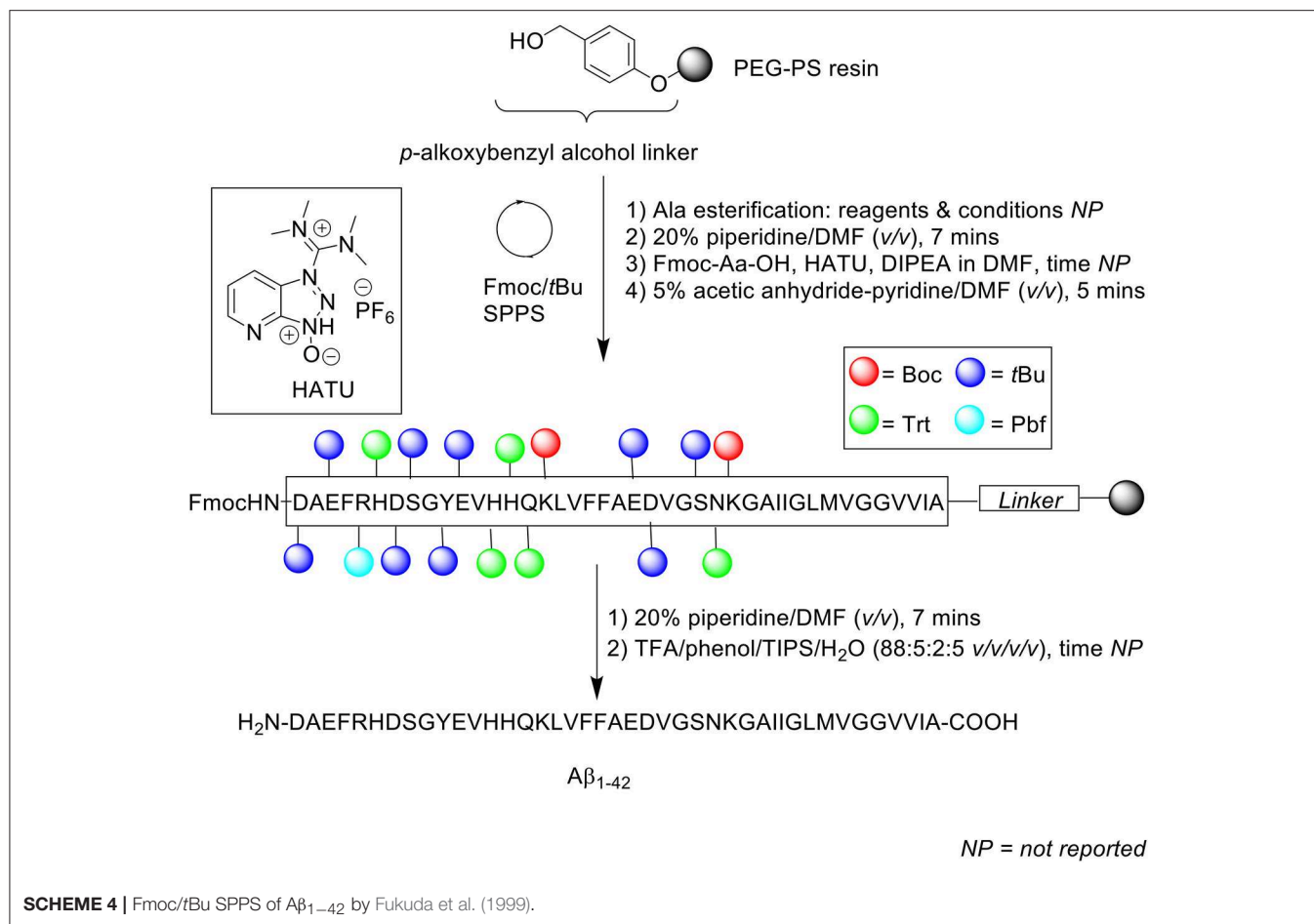
Noting one main disadvantage of stepwise SPPS for the preparation of relatively long peptides in general, which is the gradual accumulation of identical peptidic side products on resin, the group opted for a convergent approach instead, which they postulated would minimize the extent of side product formation. Using the *tert*-butyloxycarbonyl (Boc)/benzyl (Bzl) strategy, four A β _{1–42} fragments were synthesized and subsequently condensed on resin through their peptide backbone (Hendrix and Lansbury, 1992). All Boc-Aa-OH couplings were performed twice, followed by acetylation with acetic anhydride (10 eq.). The first fragment was synthesized on Kaiser oxime resin (Kaiser et al., 1989). Boc-protected leucine was bound to the resin and

TABLE 1 | Comparative A β _{1–42} yield from protocols trialed by Milton et al. (1997).

| Protocol | T _{acylation} (°C) | T _{deprotection} (°C) | Yield (%) |
|--------------|-----------------------------|--------------------------------|-----------|
| BOP/HOBt/NMM | 40 | 40 | 21 |
| BOP/HOBt/NMM | 40 | 55 | 22 |
| Fmoc-Aa-F | 22 | 40 | 23 |
| Fmoc-Aa-F | 40 | 40 | 25 |
| Fmoc-Aa-F | 40 | 55 | 28 |

Yield was calculated as a percentage ratio between purified and crude weight.





elongated to H-Y(2,6-Cl₂-Bzl)E(Bzl)VH(Bom)H(Bom)QK(Cl-Z)L-resin. This fragment was subsequently reacted with Boc-D(tBu)AE(Bzl)FR(Mts)H(Bom)DS(Bzl)G-OH (prepared with the same reagents and conditions described above) to afford the desired resin-bound **Peptide 4**, which was cleaved using low-high trifluoromethanesulfonic acid (TFMSA) /TFA protocol, purified by RP-HPLC, and characterized by amino acid analysis, ¹H nuclear magnetic resonance (NMR), and fast atom bombardment mass spectrometry (FABMS).

The second fragment was prepared on Merrifield resin. Resin-bound Boc-protected alanine was first elongated to Boc-GVVIA-resin, after which **Peptide 1** (Boc-LMVG-CO₂H) and **Peptide 2** (Boc-S(Bzl)NK(Cl-Z)GAIIG-CO₂H) (1.2–1.5 eq., BOP activation at 23°C) were coupled sequentially on resin to form Boc-S(Bzl)NK(Cl-Z)GAIIGLMVGGVVIA-resin. **Peptide 3** (Boc-VFFAE(Bzl)DVG-CO₂H) was coupled afterwards to complete the desired fragment. **Peptide 4** was coupled four successive times in the presence of BOP as an activating reagent to Boc-VFFAE(Bzl)D(Bzl)VGS(Bzl)NK(Cl-Z)GAIIGLMVGGVVIA-resin to complete the A β _{1–42} peptide chain, with each coupling step using less equivalents (2.3 eq. in total). The completed peptide chain was finally deprotected and cleaved off the resin using hydrogen fluoride.

Following analysis, it was identified that the crude product contained two truncated side products corresponding to A β _{18–42} and A β _{26–42}. These low molecular weight impurities were fortunately separable using gel-filtration HPLC in 1,1,1,3,3,3-hexafluoro-2-propanol (HFIP), permitting high recovery of the desired product. The gel-purified material was then repurified by RP-HPLC to eliminate further minor side products, which included A β _{1–37} and benzylated A β _{1–42}. The final purified product (>90% purity as determined by MS) was characterized by laser desorption MS and amino acid analysis employing Edman degeneration. The proposed method thus enabled the efficient synthesis of the peptide with minimal presence of side products. No further bio-testing was attempted by the group.

FUKUDA ET AL. (1999)

Fukuda et al. reported on the successful synthesis of A β _{1–42} and its two isoaspartyl isomers at position 7 [A β _{1–42}(isoAsp7)] and 23 [A β _{1–42}(isoAsp23)] (Fukuda et al., 1999). Syntheses of all three peptides proceeded in a stepwise fashion using the Fmoc/tBu SPPS strategy on PEG-PS resin (*loading not stated*) (Scheme 4).

Fmoc protecting group was deprotected using 20% piperidine in DMF (v/v) and Fmoc-amino acids (4 eq.) were single coupled in the presence of HATU (4 eq.) and DIPEA (8 eq.). For the isoaspartyl analogs, Fmoc-Asp-OtBu was used instead of Fmoc-Asp(OtBu)-OH at positions 7 and 23. Following each coupling step, any unreacted N-terminus was capped with 5% acetic anhydride-pyridine in DMF (v/v) for 5 min. The completed peptide chain was then cleaved off the resin using TFA/phenol/triisopropylsilane (TIPS)/water (88:5:2:5 v/v/v/v).

Given the propensity of the peptide to aggregate under acidic conditions, the lyophilized crude peptides were reconstituted in 0.1% ammonium hydroxide (NH₄OH) prior to purification using RP-HPLC on Develosil 5 μ m ODS-UG 140Å (150 \times 4.6 mm) at 0.2 mL/min flow rate at room temperature. A linear gradient of 15–36% acetonitrile in 0.1% NH₄OH was employed. Overall yields of each peptide were 10, 15, and 13% for A β _{1–42}, A β _{1–42}(isoAsp7), and A β _{1–42}(isoAsp23), respectively, relative to starting crude material. The purity of the synthetic A β _{1–42} was subsequently compared with commercial A β _{1–42} (Bachem), using RP-HPLC, matrix assisted laser desorption ionization mass spectrometry (MALDI-TOF MS), and amino acid composition analysis. The results for all three analyses indicated that their A β _{1–42} had been synthesized at a higher purity compared to commercially obtained A β _{1–42}. RP-HPLC analysis under alkaline conditions showed some impurities for commercial A β _{1–42}, which was further confirmed by MALDI-TOF MS. In contrast, the group's A β _{1–42} yielded a single, sharp chromatographic peak with retention time *ca* 19 min. Amino acid composition analysis for their A β _{1–42} also produced a result that was closer to the theoretical value, in contrast to Bachem A β _{1–42}. While purity of the final product was not reported by the authors, results obtained from thioflavin T (ThT) assay, transmission electron microscopy (TEM) imaging, and neurotoxicity assay against rat embryonic cortical neurons, carried out using their synthetic A β _{1–42}, provided ample evidence that the synthesized A β _{1–42} is sufficiently bioequivalent to endogenous A β _{1–42}.

TICKLER ET AL. (2001)

Another problematic issue for the synthesis of A β _{1–42} is the hydrophobicity of its C-terminal segment. In 2001, Tickler, Barrow, and Wade published on an improved preparation of this peptide, employing 1,8-diazabicyclo[5.4.0]undec-7-ene (DBU) as an Fmoc removal reagent (Scheme 5; Tickler et al., 2001).

Incomplete Fmoc removal is understood to be a factor that can affect overall synthetic efficiency. Thus, complete removal of temporary Fmoc protecting group from the N $^{\alpha}$ -terminus of the amino acid is of paramount importance, as this facilitates efficient coupling of subsequent Fmoc-protected amino acids. For this purpose, the stronger base DBU was preferred to the conventionally used piperidine. Peptide synthesis was undertaken on PEG-PS resin (*loading not stated*) functionalized with 4-(hydroxymethyl)phenoxyacetic acid (HMPA) linker at 0.1 mmol scale. The Fmoc protecting group was removed using 2% DBU in DMF (v/v) for 5 min, up until residue Ser8, after which 20% piperidine in DMF (v/v)

was employed to prevent aspartamide formation at residue Asp7, an established side reaction observed in the chemical synthesis of A β _{1–42}. Consequently, deprotection time for subsequent Fmoc-amino acid residues was also extended to 10 min. Fmoc-amino acids were coupled in the presence of 3-[bis(dimethylamino)methyl]imidazolium-3H-benzotriazol-1-oxide hexafluorophosphate (HBTU) and DIPEA in DMF. Cleavage of the completed peptide chain was accomplished with TFA/water/EDT/TIPS (94:2.5:2.5:1 v/v/v/v) for 3 h. The TFA filtrate was then concentrated *in vacuo*, precipitated in cold ether, reconstituted in water/acetonitrile/TFA (90:10:0.1 or 80:20:0.1 v/v/v), and recovered by lyophilization (40% yield based on 0.1 mmol PEG-PS resin loading).

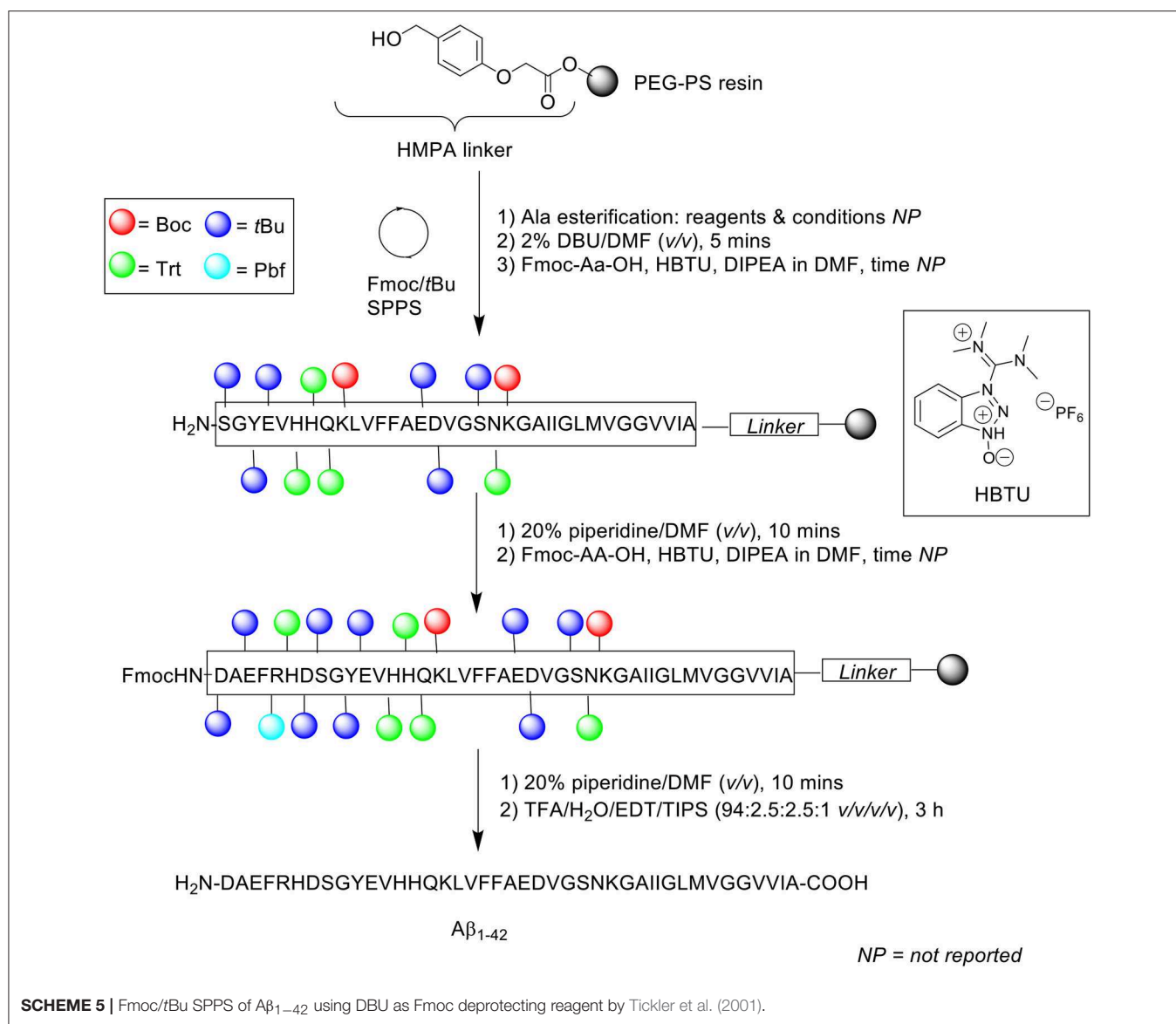
Characterization of the crude peptide was performed using RP-HPLC on a Vydac (Hesperia, USA) C4 analytical column (4.6 \times 250 mm, 5 μ m) at 1 mL/min flow rate at 60°C. A linear gradient of 15–50% B was employed over 30 min, where solvent A was 10 mM ammonium bicarbonate (NH₄CO₃) and solvent B was acetonitrile. The resulting HPLC spectrum yielded predominantly a single chromatographic peak with a retention time *ca* 19 min, which mass was confirmed by MALDI-TOF MS to correspond to the desired product. Purification of the crude product was undertaken using RP-HPLC, affording pure A β _{1–42} at 17% yield relative to purified crude weight. The purity of the final product, however, was not reported by the authors. Furthermore, employment of bicarbonate-based buffers, while shown herein to be beneficial with regards to purification of their A β _{1–42}, still required further investigation, particularly to probe the bioequivalence of the purified peptide. This was unfortunately not attempted by the group. Regardless, the employment of DBU in the synthesis of A β _{1–42} to improve Fmoc removal efficiency, especially at its hydrophobic C-terminal region, was demonstrated to afford a crude product of higher quality, thus translating to a relatively easier purification process.

CARPINO ET AL. (2004)

In the attempt to address the prevailing issue of A β _{1–42} aggregation on resin, Carpino et al. incorporated the depsipeptide method in their synthesis of A β _{1–42} (Scheme 6; Carpino et al., 2004). It is thought that the introduction of depsipeptides, a class of peptidic compounds in which the peptide bonds have been substituted with amide bonds, may restrict aggregation phenomena during synthesis (Coin, 2010).

Instead of synthesizing the linear peptide, its water-soluble O-acyl isopeptide was prepared instead, selecting Ser26 as the residue to perform O-acylation on, as the Gly25 residue does not epimerize during activation to form the ester bond. Peptide chain was subsequently elongated as normal thereafter. Following cleavage from the resin, the O-acyl isopeptide can be rearranged to yield the native peptide by treatment in aqueous buffer at pH 8.

Peptide synthesis commenced on TentaGel resin (0.25 mmol/g loading) functionalized with 4-(4-hydroxymethyl-3-methoxyphenoxy)butyric acid (HMPB) linker at 0.125 mmol scale. Fmoc-Ala-OH (1 mmol) was double coupled manually on resin in the presence of N,N'-diisopropylcarbodiimide (DIC)

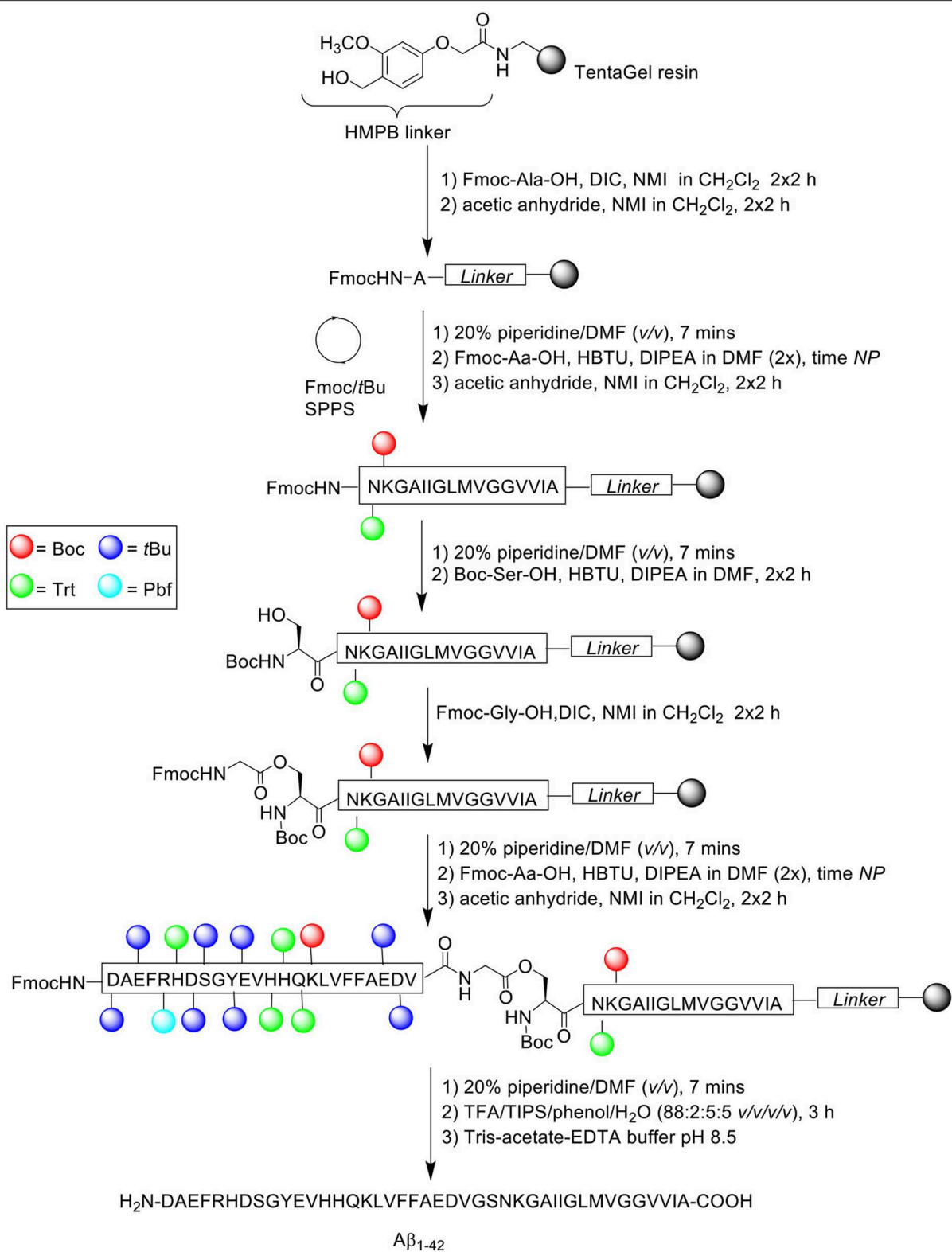


and *N*-methylimidazole (NMI) in dichloromethane (CH₂Cl₂) for 2 h each time. Any free amine at the N-terminus was capped twice with acetic anhydride/NMI (0.75 mmol) in CH₂Cl₂ for 2 h each time. Fmoc-amino acids were then double coupled up to residue Asn27 using Fmoc-Aa-OH, HBTU, and DIPEA in DMF. The Fmoc protecting group on Asn27 was removed prior to double coupling of Boc-Ser-OH using HBTU and DIPEA in DMF for 2 h each time. Resin-bound Ser26 residue was then *O*-acylated with Fmoc-Gly-OH/DIC/NMI and capped under the conditions stated above. The peptide sequence was then elongated to completion, cleaved off resin with TFA/TIPS/phenol/water (88:2:5:5 v/v/v/v) for 3 h, and recovered by lyophilization. Rearrangement of the *O*-acyl isopeptide to native A β_{1-42} was achieved by treatment with Tris-acetate-ethylenediaminetetraacetic acid (EDTA) buffer (pH 8.5). The overall yield and purity of the final peptide were not reported.

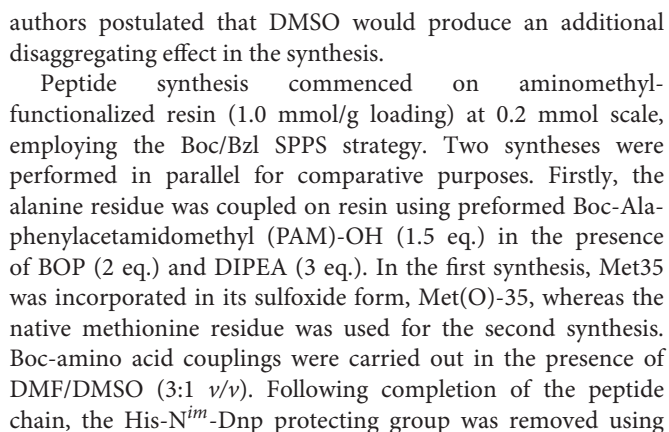
A significant by-product corresponding to A β_{26-42} was detected in the resulting crude HPLC profile, which was postulated to be due to incomplete *O*-acylation. Further bio-testing was also not undertaken by the group.

KIM ET AL. (2004)

In the same year, Kim et al. presented an optimized coupling reaction for the efficient synthesis of A β_{1-42} (Kim et al., 2004), which capitalized on the known disaggregating role of the single methionine residue in the sequence (**Scheme 7**). Intentional incorporation of oxidized methionine in the peptide synthesis consequently permitted the use of dimethylsulfoxide (DMSO) as co-solvent in all coupling reactions performed, which would normally oxidize methionine to its sulfoxide derivative. The



SCHEME 6 | Fmoc/tBu SPPS of A β_{1-42} using depsipeptide methodology by Carpino et al. (2004).



a cocktail of β -mercaptoethanol and triethylamine in DMF for 3×10 min, and the sulfoxide moiety reduced using a cocktail of silicon tetrachloride (SiCl_4)/anisole/TFA (5:5:90 v/v/v) for 15 min. The peptide was then recovered from the resin using DMSO/HF (3:1 v/v) with 5% *p*-cresol (v/v) for 2 h at 0°C , and lyophilized.

RP-HPLC analysis was performed on a Vydac 219TP5415 diphenyl column (300Å, 4.6 × 150 mm, 5 µm), using a linear gradient of solvent A (0.1% TFA in water) and B (0.09% TFA in acetonitrile). The eluted chromatographic peak (retention time 19.3 min) was identified by MALDI-TOF MS to match the desired product, although the yield and purity of the final product was not reported by the group. Furthermore, one limitation of this method, as acknowledged by the authors, is the presence

of deletion products corresponding to deletion of one or two phenylalanine residues in the sequence. No further bio-testing was attempted by the group.

SOHMA ET AL. (2005)

Sohma et al. also implemented the “O-acyl isopeptide method” in their synthesis of A β _{1–42} (Sohma et al., 2005). For comparative purposes, A β _{1–42} was also synthesized in a linear fashion on 2-chlorotrityl chloride resin (*loading not stated*) at 0.3 mmol scale. In the synthesis of the linear peptide, Fmoc-Ala-OH was coupled for 2.5 h in the presence of DIPEA in 1-ethyl-3-(3-dimethylaminopropyl)carbodiimide (EDC) under argon atmosphere, followed by capping with methanol in the presence of DIPEA in DMF for 20 min. The resin bed was afterwards washed sequentially with DMF, DMF/water (1:1 v/v), chloroform (CHCl₃), methanol, and then dried *in vacuo*. Alanine loading was photometrically quantified based on liberation of Fmoc chromophore following treatment with 50% piperidine in DMF (v/v) for 30 min at 37°C. Fmoc removal was afforded with 20% piperidine in DMF (v/v) for 20 min, and subsequent Fmoc-amino acid residues were manually coupled using DIC/HOBt in DMF for 2 h. The completed peptide chain was cleaved off the resin using TFA/*m*-cresol/thioanisole/water (92.5:2.5:2.5:2.5 v/v/v/v) for 90 min, the filtrate concentrated *in vacuo*, precipitated with cold ether, reconstituted in water, and recovered by lyophilization.

A sample of the crude product was then dissolved in TFA/water (2:1 v/v) in the presence of ammonium iodide (NH₄I) and dimethyl sulfide (CH₃)₂S, then stood for 1 h at 0°C to reduce any oxidized methionine residues. The mixture was then concentrated *in vacuo*, dissolved in HFIP, and filtered using a 0.46 μ m filter unit, before purification using preparative HPLC on a C18 column (4.6 \times 150 mm; YMC Pack ODS AM302) at 40°C. A linear gradient of 0–100% acetonitrile in 0.1% aqueous TFA was employed over 40 min at a flow rate of 5 mL/min. Peak fractions were collected and immediately lyophilized to afford pure A β _{1–42} (overall yield of 7.2% relative to starting crude material, purity >94%). MALDI-TOF MS and RP-HPLC analyses of collected fractions confirmed the presence of the desired product, which had a retention time that matched commercial A β _{1–42}.

Synthesis of “26-O-acyl-isoA β _{1–42}” was subsequently attempted. Fmoc-protected A β _{27–42} was assembled on 2-chlorotrityl chloride resin at 0.1 mmol scale, employing the same reagents and conditions as described above (Scheme 8).

Following completion of the peptide fragment, Boc-Ser-OH was coupled in the presence of DIC and HOBt in DMF for 2 h, followed by double coupling of Fmoc-Gly-OH using DIC and 4-dimethylaminopyridine (DMAP) in CH₂Cl₂ for 16 h each time. Peptide assembly was then continued to afford the completed O-acyl isopeptide chain, which was cleaved off the resin and recovered by lyophilization. The crude peptide was also pre-treated with NH₄I/(CH₃)₂S before purification, which afforded pure O-acyl isopeptide at 33.6% yield relative to purified crude weight and >96% purity. The purified peptide was subsequently

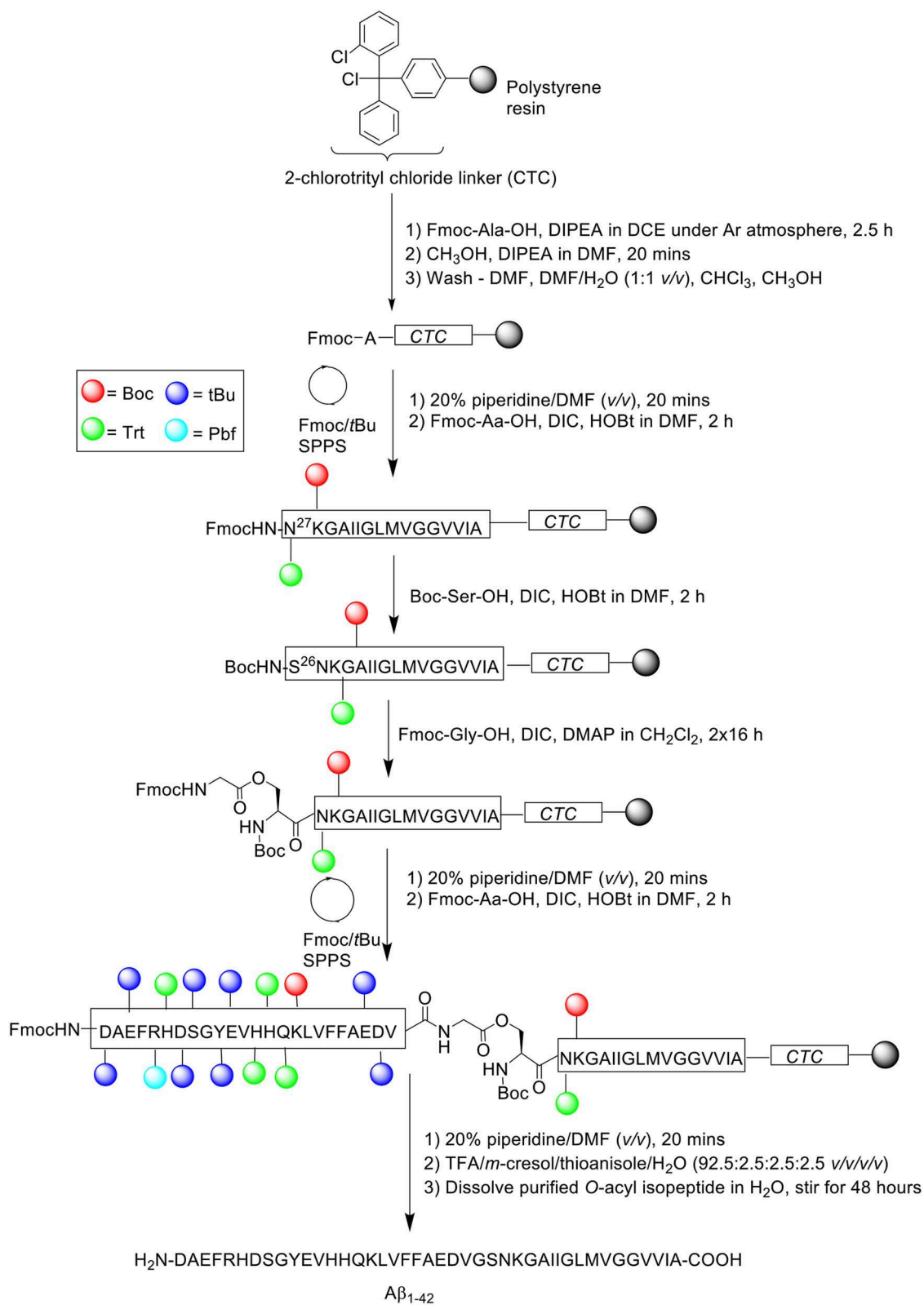
dissolved in water and stirred for 48 h to induce O- to N-acyl transfer reaction, yielding A β _{1–42} quantitatively. RP-HPLC profile and MALDI-TOF MS of A β _{1–42} synthesized using this method was again shown to be identical to that of commercial A β _{1–42}. No further bio-testing was attempted by the group.

GARCÍA-MARTÍN ET AL. (2006)

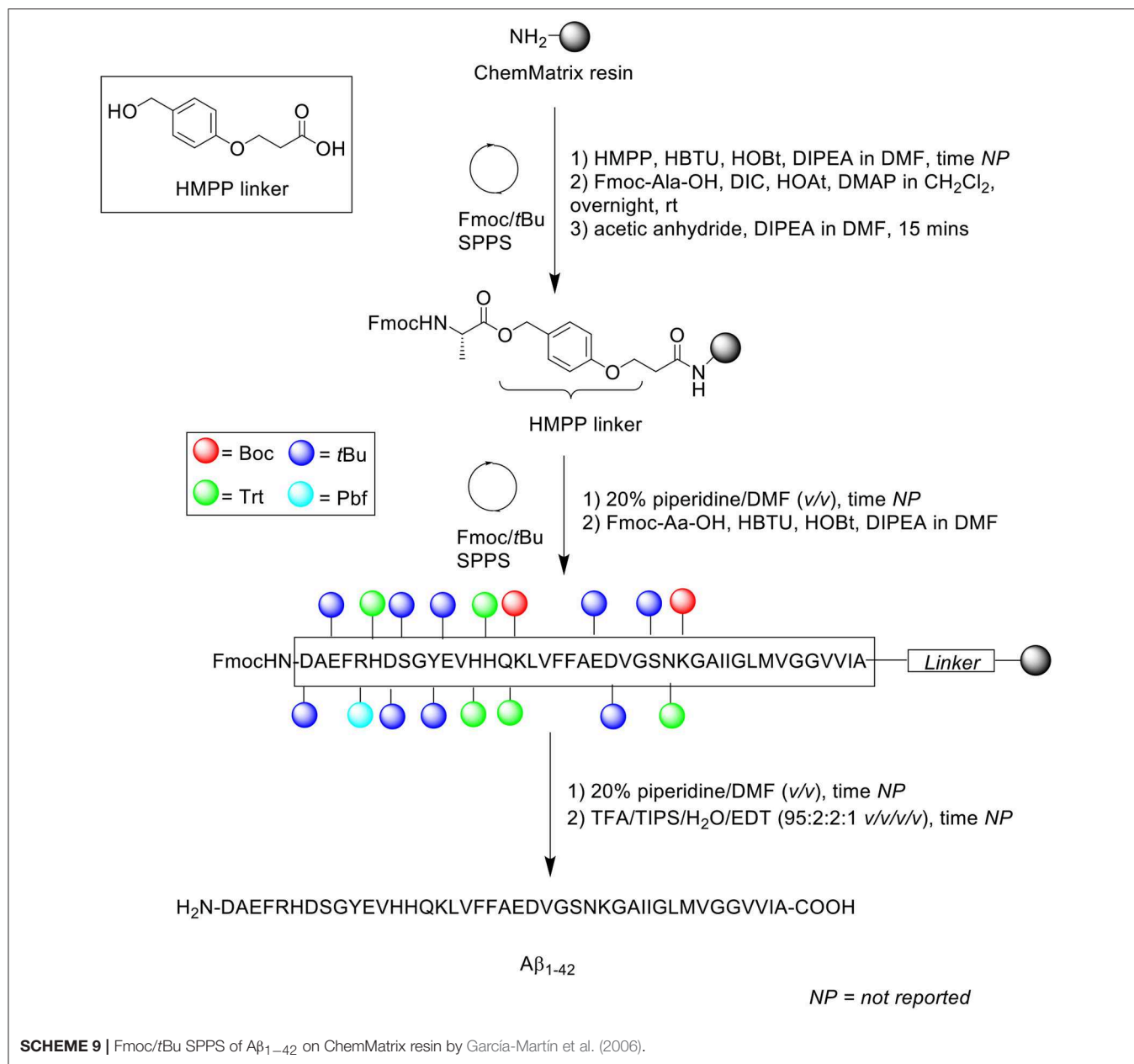
The propensity of A β _{1–42} to aggregate on resin during SPPS necessitates some considerations with regards to the choice of solid support. Particularly, the use of resins with a low degree of substitution might be more appropriate for the efficient preparation of long, hydrophobic peptides in general, as lower loading translates to lesser steric interference on resin. In 2006, García-Martín et al. introduced ChemMatrix resin as a novel, solid support for SPPS (García-Martín et al., 2006). ChemMatrix is a totally PEG-based resin which consists of only primary ether bonds, which renders it chemically stable. It also assumes a free-flowing form upon drying *in vacuo*, and is a preferable choice over PS-based resins in the synthesis of “difficult peptide sequences.” Firstly, the physical properties of ChemMatrix was contrasted with PS. The former was shown to swell in most solvents, including especially polar ones such as acetonitrile, DMSO, and methanol; none of the three can swell PS resins satisfactorily. More importantly, ChemMatrix swelled better than PS in DMF and CH₂Cl₂, and also exhibited higher chemical stability toward acid or base treatment, with the sole exception of strong Lewis acids. Microscopic analysis of ChemMatrix beads following shrinking and swelling by various solvents demonstrated no notable structural deterioration, which suggested that it was unaffected by osmotic stress. Subsequently, this resin was employed in the synthesis of four complex peptides: a decameric model peptide consisting of oligo(aminoacyl) sequences, 38-amino acid long synthetic vaccine Bacuma, polyarginine peptide, and A β _{1–42} peptide (Scheme 9).

A β _{1–42} synthesis was carried out on ChemMatrix resin (*loading not stated*) at 0.07 mmol scale in a stepwise fashion. The acid labile 3-(4-hydroxymethylphenoxy)propionic acid (HMPP) linker was coupled on resin manually with HBTU, HOBt, and DIPEA in DMF, followed by first residue attachment (Fmoc-L-Ala-OH) using DMAP in CH₂Cl₂ overnight at room temperature. Despite a prolonged reaction time, free hydroxyl groups were still present, as determined by the 4(4-nitrobenzyl)pyridine test. Consequently, the alanine coupling step was repeated for a further 2 h with fresh reagents. Acetylation of free N-terminus group was afforded using acetic anhydride/DIPEA in DMF for 15 min, followed by automated elongation to generate the desired peptide chain, which was cleaved off the resin using TFA/TIPS/water/EDT (95:2:2:1 v/v/v/v) for 90 min.

Following recovery by lyophilization, the peptide was monomerized in neat TFA, concentrated *in vacuo*, and dissolved in HFIP to retain the disaggregated state. RP-HPLC analysis was undertaken using a C8 column (size not reported; flow rate 1 mL/min) at 60°C. A linear gradient between 0.1% TFA in



SCHEME 8 | Fmoc/tBu SPPS of '26-O-acyl-isoA β_{1-42} ' by Sohma et al. (2005).



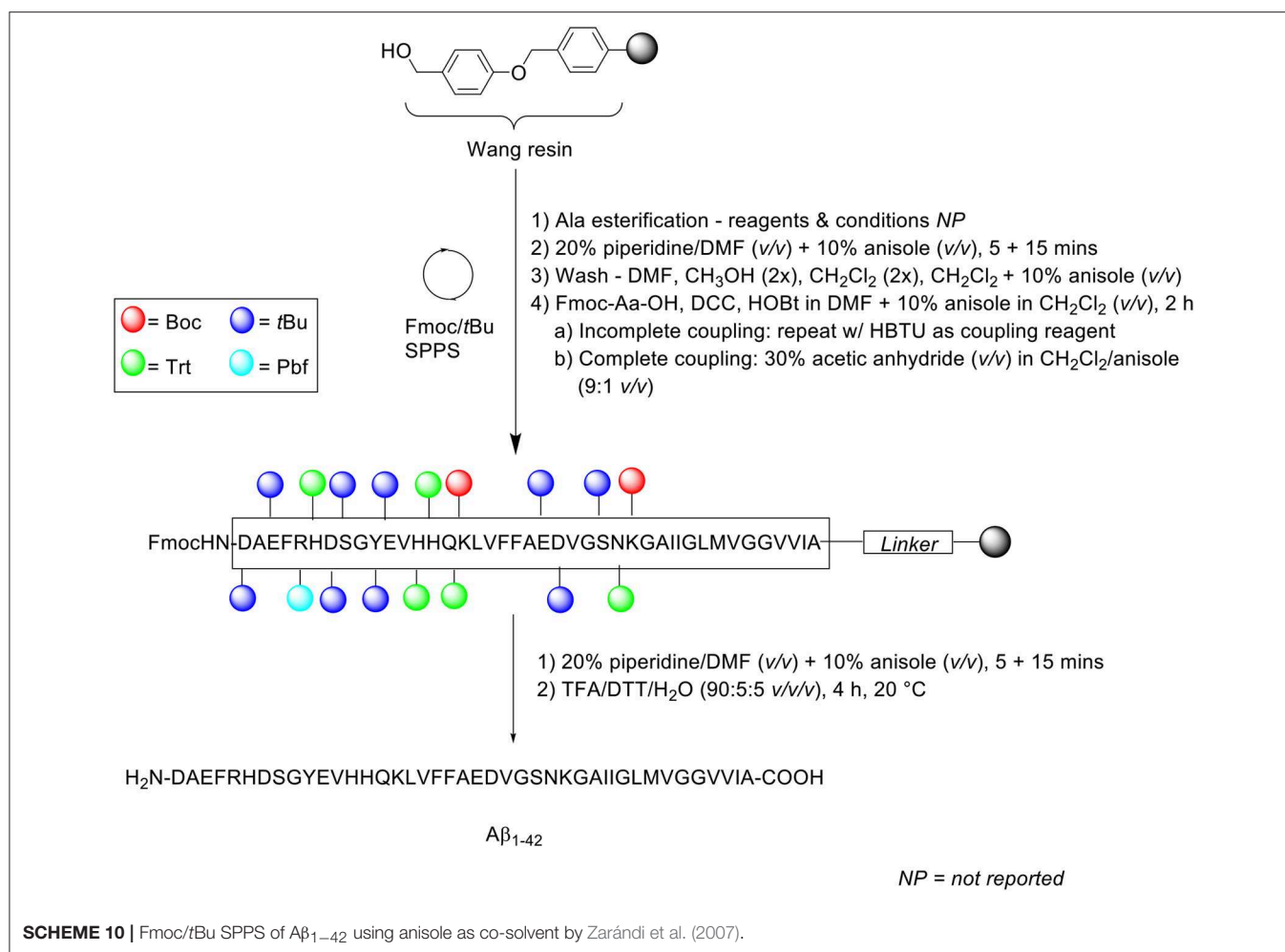
water and 0.1% TFA in acetonitrile was employed over 15 min. The resulting HPLC spectrum showed a single major peak with a retention time of 9.3 min and an estimated purity of 91%, which was confirmed by MALDI-TOF MS to correspond to the desired product. Unfortunately, the yield was not reported, and no further bio-testing was carried out by the group. Furthermore, it was not explicitly stated whether purification of the crude product was attempted in this study, although the relatively high purity percentage suggested this was the case.

ZARÁNDI ET AL. (2007)

Zarándi et al. introduced anisole as a relatively cheap and simple co-solvent for both deprotection and coupling steps in their

Fmoc/tBu SPPS of A β_{1-42} (Scheme 10; Zarándi et al., 2007). It was postulated that the use of anisole would improve the purity and yield of crude A β_{1-42} by preventing its aggregation during synthesis.

Peptide synthesis commenced on Wang resin (0.41 mmol/g loading) at 0.25 mmol scale. Fmoc removal was performed twice with 20% piperidine in DMF (v/v) containing 10% anisole (v/v) for 5 and 15 min. Following each deprotection step, the resin bed was washed sequentially with DMF, methanol (twice), CH₂Cl₂ (twice), and a final wash with 10% anisole in CH₂Cl₂ (v/v). Fmoc-amino acids were coupled in the presence of *N,N'*-dicyclohexylcarbodiimide (DCC) and HOBT in DMF, which was further diluted with 10% anisole in CH₂Cl₂ (v/v) for 2 h. The completeness of the reaction was qualitatively evaluated using the



ninhydrin test: in the case of an incomplete reaction, the coupling step was repeated with HBTU as a coupling reagent, otherwise, acetylation was carried out using 30% acetic anhydride (v/v) in CH₂Cl₂/anisole (9:1 v/v) prior to subsequent deprotection-coupling cycles. The completed peptide chain was cleaved off the resin with TFA/dithiothreitol (DTT)/water (90:5:5 v/v/v) at 20°C for 4 h.

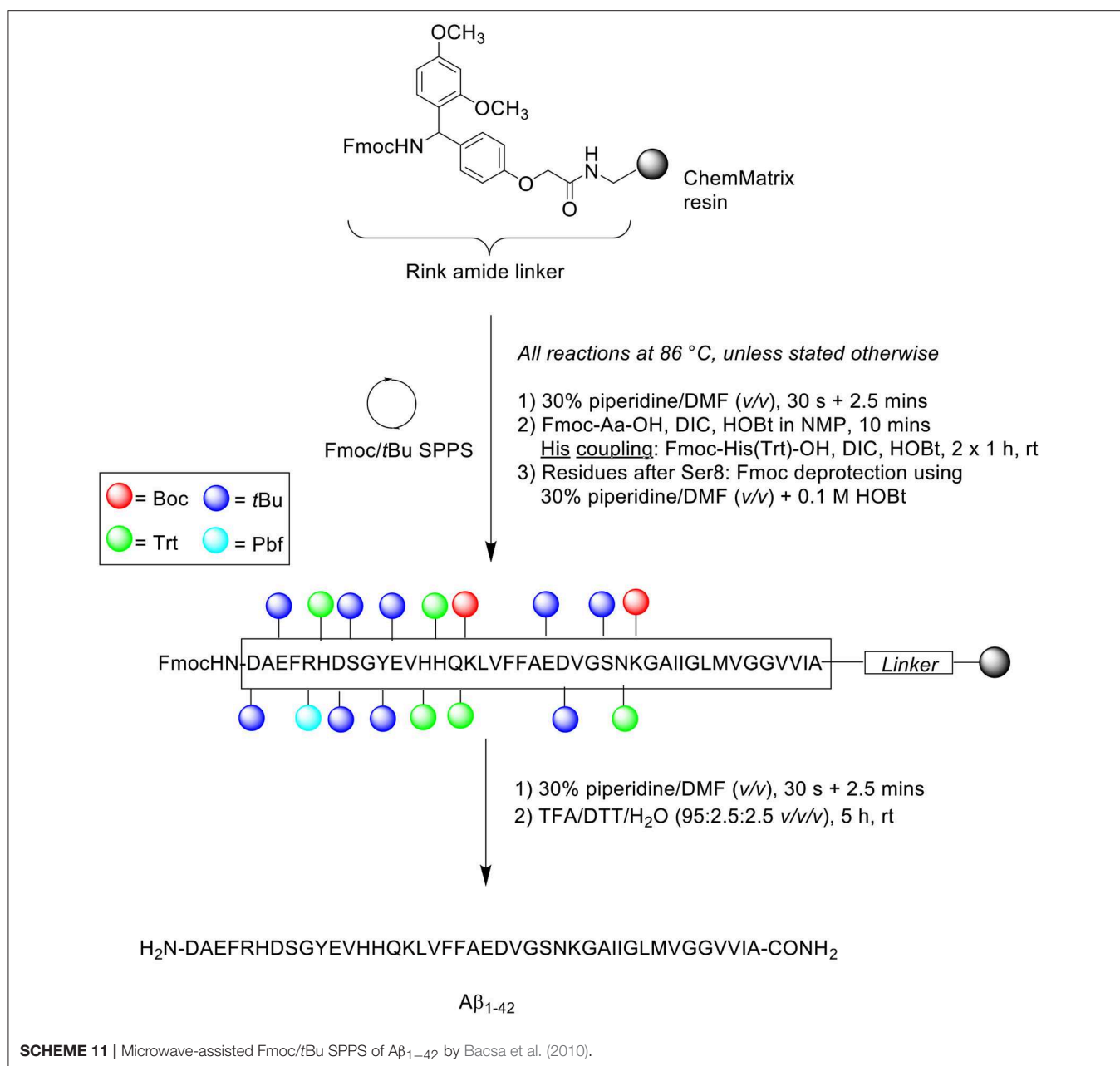
Following cleavage, the TFA filtrate was diluted with 0.1% TFA in acetonitrile to a final acetonitrile concentration of 30% (v/v), and afterwards loaded into a preparative HPLC column. Purification of the crude peptide was carried out on a PrepPak[®] Cartridge 47 x 300 mm (column no. M23582) Bakbond WP C4 15 μ Packing column at a flow rate of 80 mL/min. A linear gradient of 30–70% B was employed, where solvent B was 0.1% TFA in acetonitrile/water (4:1 v/v) and solvent A was 0.1% TFA in water. The collected fractions were analyzed by analytical RP-HPLC, ESI-MS, and amino acid composition. RP-HPLC analysis was undertaken using a Phenomenex (Jupiter) C4 column (250 \times 4.6 mm, 300 \AA , 5 μ m) at a flow rate of 0.2 mL/min. A linear gradient of 30–90% B was employed, using the same solvent system as that for peptide purification. The eluted chromatographic peak was also confirmed by ESI-MS and amino acid analysis to correspond

to the desired product, although neither its yield nor purity were reported by the authors. The 3-(4,5-dimethylthiazol-2-yl)-2,5-diphenyltetrazolium bromide (MTT) assay was subsequently carried out on a SH-SY5Y neuroblastoma cell line, which was incubated in the presence of synthetic A β _{1–42}. The results obtained showed an expected reduction in cellular viability by ~40%, compared to untreated control cells, which provided proof of bioequivalence.

BACSA ET AL. (2010)

Owing to its length, and the use of extended coupling times, preparation of synthetic A β _{1–42} typically takes up to 48 h. Bacsa et al. thus attempted to synthesize this peptide using microwave-assisted Fmoc/*t*Bu SPPS to accelerate the coupling and deprotection steps, affording the final peptide in a shorter overall preparation time (**Scheme 11**; Bacsa et al., 2010). Microwave-assisted synthesis is thought to perturb intermolecular hydrogen bonding between neighboring β -sheets, a key interaction in peptide aggregation (Paradís-Bas et al., 2016).

Peptide synthesis was undertaken on Rink amide ChemMatrix resin (0.50 mmol/g loading) at 0.075 mmol scale. All reactions were performed at 86°C, unless indicated otherwise. Fmoc



removal was afforded in two steps using 30% piperidine in DMF (v/v), first for 30 s and then 2.5 min. Fmoc-amino acids were single coupled in the presence of DIC and HOBT in *N*-methyl-2-pyrrolidone (NMP) for 10 min. Coupling of the three sensitive histidine residues had to be performed at room temperature in order to prevent racemization. This step was performed twice for 60 min each time to ensure complete coupling, using Fmoc-His(Trt)-OH and DIC/HOBT. The coupling cocktail was allowed to pre-activate for 2 min prior to addition to resin bed. Fmoc removal of residues after Ser8 was achieved using 30% piperidine in DMF (v/v) containing 0.1 M HOBT to prevent aspartamide formation at residue Asp7. The completed peptide chain was cleaved using TFA/DTT/water (95:2.5:2.5

v/v/v) for 5 h at ambient temperature. The TFA filtrate was then concentrated *in vacuo*, precipitated with cold ether, and recovered by lyophilization to afford crude peptide at 78% yield. This was immediately stored at -20°C to avoid methionine oxidation and further aggregation of the peptide.

A sample of the crude peptide was dissolved in HFIP prior to RP-HPLC analysis using an analytical Phenomenex Jupiter C4 column (250 \times 4.6 mm, 10 μm) at 60°C . A linear gradient of 30–100% B was applied over 45 min at a flow rate of 4 mL/min, where solvent B was 0.1% TFA in CH₃CN and solvent A was 0.1% TFA in H₂O. The resulting chromatogram showed a single major peak with a retention time of 4.14 min, the mass of which was confirmed by MALDI-TOF MS to correspond to the

desired product. Furthermore, this result was also corroborated by standard amino acid analysis and comparison of the ¹H NMR spectrum of the crude peptide with previously published data. The group also undertook A β _{1–42} synthesis using conventional heating at the same temperature, which interestingly also yielded similar results to that obtained from microwave-assisted synthesis. The neurotoxicity of the synthesized peptides were examined *in vitro* by conducting an MTT assay on a SH-SY5Y cell line, which produced identical results with respect to cellular viability. Taken together, these results indicated that rapid synthesis of A β _{1–42} can be achieved with microwave-assisted Fmoc/tBu SPPS, and that A β _{1–42} synthesized using this method is sufficiently bioequivalent. The latter conclusion is particularly important as the use of microwave energy in peptide synthesis has been associated with peptide backbone de-aggregation, due to its direct interactions with the generated electric field.

COLLINS ET AL. (2014)

In the attempt to further shorten the preparation time and improve yield of A β _{1–42}, Collins et al. developed the high efficiency SPPS (HE-SPPS) methodology, which was successfully implemented in the synthesis of several complex peptides, including A β _{1–42} (Collins et al., 2014). Firstly, two conventional, non-microwave-assisted syntheses of A β _{1–42} were trialed at 0.1 mmol scale on PAL-PEG-PS resin (0.16 mmol/g loading) to establish a baseline purity level. In the first synthesis, Fmoc removal was performed twice for 5 and 10 min. Fmoc-amino acid (5 eq.) coupling was achieved in the presence of DIC (5 eq.) and Oxyma (5 eq.) in DMF for 60 min. The completed peptide chain was cleaved with TFA/TIPS/water/2,2'-(ethylenedioxy)diethanethiol (DODT) (v/v/v/v) and recovered by lyophilization to afford the crude peptide at 85% yield and 56% purity. In the second synthesis, Fmoc removal was also performed twice, but at shorter times of 0.5 and 3 min. Fmoc-Aa-OH (5 eq.) was coupled using 2-(6-chloro-1H-benzotriazole-1-yl)-1,1,3,3-tetramethylammonium hexafluorophosphate (HCTU, 5 eq.) in DMF and DIPEA (10 eq.) in NMP for only 5 min. The relatively short coupling time may provide an explanation to the staggeringly low crude purity of 14%, even though the yield was 72%. A β _{1–42} synthesis was also attempted using microwave-assisted SPPS. Fmoc removal was afforded by 20% piperidine (v/v) containing 0.1 M Oxyma. TFA cleavage was performed for 30 min at 38°C, and other conditions remained as stated above. This afforded the crude peptide at 87% yield and 67% purity.

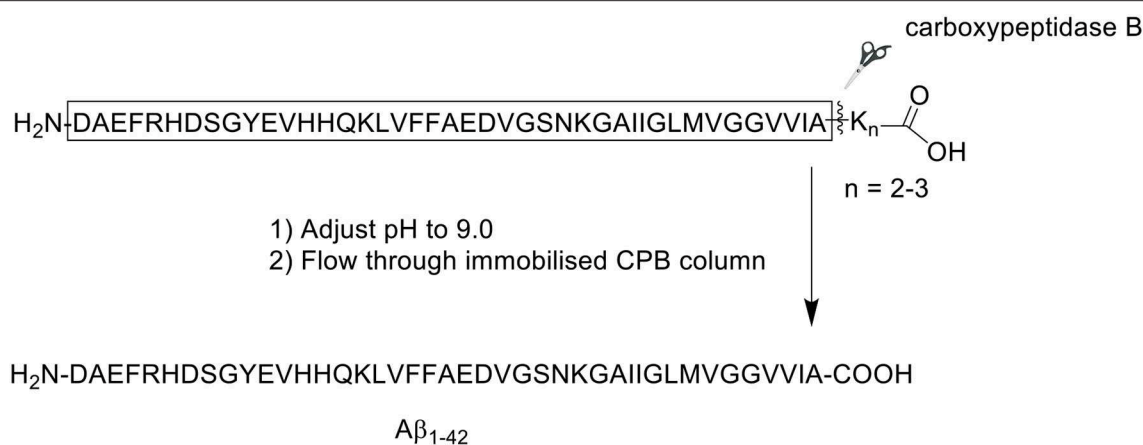
Optimizations of the microwave protocol was subsequently undertaken as follows: first, microwave conditions for deprotection and coupling steps were assessed. The group observed that the duration of these steps can be significantly shortened through utilization of a higher microwave power, whilst maintaining a high temperature within the reaction vessel. This setup allowed the vessel to reach 90°C ($T_{\text{max}} = 92^\circ\text{C}$) in just 20 s, as monitored using a fiber optic probe. Consequently, it was possible for deprotection and coupling steps to be completed in only 1 and 2 min, respectively. Next, the washing step was assessed. It was noted that following completion of each coupling

reaction, the resin bed retained a residual temperature of 50°C, which would permit diffusion at a higher rate, and thus more efficient washing steps, employing less reagent volumes and shorter time. Furthermore, the authors reasoned that post-coupling washes are not necessary, as the inherent protection afforded by SPPS meant that uncoupled, activated Fmoc-amino acids in solution would be dissolved by the large excess of base introduced in the subsequent deprotection step. Lastly, an assessment of reagents used for Fmoc removal was undertaken. Due to the classification of piperidine as a controlled substance, piperazine has often been considered as an alternative Fmoc deblocking reagents for both conventional and microwave synthesis. However, one major limitation of this reagent is that it can only reach a maximum concentration of 6% (v/v) when diluted in either DMF or NMP. A novel solvent system was thus conceived, which was aimed to increase piperazine concentration without bearing negative effects on solubility of the resin-bound peptide. Dilution of piperazine in ethanol/NMP (1:9 v/v) successfully elevated its maximum concentration to 10% (v/v), which was shown to be equally effective to 20% piperidine (v/v) with regards to its deprotecting capacity. These optimizations were implemented in the synthesis of A β _{1–42}. Aspartamide formation, an established side reaction in the synthetic process, was reasonably minimized using these reaction conditions. The proposed method enabled the efficient preparation of A β _{1–42} in just under 4 h, which is remarkably fast for a peptide of this length. All samples were analyzed by ultra-high performance liquid chromatography (UPLC) using Acquity UPLC BEH C18 column (1.7 mm and 2.1 × 100 mm). A crude 87% yield was obtained after lyophilization with 10% acetic acid (v/v) at 72% purity. Furthermore, the overall protocol also minimized chemical waste by approximately 90%, which is a forward step toward sustainability in peptide synthesis. Unfortunately, no further bio-testing was attempted by the group.

CHEMURU ET AL. (2014)

An alternative approach by which the efficient synthesis of A β _{1–42} may be achieved is through adjustment of its solubility properties, which dictate how the peptide behaves in solution. Given the presence of hydrophobic residues proximal to its C-terminus, A β _{1–42} expectedly commences aggregation almost immediately following reconstitution in conventional solvents such as acetonitrile. In 2014, Chemuru et al. reported on the ready separation of A β _{1–42} pre-synthesized with a C-terminal solubilizing tag consisting of two or three lysine residues (**Scheme 12**; Chemuru et al., 2014). Peptides were synthesized using Fmoc/tBu SPPS on PEG-PS resin (*loading not stated*). Fmoc-protected amino acids were double coupled in the presence of HBTU and NMM in DMF.

The crude product was first dissolved in 50% aqueous formic acid (v/v) prior to purification by RP-HPLC on an Agilent Zorbax SB-C3 column (9.4 × 250 mm, 5 μm). A linear gradient of 30–60% B was employed, where solvent B was 0.05% TFA in acetonitrile, and solvent A was 0.05% TFA in water. For



SCHEME 12 | Enzyme-mediated separation of lysine tag from A β_{1-42} peptide by Chemuru et al. (2014).

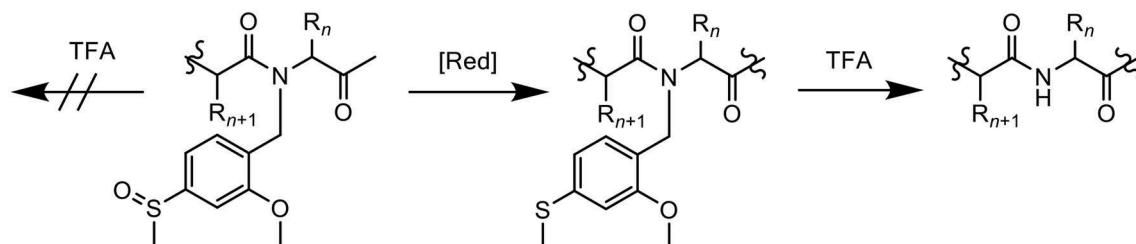


FIGURE 2 | Mmsb, a novel backbone amide-protecting group for the synthesis and purification of “difficult peptide” sequences.

comparative purposes, the group also procured synthetic wild-type A β_{1-42} . Purification of native A β_{1-42} was attempted at both room temperature and 65°C, whereas A β_{1-42} tagged with lysine residues was readily purified at room temperature. RP-HPLC analysis of A β_{1-42} at room temperature employing the solvent system described above yielded the expected asymmetrical, broad, and unresolved chromatographic peak. The yield and purity of A β_{1-42} were 2.7 and 64.9%, respectively. Repeating the purification process at 65°C resolved the peak, affording the desired product in 6.4% yield with 80.6% purity.

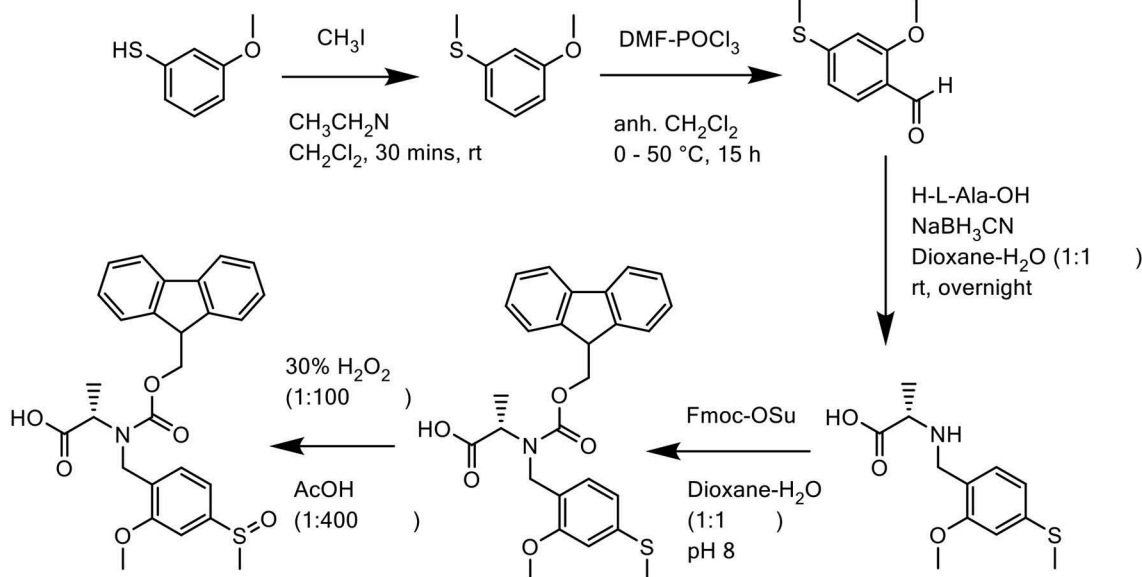
Following purification, the C-terminal lysine residues were removed using a carboxypeptidase B (CPB) agarose column, which was equilibrated to room temperature and washed at least five times with Tris-buffered saline (TBS, pH 9.0) prior to use. Purified A β_{1-42} -Lys tail peptide was flowed through the column at approximately 0.2 mL/min. The column was then washed with TBS. One-milliliter fractions were collected from both peptide load and column wash, then analyzed by liquid chromatography-mass spectrometry (LC-MS) to identify peptide-containing fractions, and confirm complete removal of the Lys residues. Fractions containing the desired product were pooled, the pH adjusted to 2.0, loaded onto RP-HPLC column, and repurified using the conditions described above. The collected fractions were assessed for purity, then pooled and lyophilized, affording pure A β_{1-42} . For A β_{1-42} synthesized with two C-terminal lysine residues (A β_{1-42} K₂), the yield and

purity of the final compound was 6.2 and 89.7%, respectively. Interestingly, the yield of A β_{1-42} synthesized with three C-terminal lysine residues (A β_{1-42} K₃) was slightly improved to 7.8%, accompanied by a slight increase in purity to 90.2%. This improvement might in part be attributed to the presence of an additional, positively-charged lysine residue at the C-terminus of the peptide, which resulted in an improved solubility. Further bio-testing was unfortunately not undertaken by the group.

PARADÍS-BAS ET AL. (2014)

Paradís-Bas et al. introduced 2-methoxy-4-methylsulfinylbenzyl (Mmsb), a novel backbone amide safety-catch protecting group in the synthesis and purification of three “difficult peptide” sequences: H-(Ala)₁₀-NH₂, Ac-(RADA)₄-NH₂, and A β_{1-42} (Paradís-Bas et al., 2014). Mmsb, which contains an electron-withdrawing sulfoxide that stabilizes a benzyl moiety, is readily reduced to its corresponding electron-donating thioether, which becomes labile to the same benzyl group. With regards to Fmoc/tBu SPPS, Mmsb is stable to TFA, however its reduced form 2-methoxy-4-methylthiobenzyl (Mmtb) is labile to the acid (**Figure 2**), therefore rendering it a suitable option.

In all three cases, the Mmsb backbone was introduced into the peptide sequence as its corresponding Fmoc



SCHEME 13 | Chemical synthesis of Fmoc-N(Mmsb)-Ala-OH.

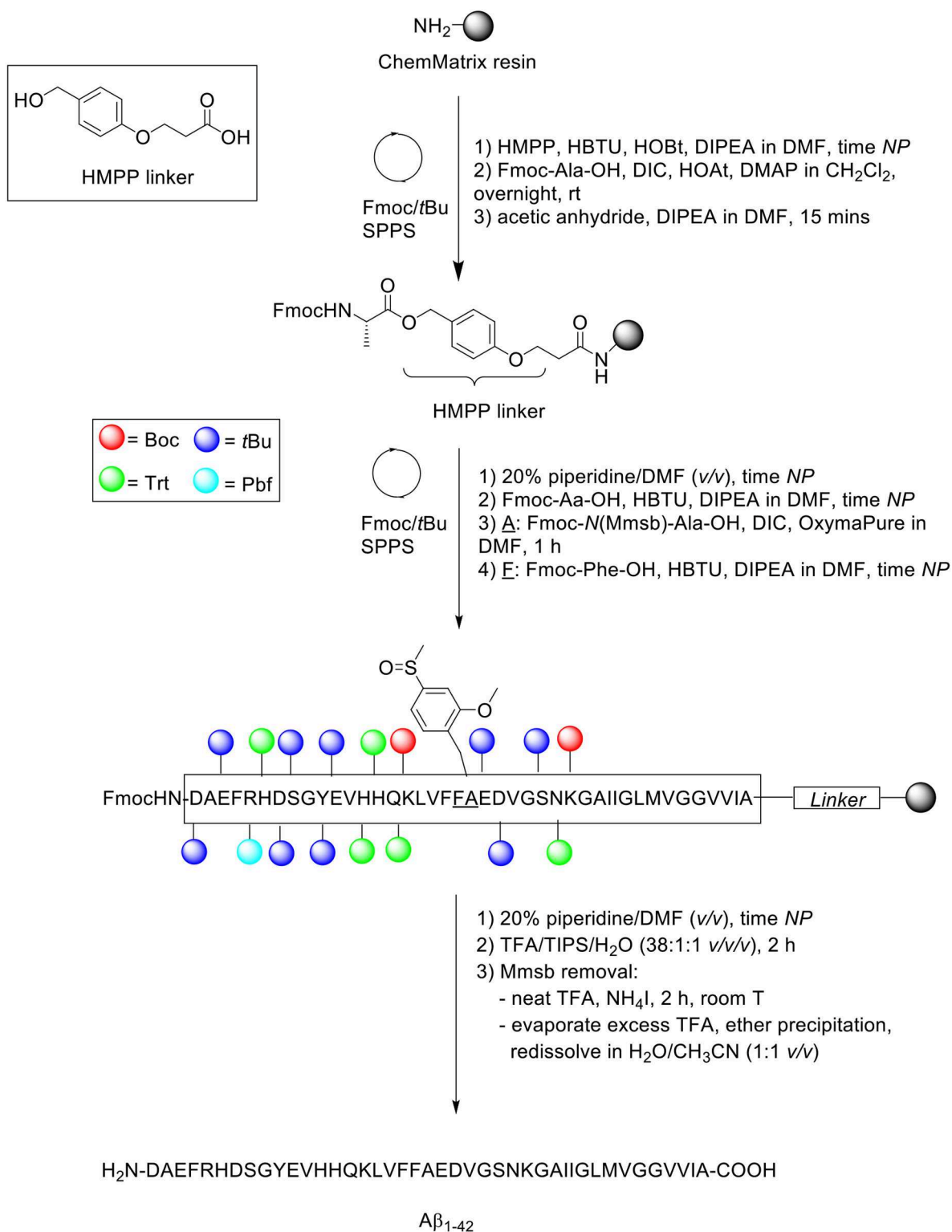
derivative Fmoc-N(Mmsb)-Ala-OH. Synthesis of this derivative was undertaken in five steps (**Scheme 13**): first, commercially available 3-methoxythiophenol was methylated with iodomethane (MeI). Trimethylamine was added dropwise to prevent dialkylation. The alkylated product was subsequently formylated using Vilsmeier reagent, affording 2-methoxy-4-methylthiobenzaldehyde, which was purified by RP-HPLC on an XBridge™ BEH130 C18 column (4.6 × 100 mm, 3.5 μm) in 48% yield. Reductive amination of this aldehyde with the amine of the unprotected alanine residue was achieved in a one-step reaction with NaBH₃CN in dioxane/H₂O (1:1 v/v). N(Mmtb)-Ala-OH was protected by Fmoc using a slight excess of Fmoc-OSu under basic conditions to afford Fmoc-N(Mmtb)-Ala-OH, which was again purified by RP-HPLC on an XBridge™ BEH130 C18 column (4.6 × 100 mm, 3.5 μm) to delineate the unreacted alanine. Lastly, oxidation of Fmoc-N(Mmtb)-Ala-OH by H₂O₂ generated Fmoc-N(Mmsb)-Ala-OH in remarkable purity (98.0%). This building block was utilized directly for SPPS of all three peptides.

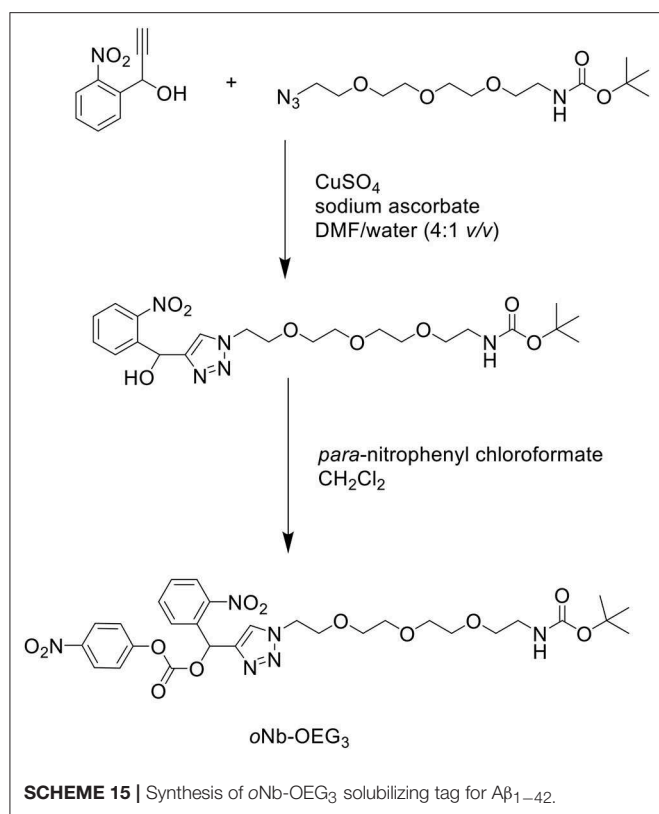
Peptide synthesis was undertaken on aminomethyl ChemMatrix resin (0.62 mmol/g loading) as solid support at 0.1 mmol scale, which was functionalized with HMPP linker (**Scheme 14**). Fmoc removal was achieved using 20% piperidine in DMF (v/v). Fmoc-AA-OH coupling was performed in the presence of HBTU as coupling reagent, with DIPEA and DMF as solvent. The Fmoc-N(Mmsb)-Ala-OH building block, which replaced Ala21 in the A β_{1-42} sequence, was coupled using DIC and OxymaPure in DMF for 1 h, followed by sequential washes with DMF and CH₂Cl₂, and Kaiser test to confirm completeness of the reaction qualitatively. Fmoc-Phe-OH, the subsequent residue in the sequence, was also coupled manually were coupled manually. The completed peptide chain was cleaved from

the resin with TFA/TIPS/H₂O (38:1:1 v/v/v) for 2 h, which demonstrated the stability of Mmsb to acids. Purity of the crude product was relatively low (35%), as determined by RP-HPLC analysis on a Symmetry300™ C4 column (4.6 × 150 mm, 5 μm) at 60°C and flow rate of 1 mL/min. A linear gradient of 10–50% B was used, where solvent B was CH₃CN + 0.036% TFA, and solvent A was H₂O + 0.045% TFA. Purification was undertaken by semi-preparative RP-HPLC using a Phenomenex Jupiter C4 column (21 × 150 mm, 10 μm) at a flow rate of 20 mL/min. A linear gradient of 0–10% B over 5 min and 10–50% B over 60 min was used, where solvent B was CH₃CN + 0.1% TFA and solvent A was H₂O + 0.1% TFA. Removal of the Mmsb amide protecting group was readily achieved by treatment with neat TFA (1 mg/mL) and ammonium iodine at room temperature for 2 h. Excess TFA was evaporated by gentle N₂ stream, and the filtrate precipitated in diethyl ether and redissolved in H₂O/CH₃CN (1:1 v/v), prior to lyophilization.

KARAS ET AL. (2017)

In another attempt to improve the solubility properties of A β_{1-42} , Karas et al. developed a short, monodisperse oligo(ethylene) glycol (OEG)-containing photolabile tag, which was functionalized on residue Lys28 of the A β_{1-42} sequence to solubilize the otherwise hydrophobic peptide (Karas et al., 2017). The tag was synthesized in two steps (**Scheme 15**): an alkyne functional group was incorporated at the benzylic position of an *ortho*-nitrobenzyl (oNb) derivative via a Grignard reaction. This was then reacted with an azide substrate through copper(I)-catalyzed alkyne-azide cycloaddition (CuAAC) in the presence of copper sulfate (CuSO₄) and sodium ascorbate in DMF/water

*NP = not reported***SCHEME 14** | Synthesis of A β_{1-42} with Mmsb protecting group by Paradis-Bas et al. (2014).



(4:1 v/v) to yield an intermediate, which was activated by *para*-nitrophenyl chloroformate in CH₂Cl₂ to afford the desired oNb-OEG₃ tag.

The group utilized microwave-assisted Fmoc/*t*Bu SPPS to synthesize their site-specific tagged A β _{1–42}. Peptide synthesis commenced on TentaGel resin (0.18 mmol/g loading) functionalized with Wang linker, and preloaded with Fmoc-Ala-OH at 0.1 mmol scale (**Scheme 16**).

The Fmoc protecting group was removed using 20% piperidine in DMF (v/v) with 0.1 M Oxyma pure at 90°C for 1 min, except for residues Asp23–Asn27 which were deprotected for 10 min at the same temperature. Fmoc-amino acids (5 eq.) were coupled in the presence of HCTU (5 eq.) and DIPEA (10 eq.). Residues Lys28–Ala42 were coupled once at 75°C, while residues Asp1–Asn27 were double coupled under the same conditions, except for the three sensitive histidine residues, which were double coupled at 50°C. Removal of the monomethoxytrityl (Mmt) side chain protecting group at Lys28 was afforded through sequential treatments with 1% TFA in CH₂Cl₂ (v/v). The resin bed was then neutralized, and resultant free amine condensed with oNb-OEG₃ tag (3 eq.) coupled using DIPEA (6 eq.) for 1 h at 75°C to afford the carbamate linkage. The completed peptide chain was cleaved from the resin using TFA/thioanisole/water/TIPS (95:2:2:1 v/v/v/v) for 3 h. The TFA filtrate was concentrated *in vacuo*, precipitated in cold ether, and recovered by lyophilization.

A sample of the crude peptide was purified by RP-HPLC using a Phenomenex Kinetex XB-C18 AXIA packed column

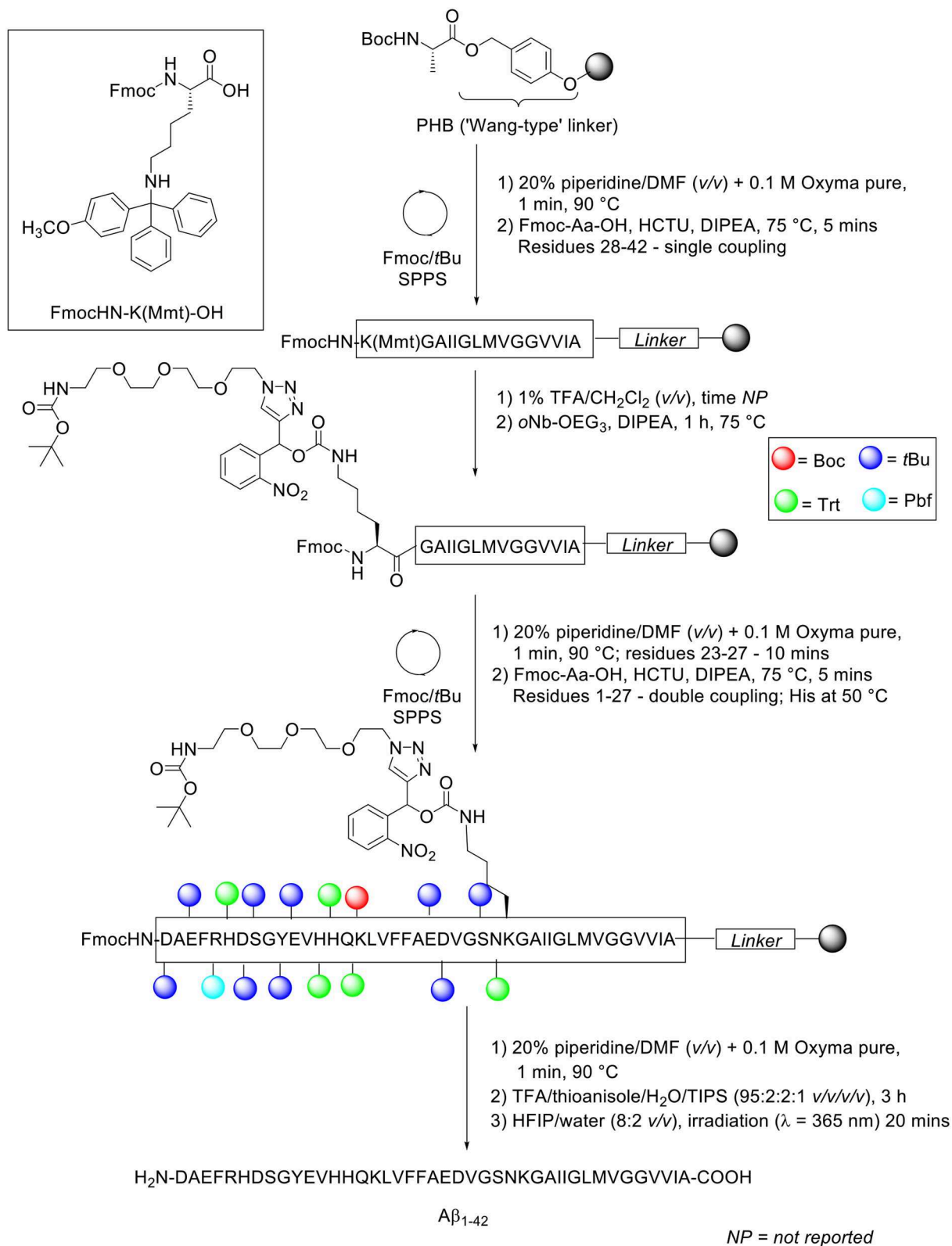
(100Å, 21.2 × 150 mm, 5μ) at 60°C. A linear gradient of 20–60% B was employed over 40 min with a flow rate of 5 mL/min. Solvent A was 10 mM ammonium acetate in water (pH 9.2), whereas solvent B was 10 mM ammonium acetate in acetonitrile/water (8:2 v/v, pH 9.2). The purified, tagged peptide was afforded at 9.6% yield relative to purified crude weight and >95% purity. The solubilizing tag was subsequently removed by photolysis at 365 nm. The photocleavable-tagged A β _{1–42} was first dissolved in HFIP/water (8:2 v/v), irradiated for 20 min, and then injected directly into RP-HPLC column for purification, which yielded pure A β _{1–42} in 60% yield. Unfortunately, the purity of the final product was not reported by the authors. Biophysical characterization of A β _{1–42} synthesized using this method was subsequently undertaken. Comparative TEM images between tagged A β _{1–42} and native A β _{1–42} obtained following photolysis showed a suppression in fibril formation, which was further quantified by a lower ThT fluorescence, after incubation in phosphate buffered saline (PBS) for 48 h at 37°C. Thus, incorporation of this tag into the A β _{1–42} peptide sequence was successfully shown by this group to improve its solubility properties, affording the desired product at higher yield and purity.

KASIM ET AL. (2019)

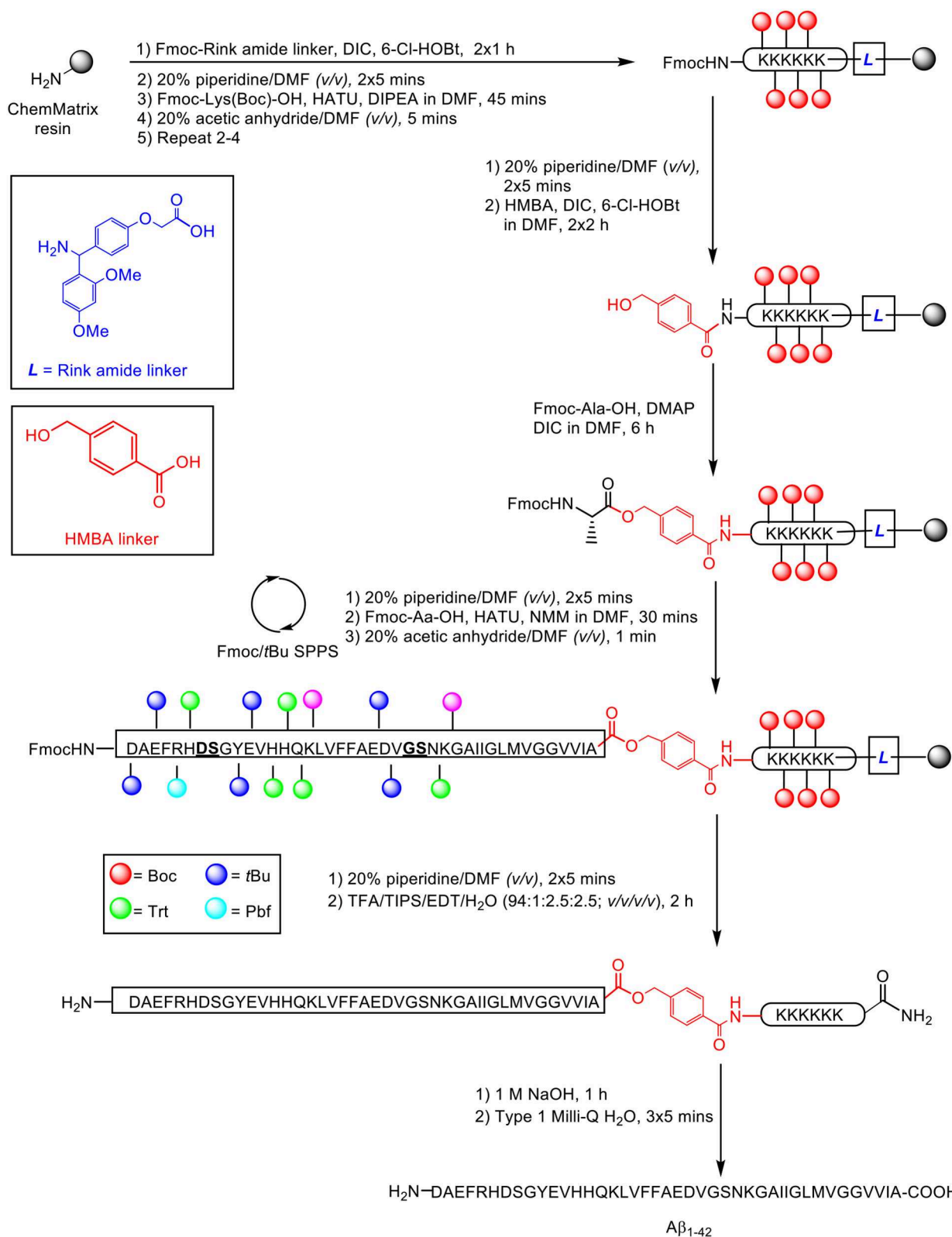
Recently, our group published an improved methodology for the synthesis and efficient characterization of the A β _{1–42} peptide (**Scheme 17**; Kasim et al., 2019).

The proposed synthetic strategy utilized a double linker system, which has previously enabled efficient synthesis of the aggregating cancer protein NY-ESO1 (Harris and Brimble, 2009) and peptide hormone vesiculin (Williams et al., 2013). Peptide synthesis commenced on the low-loading ChemMatrix resin (0.64 mmol/g loading) at 0.1 mmol scale, using Fmoc/*t*Bu SPPS. Fmoc-Rink amide linker (4 eq.) was first anchored on resin in the presence of DIC (4 eq.) and 6-chlorohydroxybenzotriazole (6-Cl-HOBt, 4 eq.) as coupling reagents, followed by sequential assembly of the hexalysine tag using HATU (4.6 eq.) and DIPEA (10 eq.), and coupling of the bifunctional 4-hydroxymethylbenzoic acid (HMBA) linker (4 eq.) using DIC (4 eq.) and 6-Cl-HOBt (4 eq.), completing the double linker construct. The first C-terminal residue alanine was then esterified on HMBA linker using Fmoc-Ala-OH (2 eq.), DIC (2 eq.) and DMAP (0.9 eq.). Peptide chain elongation was achieved using Fmoc-Aa-OH (5 eq.), HATU (4.6 eq.), and NMM (10 eq.), followed by cleavage off resin using TFA/TIPS/EDT/water (94:1:2.5:2.5 v/v/v/v). The TFA filtrate was evaporated using a gentle nitrogen stream, precipitated in cold ether, and recovered by lyophilization (56% yield based on 0.1 mmol ChemMatrix loading).

Purification of the crude product was undertaken by RP-HPLC using a semi-preparative Zorbax 300SB-C3 column (9.4 × 250 mm, 5μm) under conventional conditions (acidic mobile phases, room temperature). A linear gradient of 1–61% B was employed over 60 min, where solvent B was 0.1% TFA in acetonitrile and solvent A was 0.1% TFA in water.



SCHEME 16 | Fmoc/tBu SPPS of A β_{1-42} with oNb-OEG₃ tag functionalized on Lys28 residue by Karas et al. (2017).



SCHEME 17 | Fmoc/tBu SPPS of A β_{1-42} on a double linker system, employing pseudoproline dipeptides as aggregation disruptors by Kasim et al. (2019). Residues in bold and underlined indicate site of pseudoproline incorporation.

TABLE 2 | Comparative table of methods and conditions employed for the synthesis and purification of A β _{1–42} peptide.

| References | Method | Resin | Linker | Purification | | | Purified yield, purity (%) |
|----------------------------|----------|----------------|------------------------|--------------|---|------------|----------------------------|
| | | | | Column | Solvents | Temp. (°C) | |
| Burdick et al., 1992 | Fmoc/tBu | PEG-PS | <i>p</i> -alkoxybenzyl | C4 | CH ₃ CN (0.1% TFA)/H ₂ O (0.1% TFA) | RT | NP, NP |
| Hendrix et al., 1992 | Boc/Bzl | Merrifield | Kaiser Oxime | NP | NP | RT | NP, >90 |
| Milton et al., 1997 | Fmoc/tBu | PEG-PS | <i>p</i> -alkoxybenzyl | C4 | CH ₃ CN (0.1% TFA)/H ₂ O (0.1% TFA) | RT | 28, NP |
| Fukuda et al., 1999 | Fmoc/tBu | PEG-PS | <i>p</i> -alkoxybenzyl | C18 | CH ₃ CN (0.1% NH ₄ OH)/H ₂ O (0.1% NH ₄ OH) | RT | 10, NP |
| Tickler et al., 2001 | Fmoc/tBu | PEG-PS | HMPA | C4 | CH ₃ CN (0.1% TFA)/H ₂ O (0.1% TFA) | 60 | 17, NP |
| Carpino et al., 2004 | Fmoc/tBu | TentaGel | HMPB | NP | NP | RT | NP, NP |
| Kim et al., 2004 | Boc/Bzl | Aminomethyl PS | PAM | diphenyl | CH ₃ CN (0.09% TFA)/H ₂ O (0.09% TFA) | RT | NP, NP |
| Sohma et al., 2005 | Fmoc/tBu | Aminomethyl PS | 2-CTC | C18 | CH ₃ CN (0.1% TFA)/H ₂ O (0.1% TFA) | 40 | NP, >95 |
| García-Martín et al., 2006 | Fmoc/tBu | ChemMatrix | HMPP | C8 | CH ₃ CN (0.1% TFA)/H ₂ O (0.1% TFA) | 60 | NP, NP |
| Zarándi et al., 2007 | Fmoc/tBu | PS | Wang | C4 | CH ₃ CN/H ₂ O (0.1% TFA)/H ₂ O (0.1% TFA) | RT | NP, >95 |
| Bacsa et al., 2010 | Fmoc/tBu | ChemMatrix | Rink amide | C4 | CH ₃ CN (0.1% TFA)/H ₂ O (0.1% TFA) | 60 | NP, NP |
| Collins et al., 2014 | Fmoc/tBu | PEG-PS | PAL | C18 | CH ₃ CN (0.1% CH ₂ O ₂)/H ₂ O (0.1% CH ₂ O ₂) | RT | NP, NP |
| Chemuru et al., 2014 | Fmoc/tBu | PEG-PS | NP | C3 | CH ₃ CN (0.05% TFA)/H ₂ O (0.05% TFA) | RT | 7.8, 90.2 |
| Paradis-Bas et al., 2014 | Fmoc/tBu | ChemMatrix | HMPP | C4 | CH ₃ CN (0.1% TFA)/H ₂ O (0.1% TFA) | RT | NP, 90 |
| Karas et al., 2017 | Fmoc/tBu | TentaGel | PHB | C18 | CH ₃ CN/H ₂ O (10 mM NH ₄ OAc)/H ₂ O (10 mM NH ₄ OAc) | 60 | NP, NP |
| Kasim et al., 2019 | Fmoc/tBu | ChemMatrix | Rink amide, HMBA | C3 | CH ₃ CN (0.1% TFA)/H ₂ O (0.1% TFA) | RT | 8.6, 92 |

NP, not reported.

One highlight of this methodology is that it was possible for purification of the crude product to be carried out on a relatively large scale, up to 90 mg in a single batch. The presence of the lysine tag is proposed to facilitate this process. The purified peptide-linker was subsequently treated with 1 M sodium hydroxide for 1 h to hydrolyse the base-labile ester bond between alanine and HMBA linker. The liberated linker was then readily dissolved following sequential washes with ultrapure water, recovering the peptide quantitatively without the need for any additional HPLC purification steps, and affording the desired peptide at 92% purity. A β _{1–42} was then subjected to biophysical assessment by TEM imaging, ThT assay, and circular dichroism (CD) spectroscopy. The resulting TEM images indicated that the peptide did form fibrils over time, and possessed a concentration-dependent aggregation profile in response to ThT binding, as well as a secondary structure composition of predominantly beta-sheets and random coils, as quantified by CD. Therefore, A β _{1–42} synthesized through this methodology is sufficiently bioequivalent for use in further *in vitro* and *in vivo* biological studies.

SUMMARY

In this review, a selection of methodologies designed to facilitate the efficient synthesis of A β _{1–42} peptide has been presented and discussed in great depth. Essential details about each protocol are summarized within **Table 2**, providing a convenient point of reference for comparative purposes. In terms of SPPS methodology, the majority opted for Fmoc/*t*Bu SPPS. While there is a relatively extensive range of resins and linkers employed, these in general possess a low degree of substitution, which limited steric interference as the desired peptide elongated. With regards to purification of the crude material, there is also a great deal of variety in the chromatographic column used, but not so much with the solvent system, primarily 0.1% TFA in acetonitrile and 0.1% TFA in water, and temperature; most groups reviewed herein carried out their purification at room temperature. Yields of the final product are expectedly low, but collectively high in purity. Lastly, although this was not generally undertaken, groups that performed bioequivalence testing on their synthesized A β _{1–42} all reported on a high

similarity with the endogenous peptide, in terms of its biological profile. With regards to this, we propose that it should be made necessary for any future work in this field to include evidence of bioequivalence.

CONCLUSIONS AND FUTURE DIRECTIONS

At the present time, it is clear that significant strides have been taken toward the efficient synthesis and characterization of the amyloidogenic A β _{1–42} peptide since its maiden synthesis by Burdick et al. nearly three decades ago. Advancements in the field of “difficult peptide” synthesis, more specifically A β _{1–42}, translates to its production in ample quantities and, perhaps most importantly, with a purity that mirrors A β _{1–42} isolated from natural sources, such as post-mortem human brain tissue. Identification of the key challenge associated with its preparation, namely the propensity to aggregate both on resin during SPPS and in solution, has propelled the development of methods which have effectively addressed this issue. The so-called “A β _{1–42} problem” can thus be mitigated indirectly through optimization of the synthetic protocol employed, such as the use of PEG-based ChemMatrix resin (García-Martín et al., 2006; Kasim et al., 2019) to minimize the degree of steric interference as peptide elongation progresses, or through careful, considered choice of solvents and reagents that facilitate a more complete deprotection and coupling of amino acid residues. Furthermore, direct chemical modifications on the peptide sequence, achieved for instance through the introduction of removable solubilizing tags (Chemuru et al., 2014; Karas et al., 2017; Kasim et al., 2019) has also been proven to be an equally effective means. Thus, it would be a most logical deduction to propose that a combination of both approaches should produce a synergistic effect.

The extensive variety of methods that have been employed thus far, however, raises the curious question as to whether there is a need for a streamlined, “one-size-fits-all” protocol for the efficient synthesis of A β _{1–42}. We argue that such a generalized method is not required. Rather, any method designed specifically for the preparation of this amyloidogenic peptide must be relatively easy to reproduce by any standard peptide synthesis

laboratory. With respect to this, the reagents employed should incur a reasonable cost and be easily accessible. Consequently, A β _{1–42} synthesis using Boc/Bzl SPPS might not be especially favorable given the necessity for specialized equipment, some of which have their use restricted by local authorities. Of course, there is also the general safety issue pertaining to the use of strong acids such as HF as an essential component of this strategy. Perhaps, then, the future of A β _{1–42} lies on the more routinely employed Fmoc/tBu SPPS. Ultimately, any method employed should enable preparation of multi-milligram amounts of this peptide, and at a purity level that is identical to the endogenous peptide.

While most of the studies reviewed herein did not report their final A β _{1–42} purity, satisfactory evidence was provided in general as a proxy, in most cases through comparative assessment with commercially available A β _{1–42}, as well as *in vitro* studies employing the synthesized A β _{1–42}. The latter is perhaps of greater importance than the former, as they provide proof of bioequivalence, and suggests that even though the synthesized peptide may not be of especially high purity, it is still capable of behaving in a manner identical to endogenous A β _{1–42}, which we believe should be considered as a hallmark of a successful synthesis.

AUTHOR CONTRIBUTIONS

JK and IK conceived the review article. PH and MB proofread and provided feedback on overall structure and content of the manuscript.

FUNDING

Details of all funding sources should be provided, including grant numbers if applicable. Please ensure to add all necessary funding information, as after publication this is no longer possible.

ACKNOWLEDGMENTS

The authors would like to acknowledge the support provided by Maurice Wilkins Centre for Molecular Biodiscovery and members of the Brimble Research Group.

REFERENCES

- Atherton, E., Fox, H., Harkiss, D., Logan, C. J., Sheppard, R. C., and Williams, B. J. (1978). A mild procedure for solid phase peptide synthesis: use of fluorenylmethoxycarbonylamino-acids. *J. Chem. Soc. Chem. Commun.* 537–539. doi: 10.1039/C39780000537
- Bacsa, B., Bosze, S., and Kappe, C. O. (2010). Direct solid-phase synthesis of the β -amyloid (1–42) peptide using controlled microwave heating. *J. Org. Chem.* 75, 2103–2106. doi: 10.1021/jo100136r
- Burdick, D., Soreghan, B., Kwon, M., Kosmoski, J., Knauer, M., Henschen, A., et al. (1992). Assembly and aggregation properties of synthetic Alzheimer's A4/beta amyloid peptide analogs. *J. Biol. Chem.* 267, 546–554.
- Carpino, L. A., Krause, E., Sferdean, C. D., Schumann, M., Fabian, H., Bienert, M., et al. (2004). Synthesis of ‘difficult’ peptide sequences: application of a depsipeptide technique to the Jung–Redemann 10- and 26-mers and the amyloid peptide A β (1–42). *Tetrahedron Lett.* 45, 7519–7523. doi: 10.1016/j.tetlet.2004.07.162
- Carpino, L. A., Sadat-Aalae, D., Chao, H. G., and DeSelms, R. H. (1990). [(9-Fluorenylmethyl)oxy]carbonyl (Fmoc) amino acid fluorides. Convenient new peptide coupling reagents applicable to the Fmoc/tert-butyl strategy for solution and solid-phase syntheses. *J. Am. Chem. Soc.* 112, 9651–9652. doi: 10.1021/ja00182a041
- Chemuru, S., Kodali, R., and Wetzel, R. (2014). Improved chemical synthesis of hydrophobic A β peptides using addition of C-terminal lysines later removed by carboxypeptidase B. *Biopolymers* 102, 206–221. doi: 10.1002/bip.22470
- Choi, J. W., Kim, H. Y., Jeon, M., Kim, D. J., and Kim, Y. (2012). Efficient access to highly pure β -amyloid peptide by optimized solid-phase synthesis. *Amyloid* 19, 133–137. doi: 10.3109/13506129.2012.700287
- Coin, I. (2010). The depsipeptide method for solid-phase synthesis of difficult peptides. *J. Pept. Sci.* 16, 223–230. doi: 10.1002/psc.1224

- Collins, J. M., Porter, K. A., Singh, S. K., and Vanier, G. S. (2014). High-efficiency solid phase peptide synthesis (HE-SPPS). *Org. Lett.* 16, 940–943. doi: 10.1021/ol4036825
- Cummings, J., Lee, G., Ritter, A., and Zhong, K. (2018). Alzheimer's disease drug development pipeline: 2018. *Alzheimers Dement* 4, 195–214. doi: 10.1016/j.trci.2018.03.009
- Fukuda, H., Shimizu, T., Nakajima, M., Mori, H., and Shirasawa, T. (1999). Synthesis, aggregation, and neurotoxicity of the Alzheimer's A β _{1–42} amyloid peptide and its isoaspartyl isomers. *Bioorg. Med. Chem. Lett.* 9, 953–956. doi: 10.1016/S0960-894X(99)00121-3
- García-Martín, F., Quintanar-Audelo, M., García-Ramos, Y., Cruz, L. J., Gravel, C., Furic, R., et al. (2006). ChemMatrix, a Poly(ethylene glycol)-based support for the solid-phase synthesis of complex peptides. *J. Comb. Chem.* 8, 213–220. doi: 10.1021/cc0600019
- Glenner, G. G., and Wong, C. W. (1984). Alzheimer's disease: Initial report of the purification and characterization of a novel cerebrovascular amyloid protein. *Biochem. Biophys. Res. Commun.* 120, 885–890. doi: 10.1016/S0006-291X(84)80190-4
- Halliday, G. (2017). Pathology and hippocampal atrophy in Alzheimer's disease. *Lancet Neurol.* 16, 862–864. doi: 10.1016/S1474-4422(17)30343-5
- Hardy, J. A., and Higgins, G. A. (1992). Alzheimer's disease: the amyloid cascade hypothesis. *Science* 256, 184–185. doi: 10.1126/science.1566067
- Harris, P. W. R., and Brimble, M. A. (2009). Synthesis of an arginine tagged [Cys155-Arg180] fragment of NY-ESO-1: elimination of an undesired by-product using 'In House' resins. *Synthesis* 2009, 3460–3466. doi: 10.1055/s-0029-1216952
- Hendrix, J. C., Halverson, K. J., and Lansbury, P. T. (1992). A convergent synthesis of the amyloid protein of Alzheimer's disease. *J. Am. Chem. Soc.* 114, 7930–7931. doi: 10.1021/ja00046a060
- Hendrix, J. C., and Lansbury, P. T. (1992). Synthesis of a protected peptide corresponding to residues 1–25 of the β -amyloid protein of Alzheimer's disease. *J. Org. Chem.* 57, 3421–3426. doi: 10.1021/jo00038a034
- Herrup, K. (2015). The case for rejecting the amyloid cascade hypothesis. *Nat. Neurosci.* 18, 794–799. doi: 10.1038/nn.4017
- Kaiser, E. T., Mihara, H., Laforet, G. A., Kelly, J. W., Walters, L., Findeis, M. A., et al. (1989). Peptide and protein synthesis by segment synthesis-condensation. *Science* 243, 187–192. doi: 10.1126/science.2492114
- Karas, J. A., Noor, A., Schieber, C., Connell, T. U., Separovic, F., and Donnelly, P. S. (2017). The efficient synthesis and purification of amyloid- β (1–42) using an oligoethylene glycol-containing photocleavable lysine tag. *Chem. Commun.* 53, 6903–6905. doi: 10.1039/C7CC03147E
- Kasim, K. J., Kaviani, L., Ng, J., Harris, R. P. W., Birch, P. N., and Brimble, A. M. (2019). Efficient synthesis and characterisation of the amyloid beta peptide, A β 1–42, using a double linker system. *Org. Biomol. Chem.* 17, 30–34. doi: 10.1039/C8OB02929F
- Kim, Y. S., Moss, J. A., and Janda, K. D. (2004). Biological tuning of synthetic tactics in solid-phase synthesis: application to A β (1–42). *J. Org. Chem.* 69, 7776–7778. doi: 10.1021/jo048922y
- Maurer, K., Volk, S., and Gerbaldo, H. (1997). Auguste D and Alzheimer's disease. *Lancet* 349, 1546–1549. doi: 10.1016/S0140-6736(96)10203-8
- Milton, S. C. F., de Lisle, Milton, R. C., Kates, S. A., and Glabe, C. (1997). "Synthesis of Alzheimer's (1–42) A β -amyloid peptide with preformed Fmoc-aminoacyl fluorides," in *Techniques in Protein Chemistry*, ed D. R. Marshak (Cambridge, MA: Academic Press), 865–873. doi: 10.1016/S1080-8914(97)80083-X
- Paradis-Bas, M., Tulla-Puche, J., and Albericio, F. (2014). 2-methoxy-4-methylsulfinylbenzyl: a backbone amide safety-catch protecting group for the synthesis and purification of difficult peptide sequences. *Chemistry* 20, 15031–15039. doi: 10.1002/chem.201403668
- Paradis-Bas, M., Tulla-Puche, J., and Albericio, F. (2016). The road to the synthesis of "difficult peptides." *Chem. Soc. Rev.* 45, 631–654. doi: 10.1039/C5CS00680E
- Qiu, T., Liu, Q., Chen, Y.-X., Zhao, Y.-F., and Li, Y.-M. (2015). A β ₄₂ and A β ₄₀: similarities and differences. *J. Pept. Sci.* 21, 522–529. doi: 10.1002/psc.2789
- Scheltens, P., Blennow, K., Breteler, M. M. B., Strooper, B., de Frisoni, G. B., Salloway, S., et al. (2016). Alzheimer's disease. *Lancet* 388, 505–517. doi: 10.1016/S0140-6736(15)01124-1
- Sohma, Y., Hayashi, Y., Kimura, M., Chiyomori, Y., Taniguchi, A., Sasaki, M., et al. (2005). The 'O-acyl isopeptide method' for the synthesis of difficult sequence-containing peptides: application to the synthesis of Alzheimer's disease-related amyloid β peptide (A β) 1–42. *J. Pept. Sci.* 11, 441–451. doi: 10.1002/psc.649
- Thinakaran, G., and Koo, E. H. (2008). Amyloid precursor protein trafficking, processing, and function. *J. Biol. Chem.* 283, 29615–29619. doi: 10.1074/jbc.R800019200
- Tickler, A. K., Barrow, C. J., and Wade, J. D. (2001). Improved preparation of amyloid- β peptides using DBU as N α -Fmoc deprotection reagent. *J. Pept. Sci.* 7, 488–494. doi: 10.1002/psc.342
- Wang, P., Nilsson, J., Brinkmalm, G., Larson, G., and Huang, X. (2014). Synthesis aided structural determination of amyloid- β (1–15) glycopeptides, new biomarkers for Alzheimer's disease. *Chem. Commun.* 50, 15067–15070. doi: 10.1039/C4CC05085A
- Wenschuh, H., Beyermann, M., El-Faham, A., Ghassemi, S., Carpino, L. A., and Bienert, M. (1995). Peptide assembly in the absence of base via Fmoc amino acid fluorides. *J. Chem. Soc. Chem. Commun.* 1995, 669–670. doi: 10.1039/C39950000669
- Williams, G. M., Cooper, G. J., Lee, K., Whiting, L., and Brimble, M. A. (2013). Synthesis of the IGF-II-like hormone vesiculin using regioselective formation of disulfide bonds. *Org. Biomol. Chem.* 11, 3145–3150. doi: 10.1039/C3OB40322J
- World Health Organization (2019) *Dementia*. Available online at: <https://www.who.int/news-room/fact-sheets/detail/dementia> (accessed February 25, 2019).
- Zarándi, M., Soós, K., Fülöp, L., Bozsó, Z., Datki, Z., Tóth, G. K., et al. (2007). Synthesis of A β [1–42] and its derivatives with improved efficiency. *J. Pept. Sci.* 13, 94–99. doi: 10.1002/psc.801
- Zhang, Y. W., Thompson, R., Zhang, H., and Xu, H. (2011). APP processing in Alzheimer's disease. *Mol. Brain* 4:3. doi: 10.1186/1756-6606-4-3

Conflict of Interest Statement: The authors declare that the research was conducted in the absence of any commercial or financial relationships that could be construed as a potential conflict of interest.

Copyright © 2019 Kasim, Kaviani, Harris and Brimble. This is an open-access article distributed under the terms of the Creative Commons Attribution License (CC BY). The use, distribution or reproduction in other forums is permitted, provided the original author(s) and the copyright owner(s) are credited and that the original publication in this journal is cited, in accordance with accepted academic practice. No use, distribution or reproduction is permitted which does not comply with these terms.



Improved HaloTag Ligand Enables BRET Imaging With NanoLuc

Ovia Margaret Thirukkumaran^{1,2}, Congrong Wang¹, Nnamdi Joseph Asouzu¹, Eduard Fron², Susana Rocha², Johan Hofkens², Luke D. Lavis³ and Hideaki Mizuno^{1*}

¹ Laboratory for Biomolecular Network Dynamics, Biochemistry, Molecular and Structural Biology Section, Department of Chemistry, KU Leuven, Heverlee, Belgium, ² Chem Tech-Molecular Imaging and Photonics, Department of Chemistry, KU Leuven, Heverlee, Belgium, ³ Howard Hughes Medical Institute, Ashburn, VA, United States

OPEN ACCESS

Edited by:

Andrew Clayton,
Swinburne University of
Technology, Australia

Reviewed by:

Leigh Stoddart,
University of Nottingham,
United Kingdom
Abhijit De,
Tata Memorial Hospital, India

*Correspondence:

Hideaki Mizuno
hideaki.mizuno@kuleuven.be

Specialty section:

This article was submitted to
Chemical Biology,
a section of the journal
Frontiers in Chemistry

Received: 14 October 2019

Accepted: 23 December 2019

Published: 14 January 2020

Citation:

Thirukkumaran OM, Wang C,
Asouzu NJ, Fron E, Rocha S,
Hofkens J, Lavis LD and Mizuno H
(2020) Improved HaloTag Ligand
Enables BRET Imaging With NanoLuc.
Front. Chem. 7:938.
doi: 10.3389/fchem.2019.00938

Bioluminescence resonance energy transfer (BRET) from an exceptionally bright luciferase, NanoLuc, to a fluorescent HaloTag ligand is gaining momentum to monitor molecular interactions. The recommended use of HaloTag618 ligand for the NanoLuc-HaloTag BRET pair is versatile for ensemble experiments due to their well-separated emission bands. However, this system is not applicable for single-cell BRET imaging because of its low BRET efficiency and in turn weak acceptor signals. Here we explored the unprecedented potential of rhodamine based HaloTag ligands, containing azetidine rings, as BRET acceptors. Through a comprehensive evaluation of various commercial and Janelia Fluor HaloTag ligands for improved BRET efficiency and minimal donor signal bleed-through, we identified JF525 to be the best acceptor for microscopic BRET imaging. We successfully employed BRET imaging with JF525 to monitor the interaction of protein kinase A catalytic and regulatory subunit. Single-cell BRET imaging with HaloTag JF525 can henceforth open doors to comprehend and interpret molecular interactions.

Keywords: NanoLuc, HaloTag, BRET imaging, Janelia Fluor dyes, PKA

INTRODUCTION

Förster resonance energy transfer (FRET) is a process of transferring excited-state energy from one chromophore (donor) to another (acceptor) via non-radiative dipole-dipole coupling. FRET has been a popular choice to detect interaction and conformational change of molecules since FRET depends on distance and relative orientation between the donor and acceptor. The development of a palette of genetically-encoded fluorescent proteins (FPs) has enabled the design of a variety of FRET-based biosensors to monitor intracellular phenomena (Sanford and Palmer, 2017). However, excitation of the donor FP by light illumination, an essential requisite for fluorescence imaging, might induce undesired system perturbation such as cell damage due to phototoxicity, photobleaching, and production of autofluorescence from intrinsic molecules.

Bioluminescence resonance energy transfer (BRET) is a category of FRET with the substitution of a fluorescent donor with a luminescent protein. Since bioluminescence is an intrinsic byproduct of an enzymatic reaction catalyzed by luciferases, BRET eliminates the need for an external excitation light. Employing the previous generation of luciferases (such as Firefly or Renilla luciferases) for imaging requires long exposure time even with a sensitive detection system due to very weak luminescence. Recently a bright luciferase, NanoLuc (England et al., 2016), which is small and emits blue luminescence has been engineered to be a good BRET donor (Machleidt et al., 2015; Hiblot et al., 2017). BRET sensors with NanoLuc and acceptor FP have been developed

and applied for live cell imaging (Schaub et al., 2015; Hamer et al., 2017). Besides FPs, self-labeling protein tags such as HaloTag (Los et al., 2008) and SNAP/CLIP-tag (Keppler et al., 2003; Gautier et al., 2008) are alternative acceptors for BRET imaging. These genetically encodable enzyme tags catalyze a covalent bond formation with their fluorescently labeled cognate ligands. Amongst a series of membrane-permeable ligands for live cell assays, HaloTag NanoBRET 618 (Halo618) has been proposed as an appropriate BRET acceptor due to its well-separated emission band that minimizes the impact of signal bleed-through from NanoLuc. The NanoLuc-Halo618 pair has been employed for ensemble BRET experiments (Machleidt et al., 2015; White et al., 2017). However, from a weak absolute acceptor signal employing Halo618, it is difficult to obtain information such as dynamics and heterogeneity from non-synchronized cells via single-cell BRET imaging. The weak signal is due to the limited spectral overlap between NanoLuc emission and Halo618 absorption resulting in a lower BRET efficiency. In contrast, the superior spectral overlap of green-shifted acceptors are expected to improve BRET efficiency although the bleed-through of donor-signal into the acceptor window might become prominent. To enable live cell BRET imaging with NanoLuc, we evaluated rhodol and rhodamine based HaloTag ligands containing azetidine rings [Janelia Fluor 503 (JF503), Janelia Fluor 525 (JF525), Janelia Fluor 549 (JF549)], in comparison to oregon green (OG), tetramethylrhodamine (TMR) and Halo618, in the green-red spectral range for BRET efficiency, acceptor signal intensity and the impact of donor bleed-through.

MATERIALS AND METHODS

Protein Expression and Purification

E. coli JM109(DE3) was transformed with the respective bacterial expression vectors encoding either NanoLuc or Halo-NanoLuc. HaloTag was cloned to the C-terminus of NanoLuc with a spacer (SGGS). Transformed bacterial cells were grown, induced with IPTG for protein expression and later harvested to purify the expressed protein. The purified proteins were used for *in vitro* evaluation (details on cloning and protein purification can be found in **Supplementary Material**).

Spectral Acquisitions *in vitro*

Fluorescence Spectra of HaloTag Ligands

Synthesis of JF503, JF525, JF549, and spectroscopic measurements for HaloTag ligands (**Supplementary Figure 2**) were performed as described previously (Grimm et al., 2015, 2017). Absorption and fluorescence spectra (except for Halo618) were recorded with Cary Model 100 spectrometer (Varian) and Cary Eclipse fluorometer (Varian), respectively. The absorption spectrum of Halo618 was acquired with NanoDrop 2000 (Thermo Fischer Scientific). Quantum yields were determined using a Quantaurus-QY spectrometer (C11374, Hamamatsu) employing an integrating sphere to measure photons absorbed and emitted by a sample. Reported are average values from triplicates.

Luminescence Spectra

Halo-NanoLuc protein was incubated with HaloTag ligands (OG, JF503, JF525, JF549, TMR, and Halo618 5 μ M) at ambient temperature for \sim 4 h to facilitate complete binding. Luminescence spectra for NanoLuc alone or Halo-NanoLuc labeled with the respective ligands were acquired with a final protein concentration of 4 nM in PBS + 0.1% BSA in the presence of furimazine. Luminescence was collected within a few minutes after adding furimazine with a 30-mm lens and sent to a spectrograph (Acton SpectroPro-300i monochromator/spectrograph). The dispersed luminescence from the spectrograph was detected with a sensitive liquid nitrogen cooled CCD camera (Princeton Instruments SPEC 10:100B/LNeXcelon). The acquisition time was set to 5 s, the recorded spectra were averaged 10 times and background subtracted.

BRET Imaging in Living Cells

Imaging experiments were all performed on transfected cells (protocol in **Supplementary Material**), within a few minutes after furimazine (1:30 dilution) addition, on an inverted microscope IX83 (Olympus, Tokyo) with an APON 60XOTIRF (NA = 1.49) objective lens (Olympus). Luminescence was split into donor and acceptor windows with a dichroic mirror DM509 (Semrock, NY; OG, JM503, and JM525) or DM555 (Semrock; JF549, TMR, and Halo618). Donor and acceptor images were acquired simultaneously with two EM-CCD cameras (ImagEM C9100-13, Hamamatsu Photonics, Hamamatsu, Japan). The images for Halo-NanoLuc were acquired with 2x binning (0.55 μ M per pixel), 1200 EM gain and 0.75 s exposure time (averaged 2x). To observe PKA dissociation events, time traces were recorded for 7 min with 2x binning, 297 EM gain and 1 s exposure time (averaged 2x). After \sim 3 min, cells were stimulated by adding 10 μ M forskolin through a winged infusion set $-22\text{G} \times \frac{3}{4}$ " (Terumo, Tokyo, Japan). Acceptor/Donor emission ratios ($R_{A/D}$) were calculated from regions of interest (ROI) in individual cells using Fiji (Schindelin et al., 2012). Background from each window was calculated from an ROI without any cells. The background-corrected values were used for further analyses. The different HaloTag ligands were imaged with the same imaging parameters except for the choice of dichroic mirrors as indicated.

RESULTS

Green-Shifted HaloTag Ligands Show Better BRET Efficiency

For the *in vitro* evaluation, we acquired the emission spectrum of recombinant NanoLuc with substrate furimazine and the absorption spectra of different HaloTag ligands: OG, JF503, (Grimm et al., 2017) JF525, (Grimm et al., 2017) JF549, (Grimm et al., 2015), TMR and Halo618 (**Figure 1A**). Since the efficiency of energy transfer linearly correlates to the overlap integral (J), J was calculated using the acquired spectra (**Table 1**). JF503 had the largest J ($1.8 \times 10^{13} \text{ M}^{-1} \text{ cm}^3$) followed by OG and JF525 (83% of JF503), JF549 (72% of JF503), and TMR (56% of JF503). For Halo618, J could not be calculated since its extinction

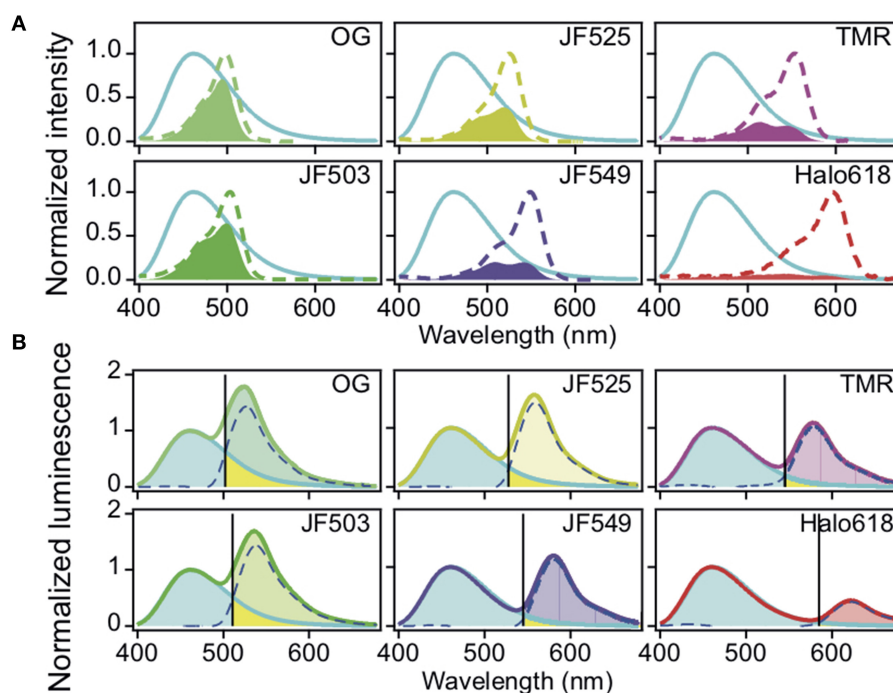


FIGURE 1 | Spectra of NanoLuc and HaloTag ligands. **(A)** Normalized absorption spectra of HaloTag ligands. The spectra of the different ligands are in dotted lines (OG, bluish green, JF503, yellowish green, JM525, yellow, JF549, violet, TMR, purple, Halo618, red) and overlaid with the normalized luminescence spectrum of NanoLuc (cyan solid line). The filled region indicates the overlap area (the products of two spectra). **(B)** Luminescence spectra of Halo-NanoLuc conjugated with Halo-ligands. Spectra were normalized with the donor peak at 460 nm. Dotted blue lines indicate the acceptor spectrum calculated by subtracting the spectrum for only NanoLuc (cyan) from that with the ligand. The wavelength where the acceptor spectrum intersects the NanoLuc spectrum ($S_{D:A}$) is denoted with a black line. R_{bt} is the ratio of yellow area over sum of yellow and cyan areas, whereas F_D is the ratio of yellow area over sum of the yellow area and the area colored with the color code of respective ligands.

TABLE 1 | Evaluation of HaloTag ligands as BRET acceptors of NanoLuc *in vitro*^a.

| Ligand | Abs _{max} (nm) | ϵ (M ⁻¹ cm ⁻¹) | Em _{max} (nm) | Φ | J (M ⁻¹ cm ³) | I_A | $S_{D:A}$ (nm) | R_{bt} (%) | F_D (%) |
|---------|----------------------------|---|---------------------------|-----------------|---|-------|-------------------|-----------------|--------------|
| OG | 496 | 8.3×10^4 | 526 | 0.88 | 1.5×10^{13} | 86.4 | 502 | 25.5 | 22.1 |
| JF503 | 503 | 8.3×10^4 | 529 | 0.87 | 1.8×10^{13} | 90.1 | 511 | 19.9 | 17.2 |
| JF525 | 525 | 9.4×10^4 | 549 | 0.91 | 1.5×10^{13} | 82.5 | 528 | 12.1 | 11.9 |
| JF549 | 549 | 1.0×10^5 | 571 | 0.88 | 1.3×10^{13} | 63.7 | 547 | 6.9 | 8.8 |
| TMR | 554 | 7.8×10^4 | 572 | 0.41 | 1.0×10^{13} | 65.7 | 545 | 7.4 | 9.8 |
| Halo618 | 595 | ND ^b | 621 ^c | ND ^b | ND ^b | 22.7 | 585 | 2.3 | 8.2 |

^aAbs_{max}, peak of the absorption spectrum; ϵ , molar extinction coefficient; Em_{max}, peak of the emission spectrum; Φ , quantum yield; J , overlap integral; I_A , bleed-through corrected signal intensity from the acceptor; $S_{D:A}$, the split point between donor and acceptor windows; R_{bt} , ratio of NanoLuc signal in the acceptor window to the entire NanoLuc signal; F_D , fraction of donor signal in the acceptor window relative to the entire acceptor signal. Refer **Supplementary Material** for calculation of J , R_{bt} , and F_D .

^bNot determinable due to lack of information on material synthesis.

^cData from Promega.

coefficient was not available. Assuming Halo618 has an extinction coefficient comparable to the other HaloTag ligands, a J smaller than TMR is expected from the overlapped area calculated with the normalized spectra.

To experimentally evaluate the BRET efficiency, we acquired the emission spectra of recombinant NanoLuc-HaloTag tandem protein (Halo-NanoLuc) conjugated with the HaloTag ligands (**Figure 1B**). After normalizing the spectra with the maximum

emission of NanoLuc (at 460 nm), signal intensity derived from the acceptor molecule was calculated by subtracting integral of the spectrum for only NanoLuc from that of Halo-NanoLuc conjugated with the ligand (I_A) (**Table 1**). Since the spectra were acquired in the dark, energy exciting the acceptor was provided exclusively through BRET, and therefore I_A reflects the BRET efficiency as well as the fluorescence quantum yield of the acceptor (Φ). As expected from calculated J and Φ , JF503

showed the highest BRET efficiency ($I_A = 90.1$) followed by OG (96% of JF503) and JF525 (92% of JF503). I_A values of JF549 and TMR were about 70% of JF503 whereas Halo618 was only 25% of JF503. Therefore, we concluded that in terms of BRET efficiency green-shifted ligands performed as better acceptors, which was in accordance with previous reports on non-JF dyes (Machleidt et al., 2015; Hiblot et al., 2017).

Quantifying Donor Signal Bleed-Through to Identify Best Acceptor

Another crucial factor we evaluated is the donor signal bleed-through. To quantify bleed-through, we determined the wavelength ($S_{D:A}$) at the intersection of NanoLuc and the acceptor spectra (Figure 1B). Based on $S_{D:A}$ value, we calculated the ratio of NanoLuc signal in acceptor window relative to entire NanoLuc signal (R_{bt}), and the fraction of signal derived from donor molecules relative to entire signal in the acceptor window (F_D). R_{bt} gives the degree of bleed-through whereas F_D indicates the impact of this bleed-through in the acceptor window. Bleed-through was insignificant for Halo618 ($R_{bt} = 2.3\%$), and it became more prominent for ligands with emission at shorter wavelengths. The R_{bt} values of the ligands in the orange range (JF549, TMR) were about three-fold higher than Halo618. Nevertheless, the impact of bleed through (F_D) was similar to Halo618 because of a three-fold better acceptor signal (I_A) (Table 1). On the other hand, ligands in green range (JF525, JF503, and OG) had R_{bt} values ~ 5 –11-fold higher than Halo618. In spite of such large R_{bt} values, the F_D values were only 1.5-, 2.1-, 2.7-fold of Halo618 due to brighter acceptor signal (I_A). From this result, we concluded that the impact of bleed-through was not significant compared to the ratio of bleed-through for green-shifted ligands.

JF525 Performs as an apt Acceptor of NanoLuc

We next evaluated the capability of these different HaloTag ligands for live cell BRET imaging. Chinese hamster ovary (CHO-K1) cells expressing Halo-NanoLuc were labeled with the respective HaloTag ligands and then imaged with a microscope (refer section BRET Imaging in Living Cells for details). The luminescent signals were split into a donor and acceptor window using a dichroic mirror DM509 for the green-shifted ligands (OG, JF503, and JF525) and with DM555 for orange-red ligands (JF549, TMR, and Halo618). Luminescence intensity varies cell by cell depending on the expression level of protein and consumption of furimazine. Therefore, the BRET efficiency was evaluated by comparing the acceptor signal to the donor signal. Bright luminescence signals were observed in a lot of OG-, JF503-, and JF525-loaded cells in both donor and acceptor windows with 0.75 s exposure time, whereas only donor signal was visible in unloaded cells (Figure 2A). In JF549-, TMR-, and Halo618-loaded cells, signals in the acceptor window were barely visible even in cells whose signal in donor window was comparable to OG-, JF503-, and JF525-loaded cells. For quantitative evaluation, signal intensities from acceptor and donor windows were measured for 70 cells or more, and their ratio ($R_{A/D}$) was calculated by performing linear regression analyses (Figures 2B–D). JF525-loaded cells gave the

best acceptor signal with the $R_{A/D}$ value of 0.82 ± 0.01 (Mean \pm SEM). It was 6.8-fold larger than the bleed-through signal measured in cells without ligands using the same experimental setup ($R_{A/D} = 0.12 \pm 0.00$). JF503 ($R_{A/D} = 0.58 \pm 0.01$) and OG ($R_{A/D} = 0.45 \pm 0.00$)-loaded cells showed signals that were 4.8- and 3.8-fold more than bleed-through. For JF549-, TMR-, and Halo618-loaded cells, the bleed-through was lower ($R_{A/D} = 0.02 \pm 0.00$) as a result of using DM555 instead of DM509, but the acceptor signal was remarkably weaker ($R_{A/D} = 0.36 \pm 0.00$, 0.21 ± 0.00 , and 0.24 ± 0.00 , respectively) than JF525-loaded cells. We concluded that JF525 was the best acceptor for BRET imaging with NanoLuc.

Monitoring PKA Activation Through BRET Imaging

Resonance energy transfer systems are frequently employed to monitor protein interactions. Therefore, we evaluated the suitability of BRET imaging with NanoLuc and JF525 for this application. We observed the interaction of regulatory and catalytic subunits of protein kinase A (PRKAR2A and PRKACA, respectively), as these subunits exist together as tetramers under resting conditions (Figure 3A) and undergo a rapid dissociation in response to increase in cAMP levels (Figure 3B) (Taylor et al., 1990; Knighton et al., 1991). We labeled the N-terminus of regulatory (RS)- and C-terminus of catalytic (CS)-subunits with NanoLuc (NL) and HaloTag (HT), respectively (NL-RS, CS-HT). Both the subunits were co-expressed in NIH3T3 cells, labeled with HaloTag ligands and were imaged in the presence of furimazine. Signals were visible in both donor and acceptor windows for cells loaded with JF525 (Figure 3C). From the intensity time trace of the donor and acceptor signal from multiple cells ($n = 8$), the signal to noise ratios (SNRs) for JF525 were determined to be 249.7 ± 18 (donor) and 165.5 ± 14.2 (acceptor) (Figures 3D,E and Supplementary Figure 1). On the contrary, only a faint acceptor signal was observed with Halo618 even for cells showing similar donor intensities as JF525. The difference in donor SNRs was insignificant between JF525 and Halo618 (191.9 ± 13.4 ; $p > 0.05$) while the acceptor SNR for Halo618 (100.9 ± 8.9) was significantly lower ($p < 0.005$). The dissociation of PKA subunits was evident through a decrease in $R_{A/D}$ upon forskolin, an agonist for adenylyl cyclase to increase cAMP level, addition for cells loaded with JF525 and Halo618 (Figure 3F). However, the response ($\Delta R_{A/D}$) for JF525 was 0.012 ± 0.006 (median \pm SD), which is twice as much as $\Delta R_{A/D}$ for Halo618 (0.007 ± 0.002 ; $p < 0.05$) (Figure 3G). JF525 evidently showed much brighter acceptor signals suitable to monitor protein interactions by BRET imaging with single-cell resolution.

DISCUSSION

Self-labeling protein tags such as HaloTag provide a sophisticated platform to evaluate the acceptors in an individual BRET system due to the availability of versatile bright, photostable, and cell permeable ligands. Usage of HaloTag618 as a recommended acceptor for NanoLuc minimizes donor signal bleed-through in the acceptor window (Machleidt et al., 2015). However, a very low energy transfer efficiency yields poor acceptor

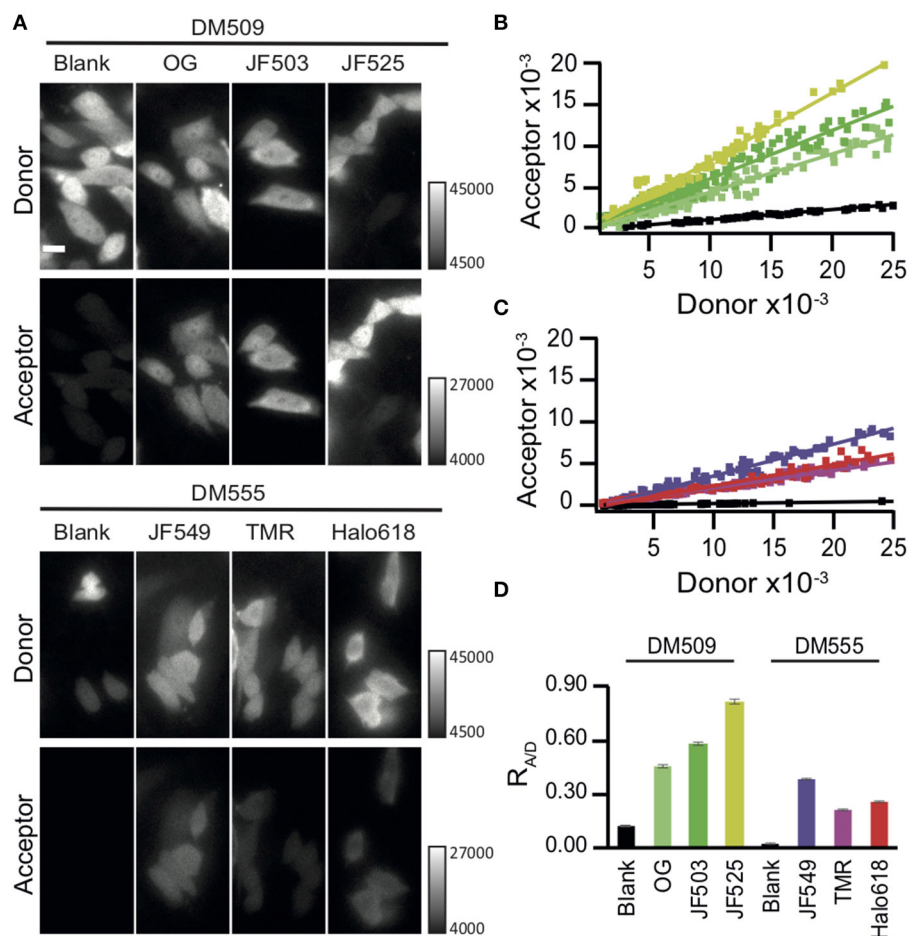
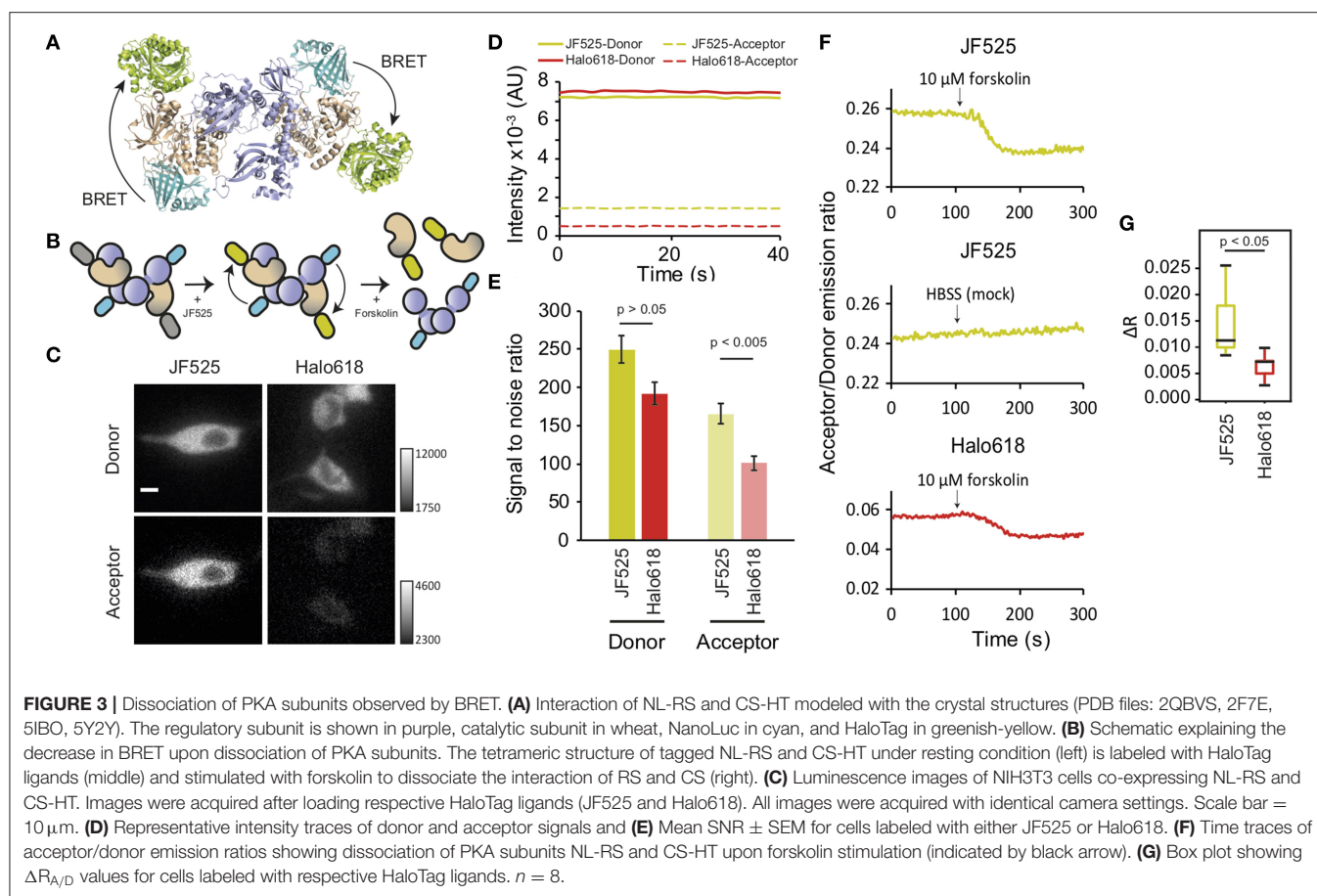


FIGURE 2 | BRET imaging in living cells. **(A)** Images of CHO-K1 cells expressing Halo-NanoLuc. Images were acquired after loading of respective ligands (OG, JF503, JF525, JM549, TMR, and Halo618) or in the absence of ligands (blank), using a dichroic mirror indicated to separate donor (upper) and acceptor (lower) windows. All images were obtained with identical acquisition settings (APON 60XOTIRF, NA = 1.49, exposure time = 0.75 s). Scale bar = 10 μm. **(B,C)** Linear regression analyses of the acceptor vs. donor signal intensities for green-shifted **(B)** or orange-red ligands **(C)**. The color codes of ligand-loaded cells are same as in **Figure 1**. Cells in the absence of ligands (blank) are shown in black. **(D)** Mean $R_{AD} \pm SEM$ calculated from the cells labeled with different ligands. $n \geq 70$.

signal largely hampering its application in the direction of cellular imaging. Employing ligands in the green spectral region, such as Alexa 488, have been reported to show higher BRET efficiency (Machleidt et al., 2015; Hiblot et al., 2017). Since higher bleed-through was expected with green ligands, they were not popularized for ensemble experiments. Conversely, higher absolute acceptor signals are appreciated for BRET imaging. Therefore, we performed a systematic evaluation of a series of HaloTag ligands to identify the best BRET acceptors of NanoLuc for live cell imaging. Brightness comparison amongst the ligands in the green-yellow spectral range (OG, JG503, and JF525) showed JF525 to be better because of a higher extinction coefficient and quantum yield although the overlap integral was lower than JF503. On the other hand, a comprehensive analysis indicated bleed-through to be 1.5-fold lower than OG. With an extensive evaluation of the bleed-through relative to BRET efficiency, we concluded that JF525 was the best *in vitro* amongst the other ligands. Endorsing the *in vitro* results, from cellular

BRET imaging it was evident that JF525 showed the highest BRET ratio.

We translated the application of this BRET system with JF525 to monitor protein-protein interaction of the labeled catalytic and regulatory subunits of PKA. Under resting conditions, we observed a basal BRET ratio which showed the interaction of these subunits. Upon stimulation with forskolin, a drop in BRET ratio was detected due to the dissociation of regulatory and catalytic subunits which enabled us to monitor PKA activation. The observed contrast upon stimulation allowed us to monitor dynamic protein-interaction within the sensor system. Apart from monitoring protein-protein interactions, the application of this system could be extended to image the interaction of proteins with small molecules that can be labeled with JF dyes. Moreover, BRET imaging could be interesting to observe interactions on light sensitive cells, avoid phototoxicity and cellular autofluorescence associated with excitation.



In addition to the photochemical properties, cellular permeability and labeling efficiency are important for live cell imaging. Since the Oregon Green fluorophore (2',7'-difluorofluorescein) has two OH groups at the 3,9' positions of the xanthene ring (Sun et al., 1997), the fluorophore itself is hydrophilic and cell impermeable. The OG HaloTag ligand is permeabilized by diacetylating these two OH groups (Supplementary Figure 2). However, the ester bonds are chemically less stable in aqueous solution (Lavis et al., 2011) and its deacetylation decreases the propensity of OG to be cell permeable. Throughout our experiments, fresh stocks of OG were used to avoid this bias. In the case of JF ligands, the presence of azetidine group at the positions 3,9' of the xanthene ring makes them hydrophobic, facilitating cell permeability. Hence, the stability of JF ligands is not expected to influence the BRET efficiency.

In order to achieve complete labeling in living cells, binding of OG, TMR, and Halo618 was done according to the protocol recommended by Promega. For the JF ligands, we established a protocol based on the reported time course of HistoneH2B labeling with JF HaloTag ligands (Grimm et al., 2017). Under these conditions, a complete labeling is expected to identify the best ligands. Ligands unable to achieve this labeling efficiency introduce underestimation of their BRET efficiencies and such ligands are in any case not appropriate as BRET acceptors.

In conclusion, we have demonstrated that the brightness, cellular permeability, labeling efficiency, photostability of HaloTag ligands, and impact of bleed-through signals relative to acceptor signals are crucial factors for BRET efficiency. Analyses *in vitro* revealed that green-shifted ligands outperformed the red-shifted ligands in terms of better BRET efficiency without marked interference from bleed-through of donor signal. Among the green-shifted ligands, JF525 was identified as the best acceptor for BRET imaging. Bright acceptor images could be acquired from single-cells employing JF525 with an exposure time of <1 s. BRET imaging with JF525 serves as an improved platform to investigate dynamic molecular interactions in single-cells.

DATA AVAILABILITY STATEMENT

All datasets from this study are included in the manuscript and the **Supplementary Files**. The raw data files would be available upon request to the corresponding author.

AUTHOR CONTRIBUTIONS

OT and HM conceptualized, designed the experiments and wrote the manuscript. OT, HM, EF, CW, and NA acquired the absorption spectra and the luminescence spectra, and

performed statistical analyses. LL synthesized and carried out the *in vitro* evaluation of Janelia Fluor (JF) ligands. JH and SR imparted microscopic knowledge and adapted the microscope for bioluminescence imaging. JH, SR, LL, and HM improvised, revised, and approved the submitted version of manuscript.

FUNDING

This work was supported by the KU Leuven Category 1 research grant from KU Leuven (C14/16/053). OT was

supported by an Aspirant PhD grant from the Research Foundation-Flanders (FWO-1147619N). This publication was made possible through funding support of the KU Leuven Fund for Fair Open Access.

SUPPLEMENTARY MATERIAL

The Supplementary Material for this article can be found online at: <https://www.frontiersin.org/articles/10.3389/fchem.2019.00938/full#supplementary-material>

REFERENCES

- England, C. G., Ehlerding, E. B., and Cai, W. (2016). NanoLuc: a small luciferase is brightening up the field of bioluminescence. *Bioconjug. Chem.* 27, 1175–1187. doi: 10.1021/acs.bioconjchem.6b00112
- Gautier, A., Juillerat, A., Heinis, C., Corrêa, I. R., Kindermann, M., Beauflis, F., et al. (2008). An engineered protein tag for multiprotein labeling in living cells. *Chem. Biol.* 15, 128–136. doi: 10.1016/j.chembiol.2008.01.007
- Grimm, J. B., English, B. P., Chen, J., Slaught, J. P., Zhang, Z., Revyakin, A., et al. (2015). A general method to improve fluorophores for live-cell and single-molecule microscopy. *Nat. Methods.* 12, 244–250. doi: 10.1038/nmeth.3256
- Grimm, J. B., Muthusamy, A. K., Liang, Y., Brown, T. A., Lemon, W. C., Patel, R., et al. (2017). A general method to fine-tune fluorophores for live-cell and *in vivo* imaging. *Nat. Methods.* 14, 987–994. doi: 10.1038/nmeth.4403
- Hamer, A., Den Dierickx, P., Arts, R., De Vries, J. S. P. M., Brunsvel, L., and Merkx, M. (2017). Bright bioluminescent BRET sensor proteins for measuring intracellular caspase activity. *ACS Sensors* 2, 729–734. doi: 10.1021/acssensors.7b00239
- Hiblot, J., Yu, Q., Sabbadini, M. D. B., Reymond, L., Xue, L., Schena, A., et al. (2017). Luciferases with tunable emission wavelengths. *Angew. Chem.* 7, 14556–14560. doi: 10.1002/anie.201708277
- Keppler, A., Gendreizig, S., Gronemeyer, T., Pick, H., Vogel, H., and Johnsson, K. (2003). A general method for the covalent labeling of fusion proteins with small molecules *in vivo*. *Nat. Biotechnol.* 21, 86–89. doi: 10.1038/nbt765
- Knighton, D. R., Zheng, J. H., Ten Eyck, L. F., Xuong, N. H., Taylor, S. S., and Sowadski, J. M. (1991). Structure of a peptide inhibitor bound to the catalytic subunit of cyclic adenosine monophosphate-dependent protein kinase. *Science* 253, 414–420. doi: 10.1126/science.1862343
- Lavis, L. D., Chao, T. Y., and Raines, R. T. (2011). Synthesis and utility of fluorogenic acetoxymethyl ethers. *Chem. Sci.* 2, 521–530. doi: 10.1039/C0SC00466A
- Los, G. V., Encell, L. P., McDougall, M. G., Hartzell, D. D., Karassina, N., Zimprich, C., et al. (2008). HaloTag: a novel protein labeling technology for cell imaging and protein analysis. *ACS Chem. Biol.* 3, 373–382. doi: 10.1021/cb800025k
- Machleidt, T., Woodroffe, C. C., Schwinn, M. K., Méndez, J., Robers, M. B., Zimmerman, K., et al. (2015). NanoBRET-a novel BRET platform for the analysis of protein-protein interactions. *ACS Chem. Biol.* 10, 1797–1804. doi: 10.1021/acschembio.5b00143
- Sanford, L., and Palmer, A. (2017). Recent advances in development of genetically encoded fluorescent sensors. *Meth. Enzymol.* 589, 1–49. doi: 10.1016/bs.mie.2017.01.019
- Schaub, F. X., Reza, M. S., Flaveny, C. A., Li, W., Musicant, A. M., Hoxha, S., et al. (2015). Fluorophore-NanoLuc BRET reporters enable sensitive *in vivo* optical imaging and flow cytometry for monitoring tumorigenesis. *Cancer Res.* 75, 5023–5033. doi: 10.1158/0008-5472.CAN-14-3538
- Schindelin, J., Arganda-Carreras, I., Frise, E., Kaynig, V., Longair, M., Pietzsch, T., et al. (2012). Fiji: an open-source platform for biological-image analysis. *Nature methods* 9, 676–682. doi: 10.1038/nmeth.2019
- Sun, W. C., Gee, K. R., Klaubert, D. H., and Haugland, R. P. (1997). Synthesis of fluorinated fluoresceins. *J. Org. Chem.* 62, 6469–6475. doi: 10.1021/jo9706178
- Taylor, S. S., Buechler, J. A., and Yonemoto, W. (1990). cAMP-dependent protein kinase: Framework for a diverse family of regulatory enzymes. *Annu. Rev. Biochem.* 59, 971–1005. doi: 10.1146/annurev.bi.59.070190.004543
- White, C. W., Vanyai, H. K., See, H. B., Johnstone, E. K. M., and Pfleger, K. D. G. (2017). Using nanoBRET and CRISPR/Cas9 to monitor proximity to a genome-edited protein in real-time. *Sci. Rep.* 7:3187. doi: 10.1038/s41598-017-03486-2

Conflict of Interest: The authors declare that the research was conducted in the absence of any commercial or financial relationships that could be construed as a potential conflict of interest.

Copyright © 2020 Thirukkumaran, Wang, Asouzu, Fron, Rocha, Hofkens, Lavis and Mizuno. This is an open-access article distributed under the terms of the Creative Commons Attribution License (CC BY). The use, distribution or reproduction in other forums is permitted, provided the original author(s) and the copyright owner(s) are credited and that the original publication in this journal is cited, in accordance with accepted academic practice. No use, distribution or reproduction is permitted which does not comply with these terms.



Cardiolipin Structure and Oxidation Are Affected by Ca^{2+} at the Interface of Lipid Bilayers

Érica G. A. Miranda^{1†}, Juliana C. Araujo-Chaves^{1†}, Cintia Kawai¹, Adrienne M. M. Brito¹, Igor W. R. Dias², Jeverson T. Arantes^{2*} and Iseli L. Nantes-Cardoso^{1*}

¹ Laboratory of Nanostructures for Biology and Advanced Materials, NanoBioMAV, Center of Natural Sciences and Humanities, Federal University of ABC, Santo André, Brazil, ² Center of Engineering, Modeling, and Applied Social Sciences, Federal University of ABC, Santo André, Brazil

OPEN ACCESS

Edited by:

Andrew Clayton,
Swinburne University of
Technology, Australia

Reviewed by:

Francisco Solano,
University of Murcia, Spain
Nicolas Puff,
Sorbonne Universités, France

*Correspondence:

Iseli L. Nantes-Cardoso
lnantes@ufabc.edu.br
Jeverson T. Arantes
jeverson.teodoro@ufabc.edu.br

[†]These authors have contributed
equally to this work

Specialty section:

This article was submitted to
Chemical Biology,
a section of the journal
Frontiers in Chemistry

Received: 05 April 2019

Accepted: 20 December 2019

Published: 21 January 2020

Citation:

Miranda ÉGA, Araujo-Chaves JC,
Kawai C, Brito AMM, Dias IWR,
Arantes JT and Nantes-Cardoso IL
(2020) Cardiolipin Structure and
Oxidation Are Affected by Ca^{2+} at the
Interface of Lipid Bilayers.
Front. Chem. 7:930.
doi: 10.3389/fchem.2019.00930

Ca^{2+} -overload contributes to the oxidation of mitochondrial membrane lipids and associated events such as the permeability transition pore (MPTP) opening. Numerous experimental studies about the Ca^{2+} /cardiolipin (CL) interaction are reported in the literature, but there are few studies in conjunction with theoretical approaches based on *ab initio* calculations. In the present study, the lipid fraction of the inner mitochondrial membrane was modeled as POPC/CL large unilamellar vesicles (LUVs). POPC/CL and, comparatively, POPC, and CL LUVs were challenged by singlet molecular oxygen using the anionic porphyrin TPPS4 as a photosensitizer and by free radicals produced by Fe^{2+} -citrate. Calcium ion favored both types of lipid oxidation in a lipid composition-dependent manner. In membranes containing predominantly or exclusively POPC, Ca^{2+} increased the oxidation at later reaction times while the oxidation of CL membranes was exacerbated at the early times of reaction. Considering that Ca^{2+} interaction affects the lipid structure and packing, density functional theory (DFT) calculations were applied to the Ca^{2+} association with totally and partially protonated and deprotonated CL, in the presence of water. The interaction of totally and partially protonated CL head groups with Ca^{2+} decreased the intramolecular P-P distance and increased the hydrophobic volume of the acyl chains. Consistently with the theoretically predicted effect of Ca^{2+} on CL, in the absence of pro-oxidants, giant unilamellar vesicles (GUVs) challenged by Ca^{2+} formed buds and many internal vesicles. Therefore, Ca^{2+} induces changes in CL packing and increases the susceptibility of CL to the oxidation promoted by free radicals and excited species.

Keywords: singlet oxygen, calcium, cardiolipin, free radicals, GUVs, lipid packing, oxidative stress

INTRODUCTION

Mitochondria are vital organelles for several metabolic processes involved in cellular function and dysfunction. Mitochondria participate in cell cycle control, growth, differentiation, and play an essential role in Ca^{2+} homeostasis (Area-Gomez et al., 2019; Madreiter-Sokolowski et al., 2019; Woods et al., 2019). For mitochondria, the consequence of placing the oxidative metabolism is the primary generation of superoxide ion that leads to the formation of secondary pro-oxidant species such as hydrogen peroxide, peroxynitrite, hydroxyl radicals, carbon-centered radicals,

triplet carbonyls, and singlet oxygen (Misztal et al., 2013; Miyamoto et al., 2014; Prasad et al., 2018; Radi, 2018; Ucar et al., 2019). Mitochondrial oxidative and nitrosative stress is implicated in degenerative and cardiovascular diseases (Liguori et al., 2018). A well-known condition leading to the increase of superoxide production in mitochondria is the ischemia and reperfusion of tissues such as the myocardium and are events associated with the opening of the mitochondrial permeability transition pore (MPTP) (Kalogeris et al., 2014; Kim-Campbell et al., 2019; Menezes-Filho et al., 2019; Neginskaya et al., 2019; Sarkar et al., 2019). MPTP is an unspecific pore for low molecular mass molecules (≤ 1.5 kDa) inhibited by cyclosporine A (Giorgio et al., 2018; Vercesi et al., 2018). MPTP opens in Ca^{2+} -overloaded mitochondria leading to mitochondrial swelling and depolarization, inhibition of oxidative phosphorylation and stimulation of ATP hydrolysis (Zhao et al., 2004; Clarke et al., 2008; Giorgio et al., 2018; Vercesi et al., 2018; Xie et al., 2019). Studies about MPTP gained high relevance due to the participation of this pore in both apoptotic and necrotic cell death (Kim-Campbell et al., 2019). The role of Ca^{2+} in the MPTP opening has been associated with the interaction with proteins and phospholipids of the inner mitochondrial membranes (IMM) (Nantes et al., 2011; Vercesi et al., 2018). In 1988, Crompton and Costi (1988) reported that cyclosporine A could inhibit the opening of a Ca^{2+} -dependent pore in heart mitochondria challenged by Ca^{2+} plus tertbutyl hydroperoxide. The studies about cyclosporine A also linked MPTP opening to oxidative stress and ischemia-reperfusion injury (Griffiths and Halestrap, 1993; Qian et al., 1997). Ischemia promotes an increase of the intracellular Ca^{2+} to levels enough to cause mitochondrial Ca^{2+} overload upon reoxygenation (Halestrap, 2006; Vercesi et al., 2018). The effect of Ca^{2+} has been related to the production of membrane defects (Fagian et al., 1990; Turin et al., 1997; Kowaltowski et al., 1998) and its binding is favored by the exclusive presence of CL ($\sim 20\%$ of total lipids) in the IMM. CL is associated with Ca^{2+} binding and modulates the structure and function of the respiratory complexes and cytochrome c (Powell et al., 1987; Hoch, 1992). The binding and effects of Ca^{2+} on the biological membranes have been extensively investigated by experimental studies (Pessoto et al., 2015). In a minor extension, CL has been the object of theoretical studies. Dahlberg et al. (2010) presented *ab initio* Density Functional Theory (DFT) calculations of the cardiolipin (CL) headgroup and its 2'-deoxy derivative (dCL). The authors estimated that protons could exchange between phosphate groups with an energy barrier of $\sim 4\text{--}5$ kcal/mol. Lemmin et al. stated that in-depth models and characterization of cardiolipins are to date rare and proposed an *ab initio* parametrization of cardiolipin species for molecular simulation and concluded that the cardiolipin protonation influences the lipid packing (Lemmin et al., 2013). The authors also investigated the interactions with Na^+ and Mg^{2+} but not Ca^{2+} . To the best of our knowledge, the literature lacks a conjugated theoretical and experimental study about the effect of Ca^{2+} and water in the whole CL structure. In the present study, it is theoretically demonstrated that Ca^{2+} affects CL structure influenced by the protonation state of the lipid headgroup. Also, experimental studies showed that the

effects of Ca^{2+} on the CL-containing lipid bilayer organization increased its susceptibility to the oxidation by singlet oxygen and free radicals.

RESULTS

The Ca^{2+} -promoted changes in CL structure and packing might affect the susceptibility of lipid membranes to the attack of free radicals to an allylic carbon and the addition of singlet oxygen to the double bonds of unsaturated acyl chains leading to the formation of lipid peroxides (LOOH). Considering this premise, we modeled the lipid fraction of the inner mitochondrial membrane arranged as POPC (1-palmitoyl-2-oleoyl-sn-glycero-3-phosphocholine)/TOCL (tetraoleoyl cardiolipin) large and giant unilamellar vesicles (LUVs and GUVs, respectively). The PC and CL fractions of the lipid bilayers were also analyzed individually by using POPC and TOCL LUVs. TOCL LUVs were replaced by BBCL (bovine brain cardiolipin) LUVs when Fe^{2+} /citrate was the pro-oxidant agent. LUVs were challenged by the oxidative attack of excited species and free radicals simulating the events occurring in photodynamic therapy (PDT) and chemical oxidative stress promoted by the Fenton reaction. A PDT model was constructed using the anionic porphyrin TPPS4 (meso-tetrakis(4-sulfonatophenyl) porphyrin) as the photosensitizer for the generation of singlet molecular oxygen via energy transfer to ground state molecular oxygen. TPPS4 irradiated by a LED array was the singlet oxygen source for POPC/TOCL (80/20 mol%), POPC (100%) and TOCL (100%). TPPS4 was chosen because this molecule does not have an affinity to negatively charged interfaces (Kawai et al., 2014a). Therefore, we excluded the interference of porphyrin binding on the susceptibility of phospholipids to oxidative damages promoted by the excited species. In this model, the singlet oxygen attack to lipids could be determined by LOOH formation (Bacellar et al., 2018). The model of chemical oxidative stress was constructed using Fe^{2+} -citrate targeting the lipid peroxides of the membranes (Pessoto et al., 2009). POPC/CL large unilamellar vesicles (LUVs) were challenged by singlet oxygen produced by the irradiation of TPPS4 added to the medium (**Figure 1A**). The presence of 3 mM Ca^{2+} increased LOOH production at late times of irradiation. Considering that LUVs have a mixture of POPC and TOCL, it was investigated the specific effect of 3 mM Ca^{2+} on each type of lipid used (Ohyashiki et al., 2002; Rodrigues et al., 2007). Therefore, POPC and TOCL LUVs were separately challenged by singlet oxygen (**Figures 1B,C**). Like observed for POPC/TOCL vesicles, Ca^{2+} increased the production of LOOH in POPC LUVs, at late times of irradiation. For TOCL LUVs, Ca^{2+} increased both the rate and the yield of LOOH produced by PDT, in comparison with the same membrane in the absence of the ion. In this condition, most of the oxidized lipid was formed at the early times of irradiation (**Figure 1C**). The presence of Ca^{2+} also increased the rate of LOOH production in BBCL LUVs challenged by Fe^{2+} -citrate (**Figure 1D**). In this case, BBCL was used because the oxidative mechanism of the Fenton reaction requires the presence of an allylic carbon in a polyunsaturated acyl chain (**Scheme 1**). It was observed a higher total LOOH

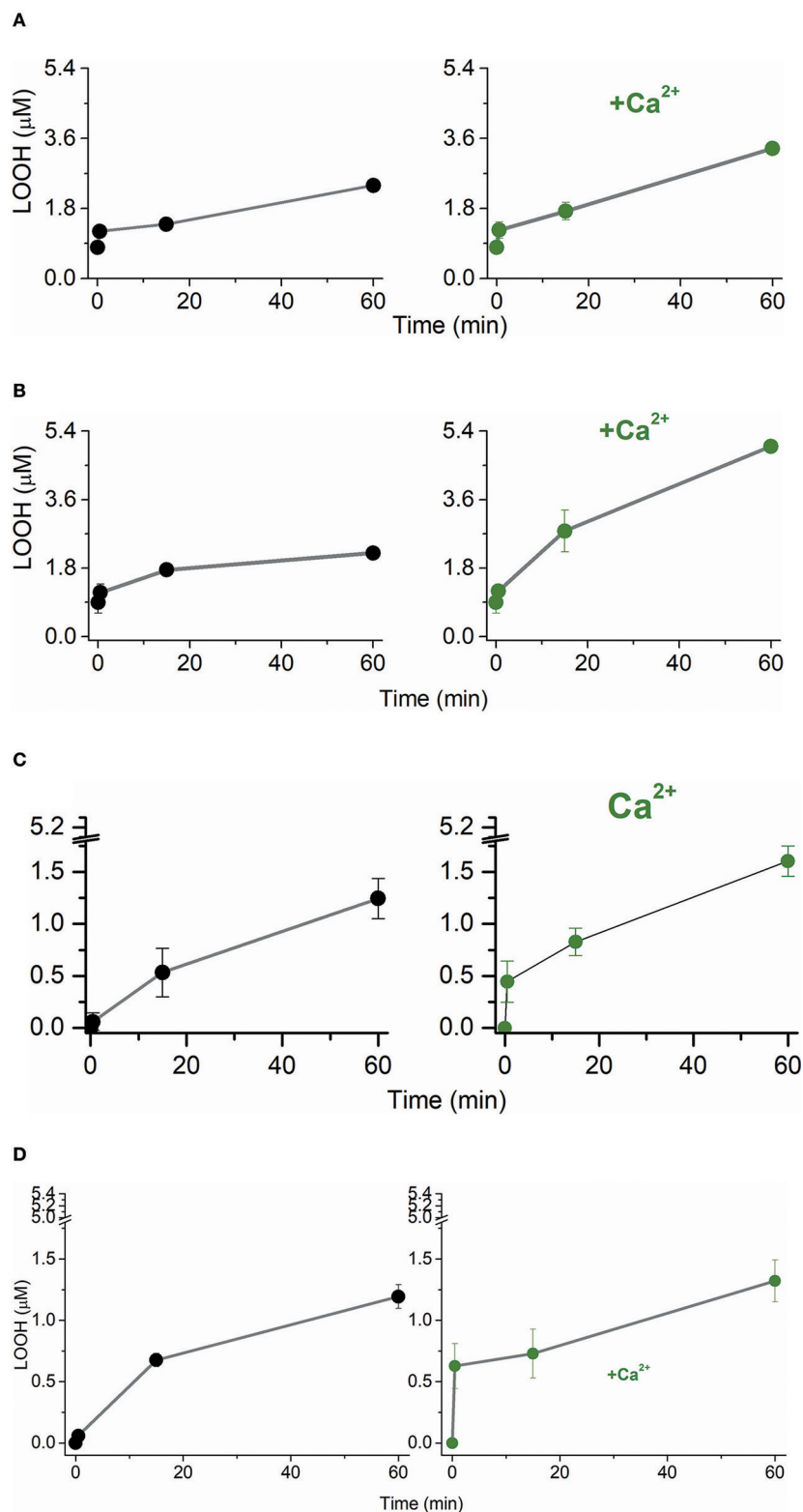
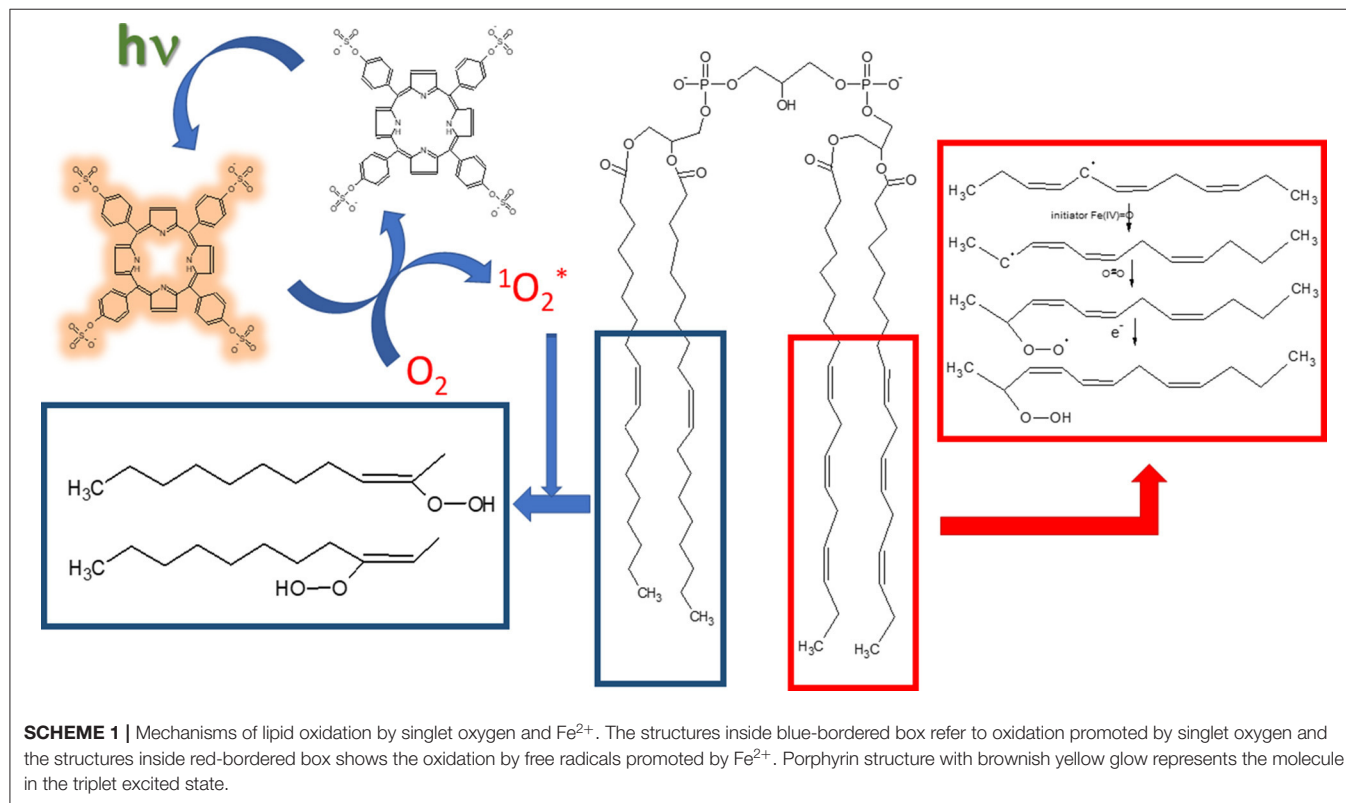


FIGURE 1 | Effect of Ca^{2+} on the LOOH production by singlet oxygen and free radicals in phospholipid bilayers. **(A)** Temporal LOOH production by singlet oxygen in POPC/TOCL LUVs in the absence (left, black line, and symbol) and presence (right, olive line, and symbol) of 3 mM Ca^{2+} . **(B)** Temporal LOOH production by singlet oxygen in POPC LUVs in the absence (left, black line, and symbol) and presence (right, olive line, and symbol) of 3 mM Ca^{2+} . **(C)** Temporal LOOH production by singlet oxygen in TOCL LUVs in the absence (left, black line, and symbol) and presence (right, olive line, and symbol) of 3 mM Ca^{2+} . **(D)** Temporal LOOH production by singlet oxygen in TOCL LUVs in the absence (left, black line, and symbol) and presence (right, olive line, and symbol) of 3 mM Ca^{2+} . (Continued)

FIGURE 1 | Fe^{2+} /citrate in BBCL LUVs in the absence (left, black line, and symbol) and presence (right, olive line, and symbol) of 3 mM Ca^{2+} . In (A–C), singlet oxygen was generated by the irradiation of 10 μM of TPPS4 using LED array that emits 200 $\mu\text{W}/\text{cm}^2$ in 532 nm. In (D), polyunsaturated BBCL was oxidized by 50 μM Fe^{2+} /citrate as described in Materials and Methods. The experiments of oxidation were performed in deionized aqueous solution of 0.2 M of glucose, pH = 6.5, at 25°C.



production for POPC vesicles in the presence of Ca^{2+} than for CL-containing vesicles (Figures 1A,C,D). This result could be due to a better membrane vulnerability to the oxidative attacks induced by a less packed membrane (Khalifat et al., 2011). Differences in the kinetics and yield of LOOH production in POPC and POPC/TOCL membranes are consistent with previous studies (Ahmed-Adrar et al., 2009) that demonstrated a strong protective effect of CL against PC peroxidation that was observed at the range of 5–15% of CL. The assignment of the apparent protective effect of CL on POPC exclusively to a higher sensitivity this lipid to oxidation can not explain the lower total yield of LOOH in membranes of 100% TOCL. In the case of LOOH production by singlet oxygen, it is important to consider the physical quenching of the excited species by lipid acyl chains (Krasnovsky et al., 1983; Vever-Bizet et al., 1989). Literature data reports that the oxidation of CL promotes conformational change both in the backbone/head group and in acyl chain of the lipid (Vähäheikkilä et al., 2018). The polar groups formed in oxidized lipids such as LOOH move to regions closer to the membrane–water interface and contributes to a higher area per lipid chain as well as a decrease of membrane thickness. These structural changes could influence the physical quenching of singlet oxygen by acyl chains. Therefore, in CL-containing membranes, a rapid

accumulation of LOOH occurs at the early times of irradiation. However, specially if the physical quencher is favored in oxidized CL membranes, although the faster rate of oxidation, the total yield of LOOH should be lower in these membranes. This is a possible mechanism that requires future investigations. Thus, the affinity of Ca^{2+} to CL affecting the lipid structure and making it more susceptible to oxidation is consistent with a higher and faster LOOH production observed in CL-containing membranes compared with the same membrane where Ca^{2+} was absent. The comparative analysis of the differences in the total LOOH yield observed in different membranes should involve other mechanisms to be elucidated in the future.

Scheme 1 depicts the mechanisms of LOOH production by singlet oxygen and by Fe^{2+} /citrate. In the photochemically-induced lipid oxidation, a sensitizer such as porphyrin is promoted to the singlet excited state by the light absorption and converted to the triplet excited state via intersystem crossing (ISC). In aerated media, the triplet sensitizer is deactivated by energy transfer to molecular oxygen, which, in turn, is converted to singlet molecular oxygen ($^1\Delta_g$). Singlet molecular oxygen adds to a double bond of the acyl chain and produces the peroxide derivatives. The lipid oxidation promoted by Fe^{2+} /citrate is initiated by the formation of oxyferryl species (Fe(IV)=O)

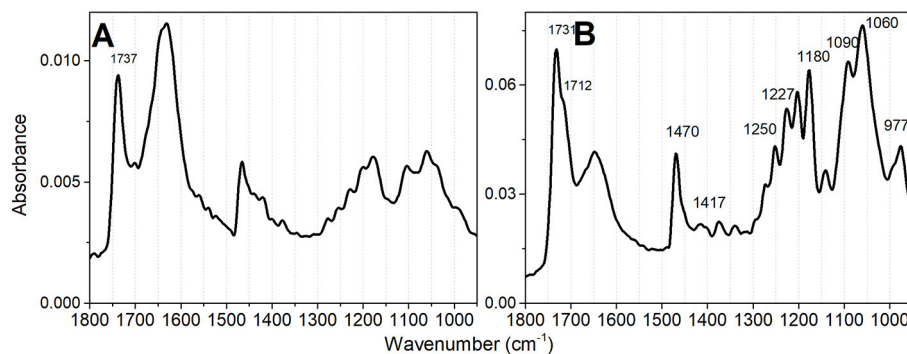


FIGURE 2 | Infrared absorbance spectra of TOCL vesicles at different pH values. **(A)** Spectrum obtained at pH 2 and **(B)** Spectrum obtained at pH 6.5. The lipid concentration was 5 mM in deionized water. The desired pH was obtained by lipid titration.

in the presence of Fe^{3+} (Ohyashiki et al., 2002). Oxyferryl abstracts one electron of an allylic carbon leading the formation of conjugated dienes. The carbon-centered radical reacts with molecular oxygen and produces the lipid peroxyl radical prone to attack another allylic carbon that leads to the propagation of the lipid oxidation. Several other oxidized products can be formed in the process of lipid oxidation promoted by singlet oxygen and Fe^{2+} /citrate. However, the focus was the effect of Ca^{2+} on the lipid oxidation, and LOOH production was used as a molecular marker of lipid oxidation.

Despite the differences in the oxidative mechanisms involved in photochemical and chemical oxidations, Ca^{2+} favored the pro-oxidant effects of electronically excited and free radical species. Ca^{2+} had peculiar effects in the oxidation kinetics according to the lipid composition, independently of the oxidative mechanism. These results are consistent with the effect of Ca^{2+} on the lipid bilayer packing that modulates the accessibility of the acyl chain double bonds to the attack of pro-oxidant species. It was performed DFT calculations for the lipid interaction with Ca^{2+} and water molecules to investigate the changes promoted by Ca^{2+} on the CL structure with repercussion on the lipid bilayer packing. DFT calculations were preceded by FTIR analysis of the CL at pH 2 and 6.5 to access the protonation state of the lipid.

The features of infrared spectra of lipids are influenced by the degree of hydration, the structural organization, and specific hydrogen bonding influenced by the protonation states of the phosphate head groups (Lewis et al., 1994; Lewis and McElhaney, 2000; Kooijman et al., 2017). CL has two phosphate groups and a complex ionization behavior, which has been thoroughly studied in different conditions and by a diversity of techniques. Most studies are consistent with CL as being fully deprotonated at physiological pH and rest on a single pK_a value for both phosphate groups of the lipid (Blume et al., 1988; Lewis et al., 1994; Lewis and McElhaney, 2000; Kooijman et al., 2017). In the minority, some studies have demonstrated two widely separated pK_a values (Hübner et al., 1991; Kates et al., 1993; Gorbenko et al., 2006; Hielscher et al., 2009) and include the theoretical study of Dahlberg et al. (2010) and Lemmin et al. (2013). It is not the main objective of the present study to approach the

question of cardiolipin pK_a values. Therefore, the lipid samples were analyzed by FTIR at pH values of 2.0 and 6.5 to assure that CL was not totally protonated at the experimental conditions of lipid oxidation (pH 6.5). The pH 6.5 corresponds to the expected value at the interface of the outer side of the inner mitochondrial membrane in the energized state of the organelle, i.e., with the transmembrane potential ($\Delta\Psi$) generated by the proton gradient in a coupled mitochondrion (Kawai et al., 2013). Different features observed in the FTIR spectra at pH 2 and 6.5 warrant that CL was not totally protonated at pH 6.5. Even in liposomes with mixed lipids, in the absence of proteins, cardiolipin forms domains (Kawai et al., 2014b) and is reasonable to consider that singly and doubly unprotonated CL molecules may be present in these lipid bilayers. In **Figure 2**, the organization of CL as vesicles, at pH 6.5 is indicated by the sharp band peaking at $1,732\text{ cm}^{-1}$ with a shoulder at $1,718\text{ cm}^{-1}$ that is assigned to the C=O ester group. The CL FTIR spectrum obtained at pH 2 (**Figure 2A**) presents low-intensity signals of $\gamma\text{ CH}_2$ wagging vibrations, i.e., the Snyder modes of CH_2 groups, between $1,400$ and $1,150\text{ cm}^{-1}$. The Snyder modes of CH_2 groups are intensified at pH 6.5 (**Figure 2B**), with a sharp band in $1,732$. The contributions of symmetric and asymmetric vibration of the P=O and the CO-PO functional groups are in the spectral region of $1,250$ – 840 cm^{-1} (Mantsch et al., 1981; Mendelsohn et al., 1984; Mantsch and McElhaney, 1991; Guan et al., 1994).

For the theoretical calculations, it was necessary to consider all the protonation states of CL and the species with head charges of 0, -1 , and -2 were calculated. The DFT calculations were performed for CL structure by combining hydration in the absence and the presence of Ca^{2+} with three protonation degrees of CL, i.e., protonated, partially and totally deprotonated states that were noted as 0, -1 , and -2 , respectively (**Figure 3A**). To the notation above, $-\text{Ca}^{2+}$ and $+\text{Ca}^{2+}$ were included in conditions in which the ion is absent and present, respectively.

The results of DFT calculations presented in **Figure 3A** were performed for hydrated CL. Consistently, **Figure 3A** shows that in the absence and presence of Ca^{2+} , deprotonation increases the P-P distance. The interaction of CL head groups with Ca^{2+} , in all the three protonation states, decreases the intramolecular P-P distance relative to the head group in the

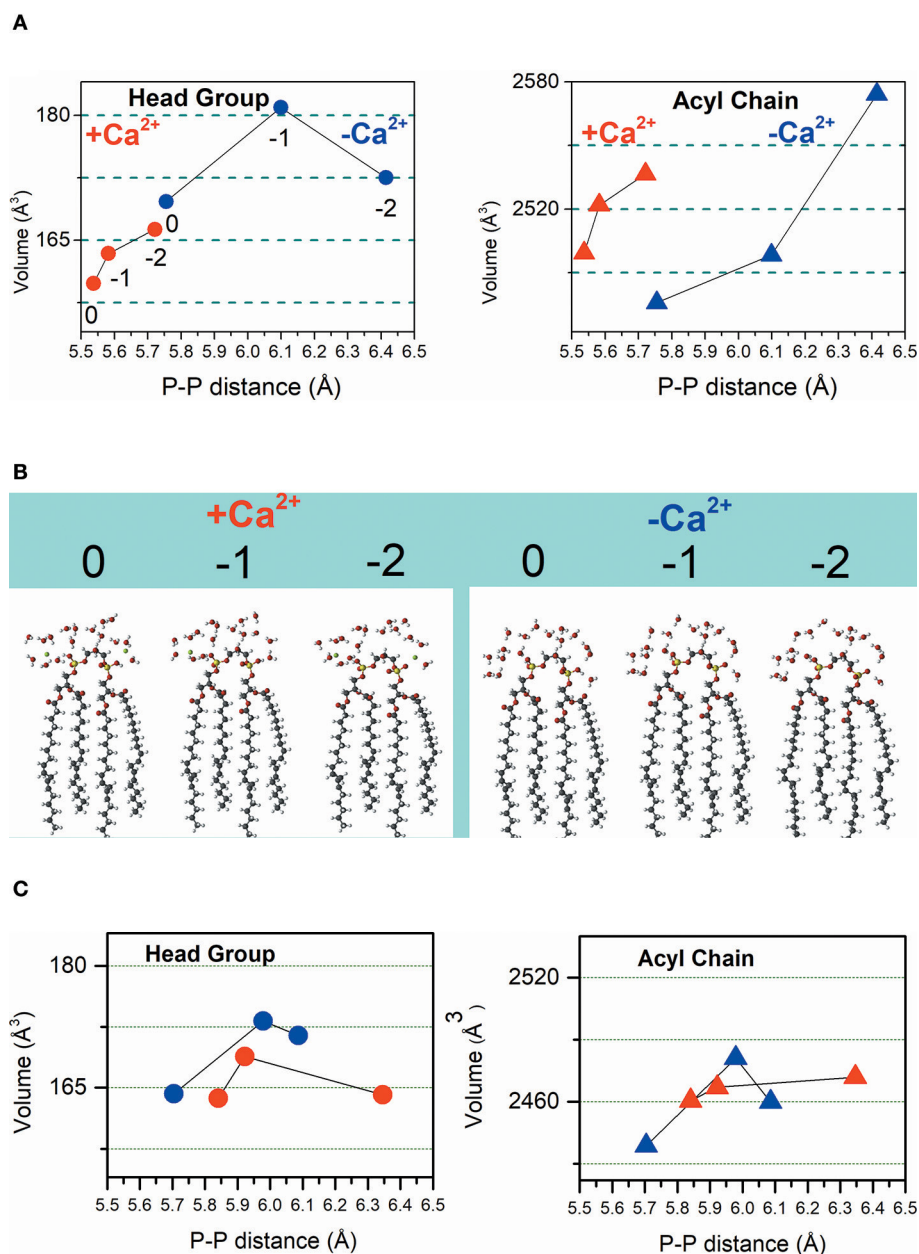


FIGURE 3 | Calculated volumes of the CL headgroup and acyl chains associated with phosphate-phosphate distance influenced by the protonation degree and hydration in the absence ($-\text{Ca}^{2+}$) and the presence ($+\text{Ca}^{2+}$) of the ion. Dimensions of head groups are represented by solid circles and dimensions of acyl chains are represented by solid triangles. **(A)** Hydrated CL. Symbols in red represent results obtained in the presence of Ca^{2+} , and the symbols in blue represent the results achieved in the absence of Ca^{2+} . **(B)** The inset shows the calculated CL structures with head group charges of 0, -1, and -2 in the presence of Ca^{2+} (left) and the absence of Ca^{2+} (right). **(C)** Non-hydrated CL. In this panel, symbols in red represent results obtained in the presence of Ca^{2+} and the symbols in blue represent the results achieved in the absence of Ca^{2+} . From left to right the CL head groups have charges of 0, -1, and -2 that is noted only in the left panel in **(A)**, for clarity.

corresponding protonation state, significantly. The interaction with Ca^{2+} increases the hydrophobic volume of the acyl chains of protonated and partially deprotonated CL relative to the CL in the corresponding protonation state. Deprotonated CL had a decrease of acyl chain volume in the presence of Ca^{2+} . Ca^{2+} propitiated a combination of decreased head group volume with increased acyl chain volume. **Figure 3B** shows the

calculated hydrated structures. Calculations were also performed for non-hydrated CL to get information about the relevance of headgroup hydration on the effects of Ca^{2+} (**Figure 3C**). **Figure 3C** shows that the effects of Ca^{2+} on CL structure are significantly different in the absence of water. The decrease of P-P distance was observed only for partially protonated CL; however, in this condition, the increase of headgroup volume

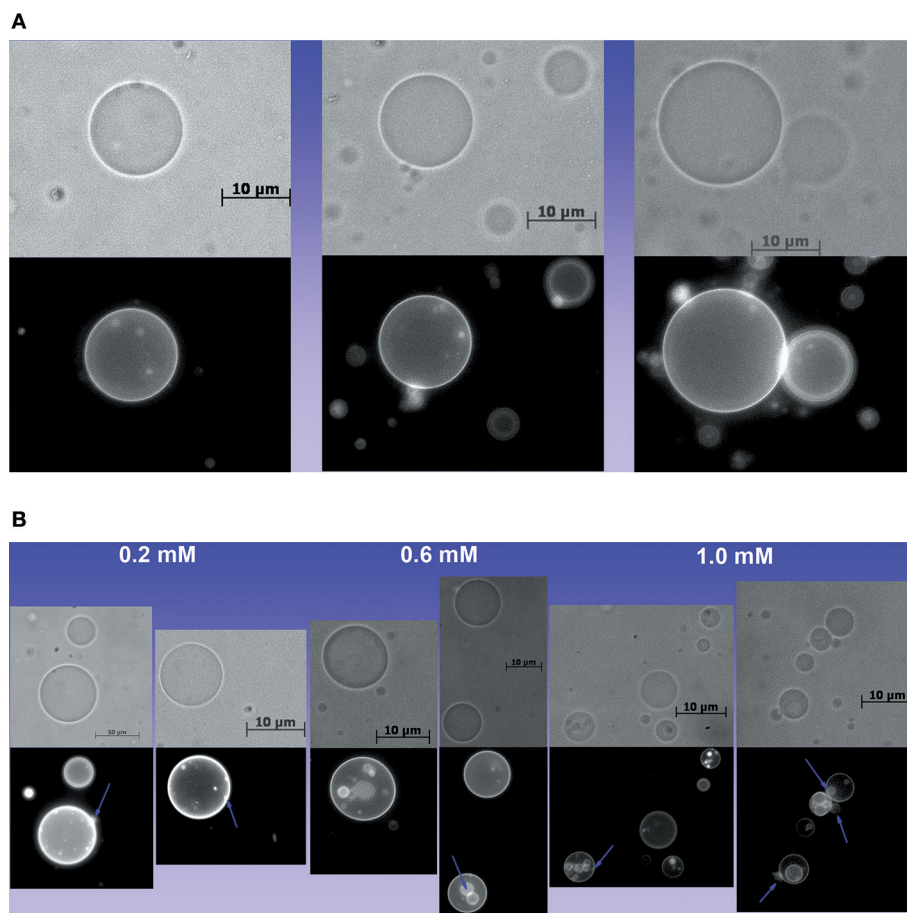


FIGURE 4 | Effect of Ca^{2+} on the structure of GUVs. **(A)** Images of POPC/TOCL GUVs in the absence of Ca^{2+} , **(B)** Images of GUVs treated with 0.2, 0.6, and 1.0 mM of Ca^{2+} in which lamellas and buds are evident. Some buds and lamellas are indicated by violet arrows.

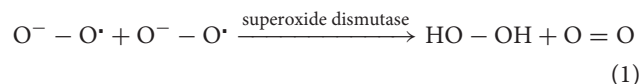
was not accompanied by increasing of acyl chain volume. Theoretical calculations predicted that the changes induced by Ca^{2+} in CL structure should affect membrane stability. The theoretically predicted effect of Ca^{2+} on hydrated CL structure was reinforced by an additional experimental study using giant unilamellar vesicles (GUVs) of POPC/TOCL at pH around 6.5. The POPC/TOCL GUVs labeled with fluorescent CL (TopFluorCL) were challenged by Ca^{2+} and analyzed by fluorescence microscopy (**Figures 4A,B**).

Figures 4A,B show that Ca^{2+} induced the formation of buds and many internal vesicles in the GUVs, some of them are indicated by violet arrows in **Figure 4B**. This result is consistent with the effect of Ca^{2+} in the lipid packing (Grijalba et al., 1999; Van Meer et al., 2008; Graber et al., 2017).

DISCUSSION

Mitochondria are organelles that place a wide variety of cellular metabolic processes, including the production of ATP and the buffering of cytosolic calcium. In cell conditions in which there is a disruption of the Ca^{2+} homeostasis, mitochondria uptake and retain Ca^{2+} trying to restore the homeostasis (Giorgi et al., 2015;

Area-Gomez et al., 2019; Trebak and Kinet, 2019). However, the accumulation of Ca^{2+} in mitochondria favors oxidative damages, which can contribute to mitochondrial permeability and cell death (Tajeddine, 2016). In mitochondria, the oxidative stress is related to the partial reduction of molecular oxygen in the respiratory chain. Molecular oxygen is the final acceptor of electrons in the respiratory chain, and about 1–2% of molecular oxygen consumed in mitochondria is partially reduced to superoxide ion at the level of complexes I and III. Thus, the respiratory chain and other mitochondrial metabolic pathways produce superoxide ion that promotes oxidative stress after being converted into hydrogen peroxide, hydroxyl radical and peroxynitrite (Equations 1–3) (Murphy, 2009).



In addition to the radical species, the electronically excited species also contribute to mitochondrial oxidative damage.

Oxidative processes promoted by the peroxidase activity of respiratory cytochromes on membrane lipids produce triplet carbonyls and singlet oxygen (Rodrigues et al., 2007). In mitochondria, cardiolipin plays a vital role in the proper functioning of the inner mitochondrial membrane proteins. Oxidative damages on mitochondrial lipids have been linked to a diversity of diseases such as muscular dystrophy, cancer, diabetes, premature aging, dementia, deafness, blindness, and male infertility (da Costa et al., 2016). The generation of pro-oxidant species in Ca^{2+} -overloaded mitochondria are well-known inducers of MPTP opening. ANT, FOF1 ATPase, VDAC, and CypD are the mitochondrial proteins that are recognized as components and regulators of MPTP. There is a piece of evidence that pro-oxidant species can directly oxidize the MPTP components and regulators, but the role played by Ca^{2+} in this process is obscure. The protein CypD was postulated as a potential target for Ca^{2+} binding and regulation of MPTP opening. However, Nakagawa et al. (2005) and Baines et al. (2005) demonstrated that MPTP opening occurred in mitochondria from the heart, liver, and brain of mice lacking cyclophilin D (CypD^{-/-}), although they required higher Ca^{2+} concentration than normal mitochondria. In a subsequent study, Giorgio et al. (2013) demonstrated the formation of Ca^{2+} -sensitive MPTP by FOF1 ATPase incorporated in a lipid bilayer model. In a previous investigation, Grijalba et al. (1999) showed that Ca^{2+} -CL complexation induces lipid packing changes and domains in submitochondrial particles (SMPs) and liposomes. The authors proposed that the Ca^{2+} -induced in-plane rearrangements of lipids respond for the increased production of carbon-centered free radicals and membrane permeability in antimycin A-poisoned SMPs. Therefore, the studies above postulated that Ca^{2+} -induced changes in lipid packing reverberate on the structure and aggregation of proteins involved in the membrane permeabilization. In the present study, it was demonstrated theoretically and experimentally that Ca^{2+} changes lipid packing and, even in the absence of proteins, the binding of Ca^{2+} favored lipid oxidation. Interestingly, oxidative effects of chemically generated free radicals and photochemically-generated singlet oxygen were similarly favored by Ca^{2+} , at least concerning the formation of LOOH (lipid peroxide). The factors behind the different LOOH production kinetics determined in this paper are a challenging issue. Some aspects should be considered in trying to answer this question. For singlet oxygen generation, porphyrin TPPS4 was chosen precisely to prevent that the binding affinity of the photosensitizer to the membrane could interfere with oxidation kinetics. Therefore, as already shown in a previous study, with the use of TPPS4, most singlet oxygen is generated in bulk water, and membrane attack depends on the diffusion of the reactive species to the membrane. As Fe^{2+} -citrate is also water-soluble under our experimental conditions, the oxidation by both singlet oxygen and Fe^{2+} -citrate depend on the access of the reactive species to the lipid bilayer. Thus, the similar effects of Ca^{2+} on the CL oxidation kinetics by singlet oxygen and free radicals are consistent with changes in lipid packing (Chen et al., 2015). Cardiolipin oxidation by singlet oxygen in the presence of Ca^{2+} cannot be related to the arm-to-arm effect either (Yin and Zhu, 2012), as this mechanism is feasible to

occur only in free radical-oxidized polyunsaturated fatty acids. Since the increase in the yield of cardiolipin peroxide in the presence of Ca^{2+} was similar for TOCL oxidation promoted by singlet oxygen and BBCL oxidation by free radicals, the significant favoring of the arm-to-arm mechanism by Ca^{2+} can be ruled out. The similarity of Ca^{2+} effects observed for TOCL and BBCL also rules out the influence of the ion on the propagation of lipid peroxidation. Subsequent steps of lipid oxidation, including fragmentation, occur when the oxidizing agent is free radical acting on polyunsaturated fatty acids. Furthermore, lipid fragmentation products that are detected in biological membranes under oxidative stress were not observed in model lipid membranes under the action of singlet oxygen and free radicals (Kim et al., 2011). The significant effect of calcium on the kinetics of LOOH production in POPC membranes suggests that this ion also affects the packing of this phospholipid bilayers. However, the cause of the different kinetic profiles of LOOH production in POPC membranes to cardiolipin-containing membranes is a challenge that requires further studies. In the case of CL, both singlet oxygen and free radical oxidation depend on the access of reactive species to the interior of the bilayer. Therefore, the effect of calcium on the structure of cardiolipin predicted by theoretical studies is in line with the observed results. The pro-oxidant effect of Ca^{2+} that was non-specific for the oxidizing agent is consistent with changes in lipid packing that increase the membrane vulnerability to a diversity of oxidative attacks. Therefore, mitochondrial dysfunction associated with Ca^{2+} overload seems to be linked to distinct effects of Ca^{2+} on lipids and proteins. In the case of lipids, Ca^{2+} promotes changes in lipid packing that are enough to increase the susceptibility of membranes to the oxidation by free radicals and electronically excited species. Lipid oxidation favored by Ca^{2+} might have repercussions on protein structure and function and can occur associated with the effect of Ca^{2+} binding on proteins. Furthermore, in our DFT calculations, we observed that the effect of Ca^{2+} on CL is modulated by the interaction of the lipid head group with water.

MATERIALS AND METHODS

Chemicals

The reagents 1-palmitoyl-2-oleoyl-sn-glycero-3-phosphocholine (POPC), tetraoleoyl cardiolipin (TOCL), and bovine brain cardiolipin (BBCL) were obtained from Avanti Polar Lipids, Inc. (Alabaster, AL, USA), TPPS4 (meso-tetrakis(4-sulfonatophenyl) porphyrin) was purchased from Sigma-Aldrich Corp. (St. Louis, MO, USA), Xylenol orange was purchased from Fluka Chemical Corp. (Ronkonkoma, NY, EUA). Glucose, sucrose, ammoniacal ferrous sulfate ((NH_4)₂Fe(SO₄)₂), chloroform, n-butanol, and ethanol were obtained from Synth (Labsynth Ltda., SP, Brazil), Deuterium oxide (D₂O) was purchased from Cambridge Isotope Laboratories, Inc. (Andover, MA, EUA). The TPPS4 stock solution concentration was checked using the absorption coefficient ϵ at 412 nm = $5.30 \times 10^5 \text{ M}^{-1} \text{ cm}^{-1}$ (Kawai et al., 2014a).

Giant Unilamellar Vesicles

Giant unilamellar vesicles of POPC/TOCL/TopFluorCL (90/9.5/0.5 mol%, respectively) were grown using the electroformation method (Riske et al., 2009; Haluska et al., 2012). The use of a lower cardiolipin percentage (10%) in GUVs than in LUVs (20%) is necessary for the better stability of the vesicles. Briefly, 40 μL of a mixture of lipids in the concentration of 2.5 mM dissolved in chloroform solution was spread on two conductive glass plates (coated with indium tin oxide). The apparatus was positioned with the conductive sides facing each other and separated by a 2-mm-thick Teflon frame. In the following, the electro swelling chamber was filled with a 0.2 M sucrose solution. The apparatus was connected to an alternating power generator at 1 V with a 10 Hz frequency for 2 h at 25°C. The vesicle suspension was removed from the chamber and diluted ~ 6 times into 0.2 M glucose solution. The optical sugar asymmetry between the interior and exterior of the giant vesicles created differences in the density and refractive index between the sucrose and glucose solutions; the vesicles were, therefore, stabilized at the bottom of the chamber by the action of gravity, and had the best contrast when observed under phase-contrast microscopy. Observation of the giant vesicles was performed under an inverted microscope, the Zeiss Observer A1 (Carl Zeiss, Jena, Germany), equipped with a 40X objective. Images were obtained using an AxioCam R3 digital camera (Carl Zeiss, Jena, Germany). The vesicle suspension was placed in a special chamber, which consists of an 8-mm-thick Teflon frame between two glass plates, through which observation was possible.

Large Unilamellar Vesicles (LUVs)

Lipids, POPC/CL (80/20 mol%), POPC (100%), and CL (100%) were initially dissolved in chloroform and the solvent evaporated under a flow of N_2 . The lipid film was kept under reduced pressure for at least 2 h, after which it was hydrated by adding a 0.2 M glucose, pH 6.5, at room temperature. Unilamellar liposomes were obtained by extrusion of hydrated lipid dispersions in an Avanti Mini-Extruder, acquired from Avanti Polar Lipids, Inc. (Alabaster, AL, USA). Multilamellar liposomes were subjected to 11 passes through two polycarbonate filters (100 nm pore size, Nucleopore, Pleasanton, CA, USA) installed in tandem. Liposome solutions were diluted with the buffer to the final lipid concentration of 250 μM .

Generation of Singlet Oxygen and Free Radicals

Where indicated, porphyrins were excited by irradiation with a white LED array. The LED array emits 200 $\mu\text{W}/\text{cm}^2$ in 532 nm measured by FieldMate PowerMeter (Coherent Inc.). Lipid photo-oxidation was promoted by 10 μM of TPPS4. For the oxidation promoted by free radical generated by Fe^{2+} /citrate polyunsaturated BBCL was used and incubated in the presence of 50 μM Fe^{2+} /citrate (Pessoto et al., 2009). Data are presented as the mean \pm s.e.m. of three experiments with different liposome preparations. Where indicated, lipid oxidation of lipids in LUVs was carried out using POPC/TOCL (80/20 mol%, respectively), POPC 100%, TOCL 100%, and BBCL 100% in a solution of 0.2 M of glucose, pH 6.5. The presence of glucose in the medium has the

objective to reproduce the same conditions of the experiments with GUVs.

Lipid Oxidation Assays

Lipid oxidation was evaluated with lipid peroxide (LOOH) production. Lipid hydroperoxide concentration was determined by the oxidation of Fe(II) in the presence of xylenol orange: aliquots of the sample (10 μL) were extracted from incubation at room temperature and mixed with 890 μL of Milli-Q[®] water and 100 μL of hydroperoxide reagent that contained 2.5 mM xylenol orange, 2.5 mM $(\text{NH}_4)_2\text{Fe}(\text{SO}_4)_2$, and 1.15 M HClO_4 in Milli-Q[®] water. The sample was rested for 30 min at room temperature. The oxidation of Fe(II) by LOOH generates Fe(III), which reacts with xylenol orange and is converted to the colored product that absorbs at 560 nm. LOOH concentration was calculated by using $\epsilon = 560 \text{ nm} = 6.45 \times 10^4 \text{ M}^{-1}\text{cm}^{-1}$. TBARS was determined at 535 nm after reaction with thiobarbituric acid (TBA), using the molar extinction coefficient $1.56 \times 10^5 \text{ M}^{-1}\text{cm}^{-1}$.

Electronic Absorption Spectra Measurements

The electronic absorption spectra of porphyrins were measured by using a Varian Cary 50, Varian Inc. (CA, United States) spectrometer. The spectral resolution for wavelength scan was 0.5 nm. The optical path length was 1 cm for the LOOH dosages, and 0.1 cm for the porphyrin spectra measurements and quantification.

FTIR Spectroscopy

An *in situ* attenuated total reflectance-Fourier transform infrared (ATR-FTIR) technique (Mudunkotuwa et al., 2014) has been used to study the protonation of 10 mM cardiolipin vesicles at pH 2 and 6 (Hielscher et al., 2009). Infrared spectra were recorded using a Varian 640-IR Spectrometer fitted with a DLaTGS detector and a PIKE MIRacleTM single reflection horizontal ATR accessory with around 1.8 mm of sampling area diamond/ZnSe crystal and 45 degrees angle of incidence. A series of spectra were measured corresponding to each sample conditions after 15 μL of the sample had been dropped in contact with the crystal and let drying at room temperature ($20^\circ\text{C} \pm 1$) for 30–40 min. These thin films as shaped have enough optically sampled surface area. The surface area allows for good quality infrared spectra to be obtained from a single internal reflection. The reference spectrum was the crystal. All spectra were calculated from 64 scans at 4 cm^{-1} resolution and were not corrected for the wavelength dependence of absorbances.

Theoretical Calculations

The *ab initio* DFT calculations were performed with the code Car-Parrinello Molecular Dynamic (CPMD), using Troullier-Martins pseudopotentials with the inclusion of London dispersion forces (DCACPs) (Kohn and Sham, 1965; Troullier and Martins, 1991; Von Lilienfeld et al., 2005)¹.

¹CPMD, Copyright IBM Corp 1990–2015, Copyright MPI für Festkörperforschung Stuttgart 1997–2001. Available online at: <https://www.cpmd.org/wordpress/index.php/the-code/> (accessed January 9, 2019).

All molecular structures were fully relaxed until the forces on which atom was <0.02 eV/Å. The Kohn-Sham orbitals were expanded in a set of plane waves with the cutoff energy of 110 Ry (Furmanchuk et al., 2010; Rössle et al., 2010; Bernardi and Pascutti, 2012; Payal et al., 2012; Dreyer et al., 2013). In all phospholipids, the interaction parameter in the z-direction (CL frontal structure) was set to 5.6 Å. This value was previously minimized for a range of 4–6.4 Å (z-axis).

DATA AVAILABILITY STATEMENT

The raw data supporting the conclusions of this manuscript will be made available by the authors, without undue reservation, to any qualified researcher.

AUTHOR CONTRIBUTIONS

IN-C conceived experiments. ÉM and JA-C conducted the experiments and analyzed part of the results. ID and JA performed theoretical calculations. IN-C and JA analyzed

the results and wrote the manuscript. CK performed GUV production and images. AB performed FTIR experiments. All authors reviewed the manuscript.

FUNDING

FAPESP (2015/17688-0, 2017/02317-2), CAPES, finance code-001 and CNPq 309247/2017-9. National System of Nanotechnology Laboratories—SisNANO, Proc. CNPq 402289/2013-7.

ACKNOWLEDGMENTS

The authors thank the financial support from FAPESP, CNPq, and CAPES Brazilian agencies for the financial supporting, the computational facilities of the Centro Nacional de Processamento de Alto Desempenho (CENAPAD-Campinas) and High-Performance Computing (HPC) of UFABC, Nucleus of Biochemistry and Biotechnology of UFABC (NBB/UFABC) and the Multiuser Experimental Central of UFABC.

REFERENCES

- Ahmed-Adrar, N. S., Collin, F., Couturier, M., Vitrac, H., Bonnefont-Rousselot, D., Jore, D., et al. (2009). Radiolytic yield of cardiolipin peroxidation by gamma rays in large unilamellar vesicles of phosphatidylcholine. *Radiat. Res.* 171, 622–630. doi: 10.1667/RR1473.1
- Area-Gomez, E., Guardia-Laguarta, C., Schon, E. A., and Przedborski, S. (2019). Mitochondria, OxPhos, and neurodegeneration: cells are not just running out of gas. *J. Clin. Invest.* 129, 34–45. doi: 10.1172/JCI120848
- Bacellar, I. O. L., Oliveira, M. C., Dantas, L. S., Costa, E. B., Junqueira, H. C., Martins, W. K., et al. (2018). Photosensitized membrane permeabilization requires contact-dependent reactions between photosensitizer and lipids. *J. Am. Chem. Soc.* 140, 9606–9615. doi: 10.1021/jacs.8b05014
- Baines, C. P., Kaiser, R. A., Purcell, N. H., Blair, N. S., Osinska, H., Hambleton, M. A., et al. (2005). Loss of cyclophilin D reveals a critical role for mitochondrial permeability transition in cell death. *Nature* 434, 658–662. doi: 10.1038/nature03434
- Bernardi, R. C., and Pascutti, P. G. (2012). Hybrid QM/MM molecular dynamics study of benzocaine in a membrane environment: how does a quantum mechanical treatment of both anesthetic and lipids affect their interaction. *J. Chem. Theory Comput.* 8, 2197–2203. doi: 10.1021/ct300213u
- Blume, A., Hiibner, W., and Messner, G. (1988). Fourier transform infrared spectroscopy of ^{13}C -labeled phospholipids hydrogen bonding to carbonyl groups. *Biochemistry* 27, 8239–8249. doi: 10.1021/bi00421a038
- Chen, Y. F., Tsang, K. Y., Chang, W. F., and Fan, Z. A. (2015). Differential dependencies on $[\text{Ca}^{2+}]$ and temperature of the monolayer spontaneous curvatures of DOPE, DOPA and cardiolipin: effects of modulating the strength of the inter-headgroup repulsion. *Soft Matter* 11, 4041–4053. doi: 10.1039/C5SM00577A
- Clarke, S. J., Khaliulin, I., Das, M., Parker, J. E., Heesom, K. J., and Halestrap, A. P. (2008). Inhibition of mitochondrial permeability transition pore opening by ischemic preconditioning is probably mediated by reduction of oxidative stress rather than mitochondrial protein phosphorylation. *Circ. Res.* 102, 1082–1090. doi: 10.1161/CIRCRESAHA.107.167072da
- Crompton, M., and Costi, A. (1988). Kinetic evidence for a heart mitochondrial pore activated by Ca^{2+} , inorganic phosphate and oxidative stress: a potential mechanism for mitochondrial dysfunction during cellular Ca^{2+} -overload. *Eur. J. Biochem.* 178, 489–501. doi: 10.1111/j.1432-1033.1988.tb14475.x
- da Costa, J. P., Vitorino, R., Silva, G. M., Vogel, C., Duarte, A. C., and Rocha-Santos, T. (2016). A synopsis on aging—Theories, mechanisms and future prospects. *Ageing Res. Rev.* 29, 90–112. doi: 10.1016/j.arr.2016.06.005
- Dahlberg, M., Marini, A., Mennucci, B., and Maliniak, A. (2010). Quantum chemical modeling of the cardiolipin headgroup. *J. Phys. Chem. A* 114, 4375–4387. doi: 10.1021/jp9110019
- Dreyer, J., Zhang, C., Ippoliti, E., and Carloni, P. (2013). Role of the membrane dipole potential for proton transport in gramicidin A embedded in a DMPC bilayer. *J. Chem. Theory Comput.* 9, 3826–3831. doi: 10.1021/ct400374n
- Fagian, M. M., Pereira-da-Silva, L., Martins, I. S., and Vercesi, A. E. (1990). Membrane protein thiol cross-linking associated with the permeabilization of the inner mitochondrial membrane by Ca^{2+} plus prooxidants. *J. Biol. Chem.* 265, 19955–19960.
- Furmanchuk, A., Shishkin, O. V., Isayev, O., Gorb, L., and Leszczynski, J. (2010). New insight on structural properties of hydrated nucleic acid bases from ab initio molecular dynamics. *Phys. Chem. Chem. Phys.* 12, 9945–9954. doi: 10.1039/c002934c
- Giorgi, C., Missiroli, S., Patergnani, S., Duszyński, J., Wieckowski, M. R., and Pinton, P. (2015). Mitochondria-associated membranes: composition, molecular mechanisms, and physiopathological implications. *Antioxid. Redox Signal.* 22, 995–1019. doi: 10.1089/ars.2014.6223
- Giorgio, V., Guo, L., Bassot, C., Petronilli, V., and Bernardi, P. (2018). Calcium and regulation of the mitochondrial permeability transition. *Cell Calcium* 70, 56–63. doi: 10.1016/j.ceca.2017.05.004
- Giorgio, V., von Stockum, S., Antoniel, M., Fabbro, A., Fogolari, F., Forte, M., et al. (2013). Dimers of mitochondrial ATP synthase form the permeability transition pore. *Proc. Natl. Acad. Sci. U.S.A.* 110, 5887–5892. doi: 10.1073/pnas.1217823110
- Gorbenko, G. P., Molotkovsky, J. G., and Kinnunen, P. K. J. (2006). Cytochrome c interaction with cardiolipin/phosphatidylcholine model membranes: effect of cardiolipin protonation. *Biophys. J.* 90, 4093–4103. doi: 10.1529/biophysj.105.080150
- Graber, Z. T., Shi, Z., and Baumgart, T. (2017). Cations induce shape remodeling of negatively charged phospholipid membranes. *Phys. Chem. Chem. Phys.* 19, 15285–15295. doi: 10.1039/C7CP00718C
- Griffiths, E. J., and Halestrap, A. P. (1993). Protection by cyclosporin A of ischemia/reperfusion-induced damage in isolated rat hearts. *J. Mol. Cell. Cardiol.* 25, 1461–1469. doi: 10.1006/jmcc.1993.1162

- Grijalba, M. T., Vercesi, A. E., and Schreier, S. (1999). Ca^{2+} -induced increased lipid packing and domain formation in submitochondrial particles. A possible early step in the mechanism of Ca^{2+} -stimulated generation of reactive oxygen species by the respiratory chain. *Biochemistry* 38, 13279–13287. doi: 10.1021/bi9828674
- Guan, Y., Wurrey, C. J., and Thomas, G. J. (1994). Vibrational analysis of nucleic acids. I. The phosphodiester group in dimethyl phosphate model compounds: $(\text{CH}_3\text{O})_2\text{PO}_2^-$, $(\text{CD}_3\text{O})_2\text{PO}_2^-$, and $(13\text{CH}_3\text{O})_2\text{PO}_2^-$. *Biophys. J.* 66, 225–235. doi: 10.1016/S0006-3495(94)80767-2
- Halestrap, A. P. (2006). Calcium, mitochondria and reperfusion injury: a pore way to die. *Biochem. Soc. Trans.* 34(Pt 2), 232–237. doi: 10.1042/BST20060232
- Haluska, C. K., Baptista, M. S., Fernandes, A. U., Schroder, A. P., Marques, C. M., and Itri, R. (2012). Photo-activated phase separation in giant vesicles made from different lipid mixtures. *Biochim. Biophys. Acta Biomembr.* 1818, 666–672. doi: 10.1016/j.bbamem.2011.11.025
- Hielscher, R., Wenz, T., Hunte, C., and Hellwig, P. (2009). Monitoring the redox and protonation dependent contributions of cardiolipin in electrochemically induced FTIR difference spectra of the cytochrome bc1 complex from yeast. *Biochim. Biophys. Acta Bioenerg.* 1787, 617–625. doi: 10.1016/j.bbambio.2009.01.006
- Hoch, F. L. (1992). Cardiolipins and biomembrane function. *BBA Rev. Biomembr.* 1113, 71–133. doi: 10.1016/0304-4157(92)90035-9
- Hübner, W., Mantsch, H. H., and Kates, M. (1991). Intramolecular hydrogen bonding in cardiolipin. *BBA Biomembr.* 1066, 166–174. doi: 10.1016/0005-2736(91)90183-9
- Kalogeris, T., Bao, Y., and Korthuis, R. J. (2014). Mitochondrial reactive oxygen species: a double edged sword in ischemia/reperfusion vs preconditioning. *Redox Biol.* 2, 702–714. doi: 10.1016/j.redox.2014.05.006
- Kates, M., Syz, J.-Y., Gosser, D., and Haines, T. H. (1993). pH-dissociation characteristics of cardiolipin and its 2'-deoxy analogue. *Lipids* 28, 877–882. doi: 10.1007/BF02537494
- Kawai, C., Araújo-Chaves, J. C., Magrini, T., Sanches, C. O. C. C., Pinto, S. M. S., Martinho, H., et al. (2014a). Photodamage in a mitochondrial membrane model modulated by the topology of cationic and anionic meso-tetrakis porphyrin free bases. *Photochem. Photobiol.* 90, 596–608. doi: 10.1111/php.12228
- Kawai, C., Ferreira, J. C., Baptista, M. S., and Nantes, I. L. (2014b). Not only oxidation of cardiolipin affects the affinity of cytochrome c for lipid bilayers. *J. Phys. Chem. B* 118, 11863–11872. doi: 10.1021/jp504518g
- Kawai, C., Pessoto, F. S., Graves, C. V., Carmona-Ribeiro, A. M., and Nantes, I. L. (2013). Effects of transmembrane potential and pH gradient on the cytochrome c-promoted fusion of mitochondrial mimetic membranes. *J. Bioenerg. Biomembr.* 45, 421–430. doi: 10.1007/s10863-013-9507-y
- Khalifat, N., Fournier, J. B., Angelova, M. I., and Puff, N. (2011). Lipid packing variations induced by pH in cardiolipin-containing bilayers: the driving force for the cristae-like shape instability. *Biochim. Biophys. Acta Biomembr.* 1808, 2724–2733. doi: 10.1016/j.bbamem.2011.07.013
- Kim, J., Minkler, P. E., Salomon, R. G., Anderson, V. E., and Hoppel, C. L. (2011). Cardiolipin: characterization of distinct oxidized molecular species. *J. Lipid Res.* 52, 125–135. doi: 10.1194/jlr.M010520
- Kim-Campbell, N., Gomez, H., and Bayir, H. (2019). "Cell death pathways: apoptosis and regulated necrosis," in *Critical Care Nephrology*, 3rd Edn. (Elsevier), 113–121.
- Kohn, W., and Sham, L. J. (1965). Self-consistent equations including exchange and correlation effects. *Phys. Rev.* 140:A1133. doi: 10.1103/PhysRev.140.A1133
- Kooijman, E. E., Swim, L. A., Graber, Z. T., Tyurina, Y., Bayir, H., and Kagan, V. E. (2017). Magic angle spinning 31 P NMR spectroscopy reveals two essentially identical ionization states for the cardiolipin phosphates in phospholipid liposomes. *Biochim. Biophys. Acta Biomembr.* 1859, 61–68. doi: 10.1016/j.bbamem.2016.10.013
- Kowaltowski, A. J., Netto, L. E. S., and Vercesi, A. E. (1998). The thiol-specific antioxidant enzyme prevents mitochondrial permeability transition: evidence for the participation of reactive oxygen species in this mechanism. *J. Biol. Chem.* 273, 12766–12769. doi: 10.1074/jbc.273.21.12766
- Krasnovsky, A. A., Kagan, V. E., and Minin, A. A. (1983). Quenching of singlet oxygen luminescence by fatty acids and lipids. Contribution of physical and chemical mechanisms. *FEBS Lett.* 155, 233–236. doi: 10.1016/0014-5793(82)80610-8
- Lemmin, T., Bovigny, C., Lançon, D., and Dal Peraro, M. (2013). Cardiolipin models for molecular simulations of bacterial and mitochondrial membranes. *J. Chem. Theory Comput.* 9, 670–678. doi: 10.1021/ct300590v
- Lewis, R. N., McElhaney, R. N., Pohle, W., and Mantsch, H. H. (1994). Components of the carbonyl stretching band in the infrared spectra of hydrated 1,2-diacylglycerol bilayers: a reevaluation. *Biophys. J.* 67, 2367–2375. doi: 10.1016/S0006-3495(94)80723-4
- Lewis, R. N. A. H., and McElhaney, R. N. (2000). Surface charge markedly attenuates the nonlamellar phase-forming propensities of lipid bilayer membranes: calorimetric and ^{31}P -nuclear magnetic resonance studies of mixtures of cationic, anionic, and zwitterionic lipids. *Biophys. J.* 79, 1455–1464. doi: 10.1016/S0006-3495(00)76397-1
- Liguori, I., Russo, G., Curcio, F., Bulli, G., Aran, L., Della-Morte, D., et al. (2018). Oxidative stress, aging, and diseases. *Clin. Interv. Aging* 13, 757–772. doi: 10.2147/CIA.S158513
- Madreiter-Sokolowski, C. T., Waldeck-Weiermair, M., Bourguignon, M.-P., Villeneuve, N., Gottschalk, B., Klec, C., et al. (2019). Enhanced inter-compartmental Ca^{2+} flux modulates mitochondrial metabolism and apoptotic threshold during aging. *Redox Biol.* 20, 458–466. doi: 10.1016/j.redox.2018.11.003
- Mantsch, H. H., Martin, A., and Cameron, D. G. (1981). Characterization by infrared spectroscopy of the bilayer to nonbilayer phase transition of phosphatidylethanolamines. *Biochemistry* 20, 3138–3145. doi: 10.1021/bi00514a024
- Mantsch, H. H., and McElhaney, R. N. (1991). Phospholipid phase transitions in model and biological membranes as studied by infrared spectroscopy. *Chem. Phys. Lipids* 57, 213–226. doi: 10.1016/0009-3084(91)90077-O
- Mendelsohn, R., Anderle, G., Jaworsky, M., Mantsch, H. H., and Dluhy, R. A. (1984). Fourier transform infrared spectroscopic studies of lipid-protein interaction in native and reconstituted sarcoplasmic reticulum. *BBA Biomembr.* 860, 491–502. doi: 10.1016/0005-2736(84)90173-1
- Menezes-Filho, S. L., Amigo, I., Luévano-Martínez, L. A., and Kowaltowski, A. J. (2019). Fasting promotes functional changes in liver mitochondria. *Biochim. Biophys. Acta Bioenerg.* 1860, 129–135. doi: 10.1016/j.bbambio.2018.11.017
- Misztal, T., Przesław, K., Rusak, T., and Tomasiak, M. (2013). Peroxynitrite - altered platelet mitochondria - a new link between inflammation and hemostasis. *Thromb. Res.* 131:e17–25. doi: 10.1016/j.thromres.2012.11.010
- Miyamoto, S., Martinez, G. R., Medeiros, M. H. G., and Di Mascio, P. (2014). Singlet molecular oxygen generated by biological hydroperoxides. *J. Photochem. Photobiol. B Biol.* 139, 24–33. doi: 10.1016/j.jphotobiol.2014.03.028
- Mudunkotuwa, I. A., Minshid, A., Al, and Grassian, V. H. (2014). ATR-FTIR spectroscopy as a tool to probe surface adsorption on nanoparticles at the liquid-solid interface in environmentally and biologically relevant media. *Analyst* 139, 870–881. doi: 10.1039/C3AN01684F
- Murphy, M. P. (2009). How mitochondria produce reactive oxygen species. *Biochem. J.* 417, 1–13. doi: 10.1042/BJ20081386
- Nakagawa, T., Shimizu, S., Watanabe, T., Yamaguchi, O., Otsu, K., Yamagata, H., et al. (2005). Cyclophilin D-dependent mitochondrial permeability transition regulates some necrotic but not apoptotic cell death. *Nature* 434, 652–658. doi: 10.1038/nature03317
- Nantes, I. L., Rodrigues, T., Caires, A. C. F., Cunha, R. L. O. R., Pessoto, F. S., Yokomizo, C. H., et al. (2011). Specific effects of reactive thiol drugs on mitochondrial bioenergetics. *J. Bioenerg. Biomembr.* 43, 11–18. doi: 10.1007/s10863-011-9328-9
- Neginskaya, M. A., Solesio, M. E., Berezhnaya, E. V., Amodeo, G. F., Mnatsakanyan, N., Jonas, E. A., et al. (2019). ATP synthase C-subunit-deficient mitochondria have a small cyclosporine A-sensitive channel, but lack the permeability transition pore. *Cell Rep.* 26, 11–17.e2. doi: 10.1016/j.celrep.2018.12.033
- Ohyashiki, T., Kadoya, A., and Kushida, K. (2002). The role of Fe^{3+} on Fe^{2+} -dependent lipid peroxidation in phospholipid liposomes. *Chem. Pharm. Bull.* 50, 203–207. doi: 10.1248/cpb.50.203
- Payal, R. S., Bharath, R., Periyasamy, G., and Balasubramanian, S. (2012). Density functional theory investigations on the structure and dissolution mechanisms for cellobiose and xylan in an ionic liquid: Gas phase and cluster calculations. *J. Phys. Chem. B* 116, 833–840. doi: 10.1021/jp207989w

- Pessoto, F. S., Inada, N. M., Nepomuceno, M. d. F., Ruggiero, A. C., Nascimento, O. R., et al. (2009). Biological effects of anionic meso-tetrakis (para-sulfonatophenyl) porphyrins modulated by the metal center. Studies in rat liver mitochondria. *Chem. Biol. Interact.* 181, 400–408. doi: 10.1016/j.cbi.2009.07.012
- Pessoto, F. S., Yokomizo, C. H., Prieto, T., Fernandes, C. S., Silva, A. P., Kaiser, C. R., et al. (2015). Thiosemicarbazone p-substituted acetophenone derivatives promote the loss of mitochondrial $\Delta\psi$, GSH depletion, and death in K562 cells. *Oxid. Med. Cell. Longev.* 2015:394367. doi: 10.1155/2015/394367
- Powell, G. L., Knowles, P. F., and Marsh, D. (1987). Spin-label studies on the specificity of interaction of cardiolipin with beef heart cytochrome oxidase. *Biochemistry* 26, 8138–8145. doi: 10.1021/bi00399a018
- Prasad, A., Balukova, A., and Pospíšil, P. (2018). Triplet excited carbonyls and singlet oxygen formation during oxidative radical reaction in skin. *Front. Physiol.* 9:1109. doi: 10.3389/fphys.2018.01109
- Qian, T., Nieminen, A.-L., Herman, B., and Lemasters, J. J. (1997). Mitochondrial permeability transition in pH-dependent reperfusion injury to rat hepatocytes. *Am. J. Physiol. Physiol.* 273, C1783–C1792. doi: 10.1152/ajpcell.1997.273.6.C1783
- Radi, R. (2018). Oxygen radicals, nitric oxide, and peroxynitrite: Redox pathways in molecular medicine. *Proc. Natl. Acad. Sci. U.S.A.* 115, 5839–5848. doi: 10.1073/pnas.1804932115
- Riske, K. A., Sudbrack, T. P., Archilha, N. L., Uchoa, A. F., Schroder, A. P., Marques, C. M., et al. (2009). Giant vesicles under oxidative stress induced by a membrane-anchored photosensitizer. *Biophys. J.* 97, 1362–1370. doi: 10.1016/j.bpj.2009.06.023
- Rodrigues, T., De França, L. P., Kawai, C., De Faria, P. A., Mugnol, K. C. U., Braga, F. M., et al. (2007). Protective role of mitochondrial unsaturated lipids on the preservation of the apoptotic ability of cytochrome c exposed to singlet oxygen. *J. Biol. Chem.* 282, 25577–25587. doi: 10.1074/jbc.M700009200
- Rössle, S., Friedrichs, J., and Frank, I. (2010). The formation of DNA photodamage: the role of exciton localization. *ChemPhysChem* 11, 2011–2015. doi: 10.1002/cphc.201000081
- Sarkar, S., Chakraborty, D., Bhowmik, A., and Ghosh, M. K. (2019). Cerebral ischemic stroke: cellular fate and therapeutic opportunities. *Front. Biosci.* 24, 435–450. doi: 10.2741/4727
- Tajeddine, N. (2016). How do reactive oxygen species and calcium trigger mitochondrial membrane permeabilisation? *Biochim. Biophys. Acta Gen. Subj.* 1860, 1079–1088. doi: 10.1016/j.bbagen.2016.02.013
- Trebak, M., and Kinet, J.-P. (2019). Calcium signalling in T cells. *Nat. Rev. Immunol.* 19, 154–169. doi: 10.1038/s41577-018-0110-7
- Troullier, N., and Martins, J. L. (1991). Efficient pseudopotentials for plane-wave calculations. *Phys. Rev. B* 43, 1993–2006. doi: 10.1103/PhysRevB.43.1993
- Turin, J., Almeida, A. M., Di Mascio, P., Vercesi, A. E., and Nantes, I. L. (1997). Singlet oxygen-promoted mitochondrial permeability transition pore (MTP) opening in rat liver mitochondria. *FASEB J.* 11.
- Ucar, E., Seven, O., Lee, D., Kim, G., Yoon, J., and Akkaya, E. U. (2019). Selectivity in photodynamic action: higher activity of mitochondria targeting photosensitizers in cancer cells. *ChemPhotoChem* 3, 129–132. doi: 10.1002/cptc.201800231
- Vähäheikkilä, M., Peltomaa, T., Róg, T., Vazdar, M., Pöyry, S., and Vattulainen, I. (2018). How cardiolipin peroxidation alters the properties of the inner mitochondrial membrane? *Chem. Phys. Lipids* 214, 15–23. doi: 10.1016/j.chemphyslip.2018.04.005
- Van Meer, G., Voelker, D. R., and Feigenson, G. W. (2008). Membrane lipids: where they are and how they behave. *Nat. Rev. Mol. Cell Biol.* 9, 112–124. doi: 10.1038/nrm2330
- Vercesi, A. E., Castilho, R. F., Kowaltowski, A. J., de Oliveira, H. C. F., de Souza-Pinto, N. C., Figueira, T. R., et al. (2018). Mitochondrial calcium transport and the redox nature of the calcium-induced membrane permeability transition. *Free Radic. Biol. Med.* 129, 1–24. doi: 10.1016/j.freeradbiomed.2018.08.034
- Vever-Bizet, C., Dellinger, M., Brault, D., Rougee, M., and Bensasson, R. V. (1989). Singlet molecular oxygen quenching by saturated and unsaturated fatty-acids and by cholesterol. *Photochem. Photobiol.* 50, 321–325. doi: 10.1111/j.1751-1097.1989.tb04165.x
- Von Lilienfeld, O. A., Tavernelli, I., Rothlisberger, U., and Sebastiani, D. (2005). Performance of optimized atom-centered potentials for weakly bonded systems using density functional theory. *Phys. Rev. B Condens. Matter Mater. Phys.* 71:195119. doi: 10.1103/PhysRevB.71.195119
- Woods, J. J., Nemani, N., Shanmugapriya, S., Kumar, A., Zhang, M., Nathan, S. R., et al. (2019). A selective and cell-permeable mitochondrial calcium uniporter (MCU) inhibitor preserves mitochondrial bioenergetics after hypoxia/reoxygenation injury. *ACS Cent. Sci.* 5, 153–166. doi: 10.1021/acscentsci.8b00773
- Xie, Y., Yang, Y., Galice, S., Bers, D. M., and Sato, D. (2019). Size matters: Ryanodine receptor cluster size heterogeneity potentiates calcium waves. *Biophys. J.* 116, 530–539. doi: 10.1016/j.bpj.2018.12.017
- Yin, H., and Zhu, M. (2012). Free radical oxidation of cardiolipin: Chemical mechanisms, detection and implication in apoptosis, mitochondrial dysfunction and human diseases. *Free Radic. Res.* 46, 959–974. doi: 10.3109/10715762.2012.676642
- Zhao, K., Zhao, G. M., Wu, D., Soong, Y., Birk, A. V., Schiller, P. W., et al. (2004). Cell-permeable peptide antioxidants targeted to inner mitochondrial membrane inhibit mitochondrial swelling, oxidative cell death, and reperfusion injury. *J. Biol. Chem.* 279, 34682–34690. doi: 10.1074/jbc.M40299200

Conflict of Interest: The authors declare that the research was conducted in the absence of any commercial or financial relationships that could be construed as a potential conflict of interest.

Copyright © 2020 Miranda, Araujo-Chaves, Kawai, Brito, Dias, Arantes and Nantes-Cardoso. This is an open-access article distributed under the terms of the Creative Commons Attribution License (CC BY). The use, distribution or reproduction in other forums is permitted, provided the original author(s) and the copyright owner(s) are credited and that the original publication in this journal is cited, in accordance with accepted academic practice. No use, distribution or reproduction is permitted which does not comply with these terms.



Solid-Phase Synthesis of Head to Side-Chain Tyr-Cyclodepsipeptides Through a Cyclative Cleavage From Fmoc-MeDbz/MeNbz-resins

Gerardo A. Acosta^{1,2,3,4}, Laura Murray^{1,2}, Miriam Royo^{3,4}, Beatriz G. de la Torre^{5,6} and Fernando Albericio^{1,2,3,4,6*}

¹ CIBER-BBN, Networking Centre on Bioengineering, Biomaterials and Nanomedicine, University of Barcelona (UB), Barcelona, Spain, ² Department of Organic Chemistry, University of Barcelona, Barcelona, Spain, ³ Institute of Advanced Chemistry of Catalonia (IQAC-CSIC), Spanish National Research Council (CSIC), Barcelona, Spain, ⁴ Associated Unit, Spanish National Research Council-University of Barcelona (CSIC-UB), Barcelona, Spain, ⁵ KwaZulu-Natal Research Innovation and Sequencing Platform (KRISP), School of Laboratory Medicine and Medical Sciences, College of Health Sciences, University of KwaZulu-Natal, Durban, South Africa, ⁶ Peptide Science Laboratory, School of Chemistry and Physics, University of KwaZulu-Natal, Durban, South Africa

OPEN ACCESS

Edited by:

Laszlo Otvos,
Olpe LLC, United States

Reviewed by:

Mare Cudic,
Florida Atlantic University,
United States
Max Julian Cryle,
Monash University, Australia

*Correspondence:

Fernando Albericio
albericio@ukzn.ac.za

Specialty section:

This article was submitted to
Chemical Biology,
a section of the journal
Frontiers in Chemistry

Received: 11 February 2020

Accepted: 25 March 2020

Published: 22 April 2020

Citation:

Acosta GA, Murray L, Royo M, de la Torre BG and Albericio F (2020) Solid-Phase Synthesis of Head to Side-Chain Tyr-Cyclodepsipeptides Through a Cyclative Cleavage From Fmoc-MeDbz/MeNbz-resins. *Front. Chem.* 8:298. doi: 10.3389/fchem.2020.00298

Cyclic depsipeptides constitute a fascinating class of natural products. Most of them are characterized by an ester formed between the β -hydroxy function of Ser/Thr -and related amino acids- and the carboxylic group of the C-terminal amino acid. Less frequent are those where the thiol of Cys is involved rendering a thioester (cyclo thiodepsipeptides) and even less common are the cyclo depsipeptides with a phenyl ester coming from the side-chain of Tyr. Herein, the preparation of the later through a cyclative cleavage using the Fmoc-MeDbz/MeNbz-resin is described. This resin has previously reported for the synthesis of cyclo thiodepsipeptides and homodetic peptides. The use of that resin for the preparation of all these peptides is also summarized.

Keywords: cyclodipeptides, heterodetic cyclic peptides, homodetic cyclic peptides, native chemical ligation, solid-phase peptide synthesis

INTRODUCTION

Peptides are an important class of Active Pharmaceutical Ingredients (APIs) (Henninot et al., 2018; Lau and Dunn, 2018; Al Shaer et al., 2020; de la Torre and Albericio, 2020). They show excellent chemical and biological diversity, as well as high activity and specificity, low toxicity, low accumulation in tissues, and minimization of drug-drug interactions. Furthermore, the production of peptides ready for use in humans is relatively affordable thanks to the development of two complementary technologies, namely solid-phase peptide synthesis (SPPS) and reversed-phase high-performance liquid chromatography (RP-HPLC). The former was first described by Bruce Merrifield (Merrifield, 1963), and later refined by several groups, while the latter, founded on the pioneering work of Jim Waters (McDonald, 2006), allows the purification of complex synthetic crude peptides. Both technologies can be used to prepare peptides to fulfill research and industrial requirements (Zompra et al., 2009; Rasmussen, 2018).

Peptide synthesis can be briefly defined as the proper combination of protecting groups (Isidro-Llobet et al., 2009) and coupling reactions—the latter based exclusively on the activation of the carboxylic group (El-Faham and Albericio, 2011). Although there are a large number of coupling reagents that cleanly render the active species (El-Faham and Albericio, 2011), the development of the native chemical ligation (NCL) technique by Stephen Kent brought about a breakthrough in the field (Dawson et al., 1994). NCL involves the preparation of an unprotected C-thioester peptide that allows reaction with an unprotected N-terminal Cys to render first the thioester involving the thiol of the Cys, which rearranges to form the natural amide bond (**Figure 1**). This technique has allowed the synthesis of difficult, large peptides, and proteins (Camarero and Muir, 1999; Camarero et al., 2001; Miller et al., 2003; Avital-Shmilovici et al., 2013; Okamoto et al., 2014a,b; Boll et al., 2015; Pala-Pujadas et al., 2018; Snella et al., 2018; Spengler et al., 2018; Ashhurst et al., 2019; Sun and Brik, 2019; Jbara et al., 2020; Serra et al., 2020).

One of the keys to the success of the NCL approach is the preparation of unprotected C-thioester peptides. Although these compounds were first synthesized using the *tert*-butoxycarbonyl (Boc)/benzyl (Bzl) strategy, several methods have been proposed for the same purpose using the friendlier fluorenylmethoxycarbonyl (Fmoc)/*tert*-butyl (tBu) approach. In this case, the main problem to overcome is the lack of stability of the thioester to the piperidine used in each step to remove the Fmoc group. In this regard, the thioester should be formed after elongation of the peptide. Although several linkers have been developed for this purpose (Camarero et al., 2004; Mulder et al., 2014; Kawakami et al., 2016; Morisaki et al., 2016; Olivier et al., 2017; Rao and Liu, 2017; Shelton et al., 2017; Flood et al., 2018),

the 3-(Fmoc-amino)-4-(methylamino) benzoic acid (Fmoc-MeDbz, the acronym derives from *N*-methyl-diaminobenzoic acid) and/or its non-methylated analog developed by Blanco-Canosa and Dawson are optimal (Blanco-Canosa and Dawson, 2008; Blanco-Canosa et al., 2015). Fmoc-MeDbz is anchored to an amino resin. After removal of the Fmoc group, peptide elongation proceeds smoothly using normal coupling reagents (the electronic deactivation of the aromatic ring by the growing peptide chain and the presence of the Me in the second amino group impede the development of a second peptide chain on the *N*-Me-amino). Once the peptide has been elongated, the resin is reacted with *p*-nitrophenyl chloroformate, followed by cyclization in basic media [*N,N*-diisopropylethylamine (DIEA)] to render *N*-acyl-*N'*-methyl-benzimidazolinone (MeNbz)-resin. As an activated *N*-acylurea (*N*-acyl-*N'*-methylurea), this resin is susceptible to being a leaving group when under the attack of a nucleophile such as a thiol and therefore to rendering, in this case, the peptide thioester (**Figure 2**). This resin is considered a “safety catch,” in the terms described by Patek and Lebl, namely stable throughout peptide elongation and then activated to be labile to a given reagent (Patek and Lebl, 1999).

This MeNbz-resin has also been used by Stockdill's group to synthesize C-terminal-modified peptides (Arbour et al., 2017, 2018a,b). In this case, the linker is released through an intermolecular reaction by the action of nucleophiles such as alcohols, thiols, amines, and even amino acids.

Our group (Acosta et al., 2017) and Olsen's (Gless et al., 2017; Gless and Olsen, 2018) have used the same strategy but in an intramolecular mode for the preparation of cyclodepsipeptides. In this strategy, after the formation of the MeNbz-activated species, the protecting group of the

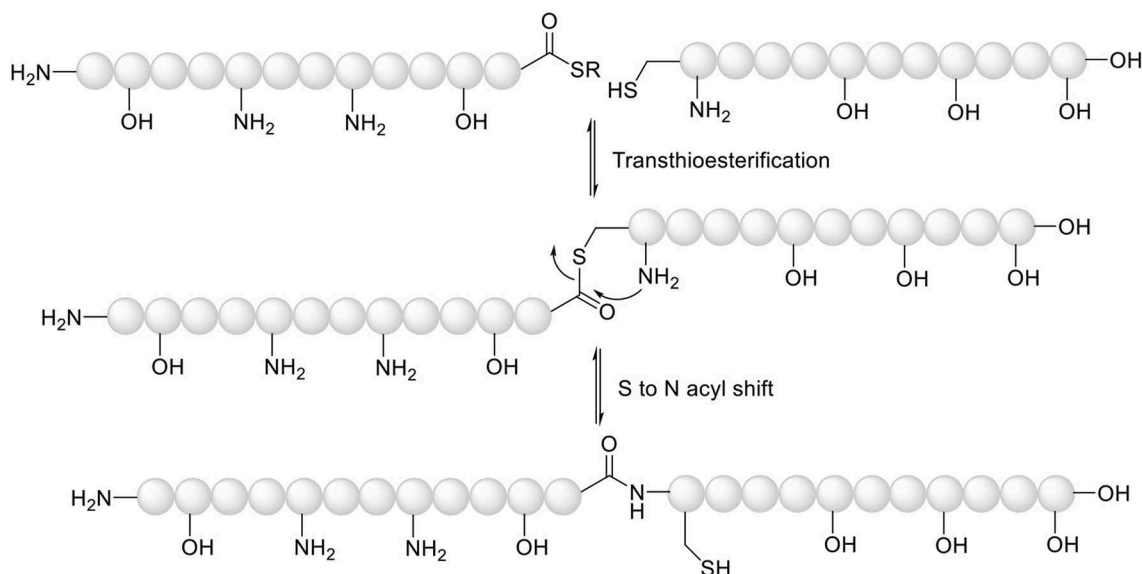
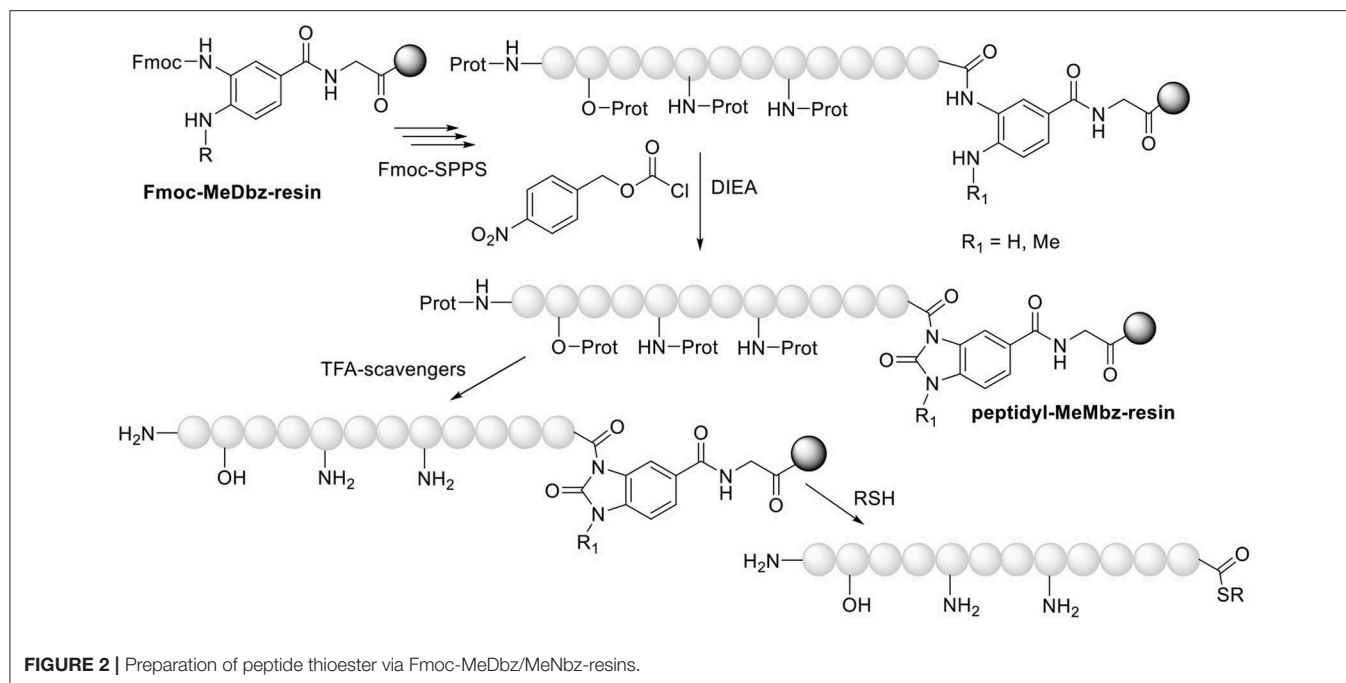


FIGURE 1 | Mechanism of native chemical ligation.



side-chain of a Cys residue is removed and the free thiol attacks the peptidyl-MeNbz-resin to render the cyclic thioester, with concomitant release of the peptide from the resin (**Figure 3**). A further advantage of this “cyclative cleavage” approach is that only the cyclic peptide is released from the resin. In this regard, those lineal sequences that have not converted to the cyclic structure remain unaltered on the resin, thereby simplifying the crude product and thus the purification step.

Our group has extended this “cyclative cleavage” to the preparation of homodetic cyclic peptides, where the nucleophile that causes the cleavage is an amino function, preferably from the side-chain of a peptide containing a basic amino acid (Abdel Monaim et al., 2018). In this case, the formation of the “head to side-chain” cyclic peptide is more favorable than the corresponding “head to tail” cyclic peptide, presumably due to the higher basicity of the ω -amino vs. the α -amino function (**Figure 3**).

Stockdill’s group has recently reported an elegant strategy combining the two previous methods for the preparation of a “head to tail” cyclic peptide containing a Cys residue (Arbour et al., 2019). Thus, the formation of the cyclic thiodepsipeptide takes place by the attack of the thiol of a *N*-terminal Cys on the peptidyl-MeNbz-resin, after which the cyclic thiodepsipeptide rearranges to form the homodetic head to tail cyclic peptide.

An important class of cyclo heterodetic peptides are the head to side-chain cyclodepsipeptides, where a residue of Ser, Thr, or other β -hydroxy amino acid forms an ester bond with the carboxylic group of *C*-terminal amino acid (Pelay-Gimeno et al., 2013). In our hands, the application of cyclative

cleavage on *N*-acyl-*N'*-MeDbz-resin for the preparation of Ser cyclodepsipeptides has proved unsuccessful, even when using strong bases such as NaH (results not shown).

Finally, less common but very intriguing peptides of the same family are those containing a phenyl ester coming from the phenol of a Tyr. These Tyr-cyclodepsipeptides are found in the fengycin family, which are lipodepsipeptides isolated from *Bacillus* strains (Sieber and Marahiel, 2003). Their syntheses are a challenge due to the inherent lability of the phenyl ester bond, which should be formed during the last steps of the synthetic strategy. Feliu and Planas’ group developed an elegant strategy (Rosés et al., 2016; Rosés et al., 2018), based on the following: incorporation of the first amino acid through the side-chain with the carboxylic acid protected in the form of the allyl ester; elongation of the peptide chain; formation of the phenyl ester with an *N*-Alloc-amino acid; treatment with Pd(0) to remove the allyl and the Alloc protecting groups; on-resin cyclization; and global deprotection and cleavage from the resin.

Here we report on a further application of the Fmoc-MeDbz/MeNbz-resin strategy for the synthesis of Tyr-cyclodepsipeptides.

RESULTS AND DISCUSSION

As the aromatic ring of the Tyr side chain should confer more rigidity to the pending unit than the side chains of Cys or Lys/Orn/Dab/Dap studied in previous works (Acosta et al., 2017; Abdel Monaim et al., 2018), we first investigated the

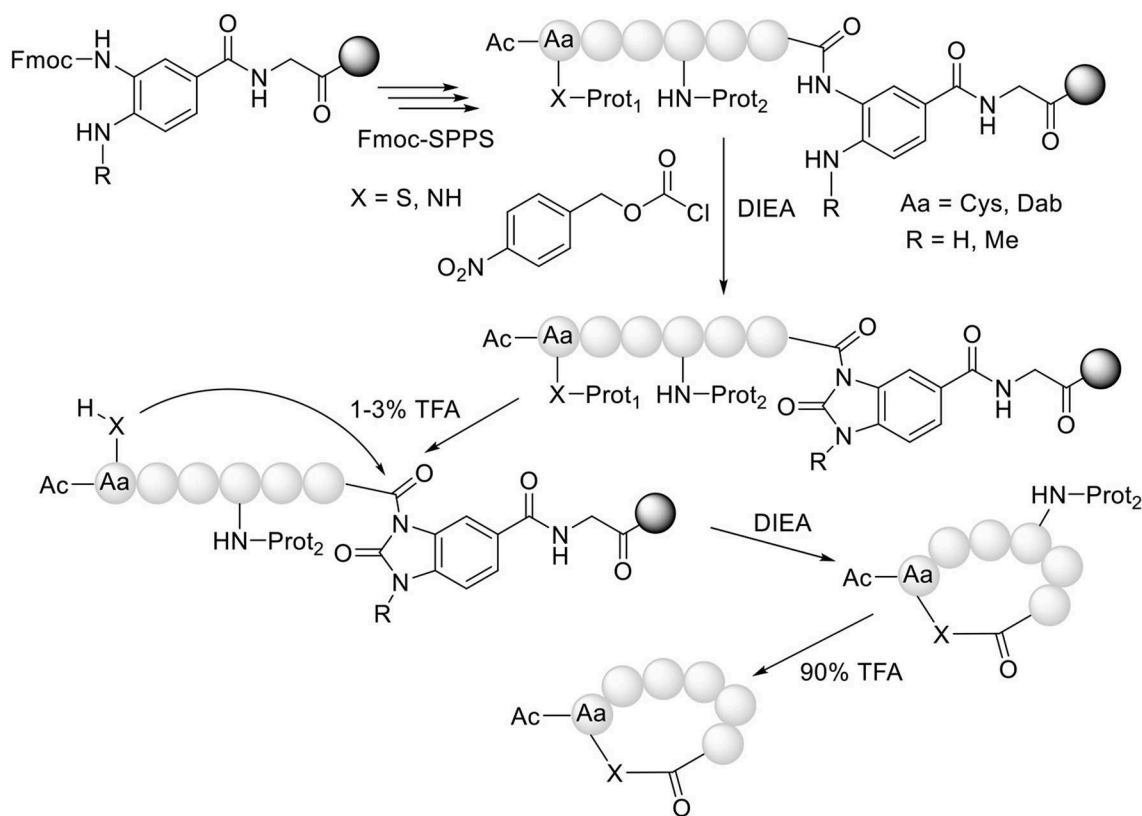


FIGURE 3 | Synthesis of head to side-chain cyclodepsipeptides ($\text{X} = \text{S}$) and cyclodepsipeptides ($\text{X} = \text{NH}$).

relevance of cyclodepsipeptide size with respect to facilitating the cyclization. Thus, model peptides with 6, 7, 8, and 9 amino acids were prepared, which correspond to cycles of 23, 26, 29, and 32-member rings, respectively (**Figure 4**). The sequence of these peptides was based on our previous works, related to the preparation of cyclo thiodepsipeptides and homodetic peptides as well (Acosta et al., 2017; Abdel Monaim et al., 2018). The peptide was built on a Fmoc-MeDbz-Gly-Rink-ChemMatrix resin with Fmoc/tBu amino acids using N,N' -diisopropylcarbodiimide (DIC) and OxymaPure in N,N -dimethylformamide (DMF) as coupling method (Subiros-Funosas et al., 2009). Tyr protected as Fmoc (α -amino) and 2-chlorotrityl (ClTrt) (phenol side-chain) was incorporated as the last amino acid. The Fmoc was removed with piperidine-DMF (2:8) and the amino function was acylated with hexanoic acid (Hx-OH). The Hx-Tyr(ClTrt)-peptidyl-MeDbz-Gly-Rink-ChemMatrix resin was activated with p -nitrophenyl chloroformate in anhydrous DCM, followed by cyclization with 0.5 M DIEA in DMF for 45 min to render Hx-Tyr-peptidyl-MeNbz-resin with concomitant appearance of an intense yellow color due to the release of the p -nitrophenol. The peptide resin was then treated with a low concentration solution of trifluoroacetic acid (TFA) in DCM to remove the ClTrt protecting group of the phenol of Tyr. The peptide-resin was

then washed thoroughly to ensure that no acid remained. The final cyclative cleavage occurred using 10% DIEA in DCM. The solutions, including the washings with DCM, were collected and concentrated. Cold diethyl ether (DEE) was added to facilitate the precipitation, and then centrifuged and decanted. The remaining solid was dissolved in $\text{CH}_3\text{CN-H}_2\text{O}$ (1:1) and lyophilized.

As shown in **Table 1**, peptides 1 and 4, the smallest and the largest cycles, were not observed. In these cases, cyclization was attempted at 60°C with 10% DIEA in DMF, but no cyclic peptides were detected. However, peptides # 2 and # 3, containing 7 and 8 amino acids, respectively, showed a major peak in HPLC (**Figures 5, 6**) and the mass was corroborated by HPLC-MS (**Supplementary Figures 3, 6**).

It is difficult to generalize about peptide cyclization; however, peptides containing the same number of amino acids as peptide # 1, having Cys and Dab instead of Tyr, were able to cyclize (Acosta et al., 2017; Abdel Monaim et al., 2018). It is therefore possible to confirm that the phenol of the Tyr side chain imposes more restrictions than Cys or Dab residues. These limitations can be translated in either an inability to achieve the cyclative cleavage or/and the instability of the Tyr-cyclodepsipeptide once formed. As the linear peptides were

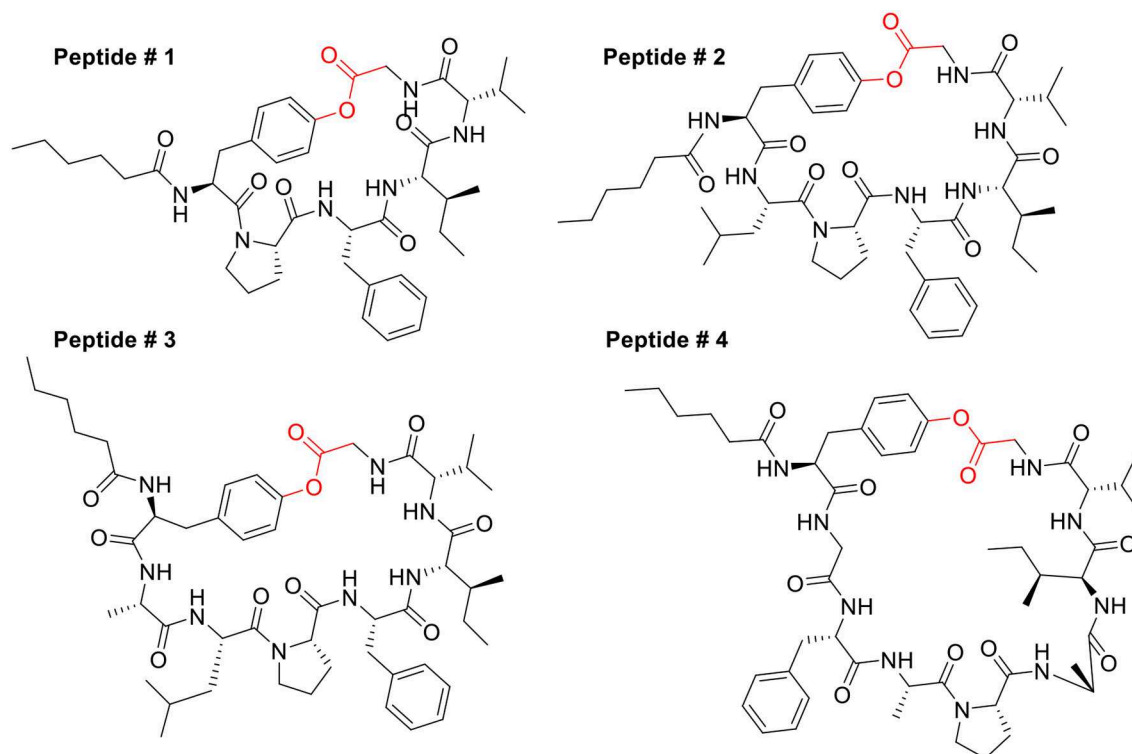


FIGURE 4 | Structures of model peptides # 1–4.

TABLE 1 | Summary of the results obtained with the model peptides.

| Peptide # | No. of AA | Peptidyl-resin | Cleaved Peptide Expected/Found mass | Cyclization |
|-----------|-----------|--------------------------|-------------------------------------|-------------|
| 1 | 6 | Hx-YPFIVG-MeNbz-resin | 774.4/- | No |
| 2 | 7 | Hx-YLPFIVG-MeNbz-resin | 888.1/888.4 | Yes |
| 3 | 8 | Hx-YALPFIVG-MeNbz-resin | 959.2/959.6 | Yes |
| 4 | 9 | Hx-YGFAPAIVG-MeNbz-resin | 974.2/- | No |

Hx, Hexanoyl.

not clearly detected, the most plausible explanation is the first one.

Next, the synthesis of the antifungal peptide BPC822 (Figure 7), first synthesized by Feliu and Planas' group, was attempted using the current methodology based on the use of the Fmoc-MeDbz/MeNbz-resin.

BPC822 contains eight amino acids similar to peptide # 3, and the phenyl ester is formed between the carboxylic group of the Ile and the phenol of the side-chain of Tyr. The involvement of the Ile, a β -substituted residue could add further difficulty to the formation of the ester. Thus, the Boc-Tyr(ClTrt)-Thr(*t*Bu)-Glu(*Ot*Bu)-Val-Pro-Gln(Trt)-D-Tyr(*t*Bu)-Ile-MeDbz-Gly-ChemMatrix-resin was constructed on a resin of reduced loading (0.33 mmol/g) to facilitate the cyclization. The resin was activated by treatment with

p-nitrophenyl chloroformate in anhydrous DCM, followed by 0.5 M DIEA in DMF for 1 h with concomitant development of an intense yellow color due to the release of the *p*-nitrophenol to render the peptidyl-MeNbz-resin. The ClTrt, protecting group of the side-chain of the Tyr, was removed by short treatments with diluted solutions of TFA in DCM, as above for the model peptides.

The cyclative cleavage was first attempted with 10% DIEA at room temperature, but after the corresponding work-up (see below) no product was obtained. The same reaction was then repeated at 60°C for 30 min and under microwave-assisted heating (100 w) at 80°C for 15 min. In both cases, the DMF was evaporated and the remaining oil was treated with concentrated solutions of TFA-H₂O-TIS (95:2.5:2.5) for 1 h to remove the remaining side-chain protecting groups. After partial evaporation of the TFA, the final product was then precipitated with cold DEE, centrifuged, decanted, and lyophilized. Although the two methods rendered the target peptide, the HPLC corresponding to the cyclative cleavage at 60°C (Figure 8) showed a much cleaner profile than that carried out under microwave conditions (Supplementary Figure 12). The final peptide was characterized by LC-MS and Maldi-TOF (Figure 9 and Supplementary Figures 9, 10, 11 and Table 1). In some cases, during the lyophilization and/or the posterior analysis, hydrolysis of the cyclic peptide was detected, thereby reinforcing the idea of the partial instability of head to side-chain Tyr-cyclodepsipeptides.

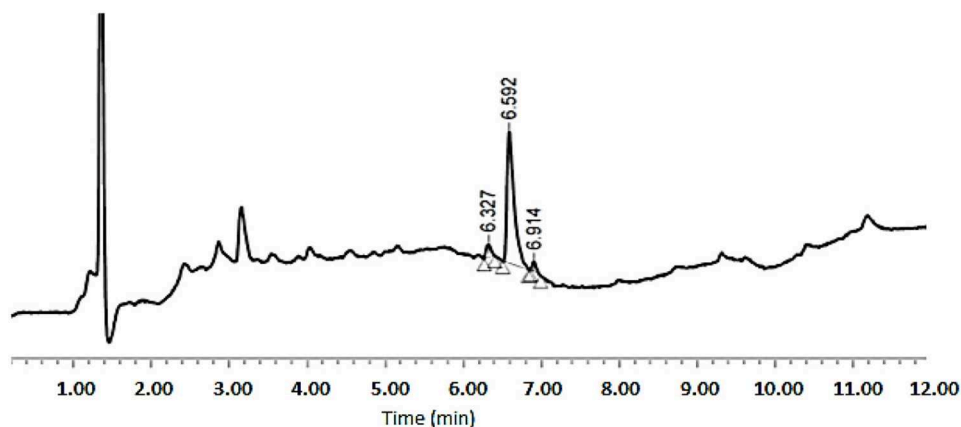


FIGURE 5 | HPLC analysis of crude peptide # 2 on a XBridge BEH130 C₁₈ 3.5 mm, 4.6 × 100 mm column. Eluents, A: H₂O with 0.045% of TFA; B: ACN with 0.036% of TFA. Gradient: 5–100% B into A in 8 min, 1.0 mL/min, 220 nm 25°C.

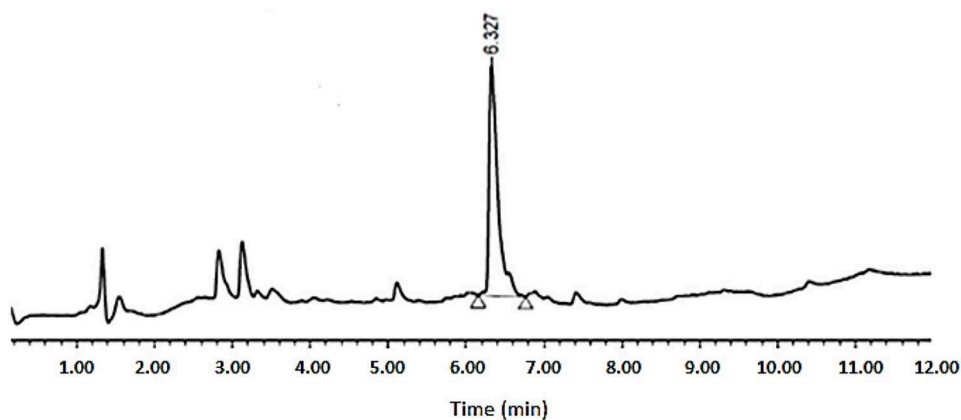


FIGURE 6 | HPLC analysis of crude peptide # 3 on XSelect C₁₈ 3.5 mm, 4.6 × 50 mm. Eluents, A: H₂O with 0.1% of formic acid; B: ACN with 0.07% of formic acid. Gradient: 5–100% B into A in 8 min, 1.6 mL/min, 220 nm, 50°C.

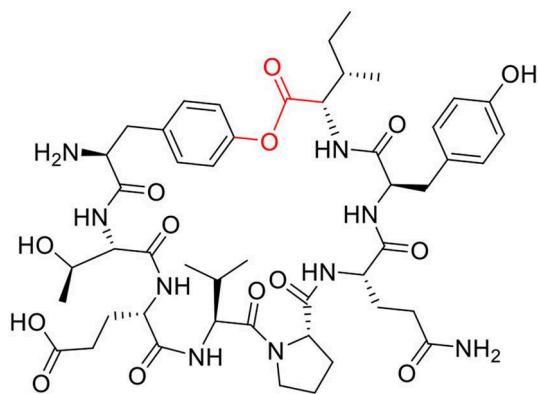


FIGURE 7 | Structure of BPC822 peptide.

CONCLUSIONS

Here, the “safety catch” Fmoc-MeDbz/MeNbz-resin developed by Blanco-Canosa and Dawson for the preparation of linear peptide thioesters was investigated to synthesize “head to side-chain” cyclodepsipeptides through a cyclative cleavage. While this strategy proved unsuccessful for the preparation of those peptides involving Ser in the formation of the ester bond, even using strong bases, it allowed the preparation of Tyr-cyclodepsipeptides using DIEA as a base. In the case of unhindered C-terminal amino acids, the cyclative cleavage took place at room temperature. When the C-terminal amino acid was more hindered, the reaction occurred at 60°C. This technology represents a friendly method for the preparation of these fascinating peptides.

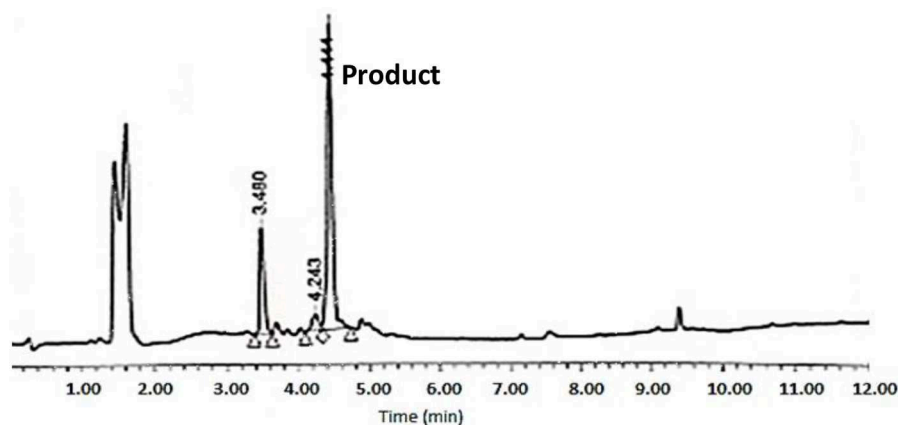


FIGURE 8 | HPLC analysis of crude BPC822 peptide cyclized at 60°C on a XBridge BEH130 C₁₈ 3.5 mm, 4.6 × 100 mm column. Eluents, A: H₂O with 0.045% of TFA; B: ACN with 0.036% of TFA. Gradient: 5–100% B into A in 8 min, 1.0 mL/min, 220 nm 25°C. The peak at 3.48 min could not be identified by MS.

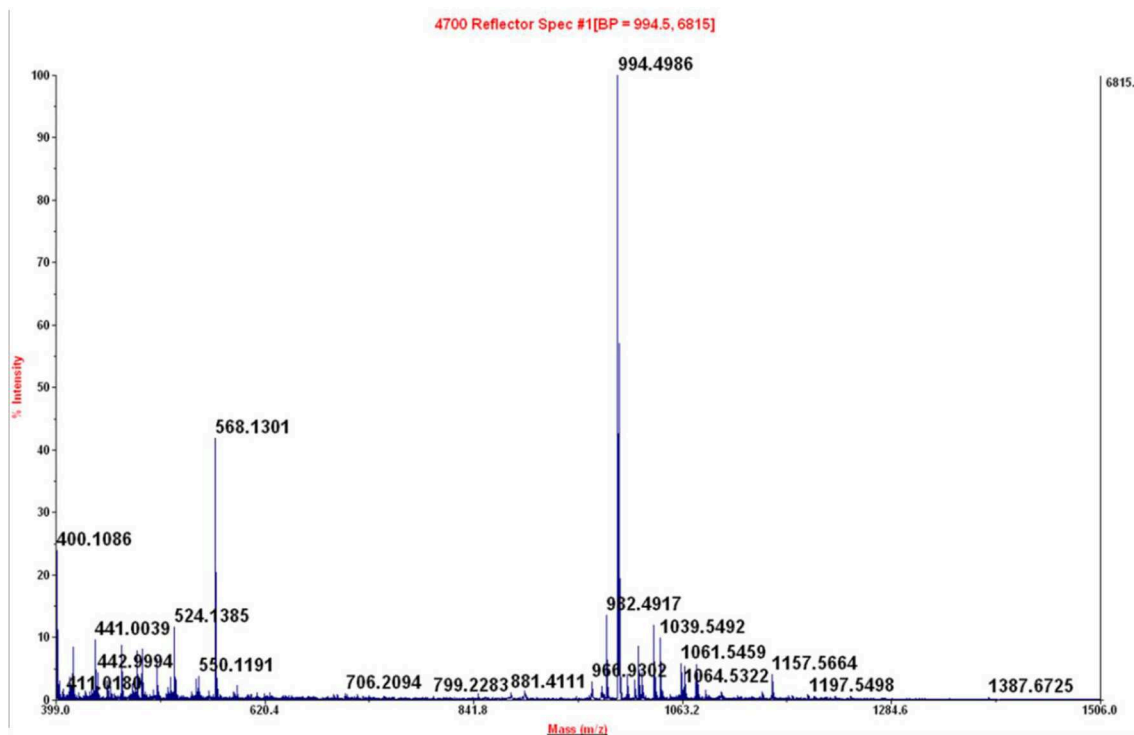


FIGURE 9 | Maldi-TOF of peak at 4.44 min of crude reaction peptide BPC822 obtained by heating at 60°C for 30 min. Calculated mass 993.48; mass found: $[M + H]^+ = 994.4986$.

EXPERIMENTAL

See **Supplementary Information** for a more detailed description of the full process. Herein, the key steps are described.

Fmoc-MeDbz-Gly-ChemMatrix-resin and SPPS

Although any amino resin can be used, aminomethyl ChemMatrix resin increases the success of the synthesis of these complex peptides (Garcia-Martin et al., 2006). To ensure

quantitative incorporation of the Fmoc-MeDbz linker, a spacer of Gly is introduced to minimize steric hindrance caused by the polymeric matrix. The incorporation of the building blocks, linker and protected amino acids took place smoothly using 3 equiv. of each component, namely carboxylic acid, DIC, and OxymaPure in DMF. The incorporation first protected acid on the H-MeDbz-resin was carried out with HATU-DIEA due to the poor nucleophilicity of the benzyl amine present in the linker. Fmoc was removed with piperidine-DMF (2×5 min). Washings with DMF and DCM were intercalated during the treatments.

Formation of the Activated *N*-acyl-*N'*-MeNbz-resin

Acylation of the NMe aniline moiety was achieved by treatment with 4-nitrophenyl chloroformate (5 equiv.) in anhydrous DCM for 1 h. Two treatments were carried out to achieve quantitative yield. Although an acyl chloride was used, the reaction was done in the absence of base. After resin filtration and washing, 0.5 M of DIEA in DMF was added for 45 min to render the cyclic urea. The release of 4-nitrophenol is shown by a strong yellow color, which indicates the formation of the cyclic urea.

Cyclative Cleavage

After the formation of the methylurea, the ClTrt of the phenol of Tyr was removed with TFA-triisopropylsilane (TIS)-DCM (2.5:2.5:95, 5×2 min washes). The resin was then washed thoroughly with DCM, DMF, and DCM, to ensure that no acid remained. The final cyclisation step occurred using 10% DIEA in DCM or DMF either at room temperature, at 60°C, or under microwave conditions, and the resin was further washed with DCM. The solution of 10% DIEA, including the DCM washings, was collected and evaporated to dryness. In the case of BCP822 peptide, the residue was treated for 1 h with TFA-TIS-DCM (95-2.5-2.5) to remove the remaining protecting groups and then evaporated to dryness.

REFERENCES

- Abdel Monaim, S. A. H., Acosta, G. A., Royo, M., El-Faham, A., de la Torre, B. G., and Albericio, F. (2018). Solid-phase synthesis of homodetic cyclic peptides from Fmoc-MeDbz-resin. *Tetrahedron Lett.* 59, 1779–1782. doi: 10.1016/j.tetlet.2018.03.084
- Acosta, G. A., Royo, M., de la Torre, B. G., and Albericio, F. (2017). Facile solid-phase synthesis of head-side chain cyclodepsipeptides through a cyclative cleavage from MeDbz-resin. *Tetrahedron Lett.* 58, 2788–2791. doi: 10.1016/j.tetlet.2017.06.008
- Al Shaer, D., Al Musaimi, O., Albericio, F., and de la Torre, B. G. (2020). 2019 FDA TIDES (Peptides and Oligonucleotides) harvest. *Pharmaceuticals*. 13:40. doi: 10.3390/ph13030040
- Arbour, C. A., Belavek, K. J., Tariq, R., Mukherjee, S., Tom, J. K., Isidro-Llobet, A., et al. (2019). Bringing macrolactamization full circle: self-cleaving head-to-tail macrocyclization of unprotected peptides via mild N-acyl urea activation. *J. Org. Chem.* 84, 1035–1041. doi: 10.1021/acs.joc.8b02418
- Arbour, C. A., Kondasinghe, T. D., Saraha, H. Y., Vorlicek, T. L., Stockdill, J. L. (2018a). Epimerization-free access to C-terminal cysteine peptide acids, carboxamides, secondary amides, and esters via complimentary strategies. *Chem. Sci.* 9, 350–355. doi: 10.1039/C7SC03553E
- Arbour, C. A., Saraha, H. Y., McMillan, T. F., and Stockdill, J. L. (2017). Exploiting the MeDbz linker to generate protected or unprotected C-terminally modified peptides. *Chem. Eur. J.* 23, 12484–12488. doi: 10.1002/chem.201703380
- In both cases, cold DEE was added in order to facilitate the precipitation of the peptide, which was then centrifuged and decanted. The remaining solid was dissolved in $\text{CH}_3\text{CN-H}_2\text{O}$ (1:1) and lyophilized.
- ## DATA AVAILABILITY STATEMENT
- The datasets generated for this study are available on request to the corresponding author.
- ## AUTHOR CONTRIBUTIONS
- Experimental part was performed mainly by GA and LM under the supervision of the rest of co-authors. The manuscript was written with contributions from of all the authors. All authors have given approval to the final version of the manuscript.
- ## FUNDING
- This work was funded in part by the following: the National Research Foundation (NRF) and the University of KwaZulu-Natal (South Africa); MINECO, (RTI2018-093831-B-I00), and the Generalitat de Catalunya (2017 SGR 1439) (Spain).
- ## ACKNOWLEDGMENTS
- The authors thank University of KwaZulu Natal for encouraging this project.
- ## SUPPLEMENTARY MATERIAL
- The Supplementary Material for this article can be found online at: <https://www.frontiersin.org/articles/10.3389/fchem.2020.00298/full#supplementary-material>
- Arbour, C. A., Stamatin, R. E., and Stockdill, J. L. (2018b). Sequence diversification by divergent C-Terminal elongation of peptides. *J. Org. Chem.* 83, 1797–1803. doi: 10.1021/acs.joc.7b02655
- Ashhurst, A. S., McDonald, D. M., Hanna, C. C., Stanojevic, V. A., Britton, W. J., and Payne, R. J. (2019). Mucosal vaccination with a self-adjuvanted lipopeptide is immunogenic and protective against mycobacterium tuberculosis. *J. Med. Chem.* 62, 8080–8089. doi: 10.1021/acs.jmedchem.9b00832
- Avital-Shmilovici, M., Mandal, K., Gates, Z. P., Phillips, N. B., Weiss, M. A., and Kent, S. B. H. (2013). Fully convergent chemical synthesis of ester insulin: determination of the high resolution X-ray structure by racemic protein crystallography. *J. Am. Chem. Soc.* 135, 3173–3185. doi: 10.1021/ja311408y
- Blanco-Canosa, J. B., and Dawson, P. E. (2008). An efficient Fmoc-SPPS approach for the generation of thioester peptide precursors for use in native chemical ligation. *Angew. Chem. Int. Ed.* 47, 6851–6855. doi: 10.1002/anie.200705471
- Blanco-Canosa, J. B., Nardone, B., Albericio, F., and Dawson, P. E. (2015). Chemical protein synthesis using a second-generation N-Acylurea linker for the preparation of peptide-thioester precursors. *J. Am. Chem. Soc.* 137, 7197–7209. doi: 10.1021/jacs.5b03504
- Boll, E., Ebran, J.-P., Drobecq, H., El-Mahdi, O., Raibaut, L., Ollivier, N., et al. (2015). Access to large cyclic peptides by a one-pot two-peptide segment ligation/cyclization process. *Org. Lett.* 17, 130–133. doi: 10.1021/ol503359w
- Camarero, J. A., Fushman, D., Cowburn, D., and Muir, T. W. (2001). Peptide chemical ligation inside living cells: *in vivo* generation

- of a circular protein domain. *Bioorg. Med. Chem.* 9, 2479–2484. doi: 10.1016/S0968-0896(01)00217-6
- Camarero, J. A., Hackel, B. J., De Yoreo, J. J., and Mitchell, A. R. (2004). Fmoc-based synthesis of peptide α -thioesters using an aryl hydrazine support. *J. Org. Chem.* 69, 4145–4151. doi: 10.1021/jo040140h
- Camarero, J. A., and Muir, T. W. (1999). Biosynthesis of a head-to-tail cyclized protein with improved biological activity. *J. Am. Chem. Soc.* 121, 5597–5598. doi: 10.1021/ja990929n
- Dawson, P. E., Muir, T. W., Clark-Lewis, I., and Kent, S. B. (1994). Synthesis of proteins by native chemical ligation. *Science* 266:776. doi: 10.1126/science.7973629
- de la Torre, B. G., and Albericio, F. (2020). The pharmaceutical industry in 2019: an analysis of FDA drug approvals from the perspective of molecules. *Molecules* 25:745. doi: 10.3390/molecules25030745
- El-Faham, A., and Albericio, F. (2011). Peptide coupling reagents, more than a letter soup. *Chem. Rev.* 111, 6557–6602. doi: 10.1021/cr100048w
- Flood, D. T., Hintzen, J. C. J., Bird, M. J., Cistrone, P. A., Chen, J. S., and Dawson, P. E. (2018). Leveraging the Knorr pyrazole synthesis for the facile generation of thioester surrogates for use in native chemical ligation. *Angew. Chem. Int. Ed.* 57, 11634–11639. doi: 10.1002/anie.201805191
- Garcia-Martin, F., Quintanar-Audelo, M., Garcia-Ramos, Y., Cruz, L. J., Gravel, C., Furic, R., et al. (2006). ChemMatrix, a Poly(ethylene glycol)-based support for the solid-phase synthesis of complex peptides. *J. Comb. Chem.* 8, 213–220. doi: 10.1021/cc0600019
- Gless, B. H., and Olsen, C. A. (2018). Direct peptide cyclization and one-pot modification using the MeDbz linker. *J. Org. Chem.* 83, 10525–10534. doi: 10.1021/acs.joc.8b01237
- Gless, B. H., Peng, P., Pedersen, K. D., Gotfredsen, C. H., Ingmer, H., and Olsen, C. A. (2017). Structure–activity relationship study based on Autoinducing Peptide (AIP) from dog pathogen, *S. schleiferi*. *Org. Lett.* 19, 5276–5279. doi: 10.1021/acs.orglett.7b02550
- Henninot, A., Collins, J. C., and Nuss, J. M. (2018). The current state of peptide drug discovery: back to the future? *J. Med. Chem.* 61, 1382–1414. doi: 10.1021/acs.jmedchem.7b00318
- Isidro-Llobet, A., Alvarez, M., and Albericio, F. (2009). Amino acid-protecting groups. *Chem. Rev.* 109, 2455–2504. doi: 10.1021/cr800323s
- Jbara, M., Maity, S. K., and Brik, A. (2020). Examining several strategies for the chemical synthesis of phosphorylated histone H3 reveals the effectiveness of the convergent approach. *Eur. J. Org. Chem.* doi: 10.1002/ejoc.201900257. [Epub ahead of print].
- Kawakami, T., Mishima, Y., Kinoshita, M., Lee, Y.-H., and Suetake, I. (2016). A thiirane linker for isopeptide mimetics by peptide ligation. *Tetrahedron Lett.* 57, 2112–2115. doi: 10.1016/j.tetlet.2016.04.006
- Lau, J. L., and Dunn, M. K. (2018). Therapeutic peptides: historical perspectives, current development trends, and future directions. *Bioorg. Med. Chem.* 26, 2700–2707. doi: 10.1016/j.bmc.2017.06.052
- McDonald, P. D. (2006). “James watters and his liquid chromatography people: a personal perspective,” in *The 350 Chromatographic Society Golden Jubilee Book: Recognising Half a Century of Supporting 351 Progress in Separation Science* (ChromSoc, ILM).
- Merrifield, R. B. (1963). Solid phase peptide synthesis. I the synthesis of a Tetrapeptide. *J. Am. Chem. Soc.* 85, 2149–2154. doi: 10.1021/ja00897a025
- Miller, J. S., Dudkin, V. Y., Lyon, G. J., Muir, T. W., and Danishefsky, S. J. (2003). Toward fully synthetic N-linked glycoproteins. *Angew. Chem. Int. Ed.* 42, 431–434. doi: 10.1002/anie.200390131
- Morisaki, T., Denda, M., Yamamoto, J., Tsuji, D., Inokuma, T., Itoh, K., et al. (2016). An N-sulfanylethylanilide-based traceable linker for enrichment and selective labelling of target proteins. *Chem. Commun.* 52, 6911–6913. doi: 10.1039/C6CC01229A
- Mulder, M. P. C., El Oualid, F., ter Beek, J., and Ovaa, H. (2014). A native chemical ligation handle that enables the synthesis of advanced activity-based probes: diubiquitin as a case study. *ChemBioChem.* 15, 946–949. doi: 10.1002/cbic.201402012
- Okamoto, R., Mandal, K., Ling, M., Luster, A. D., Kajihara, Y., and Kent, S. B. H. (2014a). Total chemical synthesis and biological activities of glycosylated and non-glycosylated forms of the chemokines CCL1 and Ser-CCL1. *Angew. Chem. Int. Ed.* 53, 5188–5193. doi: 10.1002/anie.201310574
- Okamoto, R., Mandal, K., Sawaya, M. R., Kajihara, Y., Yeates, T. O., and Kent, S. B. H. (2014b). (Quasi-)Racemic X-ray structures of glycosylated and non-glycosylated forms of the chemokine Ser-CCL1 prepared by total chemical synthesis. *Angew. Chem. Int. Ed.* 53, 5194–5198. doi: 10.1002/anie.201400679
- Olivier, N., Desmet, R., Drobecq, H., Blanpain, A., Boll, E., Leclercq, B., et al. (2017). A simple and traceless solid phase method simplifies the assembly of large peptides and the access to challenging proteins. *Chem. Sci.* 8, 5362–5370. doi: 10.1039/C7SC01912B
- Pala-Pujadas, J., Albericio, F., and Blanco-Canosa, J. B. (2018). Peptide ligations by using aryloxycarbonyl-o-methylaminoanilides: chemical synthesis of palmitoylated sonic hedgehog. *Angew. Chem. Int. Ed.* 57, 16120–16125. doi: 10.1002/anie.201810712
- Patek, M., and Lebl, M. (1999). Safety-catch and multiply cleavable linkers in solid-phase synthesis. *Biopolymers* 47, 353–363. doi: 10.1002/(SICI)1097-0282(1998)47:5<353::AID-BIP3>3.0.CO;2-I
- Pelay-Gimeno, M., Tulla-Puche, J., and Albericio, F. (2013). “Head-to-side-chain” cyclodepsipeptides of marine origin. *Mar. Drugs* 11, 1693–1717. doi: 10.3390/md11051693
- Rao, C., and Liu, C.-F. (2017). Peptide Weinreb amide derivatives as thioester precursors for native chemical ligation. *Org. Biomol. Chem.* 15, 2491–2496. doi: 10.1039/C7OB00103G
- Rasmussen, J. H. (2018). Synthetic peptide API manufacturing: a mini review of current perspectives for peptide manufacturing. *Bioorg. Med. Chem.* 26, 2914–2918. doi: 10.1016/j.bmc.2018.01.018
- Roses, C., Camo, C., Oliveras, A., Moll, L., Lopez, N., and Feliu, L., et al. (2018). Total solid-phase synthesis of dehydroxy fengycin derivatives. *J. Org. Chem.* 83, 15297–15311. doi: 10.1021/acs.joc.8b02553
- Rosés, C., Camó, C., Vogels, K., Planas, M., and Feliu, L. (2016). Solid-phase synthesis of cyclic depsipeptides containing a tyrosine phenyl ester bond. *Org. Lett.* 18, 4140–4143. doi: 10.1021/acs.orglett.6b02281
- Serra, G., Posada, L., and Hojo, H. (2020). On-resin synthesis of cyclic peptides via tandem N-to-S acyl migration and intramolecular thiol additive-free native chemical ligation. *Chem. Commun.* 56, 956–959. doi: 10.1039/C9CC07783A
- Shelton, P. M. M., Weller, C. E., and Chatterjee, C. (2017). A facile N-mercaptoethoxyglycinamide (MEGA) linker approach to peptide thioesterification and cyclization. *J. Am. Chem. Soc.* 139, 3946–3949. doi: 10.1021/jacs.6b13271
- Sieber, S. A., and Marahiel, M. A. (2003). Learning from Nature’s drug factories: nonribosomal synthesis of macrocyclic peptides. *J. Bacteriol.* 185:7036. doi: 10.1128/JB.185.24.7036-7043.2003
- Snella, B., Diemer, V., Drobecq, H., Agouridas, V., and Melnyk, O. (2018). Native chemical ligation at serine revisited. *Org. Lett.* 20, 7616–7619. doi: 10.1021/acs.orglett.8b03355
- Spengler, J., Blanco-Canosa, J. B., Forni, L., and Albericio, F. (2018). One-pot peptide ligation-oxidative cyclization protocol for the preparation of short-/medium-size disulfide cyclopeptides. *Org. Lett.* 20, 4306–4309. doi: 10.1021/acs.orglett.8b01741
- Subiros-Funosas, R., Prohens, R., Barbas, R., El-Faham, A., and Albericio, F. (2009). Oxyma: an efficient additive for peptide synthesis to replace the benzotriazole-based HOBt and HOAt with a lower risk of explosion. *Chem. Eur. J.* 15, 9394–9403. doi: 10.1002/chem.200900614
- Sun, H., and Brik, A. (2019). The journey for the total chemical synthesis of a 53 kDa protein. *Acc. Chem. Res.* 52:3361–3371. doi: 10.1021/acs.accounts.9b00372
- Zompra, A. A., Galanis, A. S., Werbitzky, O., and Albericio, F. (2009). Manufacturing peptides as active pharmaceutical ingredients. *Future Med. Chem.* 1, 361–377. doi: 10.4155/fmc.09.23

Conflict of Interest: The authors declare that the research was conducted in the absence of any commercial or financial relationships that could be construed as a potential conflict of interest.

Copyright © 2020 Acosta, Murray, Royo, de la Torre and Albericio. This is an open-access article distributed under the terms of the Creative Commons Attribution License (CC BY). The use, distribution or reproduction in other forums is permitted, provided the original author(s) and the copyright owner(s) are credited and that the original publication in this journal is cited, in accordance with accepted academic practice. No use, distribution or reproduction is permitted which does not comply with these terms.



Comparison Between O and OH Intermediates of Cytochrome c Oxidase Studied by FTIR Spectroscopy

Elena Gorbikova^{1†} and Ruslan Kalendar^{2,3*†}

¹ Institute of Biotechnology, University of Helsinki, Helsinki, Finland, ² Department of Agricultural Sciences, University of Helsinki, Helsinki, Finland, ³ National Center for Biotechnology, Nur-Sultan, Kazakhstan

OPEN ACCESS

Edited by:

Maria Luisa Mangoni,
Sapienza University of Rome, Italy

Reviewed by:

Sven Dennerlein,
University Medical Center
Göttingen, Germany
Zufeng Guo,
Johns Hopkins University,
United States

*Correspondence:

Ruslan Kalendar
ruslan.kalendar@helsinki.fi

†ORCID:

Elena Gorbikova
orcid.org/0000-0002-6078-6012
Ruslan Kalendar
orcid.org/0000-0002-3986-2460

Specialty section:

This article was submitted to
Chemical Biology,
a section of the journal
Frontiers in Chemistry

Received: 25 January 2020

Accepted: 14 April 2020

Published: 05 May 2020

Citation:

Gorbikova E and Kalendar R (2020)
Comparison Between O and OH
Intermediates of Cytochrome c
Oxidase Studied by FTIR
Spectroscopy. *Front. Chem.* 8:387.
doi: 10.3389/fchem.2020.00387

Cytochrome *c* oxidase is terminal enzyme in the respiratory chain of mitochondria and many aerobic bacteria. It catalyzes reduction of oxygen to water. During its catalysis, CcO proceeds through several quite stable intermediates (**R**, **A**, **PR/M**, **O/OH**, **E/EH**). This work is concentrated on the elucidation of the differences between structures of oxidized intermediates **O** and **OH** in different CcO variants and at different pH values. Oxidized intermediates of wild type and mutated CcO from *Paracoccus denitrificans* were studied by means of static and time-resolved Fourier-transform infrared spectroscopy in acidic and alkaline conditions in the infrared region 1800–1000 cm⁻¹. No reasonable differences were found between all variants in these conditions, and in this spectral region. This finding means that the binuclear center of oxygen reduction keeps a very similar structure and holds the same ligands in the studied conditions. The further investigation in search of differences should be performed in the 4000–2000 cm⁻¹ IR region where water ligands absorb.

Keywords: cell respiration, cytochrome *c* oxidase, oxidized state, FTIR spectroscopy, oxidoreduction

INTRODUCTION

Cytochrome *c* oxidase is the terminal complex of the respiratory chain of mitochondria, and some aerobic bacteria and archaea. CcO possesses four redox centers, in the direction of electron flow: CuA, heme *a*, heme *a*₃, and CuB. The last two centers form the binuclear center (BNC) where catalysis takes place. CcO receives electrons from a small soluble enzyme Cytochrome *c* from the positively charged side of the membrane (P-side). Cytochrome *c* passes electrons to CuA one by one. For oxygen reduction catalysis, the BNC of CcO must receive four protons (“chemical” protons; because they go for the chemistry of the catalytic cycle) from negatively charged side of membrane (N-side). This reaction is very exergonic, and the energy released is used to translocate four more protons across the membrane (these are called “pumped” protons) (Wikstrom, 1977, 2004; Babcock and Wikstrom, 1992; Brzezinski, 2004). Two H-conductive channels serve to transfer the protons needed for the chemistry and pumping: D- and K- channels, named after the conserved residues D-124 and K-354 (here *Paracoccus denitrificans* numbering used because this work was performed on *P. denitrificans* CcO enzyme), respectively (Hosler et al., 1993; Thomas et al., 1993; Fetter et al., 1995; Iwata et al., 1995; Tsukihara et al., 1996; Ostermeier et al., 1997; Yoshikawa et al., 1998). The catalytic cycle includes six relatively stable at room temperature intermediates determined mainly by time-resolved visible and Raman spectroscopies:

R (fully-reduced) \rightarrow **A** (ferrous-oxy) \rightarrow **PR/M** (“peroxy”; **PR** formed from fully reduced and **PM** formed from two electron reduced enzyme, electrons are located at the BNC) \rightarrow **F** (ferryl) \rightarrow **O/OH** (fully-oxidized “resting”/“pulsed”) \rightarrow **E/EH** (one-electron reduced “resting”/“pulsed” states). [Figure 1, reproduced from Gorbikova, 2009]. The catalytic cycle can be speculatively divided into two halves: oxidative (**R** \rightarrow **O**) and reductive (**O** \rightarrow **R**) halves (Figure 1). This work focuses on the fully-oxidized intermediate that is measured from both sides of the catalytic circle in experiments. In this intermediate all four redox centers are present in a fully-oxidized state. The fully-oxidized intermediate may exist in different forms with different rates of reduction and reactivity toward external ligands (Moody et al., 1991; John Moody, 1996). The “slow” form has a maximum in the Soret region below 418 nm and is characterized by the slow kinetic of cyanide binding to the oxidized heme a_3 . The absorption maximum of the “fast” form red-shifted by several nm. The enzyme in the “slow” form can be obtained when the protein is incubated or isolated at a low pH value. When CcO is extracted from the membrane, it exists in the slow or “resting” **O** form. Moreover, this form is heterogenic and is thought of as simply an artifact of preparation method. Incubation of “fast” oxidase with chloride or bromide at low pH produces forms of the enzyme that are similar to the “slow” form of the enzyme (Moody et al., 1991). Reduction of the enzyme in **O** state does not couple to proton pumping (Verkhovsky et al., 1999, 2001; Ruitenberget al., 2000). “Slow” oxidase shows characteristic EPR signal arising from the BNC, at $g \approx 12$ and $g = 2.95$, that are not seen in the fast form of enzyme. Reduction of this enzyme and its re-oxidation produces a fast or “pulsed” **O_H** state. The reduction of this intermediate is accompanied by the pumping of two protons across the membrane (Verkhovsky et al., 1999; Bloch et al., 2004). It was predicted that **O_H** state relaxes to the **O** state within about ~ 30 s at room temperature (Bloch et al., 2004). It was thought that the “resting” and “pulsed” states differ in their redox properties or ligands of the BNC (Bloch et al., 2004). Later it was proposed that the difference between these intermediates are in the presence of water molecules or their reorientation in the BNC or in close proximity of it (Jancura et al., 2006; Gorbikova et al., 2008). Later, Jancura et al. (2006) characterized **O** and **O_H** protein states by visible kinetic and EPR spectroscopies and found no difference between these two states. They concluded that the reduction potentials and the ligation states of heme a_3 and Cu_B are the same for CcO in the **O** and **O_H** states. Nowadays, the structure of the BNC in **O** and **O_H** states are supposed to be as follows: $\text{FeIII-OH-CuII-HOH Tyr(280)-O-}$ (as in Figure 1). This paper presents a study of **O** \rightarrow **R** transition on statically-resolved FTIR redox spectra of wild type (WT) enzyme at pH 6.0 and 9.0, and **R** \rightarrow **O** transition of WT at two pH values (6.0 and 9.0); on D124N variant at pH 9.0; and N131V mutant at pH 6.5

Abbreviations: A, ferrous-oxy intermediate; ATR, Attenuated total reflectance; BG, background; BNC, binuclear center; CcO, Cytochrome *c* oxidase; E, one-electron reduced intermediate; F, ferryl intermediate; FRCO, fully-reduced CO-inhibited enzyme; FTIR, Fourier transform infrared; IR, infrared; NHE, Normal Hydrogen Electrode; N-side, negatively charged side of the membrane; PR/M, “peroxy” intermediates; P-side, positively charged side of the membrane; R, fully-reduced intermediate, TR, time-resolved; WT, wild type.

and 9.0. **R** intermediate is assumed to be the same in all studied cases and only oxidized intermediates may vary. Here, static and time-resolved FTIR spectroscopy demonstrates that there are no clear differences in the oxidized intermediate irrespective of type of the mutant enzyme or WT and the way the **O/O_H** intermediate is produced and measured, i.e., there is no difference between “resting” and “pulsed” fully-oxidized intermediate within the measured IR spectral range.

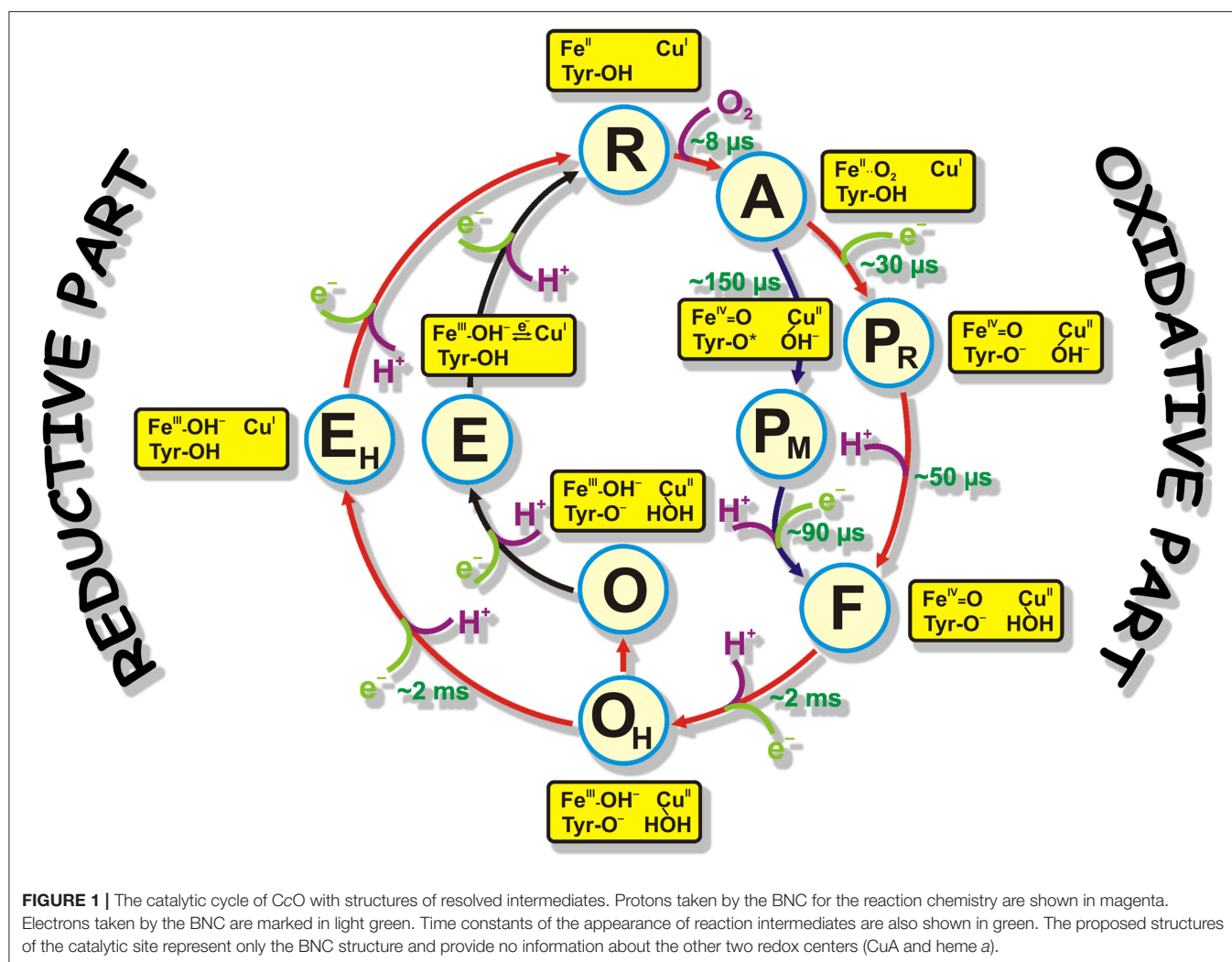
MATERIALS AND METHODS

Sample Preparation

For the preparation of “ATR-ready” sample, the variants of the enzyme were depleted of the detergent as originally described in Rich and Breton (2002) with some modifications (Ribacka et al., 2005; Gorbikova et al., 2006, 2007b). The “ATR-ready” sample of CcO was placed on a microprism slightly polished by aluminum powder ATR (Attenuated total reflectance) (Sens IR Technologies, three-bounce version, surface diameter 3 mm). The sample was dried under soft N_2 flow or under a tungsten fiber lamp positioned at a distance of ~ 30 cm from the sample film, then, rewetted with “working” buffer (= buffer in which the experiments are undertaken). In all experiments, the enzyme film was stabilized overnight, then covered with a custom designed chamber either for equilibrium FTIR measurements (Gorbikova et al., 2006) or for a time-resolved approach (Gorbikova et al., 2007b) (also see two sections below). Sample preparation for the static experiment included pumping of “working buffer” overnight in order to stabilize the protein film. In the morning, such a sample was ready for static experiments. Sample preparation for the kinetic FTIR **RO** measurements also included overnight incubation but without pumping and **FRCO** (Fully-reduced CO-inhibited) complex preparation with buffer contained 100% CO gas. Formation of **FRCO** complex was followed by the appearance of heme a_3 - $\text{C}\equiv\text{O}$ band at $1,965\text{ cm}^{-1}$ and took ~ 40 – 80 min.

Equilibrium **O** \rightarrow **R** FTIR Spectra

Equilibrium redox titration setup built in Helsinki Bioenergetics Group (Gorbikova et al., 2006; Gorbikova, 2009; Figures 9, 10 therein) allows to measure the reductive half of the catalytic cycle (Figure 1). Equilibrium redox FTIR spectra have been measured in a broad pH region before (Iwaki et al., 2004; Gorbikova et al., 2007a). The buffer composition was the following: 400 mM of K_2SO_4 , 25 mM of potassium acetate, 25 mM of potassium phosphate, and 25 mM of boric acid. The spectra were produced electrochemically with a homemade flow-by electrochemical cell (Vuorilehto et al., 2004). The picture of the cell with its description can be found in Gorbikova et al. (2006) and Vuorilehto et al. (2004). In short, gold grains were used as the working electrode, a platinum-plated titanium grid as the counter electrode and $\text{Ag/AgCl/saturated KCl}$ as the reference electrode. The “working buffer” with mediators was continuously pumped through the working electrode to the ATR chamber. The cell was connected to a Princeton Applied Research potentiostat (Oak Ridge, Tennessee, USA). To equilibrate the enzyme film



with the potential of the working electrode, two mediators were used: 1,2-diaminocyclohexane- $\text{N},\text{N},\text{N}',\text{N}'$ -tetraacetic acid + Fe, midpoint potential +95 mV; and ferrocene acetate, +370 mV. The kinetics of equilibration of the enzyme film with the potential of the working electrode was controlled in the visible region spectrophotometrically. The $\text{O} \rightarrow \text{R}$ spectra measurements were performed as follows. First, the enzyme film was equilibrated at acidic pH at -300 mV (vs NHE, Normal Hydrogen Electrode) for 15 min. Then, a background (BG) spectrum in the infrared (IR) region was measured. Then, the potential was set at $+480$ mV, again allowing 15 min for equilibration. At this point, a spectrum in the IR region was taken. Immediately after that, BG in the IR region was collected. The potential was then switched back to -300 mV and the procedure was repeated many times to collect FTIR spectra with good signal-to-noise ratio. Then, the pH of the “working buffer” was changed to another value (in this case to pH 9.0) and a series of $\text{R} \rightarrow \text{O}$ and $\text{O} \rightarrow \text{R}$ spectra were measured and summed up. To follow oxidoreduction, an FTIR spectrometer Bruker IFS 66/s (Ettlingen, Germany) equipped with a fast MCT detector and a visible spectrophotometer USB2000 (Ocean Optics) (Largo, USA) were used. FTIR spectra

were measured in the spectral range $4000\text{--}5000 \text{ cm}^{-1}$ with 4 cm^{-1} spectral resolution and IR scanner frequency 80 kHz. The number of scans in BG and sample spectra was 2000; apodization function, Blackman-Harris 3-Term. The control of the status of oxidoreduction was achieved by visible spectroscopy at 445 nm. The light guide from a visible spectrophotometer was connected to the ATR-chamber. The data acquisition system described above produced one $\text{R} \rightarrow \text{O}$ and one $\text{O} \rightarrow \text{R}$ spectrum that were summed up. All measurements were performed at room temperature. For more detailed description of the procedure of spectra collection see (Gorbikova et al., 2007a). The whole data acquisition process initializing, sending commands to/from Ocean Optics and FTIR Opus software, and collecting data was controlled by *Titration* software designed in the Helsinki Bioenergetics Group by Dr. Nikolay Belevich.

Time-Resolved $\text{R} \rightarrow \text{O}$ FTIR Spectra

With help of time-resolved $\text{R} \rightarrow \text{O}$ FTIR spectra, the oxidative part of the catalytic cycle of CcO was investigated. Time-resolved $\text{R} \rightarrow \text{O}$ FTIR spectra were measured in the following conditions: WT at pH 6.0 and 9.0; N131V at pH 6.5 and 9.0; and D124N

at pH 9.0. These spectra were measured in order to distinguish similarities and dissimilarities between **O** and **O_H** states in different conditions as much as possible. To perform time-resolved measurements of the **R**→**O** transition, a special setup was constructed. The core of this setup is an FTIR spectrometer Bruker IFS 66/s equipped with a fast MCT detector and an ATR-cell. The ATR-cell is covered with a special chamber for time-resolved oxygen reaction measurements. Enzyme on ATR-prism is prepared in **FRCO** form. CO is photolyzed from CcO **FRCO** enzyme by a laser that is delivered by a laser guide connected to the chamber. Oxygenated buffer is injected very close to the enzyme film. A light guide from a visible spectrophotometer is constructed in the ATR-chamber as well as an inlet and outlet of the pump. For more details and for pictures see [Gorbikova et al., 2007b and Figure 1 therein and Gorbikova, 2009, Figures 12–14 therein]. The “working buffer” for time-resolved FTIR measurements included 100 mM glucose [Merck (Darmstadt, Germany)], 260 μg/mL catalase [Sigma-Aldrich (St. Louis, Missouri, United States)], 3.3 mM ascorbate [Prolabo (Leicestershire, UK)], 10–100 μM hexaaminruthenium (III) chloride [Sigma-Aldrich (St. Louis, Missouri, United States)] (the amount of the last component depended on CcO variant), and 670 μg/mL glucose oxidase [Roche (Basel, Switzerland)]. Before each experiment, the sample quality control was conducted (Gorbikova et al., 2007b). Four procedures were applied in order to test the stability and functionality of the BNC of CcO. First, the intensity and the shape of the band at 1965 cm⁻¹ was analyzed. Second, CO dissociation from heme *a*₃ was followed by visible time-resolved spectroscopy with 1 ms temporal resolution. Third, CO dissociation in the dark from heme *a*₃ was followed by time-resolved (TR) rapid-scan FTIR in the region around the band at 1965 cm⁻¹. Finally, CO dissociation from **FRCO** compound at 1965 cm⁻¹ was measured after oxygenated buffer addition, delay of 3 s, and laser flash. This last test was performed before, in the middle, and at the end of each experiment. It showed the amount of enzyme capable of performing the oxygen reaction. **FRCO**→**O** spectra were acquired as initially described in (Gorbikova et al., 2007b). Spectra were measured in 1850–950 cm⁻¹ region, which was cut out by an interference filter. The spectra were collected in the rapid-scan mode with ~46 ms temporal resolution and 8 cm⁻¹ spectral resolution. Together with oxygen injection, rapid-scan acquisition started and was followed by a 3 s delay and the laser flash. The flow pump was stopped during the kinetic data collection and switched on immediately after to speed up the CcO re-reduction. This cycle was repeated many times to get spectra of a good signal-to-noise-ratio. A global fitting procedure in *Matlab* software (Natick, MA, USA) was applied to extract the slow part of kinetical spectra. The fast part of kinetical spectra was calculated as a difference between the spectrum obtained by the average of several time points before the laser flash and the spectrum obtained immediately after it. The sum of the fast and the slow components gave resulting kinetic spectrum in case of mutated CcO. The kinetic spectrum in case of WT enzyme was calculated as a spectral jump after the laser flash because oxygen reaction in WT enzyme proceeds faster than temporal resolution of the measurement setup. **FRCO** photolysis was measured separately at pH 6.5 on WT variant

and subtracted from each **FRCO**→**O** spectra to produce **R**→**O** spectra presented in the figures in the section “**Results**”. It was shown in (Heitbrink et al., 2002) that **FRCO** photolysis on WT does not depend on pH values. All measurements of kinetic **R**→**O** transitions and **FRCO** photolysis were performed in ice-cooled conditions in order to slow-down the reaction rate and increase concentration of oxygen until reaching 2.4 mM. For more details see (Gorbikova et al., 2007b, 2008).

Data Analysis

All data analysis and figure preparations were performed in *Matlab* software.

RESULTS AND DISCUSSIONS

Here, the IR spectra are compared in acidic conditions on static and time-resolved redox transitions (**O**→**R** for static transitions and **R**→**O** for the time-resolved). Altogether 6000 FTIR **O**→**R** static spectra were collected at pH 6.0 on WT (**Figure 2**, red spectrum), 173 kinetic spectra of WT at pH 6.0 (**Figure 2**, dark green spectrum), and 338 kinetic spectra of N131V at pH 6.5 (**Figure 2**, dark blue spectrum). Small differences between static and kinetic spectra are due to difference in their spectral resolution which is 4 cm⁻¹ for static and 8 cm⁻¹ for the kinetics spectra. Similar results were observed under alkaline conditions: 296 kinetic spectra for D124N at pH 9.0 (**Figure 3**, dark blue), 218 for N131V 9.0 (**Figure 3**, dark green), 82 for WT (**Figure 3**, red), and 6000 co-additions for WT in static conditions (**Figure 3**, light-green). No differences were found between oxidized intermediates in the IR region 1800–1000 cm⁻¹ for all studied cases in both acidic and alkaline conditions. There are no visible differences between static and time-resolved **R**→**O**

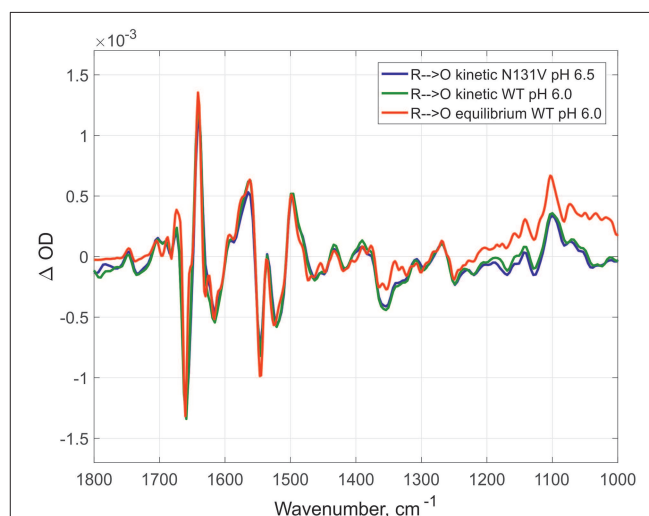


FIGURE 2 | Comparison of the **R**→**O** transitions in three different conditions. Time-resolved mode for N131V at pH 6.5 in dark blue and for WT at pH 6.0 in dark green; equilibrium mode for WT at pH 6.0 in red. All spectra normalized to 1 mM (kinetic—by amplitude of 1,965 cm⁻¹ band, equilibrium—by 1661/1641 peaks difference).

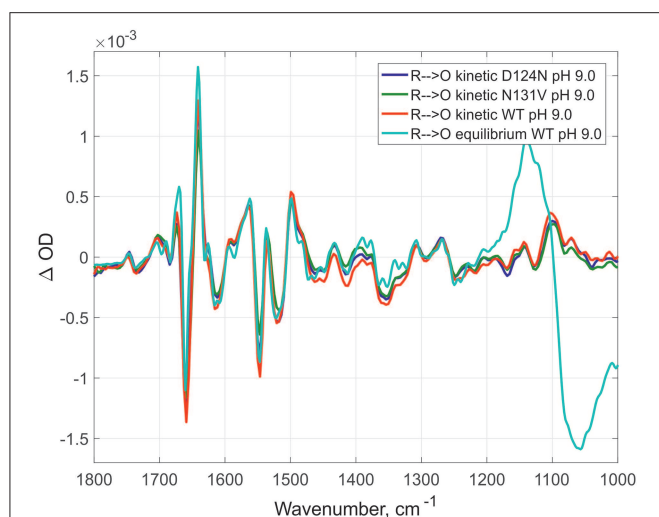


FIGURE 3 | Comparison of R→O transitions in four different conditions at pH 9.0. Time-resolved spectra for D124N (in dark blue), N131V (in dark green), and WT (in red); equilibrium spectrum for WT (light green). All spectra were measured at pH 9.0 and normalized to 1 mM (kinetic—by amplitude of 1,965 cm⁻¹ band, equilibrium—by 1661/1641 peaks difference).

FTIR spectra of WT and mutated enzymes in the IR region 1800–1000 cm⁻¹ that prove that the BNC of these variants and in these pH conditions are very similar. It does not matter what side we go R→O or O→R, oxidized intermediate provides the same findings and no difference between O and O_H is observed in the 1800–1000 cm⁻¹ infrared window for all conditions studied. Further, the difference should be sought in the so-called “water region.”

CONCLUSIONS

This paper compared the oxidized intermediates derived from different variants (WT, D124N, and N131V) and using different approaches (static O→R spectra acquisition and time-resolved R→O spectra). To perform this work, two special setups were constructed: one for static measurements and one for time-resolved measurements. This work provides an overview

of the oxidized intermediates prepared under very different conditions: different mutants and pH values. No differences are evident between all of the conditions tested, except that for static spectra spectral resolution was set at 4 cm⁻¹ and for time-resolved at 8 cm⁻¹. This similarity in oxidized intermediates under different conditions means that the structures of BNC in all these cases (O and O_H states) are very similar from the FTIR fingerprint point of view. Further investigation in the IR region 4000–2000 cm⁻¹ is required to search for differences between various oxidized intermediates.

DATA AVAILABILITY STATEMENT

The raw data supporting the conclusions of this article will be made available by the authors, without undue reservation, to any qualified researcher.

AUTHOR'S NOTE

This manuscript has been released as a pre-print at bioRxiv (Gorbikova and Kalendar, 2018).

AUTHOR CONTRIBUTIONS

EG designed research, performed research, analyzed the data, and wrote the paper. RK analyzed the data, wrote the paper.

FUNDING

EG was supported by Center of International mobility (CIMO) and Informational and Structural Biology (ISB) Graduate School. The work was supported by the Sigrid Juselius foundation, Biocentrum Helsinki and the Academy of Finland (project numbers 200726, 44895, and 115108).

ACKNOWLEDGMENTS

We warmly thank Dr. Nikolai Belevich for an excellent technical assistance, Dr. Timur Nikitin for critical reading of the manuscript and Dr. Jennifer Rowland (University of Helsinki) for outstanding editing and proofreading of the manuscript.

REFERENCES

- Babcock, G. T., and Wikstrom, M. (1992). Oxygen activation and the conservation of energy in cell respiration. *Nature* 356, 301–309. doi: 10.1038/356301a0
- Bloch, D., Belevich, I., Jasaitis, A., Ribacka, C., Puustinen, A., Verkhovsky, M. I., et al. (2004). The catalytic cycle of cytochrome c oxidase is not the sum of its two halves. *Proc. Natl. Acad. Sci. U.S.A.* 101, 529–533. doi: 10.1073/pnas.0306036101
- Brzezinski, P. (2004). Redox-driven membrane-bound proton pumps. *Trends Biochem. Sci.* 29, 380–387. doi: 10.1016/j.tibs.2004.05.008
- Fetter, J. R., Qian, J., Shapleigh, J., Thomas, J. W., Garcia-Horsman, A., Schmidt, E., et al. (1995). Possible proton relay pathways in cytochrome c oxidase. *Proc. Natl. Acad. Sci. U.S.A.* 92, 1604–1608. doi: 10.1073/pnas.92.5.1604
- Gorbikova, E. (2009). *Oxygen Reduction and Proton Translocation by Cytochrome C Oxidase (Ph.D. thesis)*. University of Helsinki, Department of Biological

and Environmental Sciences & Institute of Biotechnology & National Graduate School in Informational and Structural Biology Åbo Akademi, Helsinki, Finland.

- Gorbikova, E., and Kalendar, R. (2018). Comparison between O and O_H intermediates of cytochrome c oxidase studied by FTIR spectroscopy. *bioRxiv*. 275099. doi: 10.1101/275099
- Gorbikova, E. A., Belevich, N. P., Wikstrom, M., and Verkhovsky, M. I. (2007a). Protolytic reactions on reduction of cytochrome c oxidase studied by ATR-FTIR spectroscopy. *Biochemistry* 46, 4177–4183. doi: 10.1021/bi602523a
- Gorbikova, E. A., Belevich, N. P., Wikstrom, M., and Verkhovsky, M. I. (2007b). Time-resolved ATR-FTIR spectroscopy of the oxygen reaction in the D124N mutant of cytochrome c oxidase from *Paracoccus denitrificans*. *Biochemistry* 46, 13141–13148. doi: 10.1021/bi701614w
- Gorbikova, E. A., Vuorilehto, K., Wikstrom, M., and Verkhovsky, M. I. (2006). Redox titration of all electron carriers of cytochrome c oxidase

- by Fourier transform infrared spectroscopy. *Biochemistry* 45, 5641–5649. doi: 10.1021/bi060257v
- Gorbikova, E. A., Wikstrom, M., and Verkhovsky, M. I. (2008). The protonation state of the cross-linked tyrosine during the catalytic cycle of cytochrome c oxidase. *J. Biol. Chem.* 283, 34907–34912. doi: 10.1074/jbc.M803511200
- Heitbrink, D., Sigurdson, H., Bolwien, C., Brzezinski, P., and Heberle, J. (2002). Transient binding of CO to CuB in cytochrome c oxidase is dynamically linked to structural changes around a carboxyl group: a time-resolved step-scan fourier transform infrared investigation. *Biophys. J.* 82, 1–10. doi: 10.1016/S0006-3495(02)75368-X
- Hosler, J. P., Ferguson-Miller, S., Calhoun, M. W., Thomas, J. W., Hill, J., Lemieux, L., et al. (1993). Insight into the active-site structure and function of cytochrome oxidase by analysis of site-directed mutants of bacterial cytochrome aa3 and cytochrome bo. *J. Bioenerg. Biomembr.* 25, 121–136. doi: 10.1007/BF00762854
- Iwaki, M., Puustinen, A., Wikstrom, M., and Rich, P. R. (2004). ATR-FTIR spectroscopy and isotope labeling of the PM intermediate of *Paracoccus denitrificans* cytochrome c oxidase. *Biochemistry* 43, 14370–14378. doi: 10.1021/bi048545j
- Iwata, S., Ostermeier, C., Ludwig, B., and Michel, H. (1995). Structure at 2.8 Å resolution of cytochrome c oxidase from *Paracoccus denitrificans*. *Nature* 376, 660–669. doi: 10.1038/376660a0
- Jancura, D., Berka, V., Antalík, M., Bagelova, J., Gennis, R. B., Palmer, G., et al. (2006). Spectral and kinetic equivalence of oxidized cytochrome C oxidase as isolated and “activated” by reoxidation. *J. Biol. Chem.* 281, 30319–30325. doi: 10.1074/jbc.M605955200
- John Moody, A. (1996). ‘As prepared’ forms of fully oxidised haem/Cu terminal oxidases. *Biochim. Biophys. Acta.* 1276, 6–20. doi: 10.1016/0005-2728(96)00035-7
- Moody, A. J., Cooper, C. E., Rich, P. R. (1991). Characterisation of ‘fast’ and ‘slow’ forms of bovine heart cytochrome-c oxidase. *Biochim. Biophys. Acta.* 1059, 189–207. doi: 10.1016/S0005-2728(05)80204-X
- Ostermeier, C., Harrenga, A., Ermler, U., and Michel, H. (1997). Structure at 2.7 Å resolution of the *Paracoccus denitrificans* two-subunit cytochrome c oxidase complexed with an antibody FV fragment. *Proc. Natl. Acad. Sci. U.S.A.* 94, 10547–10553. doi: 10.1073/pnas.94.20.10547
- Ribacka, C., Verkhovsky, M. I., Belevich, I., Bloch, D. A., Puustinen, A., and Wikstrom, M. (2005). An elementary reaction step of the proton pump is revealed by mutation of tryptophan-164 to phenylalanine in cytochrome c oxidase from *Paracoccus denitrificans*. *Biochemistry* 44, 16502–16512. doi: 10.1021/bi0511336
- Rich, P. R., Breton, J. (2002). Attenuated total reflection Fourier transform infrared studies of redox changes in bovine cytochrome c oxidase: resolution of the redox Fourier transform infrared difference spectrum of heme a(3). *Biochemistry* 41, 967–973. doi: 10.1021/bi0109717
- Ruitenbergh, M., Kannt, A., Bamberg, E., Ludwig, B., Michel, H., and Fendler, K. (2000). Single-electron reduction of the oxidized state is coupled to proton uptake via the K pathway in *Paracoccus denitrificans* cytochrome c oxidase. *Proc. Natl. Acad. Sci. U.S.A.* 97, 4632–4636. doi: 10.1073/pnas.080079097
- Thomas, J. W., Puustinen, A., Alben, J. O., Gennis, R. B., and Wikstrom, M. (1993). Substitution of asparagine for aspartate-135 in subunit I of the cytochrome bo ubiquinol oxidase of *Escherichia coli* eliminates proton-pumping activity. *Biochemistry* 32, 10923–10928. doi: 10.1021/bi00091a048
- Tsukihara, T., Aoyama, H., Yamashita, E., Tomizaki, T., Yamaguchi, H., Shinzawa-Itoh, K., et al. (1996). The whole structure of the 13-subunit oxidized cytochrome c oxidase at 2.8 Å. *Science* 272, 1136–1144. doi: 10.1126/science.272.5265.1136
- Verkhovsky, M. I., Jasaitis, A., Verkhovskaya, M. L., Morgan, J. E., and Wikstrom, M. (1999). Proton translocation by cytochrome c oxidase. *Nature* 400, 480–483. doi: 10.1038/22813
- Verkhovsky, M. I., Tuukkanen, A., Backgren, C., Puustinen, A., and Wikstrom, M. (2001). Charge translocation coupled to electron injection into oxidized cytochrome c oxidase from *Paracoccus denitrificans*. *Biochemistry* 40, 7077–7083. doi: 10.1021/bi010030u
- Vuorilehto, K., Lutz, S., and Wandrey, C. (2004). Indirect electrochemical reduction of nicotinamide coenzymes. *Bioelectrochemistry* 65, 1–7. doi: 10.1016/j.bioelechem.2004.05.006
- Wikstrom, M. (2004). Cytochrome c oxidase: 25 years of the elusive proton pump. *Biochim Biophys Acta* 1655, 241–247. doi: 10.1016/j.bbabbio.2003.07.013
- Wikstrom, M. K. (1977). Proton pump coupled to cytochrome c oxidase in mitochondria. *Nature* 266, 271–273. doi: 10.1038/266271a0
- Yoshikawa, S., Shinzawa-Itoh, K., Nakashima, R., Yaono, R., Yamashita, E., Inoue, N., et al. (1998). Redox-coupled crystal structural changes in bovine heart cytochrome c oxidase. *Science* 280, 1723–1729. doi: 10.1126/science.280.5370.1723

Conflict of Interest: The authors declare that the research was conducted in the absence of any commercial or financial relationships that could be construed as a potential conflict of interest.

Copyright © 2020 Gorbikova and Kalendar. This is an open-access article distributed under the terms of the Creative Commons Attribution License (CC BY). The use, distribution or reproduction in other forums is permitted, provided the original author(s) and the copyright owner(s) are credited and that the original publication in this journal is cited, in accordance with accepted academic practice. No use, distribution or reproduction is permitted which does not comply with these terms.



A New Design for the Fixed Primer Regions in an Oligonucleotide Library for SELEX Aptamer Screening

Bin Wang*

Department of Chemistry, Marshall University, Huntington, WV, United States

OPEN ACCESS

Edited by:

John D. Wade,
University of Melbourne, Australia

Reviewed by:

Taiichi Sakamoto,
Chiba Institute of Technology, Japan
Yu Xia,
Jiangnan University, China

*Correspondence:

Bin Wang
wangb@marshall.edu

Specialty section:

This article was submitted to
Chemical Biology,
a section of the journal
Frontiers in Chemistry

Received: 10 January 2020

Accepted: 07 May 2020

Published: 05 June 2020

Citation:

Wang B (2020) A New Design for the
Fixed Primer Regions in an
Oligonucleotide Library for SELEX
Aptamer Screening.
Front. Chem. 8:475.
doi: 10.3389/fchem.2020.00475

Single-stranded DNA or RNA oligonucleotides, often called aptamers, can bind to a molecular target with both high affinity and selectivity due to their distinct three-dimensional structures. A technique called systematic evolution of ligands by exponential enrichment (SELEX) is used to screen aptamers from a random DNA or RNA pool, or library. The traditionally-designed oligonucleotides in libraries contain a randomized central region along with a fixed primer region at each end for amplifying target-bound central sequences. The single-stranded forward and reverse primer sequences may interfere with target-binding to the central region, resulting in a partial or complete loss of high-affinity aptamers during the SELEX process. To address this issue, researchers have modified the traditional oligonucleotide libraries and developed new types of oligonucleotide libraries; however, these approaches come with various limitations. The author proposes a new design that uses a conformation-changeable sequence as primers, which may open a new avenue for developing an optimized aptamer sequence with both high affinity for, and selective binding to, a particular target via SELEX.

Keywords: systematic evolution of ligands by exponential enrichment (SELEX), aptamer screening, oligonucleotide library, fixed primer regions, i-motif

Aptamers are single-stranded DNA or RNA oligonucleotides that bind to a molecular target with both high affinity and selectivity due to their distinct three-dimensional structures. Target-specific aptamers are mostly screened from a random DNA or RNA pool using a technique called systematic evolution of ligands by exponential enrichment (SELEX), which involves repetitive rounds of (1) partitioning target-bound aptamers from those not bound to the target, and (2) amplifying target-bound aptamers by the polymerase chain reaction (PCR).

Since its emergence in the 1990s, the conventional SELEX technique has undergone substantial modifications and improvements to allow the aptamer screening process to be both simpler and more efficient (Berezovski and Krylov, 2002; Mendonsa and Bowser, 2004; Berezovski et al., 2005). For example, coupling the high resolving power of capillary electrophoresis (CE) to traditional SELEX produced a substantial improvement (Mendonsa and Bowser, 2005; Mosing et al., 2005). The CE-SELEX process occurs in free solution (i.e., no need for a solid support medium), isolates high-affinity aptamers in just two to four rounds, and does not require negative screening. This flexible and high-resolution approach has allowed the successful screening of aptamers capable of targeting both macromolecules such as proteins, and small compounds such as porphyrin (Yang and Bowser, 2013; Dong et al., 2015).

The traditionally-designed DNA or RNA oligonucleotides in libraries contain a randomized central region of 30–60 nucleotides, and a fixed primer region of ~20 nucleotides at each end. The target molecule tightly binds to the central region of some of the library's fragments. However, the single-stranded forward and reverse primer sequences, which are used to amplify target-bound central sequences via PCR, may also interact with/anneal to complementary sequences in the central region, thus interfering with target-binding and resulting in a partial or complete loss of high-affinity aptamers. Furthermore, the primer sequences can participate in non-specific selection by binding to the target themselves, thus leading to false-positive results since the screened aptamers (i.e., the central sequences) do not actually bind to the target molecule (Pan and Clawson, 2009). The fixed primer regions of the oligonucleotides in libraries thus play a central role in limiting the efficiency of SELEX aptamer screening.

To address this issue, researchers have attempted to modify the traditional oligonucleotide libraries or develop new types of oligonucleotide libraries. For example, Haynes' group has modified the standard nucleic acid library by introducing nucleotides that are complementary to the fixed primer regions of the library's fragments, thus eliminating the possibility of the single-stranded primer regions becoming involved in forming any aptamer-like structures (Ouellet et al., 2014). This strategy, however, has a drawback: Since some protein families (e.g., transcription factors) preferentially bind to duplexed nucleic acids, the now double-stranded primer regions in Haynes' design create binding sites for those proteins.

Other strategies include replacing the fixed primer regions with different sequences after each round of screening or after a certain number of rounds (Shtatland et al., 2000), completely removing the fixed regions and then regenerating these regions after each round of screening (Wen and Gray, 2004; Jarosch et al., 2006; Pan et al., 2010; Lai and DeStefano, 2011), or minimizing the length of the fixed primer regions (Pan et al., 2008). These approaches have drawbacks as well, such as the involvement of many steps of cleavage and re-ligation, which is time-consuming and labor-intensive, and often causes a significant loss of the library material; or the apparent decrease of the PCR efficiency due to the reduced length of the forward and reverse primer sequences, which causes the loss of the screened aptamers.

To the author's knowledge, no study has investigated the use of highly structured, self-folded forward and reverse primers to replace the standard single-stranded primers. This may be because the self-folded primer regions are aptamer-like structures themselves, and are more likely to bind to target molecules than single-stranded primer sequences. However, the use of primers that change their conformation under different conditions may actually lead to a higher selection of the target molecule. In this study, the author proposes this new idea for primer design to be used during SELEX aptamer screening.

First, as illustrated in **Figure 1**, the binding buffer is adjusted to Condition 1, so that the forward and reverse primer regions can self-fold into a highly structured conformation. Previous studies have demonstrated that, unlike in the conventional SELEX method, the target may bind to the randomized central

region of the oligonucleotide library and/or to the folded primer regions. This is because there is little or no sequence homology among the aptamers identified using the CE-SELEX approach (Mosing et al., 2005; Yang and Bowser, 2013). Next, the target-bound fraction is separated from the unbound library, which is achieved on a CE system; the bound fraction is then collected into a vial. Since the bound fraction includes unwanted aptamers (i.e., those in which only the primer regions bind to the target), the buffer in the collecting vial is then adjusted to Condition 2, so that the self-folded primer structures unwind and the bound target is dislodged. Aptamers that use their central regions to bind to the target are not affected under Condition 2 if their central motifs do not undergo a conformation change that would release the target. The third step is to re-inject the collected solution onto the CE system, and further separate the target-bound aptamers from the unbound ones under Condition 2. This final screening produces only aptamers that have the target bound to their central regions.

This new primer design requires the use of conformation-changeable DNA or RNA sequences as primers. A potential choice for such a primer is an intercalated motif (i-motif). The i-motif is a four-stranded quadruplex structure formed by cytosine-rich DNA and RNA sequences. A cytosine nucleobase may protonate at its N3 position under slightly acidic conditions, thus allowing the formation of a C⁺:C base pair between one protonated and one unprotonated cytosine via three hydrogen bonds. The C⁺:C base pairs hold two parallel cytosine tracts together, which intercalate in an antiparallel-oriented C⁺:C duplex to form a four-stranded i-motif (Abou Assi et al., 2018). The stability of an i-motif depends on factors such as the pH and ionic strength of the solution, the DNA or RNA sequence, the length of the cytosine tract, the length and nucleobase composition in the loop regions (i.e., the nucleotides that connect the cytosine tracts in an i-motif), and the temperature. By adjusting the ionic compositions and the ionic strength of both the binding and separation buffers used in the SELEX process, modifying the length of the four cytosine tracts in an i-motif, and altering the length and/or the nucleobase composition in the loop region, an i-motif can stably fold at physiological pH (~7.2) (Fujii and Sugimoto, 2015; Gurung et al., 2015; Reilly et al., 2015; Benabou et al., 2016; Wright et al., 2017). The folded i-motif structure is disrupted and becomes single-stranded when exposed to a higher pH (e.g., ~8.0). The use of aptamers designed to include i-motifs with somewhat different sequences as the forward and reverse primers in an oligonucleotide library allows the differentiation of the 5' and 3' ends of the oligonucleotides for PCR purposes. With this design, the target-binding process first occurs at Condition 1 (i.e., pH ~7.2); the self-folded i-motif primers do not interrupt the binding of a target molecule to the central region of the library's fragments. The bound aptamers are then separated from the unbound library fragments by CE and collected into a vial containing a buffer at approximately pH 8.0 (Condition 2). The high pH causes any target molecules that bound to the i-motif primer regions in the previous step to be dislodged due to the pH-mediated conformational change of the i-motif. The collected solution is then re-injected onto the CE system, and the bound aptamers are separated from the unbound ones at Condition 2 (i.e., pH ~8.0). Phosphate buffer

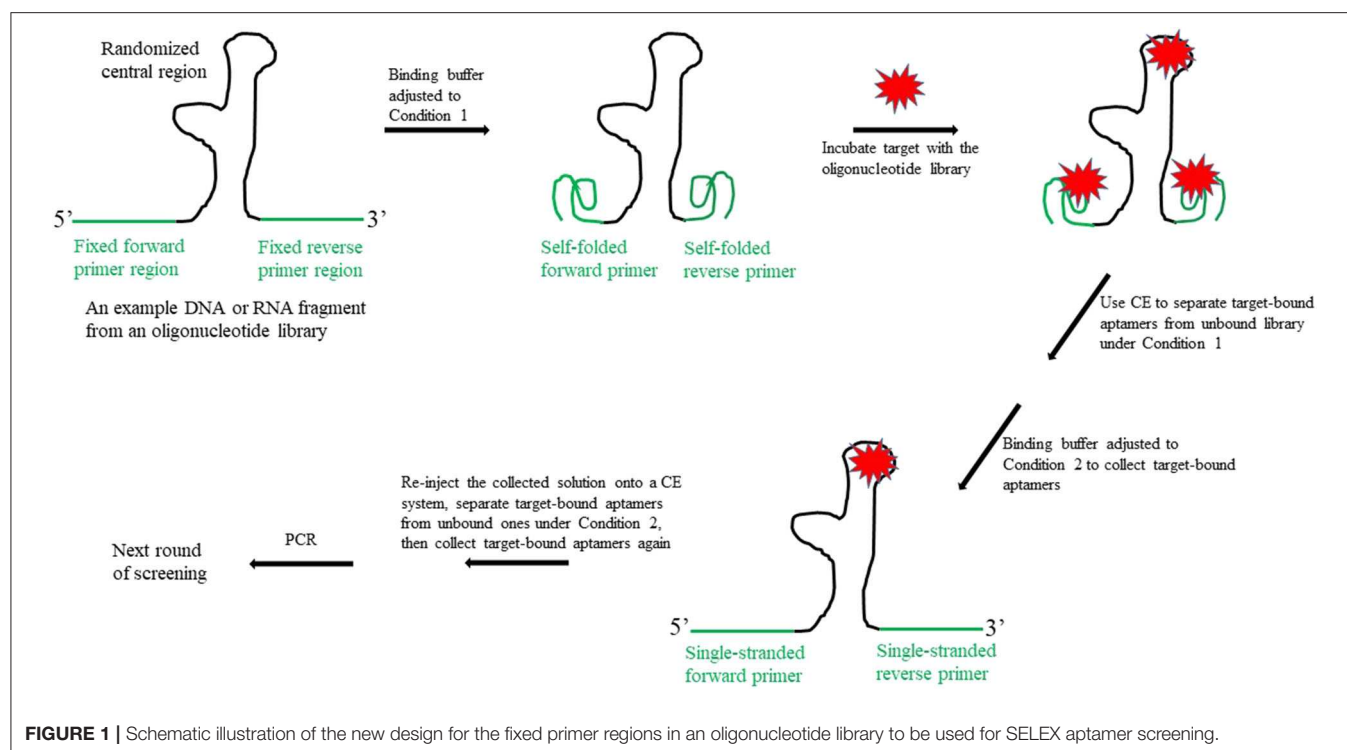


FIGURE 1 | Schematic illustration of the new design for the fixed primer regions in an oligonucleotide library to be used for SELEX aptamer screening.

is a candidate for the CE running/separation buffer, as it can be adjusted to both pH 7.2 (Condition 1) and 8.0 (Condition 2), without losing essential buffering characteristics; an uncoated fused-silica capillary is sufficient to run the entire experiment under both pH conditions. The aptamers screened using this new approach will have a high affinity to the target molecule at both physiological pH and a higher pH (~ 8.0).

Studies have demonstrated that C-rich i-motifs and G-rich G-quadruplexes can co-exist if one or both are stably folded (Phan and Mergny, 2002; Kumar et al., 2008; Bucek et al., 2009). In the new design described above, the self-folded i-motif primers that exist under Condition 1 will not interact with any G-rich sequences in the randomized central region since the base-pairing energy for the $C^+:C$ pair in an i-motif (169.7 kJ/mol) is much higher than that of canonical Watson-Crick GC pair (96.6 kJ/mol) (Yang and Rodgers, 2014). Under Condition 2, the i-motif primer regions become single-stranded; however, the likelihood that they would interrupt the identification of G-quadruplex aptamers in the central region is low because G-quadruplex motifs can stably fold under higher pH (~ 8.0). In addition, the target of interest has already bound to the central region of certain library fragments under Condition 1. If, under Condition 2, some of these potential aptamers lose their affinity for the target due to pH-induced conformational changes or interaction with now single-stranded primer sequences, our goal of only screening aptamers with high affinity to the target molecule at both physiological pH and a higher pH (~ 8.0) is achieved.

In addition to the i-motif that responds to a change in pH, other potential primers include DNA or RNA motifs that change their conformation in response to changes in temperature, or to changes in the composition of the binding buffer, such as a change in the concentration of either Mg^{2+} or a monovalent ion. The author asserts that this new type of conformation-changeable primer may render more flexibility for developing an optimized aptamer sequence with both a high affinity for and selective binding to a particular target under different conditions, and could thus be the future direction for the construction of libraries developed for SELEX aptamer screening.

DATA AVAILABILITY STATEMENT

All datasets generated for this study are included in the article/supplementary material.

AUTHOR CONTRIBUTIONS

The author confirms being the sole contributor of this work and has approved it for publication.

FUNDING

This work was supported by the National Science Foundation under Award No. OIA-1458952. Any opinions, findings, and conclusions expressed in this material are those of the author and do not necessarily reflect the views of the National Science Foundation.

REFERENCES

- Abou Assi, H., Garavis, M., Gonzalez, C., and Damha, M. J. (2018). i-Motif DNA: structural features and significance to cell biology. *Nucleic Acids Res.* 46, 8038–8056. doi: 10.1093/nar/gky735
- Benabou, S., Garavis, M., Lonnais, S., Eritja, R., Gonzalez, C., and Gargallo, R. (2016). Understanding the effect of the nature of the nucleobase in the loops on the stability of the i-motif structure. *Phys. Chem. Chem. Phys.* 18, 7997–8004. doi: 10.1039/c5cp07428b
- Berezovski, M., Drabovich, A., Krylova, S. M., Musheev, M., Okhonin, V., Petrov, A., et al. (2005). Nonequilibrium capillary electrophoresis of equilibrium mixtures: a universal tool for development of aptamers. *J. Am. Chem. Soc.* 127, 3165–3171. doi: 10.1021/ja042394q
- Berezovski, M., and Krylov, S. N. (2002). Nonequilibrium capillary electrophoresis of equilibrium mixtures—a single experiment reveals equilibrium and kinetic parameters of protein-DNA interactions. *J. Am. Chem. Soc.* 124, 13674–13675. doi: 10.1021/ja028212e
- Bucek, P., Jaumot, J., Avino, A., Eritja, R., and Gargallo, R. (2009). pH-Modulated Watson-Crick duplex-quadruplex equilibria of guanine-rich and cytosine-rich DNA sequences 140 base pairs upstream of the c-kit transcription initiation site. *Chemistry* 15, 12663–12671. doi: 10.1002/chem.200901631
- Dong, L., Tan, Q., Ye, W., Liu, D., Chen, H., Hu, H., et al. (2015). Screening and Identifying a Novel ssDNA Aptamer against Alpha-fetoprotein using CE-SELEX. *Sci. Rep.* 5:15552. doi: 10.1038/srep15552
- Fujii, T., and Sugimoto, N. (2015). Loop nucleotides impact the stability of intrastrand i-motif structures at neutral pH. *Phys. Chem. Chem. Phys.* 17, 16719–16722. doi: 10.1039/c5cp02794b
- Garung, S. P., Schwarz, C., Hall, J. P., Cardin, C. J., and Brazier, J. A. (2015). The importance of loop length on the stability of i-motif structures. *Chem. Commun.* 51, 5630–5632. doi: 10.1039/c4cc0279k
- Jarosch, F., Buchner, K., and Klusmann, S. (2006). *In vitro* selection using a dual RNA library that allows primerless selection. *Nucleic Acids Res.* 34:e86. doi: 10.1093/nar/gkl463
- Kumar, N., Sahoo, B., Varun, K. A., Maiti, S., and Maiti, S. (2008). Effect of loop length variation on quadruplex-Watson Crick duplex competition. *Nucleic Acids Res.* 36, 4433–4442. doi: 10.1093/nar/gkn402
- Lai, Y. T., and DeStefano, J. J. (2011). A primer-free method that selects high-affinity single-stranded DNA aptamers using thermostable RNA ligase. *Anal. Biochem.* 414, 246–253. doi: 10.1016/j.ab.2011.03.018
- Mendonsa, S. D., and Bowser, M. T. (2004). *In vitro* selection of high-affinity DNA ligands for human IgE using capillary electrophoresis. *Anal. Chem.* 76, 5387–5392. doi: 10.1021/ac049857v
- Mendonsa, S. D., and Bowser, M. T. (2005). *In vitro* selection of aptamers with affinity for neuropeptide Y using capillary electrophoresis. *J. Am. Chem. Soc.* 127, 9382–9383. doi: 10.1021/ja052406n
- Mosing, R. K., Mendonsa, S. D., and Bowser, M. T. (2005). Capillary electrophoresis-SELEX selection of aptamers with affinity for HIV-1 reverse transcriptase. *Anal. Chem.* 77, 6107–6112. doi: 10.1021/ac050836q
- Ouellet, E., Lagally, E. T., Cheung, K. C., and Haynes, C. A. (2014). A simple method for eliminating fixed-region interference of aptamer binding during SELEX. *Biotechnol. Bioeng.* 111, 2265–2279. doi: 10.1002/bit.25294
- Pan, W., and Clawson, G. A. (2009). The shorter the better: reducing fixed primer regions of oligonucleotide libraries for aptamer selection. *Molecules* 14, 1353–1369. doi: 10.3390/molecules14041353
- Pan, W., Xin, P., and Clawson, G. A. (2008). Minimal primer and primer-free SELEX protocols for selection of aptamers from random DNA libraries. *Biotechniques* 44, 351–360. doi: 10.2144/000112689
- Pan, W., Xin, P., Patrick, S., Dean, S., Keating, C., and Clawson, G. (2010). Primer-free aptamer selection using a random DNA library. *J. Vis. Exp.* 41:2039. doi: 10.3791/2039
- Phan, A. T., and Mergny, J. L. (2002). Human telomeric DNA: G-quadruplex, i-motif and Watson-Crick double helix. *Nucleic Acids Res.* 30, 4618–4625. doi: 10.1093/nar/gkf597
- Reilly, S. M., Morgan, R. K., Brooks, T. A., and Wadkins, R. M. (2015). Effect of interior loop length on the thermal stability and pKa of i-motif DNA. *Biochemistry* 54, 1364–1370. doi: 10.1021/bi5014722
- Shtatland, T., Gill, S. C., Javornik, B. E., Johansson, H. E., Singer, B. S., Uhlenbeck, O. C., et al. (2000). Interactions of *Escherichia coli* RNA with bacteriophage MS2 coat protein: genomic SELEX. *Nucleic Acids Res.* 28:E93. doi: 10.1093/nar/28.21.e93
- Wen, J. D., and Gray, D. M. (2004). Selection of genomic sequences that bind tightly to Ff gene 5 protein: primer-free genomic SELEX. *Nucleic Acids Res.* 32:e182. doi: 10.1093/nar/gnh179
- Wright, E. P., Huppert, J. L., and Waller, Z. A. E. (2017). Identification of multiple genomic DNA sequences which form i-motif structures at neutral pH. *Nucleic Acids Res.* 45, 2951–2959. doi: 10.1093/nar/gkx090
- Yang, B., and Rodgers, M. T. (2014). Base-pairing energies of proton-bound heterodimers of cytosine and modified cytosines: implications for the stability of DNA i-motif conformations. *J. Am. Chem. Soc.* 136, 282–290. doi: 10.1021/ja409515v
- Yang, J., and Bowser, M. T. (2013). Capillary electrophoresis-SELEX selection of catalytic DNA aptamers for a small-molecule porphyrin target. *Anal. Chem.* 85, 1525–1530. doi: 10.1021/ac302721j

Conflict of Interest: The author declares that the research was conducted in the absence of any commercial or financial relationships that could be construed as a potential conflict of interest.

Copyright © 2020 Wang. This is an open-access article distributed under the terms of the Creative Commons Attribution License (CC BY). The use, distribution or reproduction in other forums is permitted, provided the original author(s) and the copyright owner(s) are credited and that the original publication in this journal is cited, in accordance with accepted academic practice. No use, distribution or reproduction is permitted which does not comply with these terms.



Enhancing the Mitochondrial Uptake of Phosphonium Cations by Carboxylic Acid Incorporation

Laura Pala¹, Hans M. Senn¹, Stuart T. Caldwell¹, Tracy A. Prime², Stefan Warrington¹, Thomas P. Bright², Hiran A. Prag², Claire Wilson¹, Michael P. Murphy^{2,3*} and Richard C. Hartley^{1*}

¹ School of Chemistry, University of Glasgow, Glasgow, United Kingdom, ² MRC Mitochondrial Biology Unit, University of Cambridge, Cambridge, United Kingdom, ³ Department of Medicine, University of Cambridge, Cambridge, United Kingdom

OPEN ACCESS

Edited by:

John D. Wade,
University of Melbourne, Australia

Reviewed by:

Mario Zoratti,
National Research Council (CNR), Italy
Elizabeth New,
The University of Sydney, Australia

*Correspondence:

Michael P. Murphy
mpm@mrc-mbu.cam.ac.uk
Richard C. Hartley
richard.hartley@glasgow.ac.uk

Specialty section:

This article was submitted to
Chemical Biology,
a section of the journal
Frontiers in Chemistry

Received: 27 April 2020

Accepted: 27 July 2020

Published: 09 September 2020

Citation:

Pala L, Senn HM, Caldwell ST, Prime TA, Warrington S, Bright TP, Prag HA, Wilson C, Murphy MP and Hartley RC (2020) Enhancing the Mitochondrial Uptake of Phosphonium Cations by Carboxylic Acid Incorporation. *Front. Chem.* 8:783. doi: 10.3389/fchem.2020.00783

There is considerable interest in developing drugs and probes targeted to mitochondria in order to understand and treat the many pathologies associated with mitochondrial dysfunction. The large membrane potential, negative inside, across the mitochondrial inner membrane enables delivery of molecules conjugated to lipophilic phosphonium cations to the organelle. Due to their combination of charge and hydrophobicity, quaternary triarylphosphonium cations rapidly cross biological membranes without the requirement for a carrier. Their extent of uptake is determined by the magnitude of the mitochondrial membrane potential, as described by the Nernst equation. To further enhance this uptake here we explored whether incorporation of a carboxylic acid into a quaternary triarylphosphonium cation would enhance its mitochondrial uptake in response to both the membrane potential and the mitochondrial pH gradient (alkaline inside). Accumulation of arylpropionic acid derivatives depended on both the membrane potential and the pH gradient. However, acetic or benzoic derivatives did not accumulate, due to their lowered pK_a . Surprisingly, despite not being taken up by mitochondria, the phenylacetic or phenylbenzoic derivatives were not retained within mitochondria when generated within the mitochondrial matrix by hydrolysis of their cognate esters. Computational studies, supported by crystallography, showed that these molecules passed through the hydrophobic core of mitochondrial inner membrane as a neutral dimer. This finding extends our understanding of the mechanisms of membrane permeation of lipophilic cations and suggests future strategies to enhance drug and probe delivery to mitochondria.

Keywords: mitochondria, phosphonium, mitochondria-targeting, membrane permeation, membrane potential, pH gradient, computational chemistry

INTRODUCTION

Mitochondrial dysfunction contributes to a wide range of pathologies, consequently they are an important therapeutic target (Nunnari and Suomalainen, 2012; Gorman et al., 2016; Murphy and Hartley, 2018). Furthermore, the delivery of probe molecules to the organelle *in vivo* is essential in understanding how mitochondrial dysfunction arises (Yousif et al., 2009; Smith et al., 2012; Logan et al., 2014; Jean et al., 2016). There are a number of strategies to deliver molecules to

mitochondria *in vivo*, with conjugation to the alkyltriphenylphosphonium (TPP) cation being the most widespread (Smith et al., 2003, 2012; Yousif et al., 2009). TPP is used because it readily crosses biological membranes without the requirement for a protein carrier, and is chemically tractable making it easy to introduce synthetically into the molecule to be targeted (Smith et al., 2011, 2012), as well as having a good safety and toxicity profile. An important aspect of the TPP targeting system is that its positive charge and the large mitochondrial membrane potential lead to these molecules accumulating $\sim 1,000$ -fold within energized mitochondria, as described by the Nernst equation (Ross et al., 2006; Smith et al., 2011). Even so, improving mitochondria-targeting head groups to enhance mitochondrial accumulation would lead to improved therapies and probes.

To develop an improved mitochondria-targeting head group, we started from the finding that a TPP cation conjugated to a long alkyl chain carboxylic acid 1 accumulates within mitochondria to a greater extent than related compounds without an acid moiety (Figure 1) (Finichiu et al., 2013). This greater uptake occurs because of the equilibrium between the protonated (1) and deprotonated forms (2) determined by the pK_a of the carboxylic acid (~ 4.9) (Kanicky and Shah, 2003). The higher pH of the mitochondrial matrix (~ 8) relative to the cytosol (~ 7.2) and the inability of the zwitterionic TPP carboxylate 2 to cross the mitochondrial inner membrane means that the overall accumulation of the molecule is enhanced 4–10-fold compared to a comparable TPP without a carboxylic acid (Finichiu et al., 2013). Hence, we set out to develop a generic TPP-carboxylic acid targeting group so as to enhance mitochondrial uptake 4–10-fold over current TPP groups (Figure 1). The simplest way to do this is to incorporate a carboxylic acid group on one of the TPP phenyls. Both protonated and deprotonated forms of the carboxylic acid would be present in a ratio depending on the pK_a of the acid and the local pH (Figure 1). Only the protonated form of the TPP-carboxylic acid targeting group

should cross the mitochondrial membrane and once within the matrix, the higher pH should increase accumulation of the membrane-impermeant deprotonated form. Thus, this approach should generate a generic TPP-carboxylic acid targeting group to increase the delivery of the same cargo targeted with a TPP group (Figure 1). Furthermore, this combined TPP-carboxylic acid targeting group could easily be attached to any cargo using a simple phosphine-carboxylic acid precursor. Here we set out to develop such a generic TPP-carboxylic acid targeting group to enhance the delivery of drugs and probes to mitochondria *in vivo*.

MATERIALS AND METHODS

Synthetic Chemistry

The test compounds 3–19 were prepared as shown in Scheme 1. Phosphines 20 and 21 were alkylated with iodomethane, 1-bromohexane, or 1-bromododecane to give the corresponding salts 3–8 (Scheme 1). Carboxylic acids 3, 4, 7 were converted into the corresponding ethyl esters 12, 13, and 15 by stirring in ethanol with catalytic concentrated sulfuric acid. The trifluoroethyl ester 19 was prepared from carboxylic acid 7 in a similar way using trifluoroethanol as solvent. However, a better approach to trifluoroethyl esters was to esterify the carboxylic acid group of the parent phosphines 20 and 21 with trifluoroethanol using diisopropylcarbodiimide (DIC) coupling with dimethylaminopyridine (DMAP) as a nucleophilic catalyst to give the corresponding esters 23 and 24, and then alkylate the phosphine to give the phosphonium salts 16–18. Ethyl ester 14 was prepared in a similar way using dicyclohexylcarbodiimide (DCC) coupling to make ester 22 followed by alkylation with iodomethane. The synthesis of the phenylpropionic acid derivatives 9–11 began with the preparation of iodoarene 25 by the method of (Qin et al., 2015) and protection of the acid as ester 26 (Scheme 2). Adapting the procedure reported by (Dydio et al., 2014), which we had used to prepare phosphine 21, iodoarene 26 was cross-coupled with diphenylphosphine and

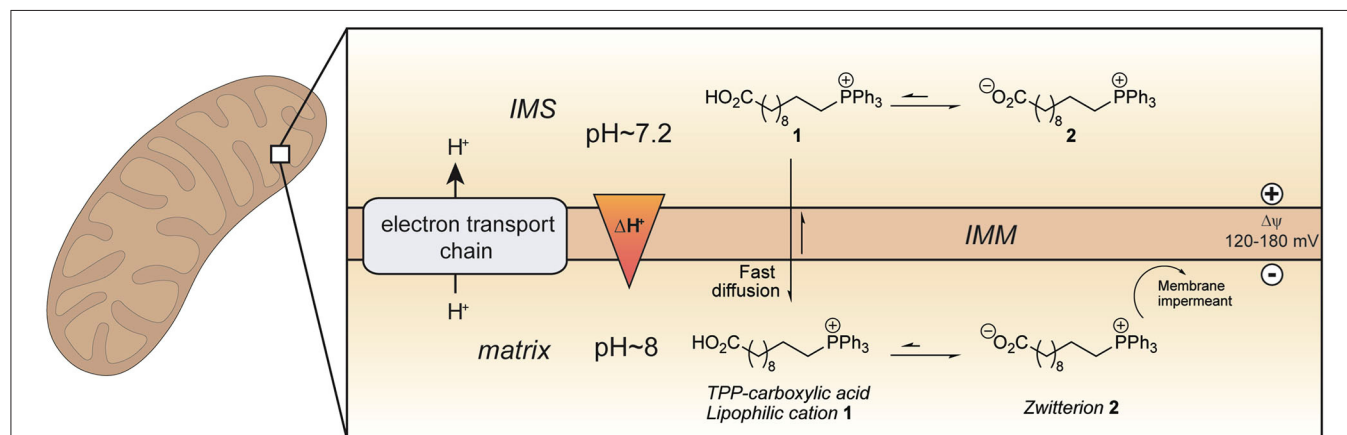
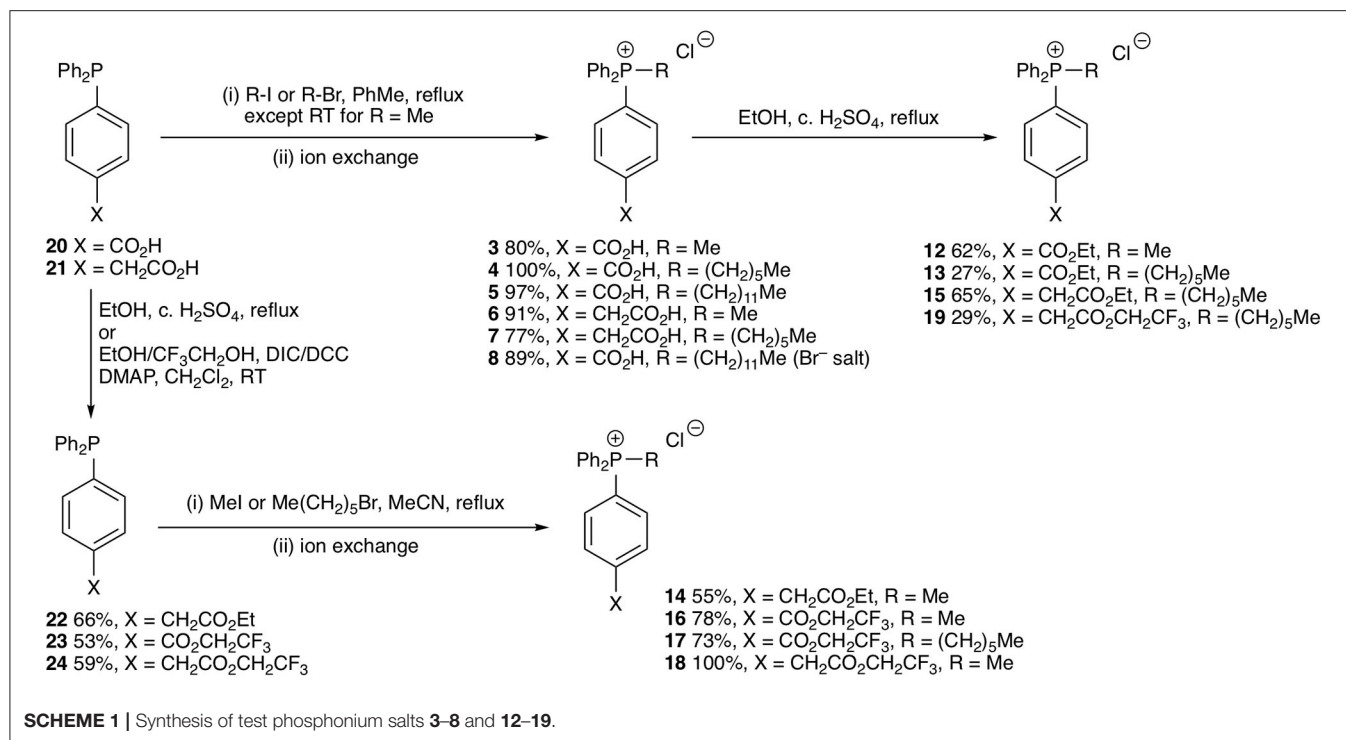


FIGURE 1 | Enhanced mitochondrial uptake by a TPP cation linked to a carboxylic acid. Model showing how a TPP long chain carboxylic acid 1 crosses the mitochondrial inner membrane and accumulates within the mitochondrial matrix in its zwitterionic form 2 due to the higher pH (~ 8) in mitochondria compared to that in the cytosol (~ 7.2). IMM, inner mitochondrial membrane; IMS, intermembrane space.



then alkylated *in situ* with iodomethane, 1-bromobutane, or 1-bromohexane to give the corresponding phosphonium salts **27–29**. Acid-catalyzed hydrolysis then gave the phosphonium salts **9–11**. The details of the synthetic procedures are described in the **Supplemental Information**.

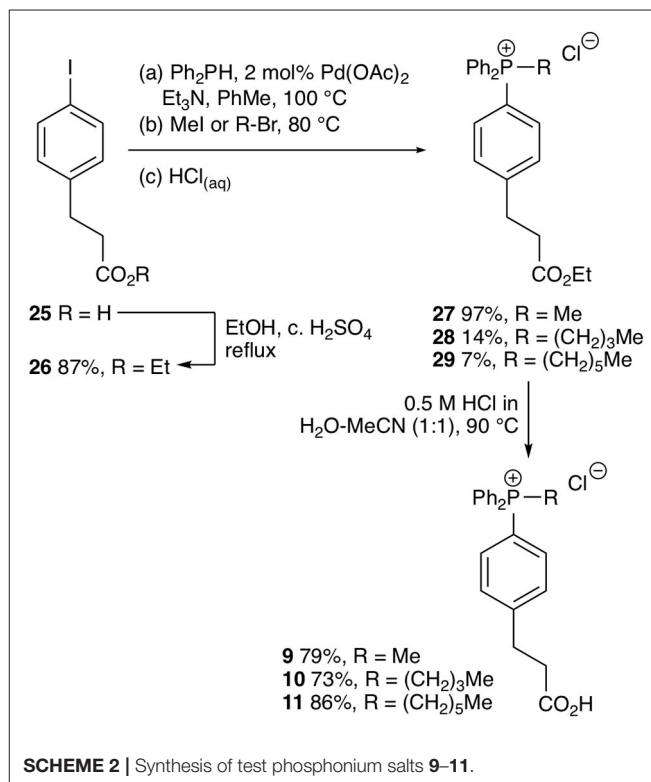
Biology-Methods

Animals

All procedures were carried out in accordance with the UK Animals (Scientific Procedures) Act 1986 and the University of Cambridge Animal Welfare Policy. Female Wistar rats (typically 6–10 weeks old, weighing ~200 g, Charles River Laboratories, UK) were housed in pathogen-free facilities at $21 \pm 2^\circ\text{C}$, humidity $57 \pm 5\%$ with a 12 h light/dark cycle and laboratory chow and water were available *ad libitum*.

Isolation of Rat Liver and Heart Mitochondria

Rats were killed by stunning and cervical dislocation and the liver or heart rapidly excised and transferred to ice cold mitochondrial isolation buffer. Mitochondria were isolated from rat liver tissue by differential centrifugation in STE buffer [250 mM sucrose, 5 mM Tris, 1 mM ethyleneglycol-bis(β -aminoethylether)-*N,N,N',N'*-tetraacetic acid (EGTA) (pH 7.4 at 4°C , adjusted with HCl)] (Chappell and Hansford, 1972). The liver was washed in ice-cold STE, chopped finely, rinsed in STE and homogenized 5–8 times using a loose PTFE pestle in a 55 ml Potter-Elvehjem tissue grinder (Wheaton, USA) and then with a tight pestle. The homogenate was centrifuged ($1,000 \times g$, 3 min, 4°C), the pellets were discarded, and the supernatants centrifuged ($10,000 \times g$, 10 min, 4°C). The supernatant was discarded and the pellet was resuspended and centrifuged again ($10,000 \times g$, 10 min, 4°C).



The final mitochondria pellet was resuspended in ~5 mL STE buffer, kept in ice and used within 4 h.

Rat hearts were washed in ice-cold STEB buffer [STE buffer supplemented with 0.1% (ws/v) fatty-acid free bovine

serum albumin (BSA)], chopped finely, washed again and then homogenized 5–8 times using a loose PTFE pestle in a 55 mL Potter-Elvehjem tissue grinder (Wheaton, USA) and then a tight pestle with roughly 8 strokes. The homogenate was centrifuged ($700 \times g$, 5 min, 4°C) and the supernatant was decanted through two layers of a pre-wetted muslin into new centrifuge tubes. The pellet was resuspended and centrifuged again ($700 \times g$, 5 min, 4°C). This supernatant was also decanted through muslin and the combined supernatants centrifuged ($10,000 \times g$, 10 min, 4°C). The mitochondrial pellet was resuspended in STEB and centrifuged again ($10,000 \times g$, 10 min, 4°C). The mitochondrial pellet was resuspended in STE without BSA ($\sim 300 \mu\text{L}$ per heart), kept on ice and used within 4 h. The protein concentration of the mitochondrial suspensions was determined using the BCA assay using BSA as a standard (Thermo Fisher Scientific, UK).

Reversed Phase-High Performance Liquid Chromatography (RP-HPLC)

For most RP-HPLC experiments, the stationary phase used was a C18 column (Jupiter 300 Å, Phenomenex) with a Widespore C18 guard column (Phenomenex). The column was connected to a 321 pump, a UV/Vis 151 system (Gilson, UK), a RIC20 Remote Controlled Chilling/Heating Dry bath (Torrey Pine Scientific) and a GX-241 liquid handler (Gilson) with Trilution LC 3.0 software (Gilson). The mobile phase was a gradient of water + 0.1% (v/v) trifluoroacetic acid (TFA) (HPLC buffer A) and acetonitrile [HPLC grade acetonitrile (Fisher Scientific, UK)] + 0.1% (v/v) TFA (HPLC buffer B) at a flow rate of 1 mL/min. Samples were prepared in 1 mL, containing 25% acetonitrile + 0.1% (v/v) TFA. Prior to analysis, they were filtered under vacuum using Protein Precipitation Plates (Porvair, $100 \mu\text{m}$ pre-filter frit, $< 10 \mu\text{m}$ secondary frit). The filtrate was transferred to centrifuge tubes and placed in the chilled sample holder. $800 \mu\text{L}$ of sample were loaded into a 2 mL sample loop and injected onto the column for analysis. Compounds were eluted using the following gradient: 0–2 min: 5% buffer B, 2–17 min: 5–100% buffer B, 17–19 min: 100% buffer B, 19–22 min: 100–5% buffer B. For some RP-HPLC experiments samples were prepared in $850 \mu\text{L}$, containing 20% acetonitrile + 0.1% (v/v) TFA. This was transferred to centrifuge tubes and placed in the chilled sample holder. $800 \mu\text{L}$ of sample were loaded into a 2 mL sample loop and injected onto the column for analysis. Compounds were eluted using the following gradient: 0–2 min: 5% buffer B, 2–4 min: 55% buffer B, 4–16 min: 70% buffer B, 16–18 min: 70–100% buffer B, 18–21 min: 100% buffer B, 21–23 min: 100–5% buffer B. All samples were detected at 220 nm and peaks identified by comparing the retention times of the known standards.

Mitochondrial Incubation of Compounds

Rat liver or heart mitochondria ($0.5 \text{ mg protein/mL}$) were incubated in 2 mL KCl buffer (120 mM KCl , 10 mM HEPES , 1 mM EGTA , adjusted with KOH to pH 7.2, 37°C) supplemented with compound and internal standard ($5 \mu\text{M}$ each, unless otherwise stated) in a shaking heat block (37°C , $1,000 \text{ rpm}$). Mitochondria were energized with succinate/rotenone ($10 \text{ mM}/10 \mu\text{M}$) or glutamate/malate (10 mM each). To abolish the mitochondrial proton motive force either FCCP ($1 \mu\text{M}$),

or a mixture of oligomycin, antimycin A and valinomycin (OAV) ($5 \mu\text{g/mL}$, 100 nM , 1 nM , respectively) were used. After the appropriate incubation time, the mitochondrial suspensions were rapidly cooled on ice and the mitochondria pelleted by centrifugation ($10,000 \times g$, 5 min, 4°C). The mitochondrial pellet was dried by aspirating the supernatant, snap frozen and stored at -80°C until RP-HPLC analysis. For this, the pellet was thawed and extracted by resuspension in $250 \mu\text{L}$ HPLC buffer B with vortexing, and then centrifuged ($16,000 \times g$, 10 min, 4°C). The resulting supernatant was removed and $750 \mu\text{L}$ HPLC buffer A was added.

Mitochondrial Respiration Assay

Respiration of isolated mitochondria was assessed using the Oroboros Oxygraph-2K (O2K) high resolution respirometer (Oroboros Instruments, Austria), equipped with two stirred (200 rpm), and temperature controlled (37°C) chambers. Before starting experiments, 2 mL KCl buffer was left to equilibrate for approximately 1 h and the Oroboros was calibrated. Rat liver mitochondria (2 mg protein/mL) were then added to the chamber with glutamate and malate (10 mM each). The lid was closed, and respiration assessed. Compounds were added in increasing concentrations using gastight syringes (Hamilton Robotics, UK), with equal volumes of control compound being used in parallel experiments. Additions did not exceed $10 \mu\text{L}$ per addition.

QUANTUM-CHEMICAL CALCULATIONS

Computational Details

Free energies of transfer and of ion-pairing/dimerisation were calculated using density-functional theory (DFT) with the TPSS exchange-correlation functional (Tao et al., 2003) (which is a pure meta-GGA functional) supplemented by Grimme's D3 correction (Grimme et al., 2010, 2011) to account for dispersive interactions. Structures and vibrational frequencies were calculated with the def2-SVP (cations) and def2-SVP+ (ion pairs and anions) basis sets, final energies with def2-TZVP+ in all cases (Weigend and Ahlrichs, 2005; Weigend, 2006). The “+” indicates augmentation of the published sets with one diffuse Gaussian function per valence angular momentum on all atoms; the exponents of the diffuse functions were derived such as to form a geometric series with the existing two outermost functions (even-tempered).

Structure optimisations and frequency calculations were performed with Turbomole 6.4 (Ahlrichs et al., 1989; Häser and Ahlrichs, 1989; Treutler and Ahlrichs, 1995; von Arnim and Ahlrichs, 1998, 1999), making use of the efficient MARI-J technique (Sierka et al., 2003). SCF energies were converged to $10^{-8} E_h$; structures to $10^{-6} E_h$ in the energy and $10^{-4} E_h a_0^{-1}$ in the gradient. The COSMO continuum solvent model (Klamt and Schüürmann, 1993; Klamt and Jonas, 1996) was applied throughout, with default solvation radii and relative permittivity $\epsilon_r = 78.3553$ and refractive index $n = 1.3334$ for water and $\epsilon_r = 1.8819$, $n = 1.3749$ for hexane. Frequencies were obtained by numerical differentiation (NumForce), using only the “slow” component of solvent polarization (Klamt, 1996). All structures

were confirmed by the absence of imaginary frequencies to be minima on the potential-energy surface in the respective solvent.

Final energies were calculated with Gaussian 09 (Frisch et al., 2013), using the SMD solvation model, which combines the IEF-PCM polarisable continuum model for electrostatic solvation (Tomasi et al., 2005) with the SMD non-electrostatic terms (Marenich et al., 2009). The same values of ϵ_r and n were used as above (which are G09 default values, noting that $n = \epsilon_\infty^{1/2}$). Default solvation radii were used, except for Cl, whose solvation radius was reduced from 2.38 Å to 1.8 Å in order to reproduce better the experimental free energy of hydration (Hünenberger and Reif, 2011) of Cl^- , $\Delta_{\text{solv}}G^*(\text{Cl}^-, \text{aq}) = -316.55 \text{ kJ mol}^{-1}$; the default radius yielded -271 kJ mol^{-1} , the adjusted radius -307 kJ mol^{-1} . The solvation radius of Na was similarly reduced from 2.27 Å to 1.6 Å; experimental $\Delta_{\text{solv}}G^*(\text{Cl}^-, \text{aq}) = -427.41 \text{ kJ mol}^{-1}$, calculated using default radius: -302 kJ mol^{-1} , calculated using adjusted radius: -429 kJ mol^{-1} .

The thermal contributions to the free energy (including the zero-point vibrational energy) were calculated according to the standard ideal-gas/rigid-rotor/harmonic-oscillator approximation at $T = 298.15 \text{ K}$, $p^\circ = 100 \text{ kPa}$. Frequencies were not scaled; however, to avoid spurious large entropy contributions from low-frequency vibrational modes, for which the harmonic-oscillator approximation is unreliable, frequencies below 100 cm^{-1} were raised (Ribeiro et al., 2011) to 100 cm^{-1} .

pK_a values were calculated from free energies obtained at the M06-2X/def2-TZVP+ level (Zhao and Truhlar, 2008) using the SMD continuum model for water in Gaussian 09. Frequencies were scaled (Alecu et al., 2010; Kanchanakungwankul et al., 2018) by a factor of 0.972 and raised (Ribeiro et al., 2011) to $\geq 100 \text{ cm}^{-1}$ using the GoodVibes program (Funes-Ardoiz and Paton, 2018) for the calculation of free energies. The pK_a value of an acid HA was then computed with respect to a reference acid HRef with experimentally known pK_a as follows:

$$\text{pK}_a(\text{HA}) = \lg(e)\Delta G_a(\text{HA})/(RT) + \text{pK}_a^{\text{expt}}(\text{HRef}) - \text{pK}_a^{\text{calc}}(\text{HRef})$$

where $\lg(e)$ is the decadic logarithm of Euler's number, $\Delta G_a(\text{HA}) = G^*(\text{A}^-) - G^*(\text{HA})$, and $\text{pK}_a^{\text{calc}}(\text{HRef}) = \lg(e)\Delta G_a(\text{HRef})$.

Choice of Standard States

We express all thermodynamic quantities in solution with reference to a fixed-solute equal-concentrations standard state as defined by Ben-Naim (Ben-Naim, 1987, 1992), indicated by *, with a concentration of $c^* = 1 \text{ mol L}^{-1}$. The usual gas-phase standard state with $p^\circ = 100 \text{ kPa}$ is indicated by $^\circ$; the standard temperature is $T = 298.15 \text{ K}$ in both cases. The free energy of solute S in solution contains a liberational term, which replaces the gas-phase translational free energy. In the * standard, these terms are exactly equal,

$$G_{\text{lib}}^*(S, \text{sln}) = G_{\text{trans}}^*(S, \text{g}).$$

The liberational free energy can therefore be calculated as

$$G_{\text{lib}}^*(S, \text{sln}) = G_{\text{trans}}^\circ(S, \text{g}) + \Delta G^{\circ \rightarrow *},$$

where $\Delta G^{\circ \rightarrow *} = RT \ln(RTc^*/p^\circ) = 8.0 \text{ kJ mol}^{-1}$ is the conversion between standard states, associated with the isothermal compression of 1 mol of ideal gas from its concentration at p° to c^* . For a process in solution where the number of particles changes, e.g., ion-pairing, the free-energy change ΔG_{sln}^* therefore includes a term $\Delta G^{\circ \rightarrow *} \times \sum_i \nu_i$, where ν_i are the (signed) stoichiometric coefficients of reactants and products.

RESULTS AND DISCUSSION

Enhanced Mitochondria-Targeting With a Triphenylphosphonium Carboxylic Acid

To develop an enhanced mitochondria-targeting head group, we first made a series of alkyltriphenylphosphonium (TPP) salts with a carboxylic acid group on one phenyl group *para* to the phosphorus (Figure 2A). The uptake of these compounds by energized mitochondria, which will have a large membrane potential, was studied alongside TPP-containing internal standards (IS). Uptake of the IS confirmed that the test compound did not significantly disrupt mitochondrial membrane potential and showed that the mitochondria continued to respond as expected to different additives known to affect the membrane potential. Energized mitochondria were incubated with carboxylic acid 3 and IS and uptake of the compounds into mitochondria measured by RP-HPLC (Figure 2B) and quantified (Figure 2C). The IS was taken up by energized mitochondria and abolishing the membrane potential with the uncoupler FCCP (Nicholls and Ferguson, 2013), blocked this uptake (Figures 2B,C). However, carboxylic acid 3 was not taken up by energized mitochondria (Figures 2B,C). A hydrophobicity threshold is required for mitochondrial uptake of alkylTPP molecules (Ross et al., 2006; Finichiu et al., 2015; Hu et al., 2017), but when hydrophobicity was increased by replacing the methyl (3) with a hexyl group (4) there was still no mitochondrial uptake compared to IS (Figure 2D). Incorporating the more hydrophobic dodecyl group (5) led to extensive adsorption to mitochondria that was unaffected by uncoupling with FCCP (Figure 2E). Extending incubation time to 15 min did not lead to uptake (data not shown). We conclude that alkylTPP salts with a carboxylic acid on one of the phenyl groups of TPP are not taken up by energized mitochondria.

The pK_a values of 3–5 may have influenced mitochondrial uptake. The enhanced mitochondrial uptake reported previously was for a carboxylic acid attached to a TPP via an undecyl chain (1) with a $\text{pK}_a \sim 4.9$ (Finichiu et al., 2013). Stabilization of the deprotonated form by the phenyl and the phosphonium cation in 3–5 may lower the pK_a , decreasing the proportion in the membrane permeant, protonated form (Figure 1). The pK_a of 3 was determined computationally by reference to experimental pK_a values for benzoic acid and phenylacetic acid, giving a pK_a of 2.5 ± 0.1 (Table 1). At intracellular pH (7.2) the TPP undecylcarboxylic acid ($\text{pK}_a \sim 4.9$) (Kanicky and Shah, 2003) would be $\sim 0.5\%$ in the protonated form, compared to 0.002% for 3, ~ 300 -fold lower. We next distanced

TABLE 1 | Calculated pK_a values of carboxylic acids **3**, **6**, and **9**, with reference to benzoic acid and phenylacetic acid.

| Compound | pK_a | | |
|--|------------|----------------------------|----------------------------------|
| | PhCOOH ref | PhCH ₂ COOH ref | Experiment (Rumble et al., 2018) |
| PhCOOH | 4.204 | 4.4 | 4.204 |
| PhCH ₂ COOH | 4.1 | 4.31 | 4.31 |
| TPMP ⁺ -COOH (3) | 2.4 | 2.6 | |
| TPMP ⁺ -CH ₂ COOH (6) | 2.6 | 2.8 | |
| TPMP ⁺ -CH ₂ CH ₂ COOH (9) | 5.1 | 5.3 | |

Reference values are printed in italics.

the acid group from the phenyl and phosphonium, to make phenylacetic and phenylpropionic derivatives with a range of hydrophobicities (**6–11**) (**Figure 3A**). The pK_a values of **6** and **9** were then computationally determined by reference to the experimental values for benzoic and phenylacetic acid, yielding pK_a values of 2.7 ± 0.1 (**6**) and 5.2 ± 0.1 (**9**) (**Table 1**). So, if **3** was excluded from mitochondria by its low pK_a then **6–8** should also be excluded, while **9–11** should be accumulated. The phenylacetic acid derivatives **6** and **7** showed no uncoupler-sensitive mitochondrial uptake (**Figures 3B,C**), while the more hydrophobic **8** adsorbed to mitochondria independently of membrane potential (**Figure 3D**). For the propionic acid derivatives (**9–11**) we made methyl, butyl and hexyl versions as the hydrophobicity of the dodecyl compounds

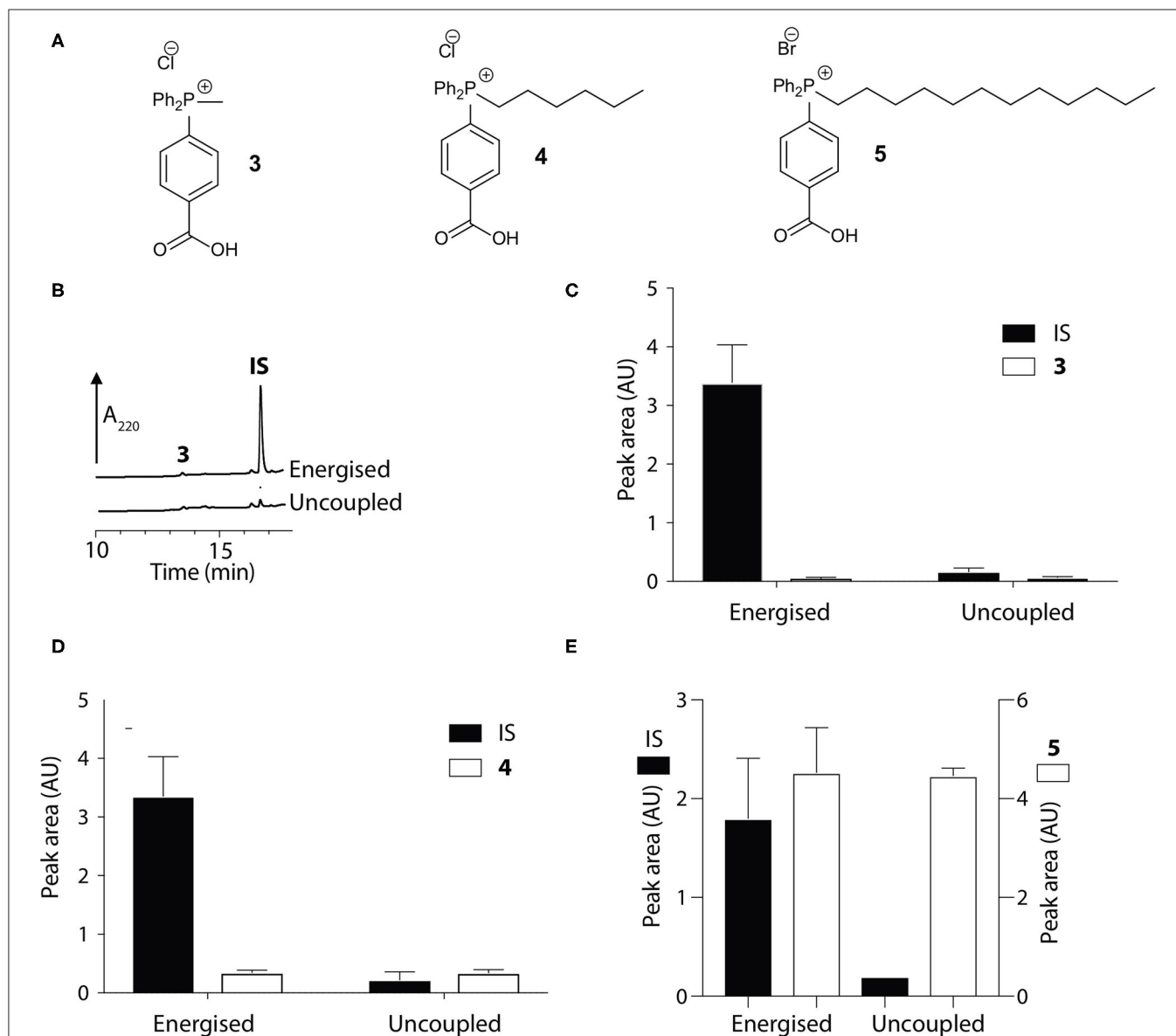


FIGURE 2 | Mitochondrial uptake of TPP benzoic acids. **(A)** Structure of TPP benzoic acids **3**, **4**, and **5**. **(B)** Liver mitochondria (0.5 mg protein/ml) supplemented with succinate and rotenone, were incubated with **3** and an internal standard (IS; isoamyl TPP) at 37°C for 5 min \pm FCCP. Mitochondria were pelleted by centrifugation and extracted for analysis by RP-HPLC. **(C–E)** Quantification of mitochondrial uptake of **3**, **4**, and **5**. **(C)**, **3**, IS = isoamyl TPP; **(D)**, **4**, IS = TPMP; **(E)**, **5**, IS = propylITPP. Data are mean \pm S.E.M. of peak areas from three biological replicates.

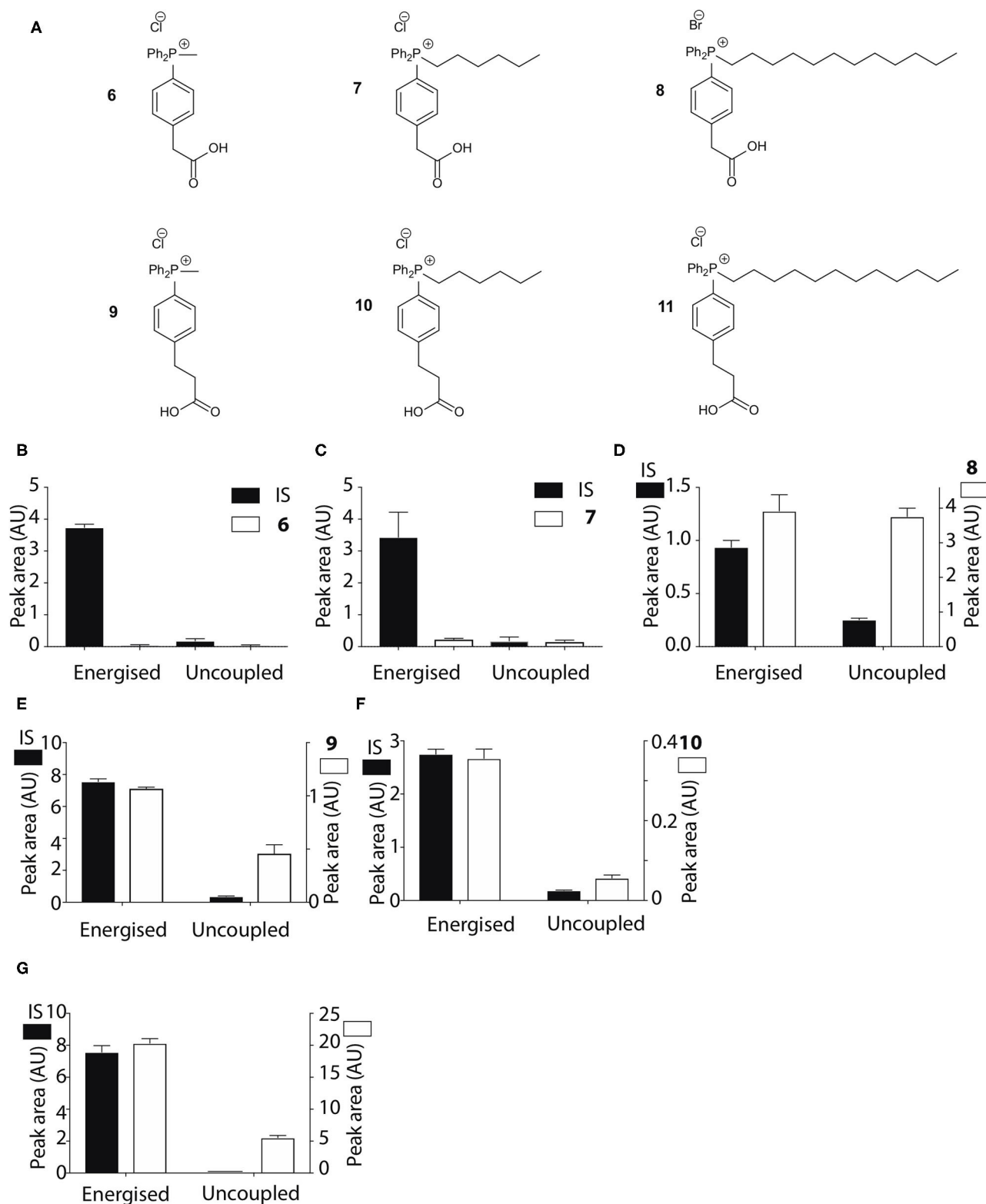


FIGURE 3 | Mitochondrial uptake of TPP acetic and propionic acids. **(A)** Structure of TPP carboxylic acids **6–11**. **(B–G)** Quantification of mitochondrial uptake of **6–11**. Mitochondria were incubated as described in **Figure 2B**, except for the indicated alterations. **(B)**, **6**, IS = isoamylTPP; **(C)**, **7**, IS = TPMP; **(D)**, **8**, IS = TPMP; **(E)**, **9** (10 μ M), IS = propylTPP (2.5 μ M), and data shown are for incubation with heart mitochondria. The same result was obtained with liver mitochondria; **(F)**, **10**, (10 μ M), IS = TPMP (5 μ M), and data shown are for liver mitochondria. The same result was obtained with heart mitochondria; **(G)**, **11**, (20 μ M) IS = TPMP (2.5 μ M). Data shown are for incubation with heart mitochondria. The same result was obtained with liver mitochondria. Data are mean \pm S.E.M. of RP-HPLC peak areas from three biological replicates except for panel G, where the +FCCP data are mean \pm range ($n = 2$).

5 and 8 made mitochondrial experiments uninformative. We found that 9–11 were all taken up by energized mitochondria, but not by uncoupled mitochondria (Figures 3E–G). Thus, the lack of mitochondrial uptake of the benzoic and phenylacetic derivatives was due to their low pK_a . Note that the accumulation of the IS were significantly higher than the carboxylic acids 9–11 (hence two Y-axes are used in Figures), even when the least lipophilic TPP-derivative, TPMP, was used as IS (Figure 3F).

We next assessed whether the mitochondrial uptake of the propionic acid TPP derivatives was enhanced by the pH gradient as shown in Figure 1. To do this we incubated 10 and TPMP with energized mitochondria and measured the accumulation ratio (ACR), that is the amount of the compound accumulated within mitochondria, normalized to the amount in the medium outside the mitochondria (Finichiu et al., 2013). The ACRs for 10 and TPMP were both substantial and were decreased by uncoupling

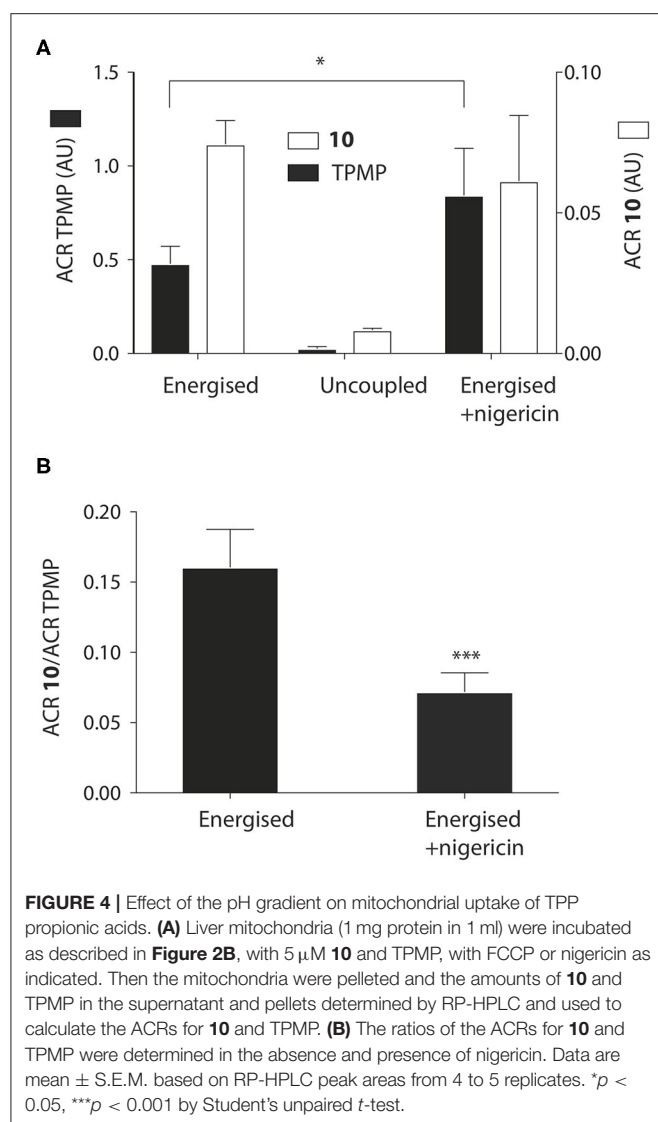
with FCCP (Figure 4A). When the K^+/H^+ exchanger nigericin (Nicholls and Ferguson, 2013) was added to abolish the pH gradient and thereby increase the membrane potential, the ACR for TPMP increased as expected, but that for 10 stayed about the same (Figure 4A). This behavior is consistent with the uptake of 10 being in response to both the membrane potential and the pH gradient, while that of TPMP is solely determined by the membrane potential (Finichiu et al., 2013). Hence, the addition of nigericin will increase the uptake of TPMP due to the elevation of the membrane potential, but for 10 the abolition of the pH gradient will counteract any increased uptake due to an elevated membrane potential. To confirm this, we next compared the ratio of the ACRs for 10 and TPMP in the presence and absence of nigericin, which showed that nigericin lowered the ratio of these ACRs (Figure 4B). We conclude that the uptake of 10 into mitochondria is driven by both the membrane potential and the pH gradient as anticipated in Figure 1.

Utilizing TPP Carboxylic Ester Head Groups to Retain Compounds Within Mitochondria

The TPP compounds containing benzoic and phenylacetic acid derivatives were not taken up by energized mitochondria because their low pK_a prevented passage across the mitochondrial inner membrane. However, their esters should be taken up with subsequent enzymatic hydrolysis within mitochondria then generating the membrane-impermeant acids (Figure 5). This would enable the prolonged delivery of drugs and probes to the mitochondrial matrix where enzymatic hydrolysis generates a TPP carboxylic acid “locked” within the mitochondrial matrix (Figure 5). To test this possibility we made ethyl esters (12–15) of the membrane impermeant TPP benzoic and phenylacetic acids while we also modulated the lipophilicity with methyl and hexyl alkyl groups (Figure 6A).

The esters 12–15 were all taken up by energized liver mitochondria and partially hydrolysed within mitochondria (Figures 6B–E), with the benzoate esters 12 and 13 hydrolysing faster than the phenylacetate esters 14 and 15. To further accelerate ester hydrolysis we next made esters (16–19) incorporating the electron-withdrawing trifluoroethyl group (Figure 6F). Trifluoroethyl esters of phenylacetic acid are known to be hydrolysed 40 times more quickly than ethyl esters by the archetypical esterase, pig liver esterase (Barton et al., 1994). All these esters 16–19 were taken up into energized mitochondria and almost completely hydrolysed (Figures 6G–J). The methyl derivatives 12, 16, and 18 were also taken up by energized heart mitochondria where the lower esterase activity enabled both acid and ester to be detected (Figures 6K–M).

Thus, the ethyl and trifluoroethyl esters 12–19 are accumulated by energized mitochondria and are there hydrolysed within the matrix to the corresponding acid. To see if the acid was retained in the matrix, we incubated mitochondria with the esters for 5 min to generate the acid within the matrix, and then abolished the membrane potential with FCCP. As expected, the IS and the remaining ester



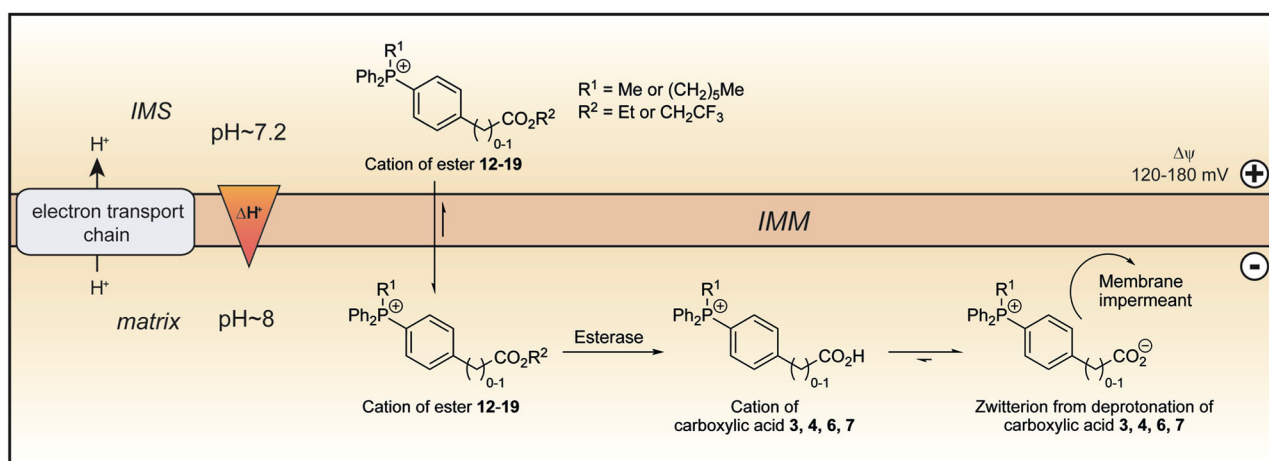


FIGURE 5 | Model of ester uptake and hydrolysis within mitochondria. The lipophilic cations of the esters **12–19** readily cross the mitochondrial inner membrane and are accumulated in the matrix in response to the membrane potential. Within mitochondria, hydrolysis forms the cations of the corresponding carboxylic acids, which exist almost exclusively as their highly charged zwitterions at pH 8.0. The zwitterions should be unable to cross the mitochondrial inner membrane and so be trapped within the mitochondrial matrix. IMM, inner mitochondrial membrane; IMS, intermembrane space.

were lost from the uncoupled mitochondria (**Figures 7A–D**). However, for **12** and **18** the acid accumulated within liver or heart mitochondria was also lost upon uncoupling to similar extents as the IS and ester (**Figures 7A–D**). Esters **13–17** and **19** showed similar behavior (data not shown). FCCP is a lipophilic anion, so to eliminate the possibility that this affected membrane permeability we also used a mixture of mitochondrial inhibitors to abolish the mitochondrial membrane potential. For **12** and **18** (**Figures 7E,F**) and **14**, **16** (data not shown) there was similar loss of the acid upon abolition of the membrane potential as was found with FCCP. Finally, to assess how quickly the acid left mitochondria upon uncoupling we incubated mitochondria with **14** for 5 min, then added FCCP and then isolated mitochondria at various time points subsequently (**Figure 7G**). The rate of efflux of the acid was indistinguishable from that of the IS and the ester at the earliest time point accessible in this experiment (**Figure 7G**). We conclude that these acids rapidly efflux from mitochondria upon loss of the membrane potential.

To see if the acids were retained within mitochondria by a membrane potential we next assessed their retention over time. When mitochondria were incubated with **13**, **17** and **19**, for up to 15 min IS accumulation was constant, but the amount of the acid present within mitochondria decreased over time (**Figures 7H,I,J**), with similar data for esters **12**, **13**, **16**, and **18** (data not shown). To further confirm that acids are lost from energized mitochondria, we incubated mitochondria with **18** for 5 min, and then pelleted the mitochondria and resuspended in fresh incubation medium. The IS was retained by the resuspended mitochondria while the acid was lost (**Figure 7K**). We conclude that the acids are rapidly lost from energized mitochondria.

The acids **3–8** are not taken up by energized mitochondria, but when generated within mitochondria they are not retained,

whether or not there is a membrane potential. One possibility is that the acid can cross the membrane as both the protonated cation and also as the neutral zwitterion. Thus, membrane potential driven uptake of the acids **3–8** in their cationic protonated form, followed by deprotonation and loss of the zwitterion might explain the lack of accumulation. However, this would involve a net influx of protons into the mitochondrial matrix and consequent mitochondrial uncoupling. As increased mitochondrial oxygen consumption is diagnostic of such uncoupling, we measured the effect on this of **3**, **4**, **6**, and **7**, compared to corresponding methyl or hexyl TPPs controls (**Figures 8A,B**). In all cases the effect of the acid on oxygen consumption was lower than the control compound, which showed the mild uncoupling expected for TPP-compounds (Reilly et al., 2013). We conclude that our data cannot be explained by the acids entering as a cation and leaching out as the neutral zwitterion, unless the membrane potential-driven uptake of the cation is very slow and matched by the efflux of the zwitterion (**Figure 8A**).

Computational Analysis of Membrane Transport by TPP Derivatives

Low- pK_a TPP-carboxylic acids are not accumulated by energized mitochondria. It is probable that the protonated cation can cross membranes in response to the membrane potential, but that the low concentration of this species renders the flux negligible compared to efflux pathway(s). Once generated within the mitochondrial matrix, the acids are rapidly lost. As this efflux is unaffected by the membrane potential, the acid must cross the membrane as a neutral species. To explore how this might occur we next carried out computational studies to evaluate the Gibbs free energy of membrane crossing of simple salts of TPMP and some of the acids.

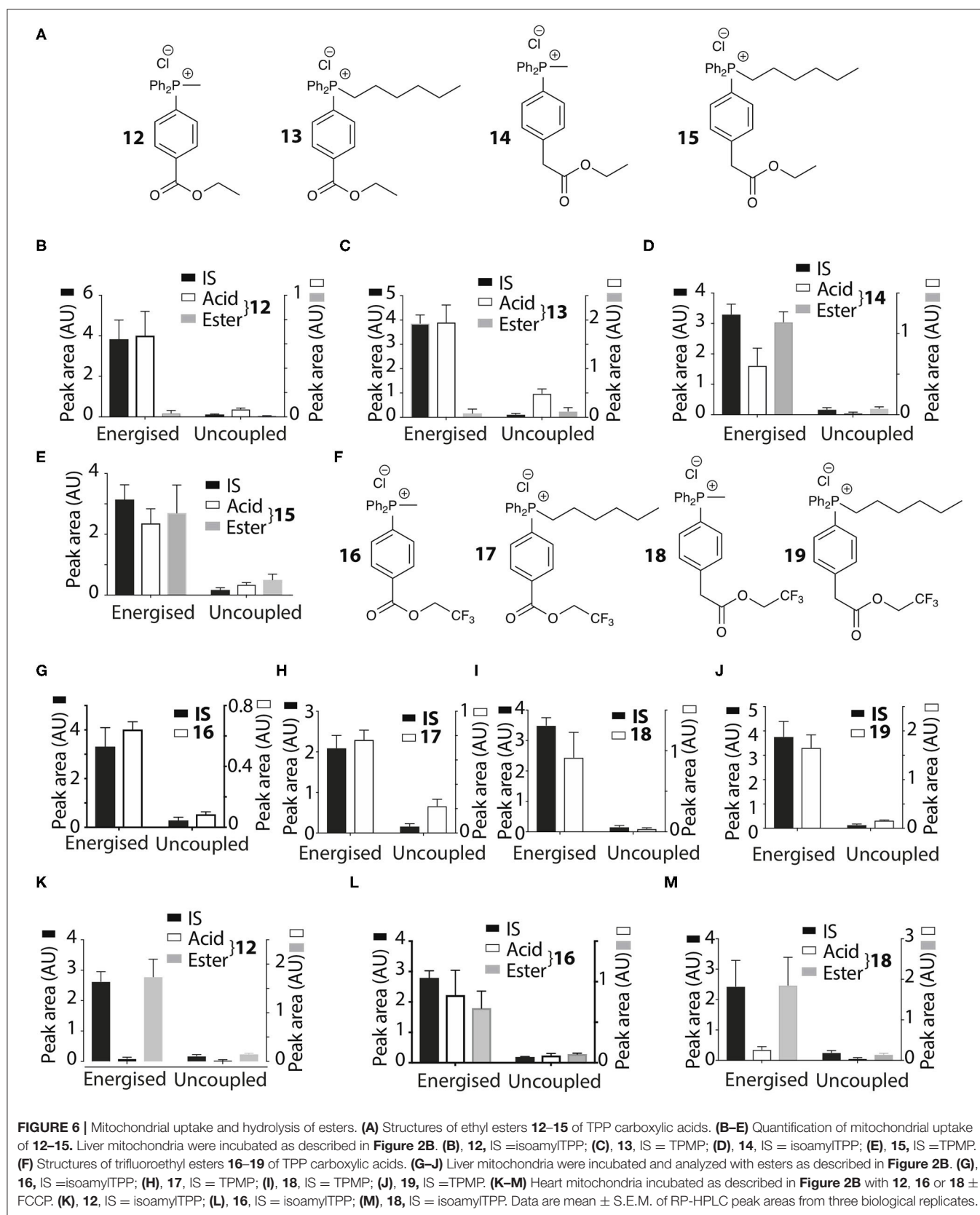


FIGURE 6 | Mitochondrial uptake and hydrolysis of esters. **(A)** Structures of ethyl esters **12–15** of TPP carboxylic acids. **(B–E)** Quantification of mitochondrial uptake of **12–15**. Liver mitochondria were incubated as described in **Figure 2B**. **(B)**, **12**, IS = isoamylTPP; **(C)**, **13**, IS = TPMP; **(D)**, **14**, IS = isoamylTPP; **(E)**, **15**, IS = TPMP. **(F)** Structures of trifluoroethyl esters **16–19** of TPP carboxylic acids. **(G–J)** Liver mitochondria were incubated and analyzed with esters as described in **Figure 2B**. **(G)**, **16**, IS = isoamylTPP; **(H)**, **17**, IS = TPMP; **(I)**, **18**, IS = TPMP; **(J)**, **19**, IS = TPMP. **(K–M)** Heart mitochondria incubated as described in **Figure 2B** with **12**, **16** or **18** \pm FCCP. **(K)**, **12**, IS = isoamylTPP; **(L)**, **16**, IS = isoamylTPP; **(M)**, **18**, IS = isoamylTPP. Data are mean \pm S.E.M. of RP-HPLC peak areas from three biological replicates.

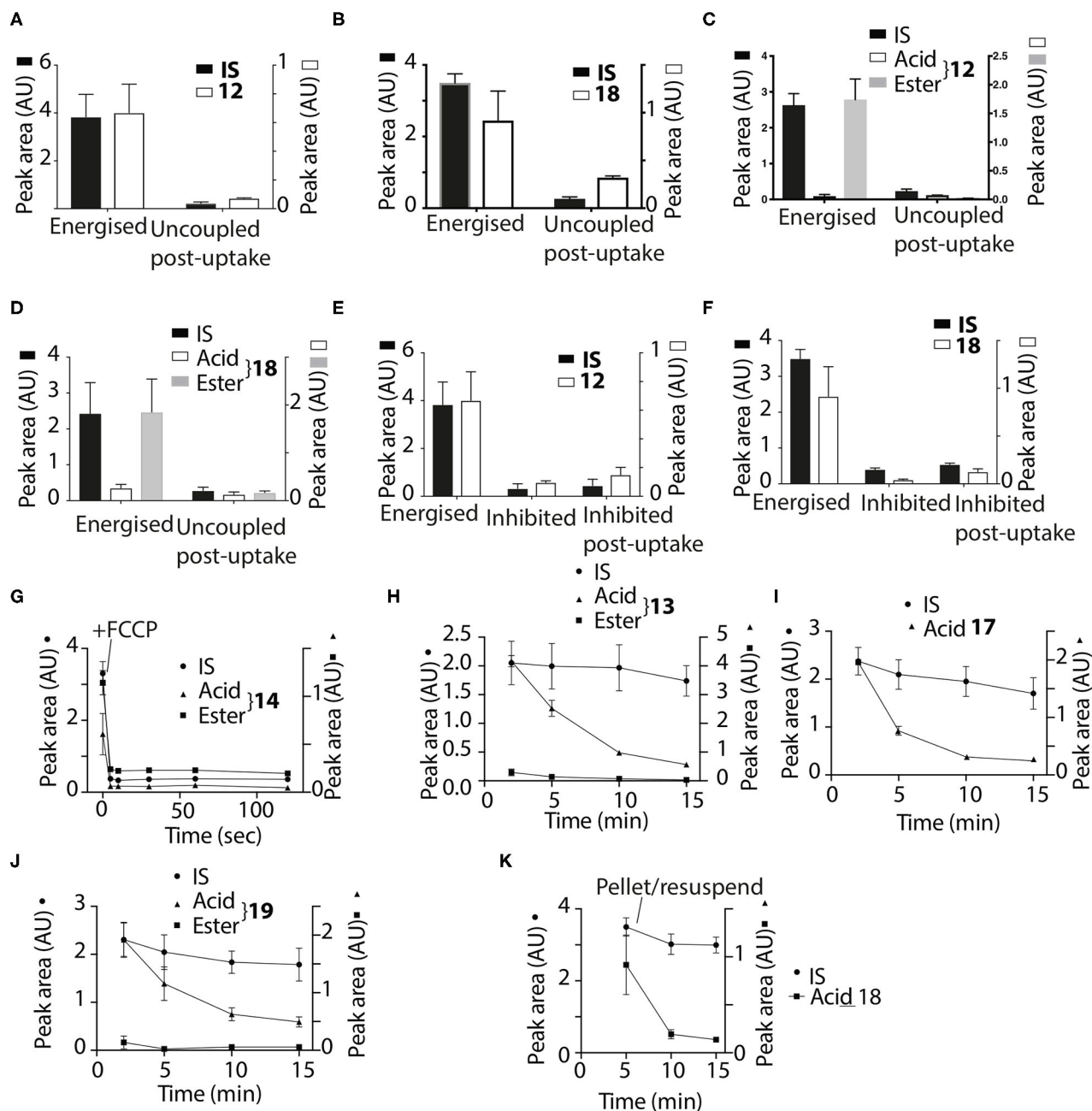


FIGURE 7 | Assessment of retention of acids within mitochondria. Liver (A,B,E,F) or heart (C,D) mitochondria were incubated with 12 or 18 as described in Figure 2B for 5 min and then either incubated for a further 5 min and then pelleted, or FCCP (B,D) was added and after 5 min further incubation the mitochondria were then pelleted. (A), 12, IS = isoamylTPP; (B), 18, IS = isoamyl TPP; (C), 12, IS = isoamyl TPP; (D), 18, IS = isoamyl TPP. (E,F) Liver mitochondria were incubated as described in Figure 2B for 5 min with esters (E), 12 IS = isoamylTPP, or (F), 18 IS = TPMP] for 10 min \pm a mixture of oligomycin/antimycin A/valinomycin or were incubated for 5 min and then a mixture of oligomycin/antimycin A/valinomycin was added after 5 min incubation followed by 5 min further incubation. (G), Liver mitochondria were incubated with 14 and isoamyl TPP as an IS for 5 min, then FCCP was added and the uptake into mitochondria analyzed at the indicated times. (H,I) Liver mitochondria were incubated as described in Figure 2B with the esters 17–19 for various times and the amounts within the mitochondria were analyzed. (H), 13, IS = TPMP; (I), 17, IS = TPMP; (J), 19, IS = TPMP. (K) Liver mitochondria were incubated with 18 and IS = isoamyl TPP for 5 min. Mitochondria were then pelleted by centrifugation and resuspended for 5 or 10 min and then pelleted again. Data are presented as mean \pm S.E.M. of quantified peak areas from three biological replicates.

The thermodynamics of transfer of ions through, or their partitioning into, a phospholipid membrane can be approximated by considering the transfer of ions from aqueous

solution to an apolar medium that mimics the hydrophobic membrane core; here, we chose hexane as the apolar medium. We have used this model previously in calculations to explain

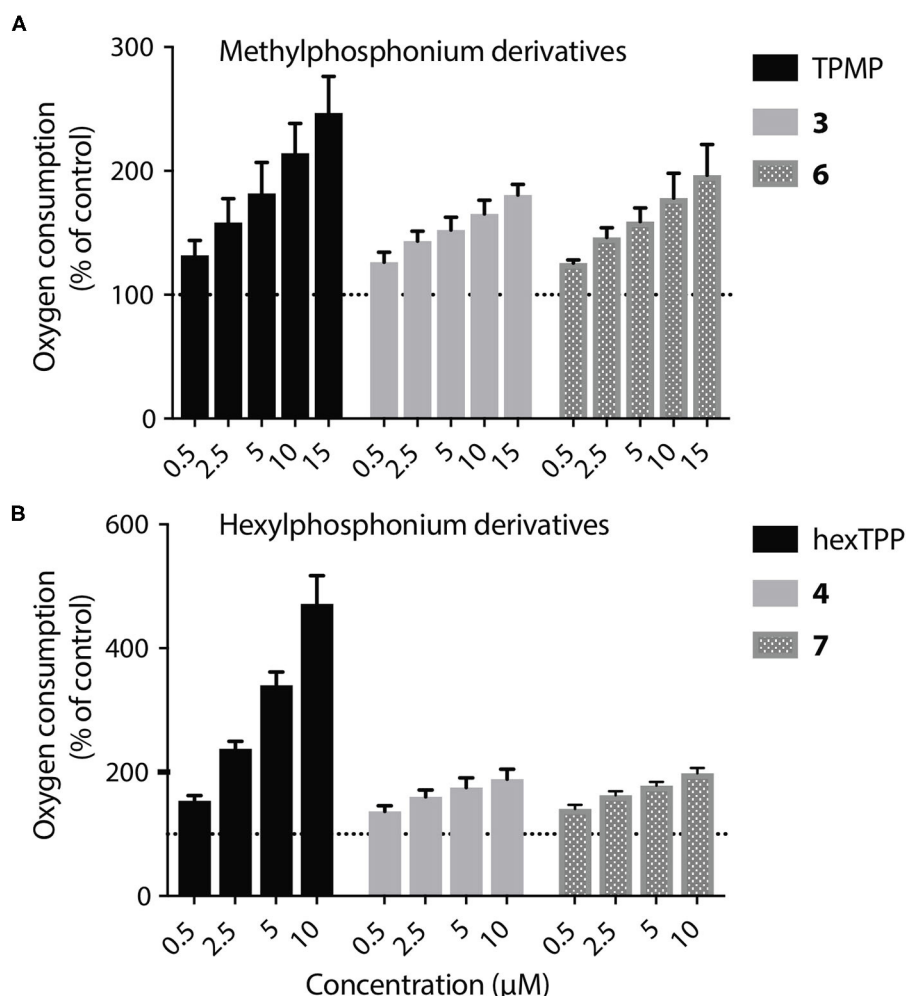
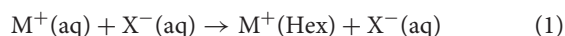


FIGURE 8 | Lack of mitochondrial uncoupling by TPP acids. **(A,B)** Liver mitochondria (0.25 mg mitochondrial protein/mL) respiring on succinate were incubated in KCl buffer (pH 7.2, 37°C) were in an Oroboros O2K high resolution respirometer. A range of concentrations of **3**, **4**, **6**, or **7**, or of appropriate ISs, were incubated and the effect on respiration rate, relative to controls without additions were determined. Data are percentage of initial respiration rate before addition of test compounds and are mean \pm S.E.M. of three biological replicates.

differences in the behavior of cations crossing membranes and accumulating in response to a membrane potential (Robb et al., 2015). It has since received some experimental validation, when (Rokitskaya et al., 2019) showed that calculations on partitioning into an alkane solvent correlate exceptionally well with experiments on transmembrane movement of lipophilic ions across black lipid membranes. The ion can transfer from water to hexane as a free ion, or together with a counter-ion such as Cl^- as a charge-neutral ion pair. For the transfer of a single monovalent cation from water to hexane, we write

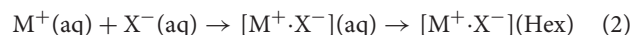


The biologically relevant counter-anions X^- are typically small and strongly hydrophilic, so their partitioning into the apolar phase is negligible and is only shown here to facilitate comparison with the transfer of an ion pair, as is discussed below. The cation is

sufficiently lipophilic to transfer to the apolar phase. The change in free energy associated with Equation (1) is therefore the single-ion free energy of transfer, $\Delta_t G^*(\text{M}^+, \text{aq} \rightarrow \text{Hex})$. The transfer free energy of a solute S is defined as the difference in solvation energy of S between the two solvents:

$$\Delta_t G^*(S, \text{aq} \rightarrow \text{Hex}) = \Delta_{\text{solv}} G^*(S, \text{Hex}) - \Delta_{\text{solv}} G^*(S, \text{aq})$$

If we start from the same initial state of free solvated ions, the transfer of a neutral ion pair (IP) contains two components: firstly, the formation of the IP in water and secondly, the transfer of the IP to the apolar phase.



Accordingly, the free-energy change associated with Equation (2) is the sum of the free energies of ion-pairing and of transfer of the

ion pair.

$$\Delta_{ip}G^*(aq) + \Delta_tG^*(IP, aq \rightarrow Hex)$$

Depending on how well solvated the ion is in the respective phase and the stability of the ion pair, it will be more thermodynamically favorable for an ion to cross either as a free ion (Equation 1) or as an ion pair (Equation 2).

Consider TPMP⁺ (Ph₃PMe⁺) and its ion pair with chloride, [TPMP⁺ · Cl[−]]: **Table 2** lists the calculated free energies of transfer for the free ion and the ion pair; for the ion pair, the free energy of pairing is given together with the sum of pairing + transfer of the pair, which is the relevant free energy for crossing as a pair. Unsurprisingly, the free TPMP⁺ cation is better solvated in water than in hexane, making the transfer from water to hexane thermodynamically unfavorable, albeit far less so than for small ions with localized, concentrated charge, such as Na⁺. Larger ions, such as TPMP⁺, have smaller surface charge densities and expose apolar surface patches to the solvent. Hence, they are relatively less well stabilized in water and so the difference between stabilization in the aqueous phase and stabilization by favorable apolar interactions in hexane is less, and the energy cost of transfer from water to hexane is lower (Reichardt and Welton, 2011).

Despite any free ion being strongly solvated in water, the formation of ion pairs in water is only relatively weakly endergonic. All the ion pairs considered here are still more stable in water than in hexane, but their transfer free energies are smaller than for ions in many cases. Generally speaking, the more hydrophilic/polar the free ion is, the more it benefits from ion-pairing in terms of reducing the energetic disadvantage associated with transferring to hexane.

For the example of TPMP⁺, it transfers relatively easily as a free cation; the transfer as an ion-pair [TPMP⁺ · Cl[−]] is disfavoured by another 14 kJ mol^{−1}. In summary, “lipophilic” ions (low overall charge, small surface charge, large apolar surface patches) can transfer as free ions from water to hexane at modest thermodynamic cost. They do not benefit from ion-pairing. On the other hand, for hydrophilic ions (high overall charge, concentrated surface charge, little apolar surface area), it is thermodynamically prohibitive to transfer as free ions. However, when paired with a strongly hydrophilic counter ion the cost of transferring is significantly reduced (Robb et al., 2015).

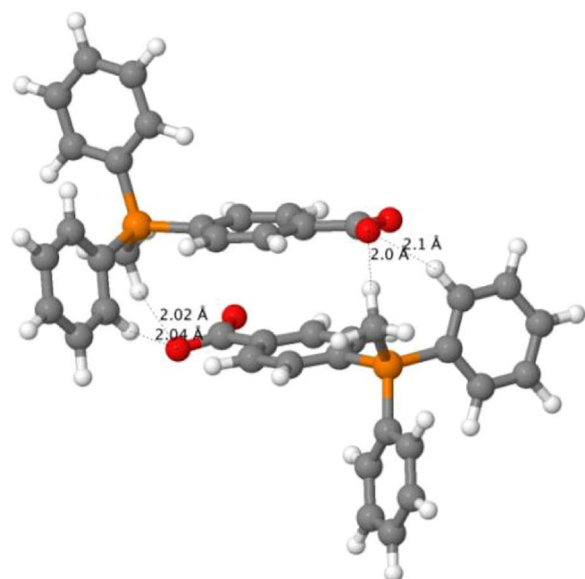
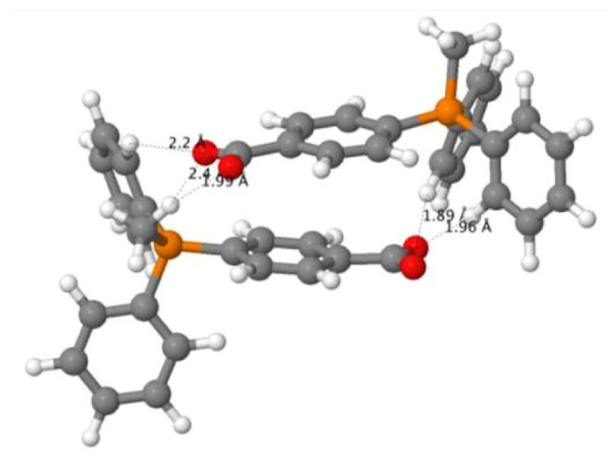
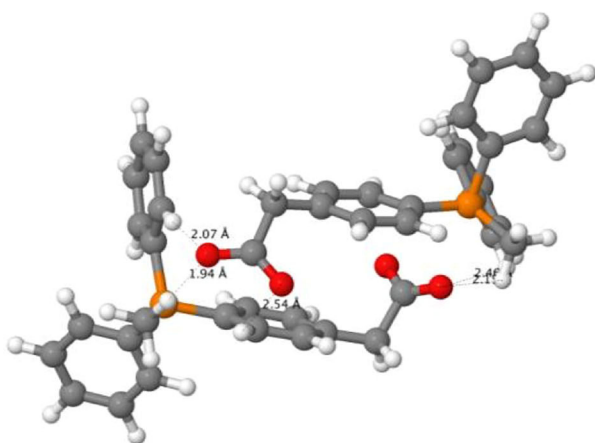
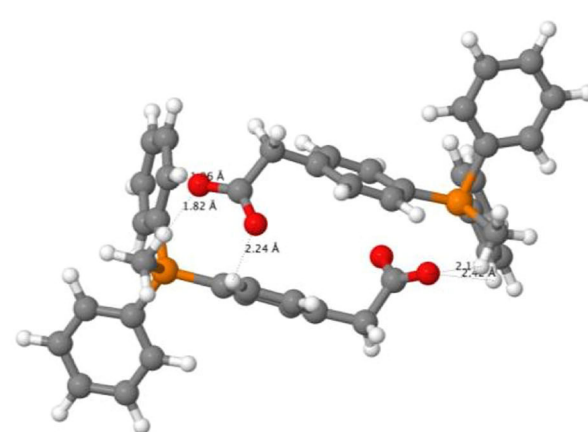
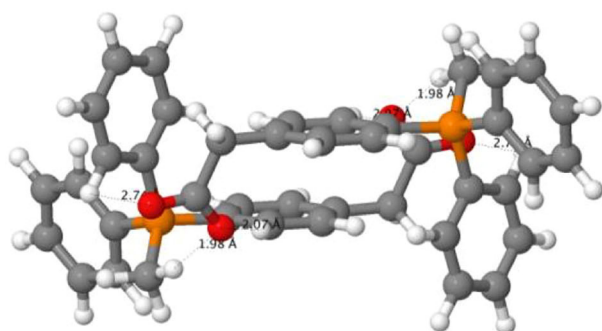
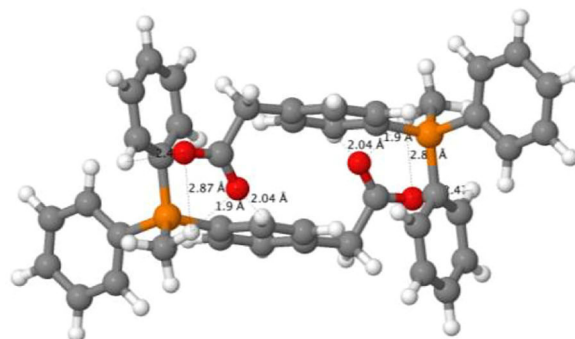
We now consider derivatives of TPMP⁺ where one of the phenyl rings has been substituted in *para* position with a carboxyl or carboxymethyl group. There are therefore multiple possibilities of forming ion pairs with counter-anions or cations (**Table 2**). Comparing the transfer free energies of the single species, TPMP⁺, TPMP⁺-COOH, and TPMP⁺-COO[−], it can be seen that introducing the neutral, protonated carboxyl group makes the transfer ~20 kJ mol^{−1} more unfavorable (compared to unsubstituted TPMP⁺) (**Table 2**). Transferring the zwitterionic carboxylate is significantly disfavored (by ~40 kJ mol^{−1}) despite the overall neutral charge because the negative charge of the carboxylate is solvent-exposed and relatively localized. Depending on whether the carboxylic acid is deprotonated or neutral, the following ion pairs were considered: [TPMP⁺-COOH · Cl[−]], [TPMP⁺-COO[−] · Cl[−]][−], [TPMP⁺-COO[−] · Na⁺]⁺. None of these ion pairs transfers more easily than the corresponding single species (**Table 2**).

However, the zwitterions TPMP⁺-COO[−] and TPMP⁺-CH₂COO[−] have the ability to form self-complementary (“head-to-tail”) dimers (**Figure 9**). In these structures, the negatively

TABLE 2 | Calculated free energies of transfer of solute S from water to hexane, $\Delta_tG^*(S, aq \rightarrow Hex)$, and free energies of ion-pairing in water, $\Delta_{ip}G^*(aq)$.

| Solute S | $\Delta_tG^*(S, aq \rightarrow Hex)$ | $\Delta_{ip}G^*(aq)$ | $\Delta_{ip}G^*(aq) + \Delta_tG^*(S, aq \rightarrow Hex)$ | Ion-pair preference |
|--|--------------------------------------|----------------------|---|---------------------|
| TPMP ⁺ | 44 | | | |
| TPMP ⁺ -COOH | 64 | | | |
| TPMP ⁺ -COO [−] | 86 | | | |
| TPMP ⁺ -CH ₂ COOH | 59 | | | |
| TPMP ⁺ -CH ₂ COO [−] | 88 | | | |
| Cl [−] | 157 | | | |
| Na ⁺ | 229 | | | |
| TPMP ⁺ · Cl [−] | 39 | 19 | 58 | 14 |
| TPMP ⁺ -COOH · Cl [−] | 55 | 18 | 73 | 9 |
| TPMP ⁺ -COO [−] · Cl [−] | 160 | 19 | 179 | 93 |
| TPMP ⁺ -COO [−] · Na ⁺ | 126 | −3 | 123 | 40 |
| TPMP ⁺ -COO ₂ [−] ^a | 39 | 16 | 55 | −30 |
| TPMP ⁺ -CH ₂ COO ₂ [−] (Conf 1) ^a | 16 | 34 | 50 | −39 |
| TPMP ⁺ -CH ₂ COO ₂ [−] (Conf 2) ^a | 30 | 12 | 41 | −47 |

All free energies are in kJ mol^{−1}.
The preference for crossing as ion pair is defined as $\Delta_{ip}G^*(aq) + \Delta_tG^*(IP, aq \rightarrow Hex) - \Delta_tG^*(free\ ion, aq \rightarrow Hex)$; a negative value means that crossing as an ion pair is preferred to crossing as a free ion. The term “ion-pairing” is used here to designate both the association with a small counter-ion and the dimerisation of zwitterions.
^aEnergies are per mol of monomer.
Comparable values for the transfer of free ions vs. ion-pairs are highlighted in bold.

[TPMP⁺-COO⁻]₂ (H₂O)[TPMP⁺-COO⁻]₂ (Hex)[TPMP⁺-CH₂COO⁻]₂ (Conf 1) (H₂O)[TPMP⁺-CH₂COO⁻]₂ (Conf 1) (Hex)[TPMP⁺-CH₂COO⁻]₂ (Conf 2) (H₂O)[TPMP⁺-CH₂COO⁻]₂ (Conf 2) (Hex)**FIGURE 9** | Optimized structures of self-complementary dimers of the assessed zwitterions in water and hexane.

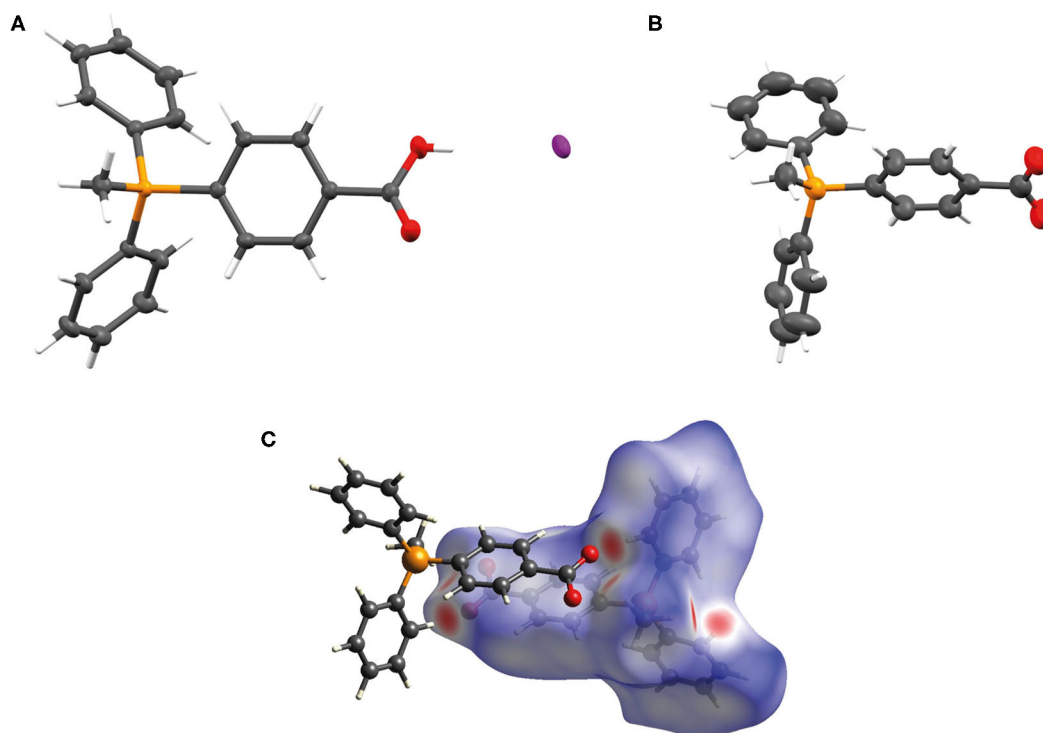
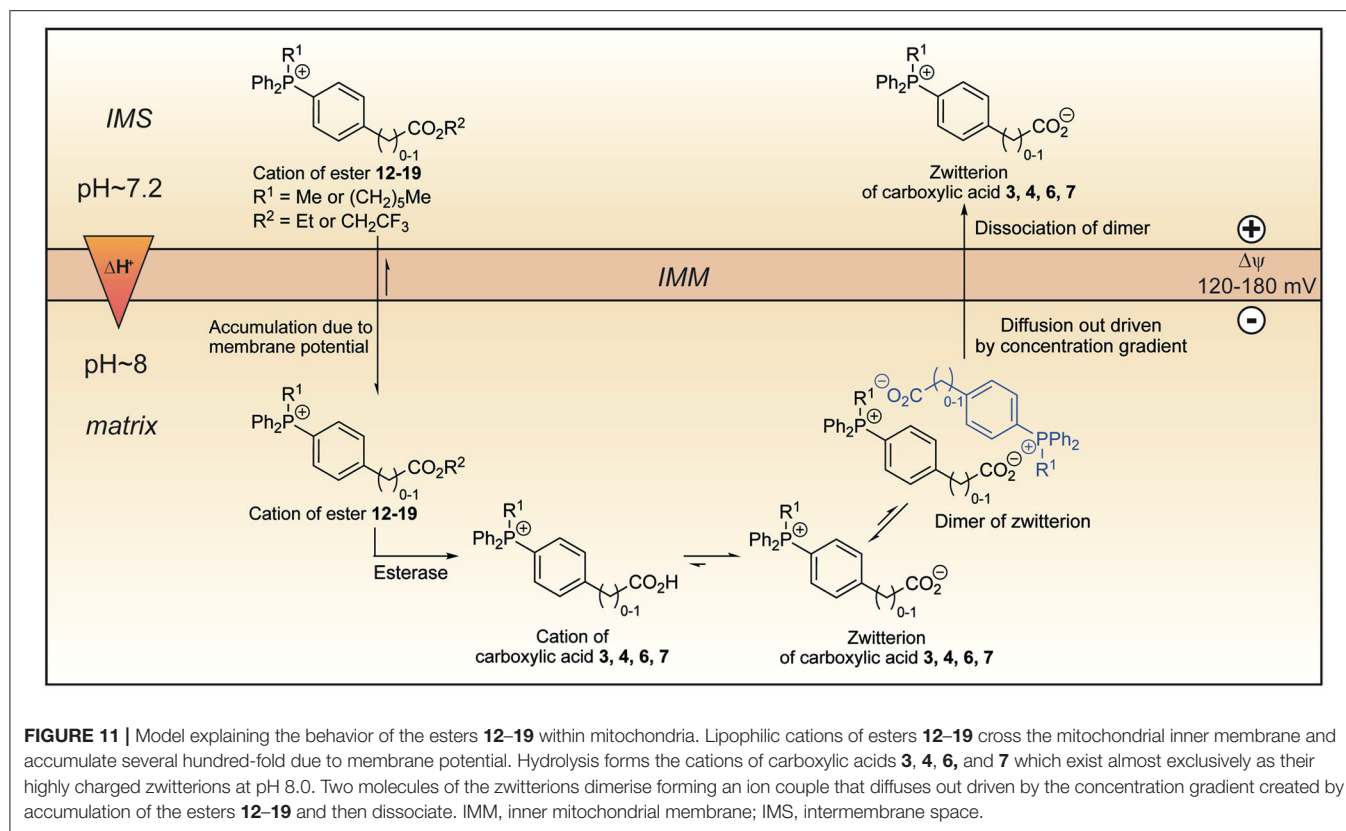


FIGURE 10 | (A) The X-ray crystal structure of [TPMP⁺-COOH · I⁻] with atomic displacement ellipsoids drawn at 50% probability level for non-hydrogen atoms. **(B)** The X-ray crystal structure of TPMP⁺-COO⁻ with atomic displacement ellipsoids drawn at 50% probability level for non-hydrogen atoms. **(C)** View of the Hirshfeld surface of TPMP⁺-COO⁻ mapped with d_{norm} property (calculated using CrystalExplorer), contact distance < van der Waals contact are shown in red, equal to it in white and longer as blue. (Spackman and Jayatilaka, 2009).

charged carboxylate groups are partially buried within the pocket formed by the α - and β -hydrogens of the methyl and phenyl substituents of the phosphonium, respectively, which carry a significant fraction of the positive charge (Figure 9). These stabilizing electrostatic interactions make the dimer formation in water similarly favorable to ion-pairing with a small single ion like Cl⁻, that is, endergonic by ~ 15 – 20 kJ mol⁻¹. At the same time, in the dimers, the negative charges of the carboxylates are locally compensated for and partially shielded from the solvent so that there is less stabilization from interactions with water. Therefore, transfer to hexane is less unfavorable than for the single zwitterions. For the dimer [TPMP⁺-CH₂COO⁻]₂, we considered two minimum energy structures. Conformer 2 is more stable than Conformer 1 by 45 kJ mol⁻¹ in water, but only by 17 kJ mol⁻¹ in hexane. Dimerisation in water is therefore more favorable for Conformer 2, but the transfer energy is less endergonic for Conformer 1 (see Table 2). The two effects largely compensate each other, such that transferring as dimers is clearly preferred for both conformers. Overall, therefore, the dimers transfer significantly more easily than the corresponding single species. The calculated Gibbs energies for all the species taken into consideration (cations, ion pairs, and dimers) are reported in Table 2. We conclude that the most likely way in which the TPP acid derivatives can leave mitochondria is as a neutral dimer of two zwitterionic molecules (Figure 9).

X-ray Crystallography Support for Dimers

Finally, we sought crystallographic evidence of the benefit of the interactions identified in our models of the dimer [TPMP⁺-COO⁻]₂. To do this, we synthesized the pure zwitterionic species without any counterion. First, the iodide salt was prepared by the method used to make the chloride salt 3 of the carboxylic acid (Scheme 1), but without ion exchange. Single crystals of this compound, [TPMP⁺-COOH · I⁻], were grown. Treatment of the iodide salt with silver carbonate removed the iodide and allowed single crystals of the zwitterion, TPMP⁺-COO⁻, also to be grown. Single crystal X-ray diffraction revealed the structures of both [TPMP⁺-COOH · I⁻] and TPMP⁺-COO⁻ (Figures 10A,B). [TPMP⁺-COOH · I⁻] has a C–OH length of 1.325(2) Å and a C=O length of 1.204(2) Å, which are close to the typical C–O (1.308 Å) and C=O (1.214 Å) bond lengths in carboxylic acids (Allen et al., 2006). As expected, there is no halogen present in the structure of TPMP⁺-COO⁻ with the positive charge of the phosphonium ions balanced in the crystal by the negatively charged carboxylate ions. The C–O bond lengths of 1.233(3) and 1.246(3) Å match closely the typical bond length of 1.254 Å for a delocalised C=O carboxylate bond (Allen et al., 2006). Within the crystal lattice multiple individual molecules interact to satisfy the attractive electrostatic interactions in a range of packing motifs. Among these, evidence for the proposed “head-to-tail” dimers was observed (Figure 10C).



Here, the carboxylate group of one molecule is in close proximity to the α -hydrogen of the methyl (2.440 Å) and the β -hydrogen of the phenyl (2.237 Å) of its neighbor's phosphonium group. These distances agree well with those predicted in our theoretical models of the dimer $[\text{TPMP}^+-\text{CH}_2\text{COO}^-]_2$ (Figure 9).

CONCLUSION

We set out to develop a mitochondria-targeting strategy that would enhance uptake into mitochondria using a targeting head group that would increase mitochondrial uptake of simple TPP cations by responding not only to the membrane potential but also to the pH gradient across the mitochondrial inner membrane. Here we show that incorporation of a propionic acid into a TPP moiety provides derivatives that accumulate in response to both these factors, albeit with a lower ACR than simple TPP compounds. On the other hand, we found that TPP moieties derivatised with benzoic or phenylacetic acid groups on the phosphonium were not taken up by mitochondria due to the low pK_a of these acids depleting the amount of cation available to cross the membrane. This suggested that this finding could be exploited to generate esters that would generate such membrane impermeant acids within the mitochondrial matrix thereby locking molecules within the mitochondrial matrix. As the ability to lock molecules within mitochondria might facilitate the development of more

persistent mitochondrial probes and therapies, we explored this possibility. To our surprise, we found that despite their low pK_a these acids were rapidly lost from mitochondria, irrespective of the presence of a membrane potential. A computational approach suggested that this occurred by the zwitterions forming dimers and that these neutral dimers were then able to pass through the mitochondrial inner membrane. Thus, esters **12–19** accumulate in the matrix driven by the membrane potential, but upon hydrolysis, the corresponding carboxylic acids **3, 4, 6, and 7** are not trapped (Figure 11). Instead, they diffuse out of the matrix as dimers of their zwitterions, driven by the concentration gradient. Our work suggests that making TPP carboxylic compounds in which the ability to form dimers was prevented (e.g., by incorporating bulky groups) would improve delivery and open up a new mitochondrial lock in strategy.

In summary, by investigating methods to enhance TPP delivery to mitochondria we have revealed the factors that govern uptake of TPP-carboxylic acids and exposed new potential strategies, which we will explore in future work.

DATA AVAILABILITY STATEMENT

The NMR data, the Fourier transformed NMR spectra for the synthesised compounds and xyz coordinates and energies of all optimised structures can be found in the University of Glasgow repository <http://dx.doi.org/10.5525/gla.researchdata.1004>. The

CIF files CCDC 1998454 [TPMP⁺-COO⁻] and 1998455 (TPMP⁺-COOH.I⁻) contain the supplementary crystallographic data for this paper. These data can be obtained free of charge from The Cambridge Crystallographic Data Centre via www.ccdc.cam.ac.uk/structure.

ETHICS STATEMENT

All experiments were conducted according to the Animals Scientific Procedures Act 1986 (UK) and directive 2010/63/EU of the European Parliament guidelines on the protection of animals used for scientific purposes. All experiments were approved by the University of Cambridge Institutional Animal Welfare and Ethical Review Body.

AUTHOR CONTRIBUTIONS

LP synthesized the majority of the compounds and carried out most biological testing. HS carried out the computational calculations. SC synthesized some of the compounds. SW and CW carried out and interpreted the single X-ray crystallography study. TP and TB carried out biological testing. HP helped design of biological experiments. RH and MM supervised the project

and the manuscript writing. All authors contributed to the article and approved the submitted version.

FUNDING

Work in the MM laboratory was supported by the Medical Research Council UK (MC_U105663142) and by a Wellcome Trust Investigator award (110159/A/15/Z). Work in the RH laboratory was supported by a Wellcome Trust Investigator award (WT110158/Z/15/Z) and LP was supported by a studentship from the University of Glasgow.

ACKNOWLEDGMENTS

HS is grateful to Kristiāns Čerņevičs for performing some of the calculations reported here as part of his MSci thesis at the University of Glasgow.

SUPPLEMENTARY MATERIAL

The Supplementary Material for this article can be found online at: <https://www.frontiersin.org/articles/10.3389/fchem.2020.00783/full#supplementary-material>

REFERENCES

- Ahlrichs, R., Bär, M., Häser, M., Horn, H., and Kölmel, C. (1989). Electronic structure calculations on workstation computers: the program system turbomole. *Chem. Phys. Lett.* 162, 165–169. doi: 10.1016/0009-2614(89)85118-8
- Alecú, I. M., Zheng, J., Zhao, Y., and Truhlar, D. G. (2010). Computational thermochemistry: scale factor databases and scale factors for vibrational frequencies obtained from electronic model chemistries. *J. Chem. Theory Comput.* 6, 2872–2887. doi: 10.1021/ct100326h
- Allen, F. H., Watson, D. G., Brammer, L., Orpen, A. G., and Taylor, R. (2006). Typical interatomic distances: organic compounds. *Int. Tables Crystallog.* C 9, 790–811. doi: 10.1107/9780955360206000062
- Barton, P., Laws, A. P., and Page, M. I. (1994). Structure-activity relationships in the esterase-catalysed hydrolysis and transesterification of esters and lactones. *J. Chem. Soc. Perkin Trans. 2*, 2021–2029. doi: 10.1039/P29940002021
- Ben-Naim, A. (1987). *Solvation Thermodynamics*. New York, NY: Plenum Press.
- Ben-Naim, A. (1992). *Statistical Thermodynamics for Chemists and Biochemists*. New York, NY: Plenum Press.
- Chappell, J. B., and Hansford, R. G. (1972). "Preparation of mitochondria from animal tissues and yeasts," in *Subcellular Components: Preparation and Fractionation*, ed. G. Birnie (London: Butterworths), 77–91.
- Dydyo, P., Detz, R. J., de Bruin, B., and Reek, J. N. (2014). Beyond classical reactivity patterns: hydroformylation of vinyl and allyl arenes to valuable beta- and gamma-aldehyde intermediates using supramolecular catalysis. *J. Am. Chem. Soc.* 136, 8418–8429. doi: 10.1021/ja503033q
- Finichiu, P. G., James, A. M., Larsen, L., Smith, R. A., and Murphy, M. P. (2013). Mitochondrial accumulation of a lipophilic cation conjugated to an ionisable group depends on membrane potential, pH gradient and pK_a: implications for the design of mitochondrial probes and therapies. *J. Bioenerg. Biomembr.* 45, 165–173. doi: 10.1007/s10863-012-9493-5
- Finichiu, P. G., Larsen, D. S., Evans, C., Larsen, L., Bright, T. P., Robb, E. L., et al. (2015). A mitochondria-targeted derivative of ascorbate: MitoC. *Free Radic. Biol. Med.* 89, 668–678. doi: 10.1016/j.freeradbiomed.2015.07.160
- Frisch, M. J., Trucks, G. W., Schlegel, H. B., Scuseria, G. E., Robb, M. A., and Cheeseman, J. R. (2013). *Gaussian 09. Version Revision E.01*. Wallingford, CT: Gaussian, Inc.
- Funes-Ardoiz, I., and Paton, R. S. (2018). *GoodVibes* V. 2.0.3. doi: 10.5281/zenodo.1435820
- Gorman, G. S., Chinnery, P. F., DiMauro, S., Hirano, M., Koga, Y., McFarland, R., et al. (2016). Mitochondrial diseases. *Nat. Rev. Dis. Primers.* 2:16080. doi: 10.1038/nrdp.2016.80
- Grimme, S., Antony, J., Ehrlich, S., and Krieg, H. (2010). A consistent and accurate ab initio parametrization of density functional dispersion correction (DFT-D) for the 94 elements H–Pu. *J. Chem. Phys.* 132:154104. doi: 10.1063/1.3382344
- Grimme, S., Ehrlich, S., and Goerigk, L. (2011). Effect of the damping function in dispersion corrected density functional theory. *J. Comput. Chem.* 32, 1456–1465. doi: 10.1002/jcc.21759
- Häser, M., and Ahlrichs, R. (1989). Improvements on the direct SCF method. *J. Comput. Chem.* 10, 104–111. doi: 10.1002/jcc.540100111
- Hu, Z., Sim, Y., Kon, O. L., Ng, W. H., Ribeiro, A. J., Ramos, M. J., et al. (2017). Unique triphenylphosphonium derivatives for enhanced mitochondrial uptake and photodynamic therapy. *Bioconjugate Chem.* 28, 590–599. doi: 10.1021/acs.bioconjchem.6b00682
- Hünenberger, P., and Reif, M. (2011). *Single-Ion Solvation: Experimental and Theoretical Approaches to Elusive Thermodynamic Quantities*. London: Royal Society of Chemistry.
- Jean, S. R., Ahmed, M., Lei, E. K., Wisnovsky, S. P., and Kelley, S. O. (2016). Peptide-mediated delivery of chemical probes and therapeutics to mitochondria. *Acc. Chem. Res.* 49, 1893–1902. doi: 10.1021/acs.accounts.6b00277
- Kanchanakungwankul, S., Bao, J. L., Zheng, J., Alecú, I. M., Lynch, B. J., Zhao, Y., et al. (2018). *Database of Frequency Scale Factors for Electronic Model Chemistries. 4th Edn*. Available online at: <https://comp.chem.umn.edu/freqscale/>
- Kanicky, J. R., and Shah, D. O. (2003). Effect of premicellar aggregation on the pK_a of fatty acid soap solutions. *Langmuir* 19, 2034–2038. doi: 10.1021/la020672y
- Klamt, A. (1996). Calculation of UV/Vis spectra in solution. *J. Phys. Chem.* 100, 3349–3353. doi: 10.1021/jp950607f
- Klamt, A., and Jonas, V. (1996). Treatment of the outlying charge in continuum solvation models. *J. Chem. Phys.* 105, 9972–9981. doi: 10.1063/1.472829
- Klamt, A., and Schüürmann, G. (1993). COSMO–A new approach to dielectric screening in solvents with explicit expressions for the screening energy and its gradient. *J. Chem. Soc. Perkin Trans. 2*, 799–805. doi: 10.1039/P29930000799

- Logan, A., Cocheme, H. M., Li Pun, P. B., Apostolova, N., Smith, R. A., Larsen, L., et al. (2014). Using exomarkers to assess mitochondrial reactive species *in vivo*. *Biochim. Biophys. Acta* 1840, 923–930. doi: 10.1016/j.bbagen.2013.05.026
- Marenich, A. V., Cramer, C. J., and Truhlar, D. G. (2009). Universal solvation model based on solute electron density and on a continuum model of the solvent defined by the bulk dielectric constant and atomic surface tensions. *J. Phys. Chem. B* 113, 6378–6396. doi: 10.1021/jp810292n
- Murphy, M. P., and Hartley, R. C. (2018). Mitochondria as a therapeutic target for common pathologies. *Nat. Rev. Drug Discov.* 17, 865–886. doi: 10.1038/nrd.2018.174
- Nicholls, D. G., and Ferguson, S. J. (2013). *Bioenergetics* 4. London: Academic Press.
- Nunnari, J., and Suomalainen, A. (2012). Mitochondria: in sickness and in health. *Cell* 148, 1145–1159. doi: 10.1016/j.cell.2012.02.035
- Qin, L., Hu, B., Neumann, K. D., Linstad, E. J., McCauley, K., Veness, J., et al. (2015). A mild and general one-pot synthesis of densely functionalized diaryliodonium salts. *Eur. J. Org. Chem.* 2015, 5919–5924. doi: 10.1002/ejoc.201500986
- Reichardt, C., and Welton, T. (2011). *Solvents and Solvent Effects in Organic Chemistry*, 4th Edn. Weinheim: Wiley-VCH.
- Reily, C., Mitchell, T., Chacko, B. K., Benavides, G. A., Murphy, M. P., and Darley-Usmar, V. M. (2013). Mitochondrially targeted compounds and their impact on cellular bioenergetics. *Redox Biol.* 1, 86–93. doi: 10.1016/j.redox.2012.11.009
- Ribeiro, R. F., Marenich, A. V., Cramer, C. J., and Truhlar, D. G. (2011). Use of solution-phase vibrational frequencies in continuum models for the free energy of solvation. *J. Phys. Chem. B* 115, 14556–14562. doi: 10.1021/jp205508z
- Robb, E. L., Gawel, J. M., Aksentijevic, D., Cocheme, H. M., Stewart, T. S., Shchepinova, M. M., et al. (2015). Selective superoxide generation within mitochondria by the targeted redox cycler MitoParaquat. *Free Radic. Biol. Med.* 89, 883–894. doi: 10.1016/j.freeradbiomed.2015.08.021
- Rokitskaya, T. I., Luzhkov, V. B., Korshunova, G. A., Tashlitsky, V. N., and Antonenko, Y. N. (2019). Effect of methyl and halogen substituents on the transmembrane movement of lipophilic ions. *Phys. Chem. Chem. Phys.* 21, 23355–23363. doi: 10.1039/c9cp03460a
- Ross, M. F., Da Ros, T., Blaikie, F. H., Prime, T. A., Porteous, C. M., Severina, I. I., et al. (2006). Accumulation of lipophilic dications by mitochondria and cells. *Biochem. J.* 400, 199–208. doi: 10.1042/BJ20060919
- Rumble, J. R., Lide, D. R., Bruno, T. J. (eds.) (2018). *CRC Handbook of Chemistry and Physics*. 99th edn. Boca Raton, FL: CRC Press.
- Sierka, M., Hoge Kamp, A., and Ahlrichs, R. (2003). Fast evaluation of the Coulomb potential for electron densities using multipole accelerated resolution of identity approximation. *J. Chem. Phys.* 118, 9136–9148. doi: 10.1063/1.1567253
- Smith, R. A., Hartley, R. C., Cocheme, H. M., and Murphy, M. P. (2012). Mitochondrial pharmacology. *Trends Pharmacol. Sci.* 33, 341–352. doi: 10.1016/j.tips.2012.03.010
- Smith, R. A., Hartley, R. C., and Murphy, M. P. (2011). Mitochondria-targeted small molecule therapeutics and probes. *Antioxid. Redox Sign.* 15, 3021–3038. doi: 10.1089/ars.2011.3969
- Smith, R. A., Porteous, C. M., Gane, A. M., and Murphy, M. P. (2003). Delivery of bioactive molecules to mitochondria *in vivo*. *Proc. Natl. Acad. Sci. U.S.A.* 100, 5407–5412. doi: 10.1073/pnas.0931245100
- Spackman, M. A., and Jayatilaka, D. (2009). Hirshfeld surface analysis *Cryst. Eng. Comm.* 11, 19–32. doi: 10.1039/B818330A
- Tao, J. M., Perdew, J. P., Staroverov, V. N., and Scuseria, G. E. (2003). Climbing the density functional ladder: nonempirical meta-generalized gradient approximation designed for molecules and solids. *Phys. Rev. Lett.* 91, 146401. doi: 10.1103/PhysRevLett.91.146401
- Tomasi, J., Mennucci, B., and Cammi, R. (2005). Quantum mechanical continuum solvation models. *Chem. Rev.* 105, 2999–3093. doi: 10.1021/cr9904009
- Treutler, O., and Ahlrichs, R. (1995). Efficient molecular numerical integration schemes. *J. Chem. Phys.* 102, 346–354. doi: 10.1063/1.469408
- von Arnim, M., and Ahlrichs, R. (1998). Performance of parallel Turbomole for density functional calculations. *J. Comput. Chem.* 19, 1746–1757. doi: 10.1002/(SICI)1096-987X(19981130)19:15<1746::AID-JCC7>3.0.CO;2-N
- von Arnim, M., and Ahlrichs, R. (1999). Geometry optimization in generalized natural internal coordinates. *J. Chem. Phys.* 111, 9183–9190. doi: 10.1063/1.479510
- Weigend, F. (2006). Accurate Coulomb-fitting basis sets for H to Rn. *Phys. Chem. Chem. Phys.* 8, 1057–1065. doi: 10.1039/B515623H
- Weigend, F., and Ahlrichs, R. (2005). Balanced basis sets of split valence, triple zeta valence and quadruple zeta valence quality for H to Rn: design and assessment of accuracy. *Phys. Chem. Chem. Phys.* 7, 3297–3305. doi: 10.1039/B508541A
- Yousif, L. F., Stewart, K. M., and Kelley, S. O. (2009). Targeting mitochondria with organelle-specific compounds: strategies and applications. *ChemBiochem* 10, 1939–1950. doi: 10.1002/cbic.200900185
- Zhao, Y., and Truhlar, D. G. (2008). The M06 suite of density functionals for main group thermochemistry, thermochemical kinetics, noncovalent interactions, excited states, and transition elements: two new functionals and systematic testing of four M06-class functionals and 12 other functionals. *Theor. Chem. Acc.* 120, 215–241. doi: 10.1007/s00214-007-0310-x

Conflict of Interest: The authors declare that the research was conducted in the absence of any commercial or financial relationships that could be construed as a potential conflict of interest.

Copyright © 2020 Pala, Senn, Caldwell, Prime, Warrington, Bright, Prag, Wilson, Murphy and Hartley. This is an open-access article distributed under the terms of the Creative Commons Attribution License (CC BY). The use, distribution or reproduction in other forums is permitted, provided the original author(s) and the copyright owner(s) are credited and that the original publication in this journal is cited, in accordance with accepted academic practice. No use, distribution or reproduction is permitted which does not comply with these terms.

Advantages of publishing in Frontiers



OPEN ACCESS

Articles are free to read
for greatest visibility
and readership



FAST PUBLICATION

Around 90 days
from submission
to decision



HIGH QUALITY PEER-REVIEW

Rigorous, collaborative,
and constructive
peer-review



TRANSPARENT PEER-REVIEW

Editors and reviewers
acknowledged by name
on published articles

Frontiers

Avenue du Tribunal-Fédéral 34
1005 Lausanne | Switzerland

Visit us: www.frontiersin.org

Contact us: frontiersin.org/about/contact



REPRODUCIBILITY OF RESEARCH

Support open data
and methods to enhance
research reproducibility



DIGITAL PUBLISHING

Articles designed
for optimal readership
across devices



FOLLOW US

@frontiersin



IMPACT METRICS

Advanced article metrics
track visibility across
digital media



EXTENSIVE PROMOTION

Marketing
and promotion
of impactful research



LOOP RESEARCH NETWORK

Our network
increases your
article's readership